



A COMPARATIVE STUDY OF TRABECULAR ARCHITECTURE IN THE DISTAL TIBIA OF HUMANS, HOMINOIDS AND AUSTRALOPITHS FROM SOUTH AFRICA

A dissertation submitted to the Faculty of Science, University of the Witwatersrand, in
fulfillment of the requirements for the degree of

MASTER OF SCIENCE
(PALAEOLOGY)

By Kimberleigh Ashley Tommy

Student number: 539205

Supervisor: Dr. Bernhard Zipfel

Co-Supervisor: Prof. Kristian Carlson

Evolutionary Studies Institute, University of the Witwatersrand, Private Bag 3, WITS
2050, Johannesburg, South Africa.

CENTRE OF  XCELLENCE
PALAEOSCIENCES



 P2A9
ALL FROM ONE

DECLARATION

I, Kimberleigh Tommy (Student number: 539205), am a student registered for the degree in Master of Science by Dissertation (SR000) in the academic year 2016 completing in January 2018. I herewith submit the following research “A comparative study of trabecular architecture in the distal tibia of humans, hominoids and australopiths from South Africa”

I declare that this Dissertation is my own, unaided work. It is being submitted for the Degree of Master of Science at the University of the Witwatersrand, South Africa. It has not been submitted before for any degree or examination at any other University.

A handwritten signature in black ink, appearing to read 'K. Tommy', with a long horizontal stroke extending to the right.

Signature of candidate:

On this 15th day of January 2018.

In loving memory of my grandparents

Victor Botha

17 August 1941

11 January 1995

Clive Tommy

2 October 1938

9 November 2009

Carol Tommy

21 March 1937

26 July 2015

ACKNOWLEDGEMENTS

Firstly, I would like to thank my supervisors Prof. Kristian Carlson and Dr. Bernhard Zipfel, I have often called you “the dream team” and there is no better way to describe the two of you. Thank you for believing in me from my honours year when I was a shy new postgraduate, a small fish in a newly expanded pond and for nurturing my scientific interest. I am forever grateful for the advice and guidance you have given me throughout the past year as I worked toward completing this dissertation. Thank you for cultivating my interest, passion and love for trabecular bone and the unending amount of potential insight it may offer. Apart from the professional support regarding the dissertation topic, I would more importantly like to take this opportunity to thank you for being my mentors and often my psychologists. Thank you for allowing me to pace about your offices during moments of anxiety, email you at all hours with questions that popped into my head and for taking the time to encourage me to explore beyond the boundaries of my comfort zones as I presented not only my research but myself as a young researcher to the scientific community. Thank you for reminding me of my potential.

I would like to thank Dr. Job Kibii of the National Museums of Kenya for providing me with the initial funding to begin this project. Although you are far away physically, you have always been in my corner, cheering me on. Thank you for the guidance in my honours year, for introducing me to trabecular bone and for encouraging me to pursue my studies. Thank you for never giving up on me and for providing me with the opportunity to visit Kenya on a workshop that has changed my perspective on integration work across African countries. I look forward to the day I meet with you again, in East Africa over a Tusker and chapatti.

Thank you to Dr. Biren Patel and the rest of the amazing team at Keck School of Medicine USC, for welcoming me with open arms during my visit and for teaching me, and in turn, learning with me regarding my data processing. Thank you to Prof. Tim Ryan for his input on methods involved in generating my results, I look forward to working with you on projects in the near future!

The data collection for this project would not have been possible without Dr. Anne Su (Ohio State University), Dr. Tea Jashashvilli (University of Southern California) and Prof. Kristian Carlson (University of Southern California). Thank you all for willingly providing me with the comparative scanning material in your possession. I look forward to much collaboration on our findings.

Thank you to my funding bodies, the National Research Foundation and the African Origins Platform (AOP), The Palaeontological Society Trust (PAST) and The Centre of Excellence in Palaeosciences (CoE Pal) for the funding required to complete this project and the additional support for conferences. Thank you to the director of the Evolutionary Studies Institute, Prof Marion Bamford for hosting me for the duration of my degree.

To my friends and colleagues at the Evolutionary Studies Institute, Safiyyah Iqbal, Silindokuhle Mavuso, Kimi Chapelle, Cebisa Mdakazi, Meriska Singh and my extended academic family at UCT and Grahamstown. Thank you for making the journey a memorable one and for offering support during difficult times.

A special thank you to Mr. Marco Fonto and the wonderful staff of Stratum Benefits for believing in me and for providing financial aid throughout my postgraduate studies. Thank you for reminding me that it takes a village, sometimes not to raise a child but to raise a scientist. Your contribution towards my education, without question, has served as my greatest motivation to always give back with the gifts I have been afforded. Your kindness and generosity will always be remembered.

To my family, the road has not been easy and the sacrifices you have made have not gone unnoticed. Thank you for the unending well of support, this is as much my celebration as it is all of ours. I could not have asked for a better foundation. Thank you Mommy, Daddy and Sissy. I would not be here today if not for you all. Thank you to my extended family, as well as the Rigney troops for always supporting me with such enthusiasm!

Finally, to my partner Ramon Rigney, thank you for sometimes losing a bit of your sanity in efforts to help me hold onto some of mine. I look forward to all of the adventures we are still to have. Your encouragement, support and abundance of wine have gotten me through the toughest hurdles. Thank you for inspiring me, motivating me and growing with me on this journey.

ABSTRACT

Trabecular fabric in the distal tibia has been shown to be sensitive to subtle variation in ankle sagittal plane kinematics during locomotor-related loading in both mammals (Barak *et al* 2011) and birds (Pontzer *et al* 2006). Differences or similarities within hominoid trabecular structure can be insightful for interpreting gait kinematic experimentation in the hominin lineage leading to the evolution of obligate bipedalism. This study assessed trabecular structure in the distal tibia of extant hominoids, and an outgroup of baboons, to infer locomotor kinematics of the ankle joint in fossil hominin species. Four hypotheses were tested through analyses of trabecular properties in the distal tibia:

1. Trabecular architecture deep to the tibial plafond of primates is effective at distinguishing species characterized by divergent locomotor behaviours.
2. Trabecular structure deep to the tibial plafond in primates mirrors known kinematics of extant species and will therefore reflect loading conditions imposed by posture and locomotion.
3. Trabecular structure in the distal tibiae of *Australopithecus africanus* specimens from Sterkfontein Member 4 is more human-like than ape-like in structure, reflective of bipedality.
4. Trabecular structure of the medial malleolus in the primate ankle contains a locomotor signal.

High resolution computed tomography (MicroCT) images (25 μ m -48 μ m voxels) were used to quantify trabecular bone structure deep to the tibial plafond and the medial malleolus in extant comparative species attributed to modern human hunter-gatherers (*Homo sapiens*), *Pan troglodytes*, *Gorilla gorilla*, *Pongo pygmaeus* and *Papio hamadryas* as well as four fossil hominins from Sterkfontein Cave (Member 4), South Africa attributed to *A. africanus*. Nine trabecular subregions were isolated beneath the articular surface of the tibial plafond and two subregions were isolated beneath the articular surface of the medial malleolus. Subregions were segmented into spherical trabecular volumes for quantification of localized structure. Descriptive statistics were used to visualize variation among and within species, followed by an analysis of variance (ANOVA) of trabecular parameters between species to test for statistical significance of observed group differences ($p=0.05$). A further stepwise discriminant function analysis (DFA) was conducted to assess the capability of trabecular

structure to discriminate between species with divergent locomotor behaviours based on trabecular structural properties.

The results of this study suggest that trabecular bone structure in the distal tibia of the primate species sampled is effective at distinguishing between species that are characterized by different locomotor behaviour repertoires. Differentiation in homologous regions is greater in presumed highly loaded regions (anterior) and less in regions of presumed low locomotor imposed loading. Trabecular structure in the distal tibia of extant comparative species sometimes matched predictions based on known kinematic data, indicating that these trabecular signals are functionally driven by posture and locomotion. Trabecular fabrics of the medial malleolus in extant non-human primates exhibited structural properties that reflected increased bone strength in their anterior region, suggesting a difference in loading exists across the anteroposterior axis of the medial malleolus (e.g., possibly differentiating relative amounts of climbing), although this difference could not be statistically tested due to small sample sizes.

Trabecular structure of *A. africanus* distal tibiae was highly variable, with some properties exhibiting greater variation than observed in any single extant species. The extent of this intraspecific variability in trabecular structure suggests the presence of two potentially different morphs in Sterkfontein Member 4. One morph resembled a baboon-like structure, composed of numerous thin trabecular struts that were highly oriented (i.e., anisotropically distributed), while the other morph resembled overlapping human-like and ape-like traits observed in previous studies of trabecular architecture in *A. africanus*. Based on the findings of this study, it can be concluded that trabecular structure in the distal tibia is effective at distinguishing species based on locomotor behaviour repertoires, provided that homologous regions are sampled, and that trabecular bone structure and organization mirrors kinematic indicators of ankle loading regimes. When these criteria are met, trabecular fabrics may be a useful tool for reconstructing behaviour in fossil hominin specimens in order to corroborate external morphological studies.

TABLE OF CONTENTS

Declaration	i
Dedication	ii
Acknowledgments	iii
Abstract	v
Table of contents	vii
List of tables and figures	x
List of abbreviations	xiv

CHAPTER 1: INTRODUCTION

1.1. Hypotheses for the current study	2
1.2. Predictions for interspecific and intraspecific trabecular structure in the primate tibial plafond	3
1.3. Predictions for interspecific and intraspecific trabecular structure in the primate medial malleolus	5
1.4. Predictions for trabecular structure in the distal tibia of <i>Australopithecus africanus</i> .	6
1.5. Significance of study	7

CHAPTER 2: LITERATURE REVIEW

2.1. Experimental evidence for bone functional adaptation	8
2.2. A review of trabecular structure and bone functional adaptation	10
2.3. Kinematics of extant non-human primates	13
2.4. Trabecular bone functional adaptation in extant non-human primates	15
2.5. Human gait kinematics	16
2.6. Trabecular bone functional adaptation in modern humans	17
2.7. The role of the ankle in human gait	18
2.8. Trabecular bone functional adaptation in the hindfoot of fossil hominins	22

CHAPTER 3: MATERIALS AND METHODS

3.1. Materials	28
3.1.1. Comparative sample	28
3.1.2. Fossil sample	31
3.2. Methods	33
3.2.1. Data collection	33
3.2.2. Image segmentation	35
3.2.3. Division into volumes of interest (VOIs)	36
3.2.4. Thresholding and quantification of trabecular parameters	37
3.3. Statistical analyses	37

CHAPTER 4: RESULTS

4.1. Interspecific comparison of trabecular structure in the distal tibia of humans, extant non-human primates and australopiths from South Africa	40
4.1.1. Structural patterns in BV/TV, Tb.Th, Tb.Sp and Conn.D across extant species	40
4.1.2. Structural patterns in DA, SMI and BS/BV across extant species.	42
4.2. Trabecular properties of <i>A. africanus</i> specimens in comparison to extant species sampled	42
4.2.1. Structural patterns in BV/TV, Tb.Th, Tb.Sp and Conn.D in <i>A. africanus</i>	42
4.2.2. Structural patterns in DA, SMI and BS/BV in <i>A. africanus</i>	44
4.3. Intraspecific variation in trabecular properties of the distal tibia in humans and extant non-human primates	56
4.3.1. Trabecular analyses of distal tibia in <i>H. sapiens</i> (modern human hunter-gatherers)	56
4.3.1.1. BV/TV, Tb.Th, Tb.Sp, and Conn.D structural patterns in <i>H. sapiens</i> (modern hunter-gatherers)	56
4.3.1.2. DA, SMI and BS/BV structural patterns in <i>H. sapiens</i> (modern hunter-gatherers)	57
4.3.2. Trabecular analyses of distal tibia in <i>P. troglodytes</i> (common chimpanzee)	58
4.3.2.1. BV/TV, Tb.Th, Tb.Sp, and Conn.D structural patterns in <i>P. troglodytes</i> (common chimpanzee)	58
4.3.2.2. DA, SMI and BS/BV structural patterns in <i>P. troglodytes</i> (common chimpanzee)	59
4.3.3. Trabecular analyses of distal tibia in <i>G. gorilla</i> (western lowland gorilla).	60
4.3.3.1. BV/TV, Tb.Th, Tb.Sp, and Conn.D structural patterns in <i>G. gorilla</i> (western lowland gorilla)	60
4.3.3.2. DA, SMI and BS/BV structural patterns in <i>G. gorilla</i> (western lowland gorilla)	61
4.3.4. Trabecular analyses of distal tibia in <i>P. pygmaeus</i> (Bornean orangutan)	62
4.3.4.1. BV/TV, Tb.Th, Tb.Sp, and Conn.D structural patterns in <i>P. pygmaeus</i> (Bornean orangutan)	62
4.3.4.2. DA, SMI and BS/BV structural patterns in <i>P. pygmaeus</i> (Bornean orangutan)	62
4.3.5. Trabecular analyses of distal tibia in <i>P. hamadryas</i> (Hamadryas baboon)	63
4.3.5.1. BV/TV, Tb.Th, Tb.Sp, and Conn.D structural patterns in <i>P. hamadryas</i> (Hamadryas baboon)	63
4.3.5.2. DA, SMI and BS/BV structural patterns in <i>P. hamadryas</i> (Hamadryas baboon)	65
4.4. Interspecific comparison of trabecular structure in the medial malleolus of humans, extant non-human primates and australopiths from South Africa	76
4.4.1. Structural patterns in BV/TV, Tb.Th, Tb.Sp and Conn.D in extant species.	76
4.4.2. Structural patterns in DA, SMI and BS/BV in extant species	77
4.5. Trabecular properties of <i>A. africanus</i> medial malleolus in comparison to extant species sampled	77

4.5.1. Structural patterns in BV/TV, Tb.Th, Tb.Sp and Conn.D in medial malleolus of <i>A. africanus</i>	77
4.5.2. Structural patterns in DA, SMI and BS/BV in medial malleolus of <i>A. africanus</i>	78
4.6. Intraspecific variation in trabecular properties of the medial malleolus in humans and extant non-human primates	84
4.6.1. Trabecular analyses of medial malleolus in <i>H. sapiens</i> (modern human hunter-gatherers)	84
4.6.2. Trabecular analyses of medial malleolus in <i>P. troglodytes</i> (chimpanzee)	84
4.6.3 Trabecular analyses of medial malleolus in <i>G. gorilla</i> (western lowland gorilla)	85
4.6.4. Trabecular analyses of the medial malleolus in <i>P. pygmaeus</i> (Bornean orangutan)	85
4.6.5. Trabecular analysis medial malleolus in <i>P. hamadryas</i> (Hamadryas baboon)	86
4.7. Discriminant Function Analysis of distal tibia in extant species	98
CHAPTER 5: DISCUSSION AND CONCLUSION	
5.1 Trabecular architecture in the primate distal tibia differs between species	102
5.2 Trabecular architecture in non-human primates is reflective of known kinematics	104
5.2.1. Trabecular structure in extant non-human hominoids	104
5.2.2. Trabecular structure in the distal tibia of digitigrade quadrupedal <i>Papio</i>	107
5.3. Trabecular architecture in modern human hunter-gatherers is highly variable and isotropic	109
5.4. Trabecular structure in the distal tibia of <i>A. africanus</i> indicates the possibility of two potentially different morphs in Sterkfontein Member 4	112
5.4.1. A potentially second morph in Sterkfontein.	113
5.5. Unique trabecular structure of StW 358 from Sterkfontein Member 4	114
5.6. Trabecular structure of StW 567, presumed <i>Homo sp.</i> from Sterkfontein Member 5	114
5.7. The distal tibia of StW 515 and links to the proximal StW514	115
5.8. Trabecular structure and the probability of climbing in <i>A. africanus</i> from Sterkfontein Member 4	116
5.9. Limitations of this study and future work	117
5.10. Conclusion	119
CHAPTER 6: REFERENCES	123
CHAPTER 7: APPENDICES	139
Table A1: Tukey-HSD for interspecific pairwise comparisons in distal tibia of extant primates (p=0.05)	139
Table A2: Tukey-HSD for intraspecific pairwise comparisons in distal tibia of extant primates (p=0.05)	142
Table A3: Pearson's Correlation by VOI for trabecular parameters examined in distal tibia.	146
Table A4: Trabecular properties of fossil hominins from Sterkfontein Member 4 in relation to comparative extant species	148

LIST OF TABLES AND FIGURES

Table 1.1 Interspecific predictions for trabecular parameters for distal tibia and medial malleolus of extant non-human primates species used in this dissertation.

Table 3.1: Comparative primate species used in this study.

Table 3.2: Relative body weight according to sex in extant primate species sampled.

Table 3.3: Trabecular parameters quantified in the present study.

Table 4.1: Bone volume fraction (BV/TV) mean and standard deviation of structural variables by region, along with results of analysis of variance ($p=0,05$).

Table 4.2: Trabecular thickness (Tb.Th) mean and standard deviation of structural variables by region, along with results of analysis of variance ($p=0,05$).

Table 4.3: Trabecular spacing (Tb.Sp) mean and standard deviation of structural variables by region, along with results of analysis of variance ($p=0,05$).

Table 4.4: Connectivity Density (Conn.D) mean and standard deviation of structural variables by region, along with results of analysis of variance ($p=0,05$).

Table 4.5: Degree of anisotropy (DA) mean and standard deviation of structural variables by region, along with results of analysis of variance ($p=0,05$).

Table 4.6: Structural Model Index (SMI) mean and standard deviation of structural variables by region, along with results of analysis of variance ($p=0,05$).

Table 4.7: Bone surface to bone volume ratio (BS/BV) mean and standard deviation of structural variables by region, along with results of analysis of variance ($p=0,05$).

Table 4.8. Summary of analysis of variance for trabecular parameters in the distal tibia of modern *H. sapiens*

Table 4.9. Summary of analysis of variance for trabecular parameters in the distal tibia of *P. troglodytes*.

Table 4.10. Summary of analysis of variance for trabecular parameters in the distal tibia of *G. gorilla*.

Table 4.11. Summary of analysis of variance for trabecular parameters in the distal tibia of *P. pygmaeus*.

Table 4.12. Summary of analysis of variance for trabecular parameters in the distal tibia of *P. hamadryas*.

Table 4.13. Summary statistics (mean and standard deviation) of trabecular parameters in the medial malleolus of extant hominoids and *A. africanus*.

Table 4.14. Predicted group membership summary for discriminant function analyses.

Table 4.15. Summary of discriminant function analysis of the distal tibia.

Figure 1.1. Transverse slice through the distal tibia in A) *Homo*, B) *Pan*, C) *Gorilla*, D) *Pongo* and E) *Papio*.

Figure 1.2. Transverse slice through the medial malleolus. The two volumes of interest (VOIs) sampled within the medial malleolus are situated anteriorly and posteriorly (red circles).

Figure 2.1. The macro-structure of trabecular bone. From Mathieu *et al* (2006).

Figure 2.2. After Dawe & Davis (2011). Image depicting the three subphases of stance phase, A) first rocker (heel rocker), B) second rocker (ankle rocker), C) third rocker (forefoot rocker).

Figure 2.3. Osteological components of the tibiotalar. A) distal tibia, B) fibula, C) talus adapted from Gray's Anatomy (2009).

Figure 2.4. Morphology of the distal tibia. A) Inferior aspect, tibial plafond (articulating surface with talus); B) Superior aspect; C) Anterior aspect; D) Posterior aspect; E) Medial aspect of distal tibia, showing medial malleolus projection; F) Lateral aspect.

Figure 2.5. From Brockett & Chapman (2016). Figure adapted from Visual 3D (C-Motion, Rockville, Maryland). Diagram illustrating relative osteokinematic movements of the ankle joint complex.

Figure 2.6. Volume of interest (VOI) locations (white circles), A) *P. ursinus*, B) *P. troglodytes*, C) StW 352, D) *G. gorilla*, and E) *H. sapiens* calcanei examined in Zeininger *et al* 2016.

Figure 2.7. Adjusted from Su & Carlson (2017). The nine volumes of interest sampled in the study in relationship to the articular surface of the trochlea.

Figure 2.8. Representation of location of the lateral and medial VOIs in the distal tibia examined in Barak *et al* (2013).

Figure 3.1. 3D reconstruction representative distal tibiae plafond of extant comparative species used in this study.

Figure 3.2. 3D reconstruction of fossil tibiae used in this study showing the tibial plafond.

Figure 3.3. Hominin fossil distal tibiae from Sterkfontein Member 4 attributed to *A. africanus* examined in this study.

Figure 3.4. Standardized anatomical positions for distal tibia in VG Studio MAX 3.0.

Figure 3.5. Orientation of tibial plafond and division into nine volumes of interest.

Figure 3.6. Orientation of medial malleolus and division into nine volumes of interest.

Figure 3.7. Visual representation of a spherical trabecular volume as analysed in this study.

Figure 4.1. Boxplots indicating bone volume fraction (BV/TV) by subregion across groups.

Fig 4.2. Boxplots indicating trabecular thickness (Tb.Th) by subregion across groups.

Fig 4.3. Boxplots indicating trabecular spacing (Tb.Sp) by subregion across groups.

Fig 4.4. Boxplots indicating connectivity density (Conn.D) by subregion across groups.

Fig 4.5. Boxplots indicating degree of anisotropy (DA) by subregion across groups.

Fig 4.6. Boxplots indicating structural model index (SMI) by subregion across groups.

Fig 4.7. Boxplots indicating bone surface to bone volume ratio (BS/BV) by subregion across groups.

Figure 4.8. Boxplots indicating A) bone volume fraction (BV/TV), B) trabecular thickness (Tb.Th), C) trabecular spacing (Tb.Sp) and D) connectivity density (Conn.D) by subregion in *H. sapiens*.

Figure 4.9. Boxplots indicating A) degree of anisotropy (DA), B) structural model index (SMI) and C) bone surface to bone volume ratio (BS/BV) by subregion in *H. sapiens*.

Figure 4.10. Boxplots indicating A) bone volume fraction (BV/TV), B) trabecular thickness (Tb.Th), C) trabecular spacing (Tb.Sp) and D) connectivity density (Conn.D) by subregion in *P. troglodytes*.

Figure 4.11. Boxplots indicating A) degree of anisotropy (DA), B) structural model index (SMI) and C) bone surface to bone volume ratio (BS/BV) by subregion in *P. troglodytes*.

Figure 4.12. Boxplots indicating A) bone volume fraction (BV/TV), B) trabecular thickness (Tb.Th), C) trabecular spacing (Tb.Sp) and D) connectivity density (Conn.D) by subregion in *G. gorilla*.

Figure 4.13. Boxplots indicating A) degree of anisotropy (DA), B) structural model index (SMI), and C) bone surface to bone volume ratio (BS/BV) by subregion in *G. gorilla*.

Figure 4.14. Boxplots indicating A) bone volume fraction (BV/TV), B) trabecular thickness (Tb.Th), C) trabecular spacing (Tb.Sp) and D) connectivity density (Conn.D) by subregion in *P. pygmaeus*.

Figure 4.15. Boxplots indicating A) degree of anisotropy (DA), B) structural model index (SMI) and C) bone surface to bone volume ratio (BS/BV) by subregion in *P. pygmaeus*.

Figure 4.16. Boxplots indicating A) bone volume fraction (BV/TV), B) trabecular thickness (Tb.Th), C) trabecular spacing (Tb.Sp) and D) connectivity density (Conn.D) by subregion in *P. hamadryas*.

Figure 4.17. Boxplots indicating A) degree of anisotropy (DA), B) structural model index (SMI) and C) bone surface to bone volume ratio (BS/BV) by subregion in *P. hamadryas*.

Fig 4.18. Boxplots indicating bone volume fraction (BV/TV) in the medial malleolus by subregion across extant groups.

Fig 4.19. Boxplots indicating mean trabecular thickness (Tb.Th) in the medial malleolus by subregion across extant groups.

Fig 4.20. Boxplots indicating trabecular spacing (Tb.Sp) in the medial malleolus by subregion across extant groups.

Fig 4.21. Boxplots indicating connectivity density (Conn.D) in the medial malleolus by subregion across extant groups.

Fig 4.22. Boxplots indicating degree of anisotropy (DA) in the medial malleolus by subregion across extant groups.

Fig 4.23. Boxplots indicating structural model index (SMI) in the medial malleolus by subregion across extant groups.

Fig 4.24. Boxplots indicating bone surface to bone volume ratio (BS/BV) in the medial malleolus by subregion across extant groups.

Figure 4.25. Boxplots indicating A) bone volume fraction (BV/TV), B) trabecular thickness (Tb.Th), C) trabecular spacing (Tb.Sp) and D) connectivity density (Conn.D) by subregion in the medial malleolus of *H. sapiens*.

Figure 4.26. Boxplots indicating A) degree of anisotropy (DA), B) structural model index (SMI) and C) bone surface to bone volume ratio (BS/BV) by subregion in the medial malleolus of *H. sapiens*.

Figure 4.27. Boxplots indicating A) bone volume fraction (BV/TV), B) trabecular thickness (Tb.Th), C) trabecular spacing (Tb.Sp) and D) connectivity density (Conn.D) by subregion in the medial malleolus of *P. troglodytes*.

Figure 4.28. Boxplots indicating A) degree of anisotropy (DA), B) structural model index (SMI) and C) bone surface to bone volume ratio (BS/BV) by subregion in the medial malleolus of *P. troglodytes*.

Figure 4.29. Boxplots indicating A) bone volume fraction (BV/TV), B) trabecular thickness (Tb.Th), C) trabecular spacing (Tb.Sp) and D) connectivity density (Conn.D) by subregion in the medial malleolus of *G. gorilla*.

Figure 4.30. Boxplots indicating A) degree of anisotropy (DA), B) structural model index (SMI) and C) bone surface to bone volume ratio (BS/BV) by subregion in the medial malleolus of *G. gorilla*.

Figure 4.31. Boxplots indicating A) bone volume fraction (BV/TV), B) trabecular thickness (Tb.Th), C) trabecular spacing (Tb.Sp) and D) connectivity density (Conn.D) by subregion in the medial malleolus of *P. pygmaeus*.

Figure 4.32. Boxplots indicating A) degree of anisotropy (DA) B) structural model index (SMI) and C) bone surface to bone volume ratio (BS/BV) by subregion in the medial malleolus of *P. pygmaeus*.

Figure 4.33. Boxplots indicating A) bone volume fraction (BV/TV), B) trabecular thickness (Tb.Th), C) trabecular spacing (Tb.Sp) and D) connectivity density (Conn.D) by subregion in the medial malleolus of *P. hamadryas*.

Figure 4.34. Boxplots indicating A) degree of anisotropy (DA), B) structural model index (SMI) and C) bone surface to bone volume ratio (BS/BV) by subregion in the medial malleolus of *P. hamadryas*.

Figure 4.35. Plots of Discriminant Function 1 versus Discriminant Function 2 of individuals in groups summarizing scalar values by subregions in the distal tibia.

LIST OF ABBREVIATIONS

Institutional abbreviations

ESI: Evolutionary Studies Institute, University of Witwatersrand, Johannesburg.

CMNH: Cleveland Museum of Natural History, Cleveland.

AMNH: American Museum of Natural History, New York.

NMNH: Smithsonian National Museum of Natural History, Washington D.C.

VIP Lab: Virtual Imaging Processing Lab, University of the Witwatersrand, Johannesburg

List of programs

VG Studio MAX 3.0 (Volume Graphics, Heidelberg, Germany)

AVIZO LITE 9.0.0 (FEI Visualization Sciences Group, France)

JMP (Version 13, SAS Institute Inc, Cary, NC, 1989-2007)

ImageJ with BoneJ plugin (ImageJ 1.50i, Java 1.6.0_20, <https://imagej.nih.gov/ij/>).

Trabecular structural abbreviations

BV/TV: Bone volume fraction

Tb.Th: Trabecular thickness

Tb.Sp: Trabecular separation

Conn.D: Connectivity density

DA: Degree of anisotropy

SMI: Structural Model Index

BS/BV: Bone surface to bone volume ratio

Anatomical abbreviations

CCJ: Calcaneocuboid joint

TCJ: Talcocrural joint

A-M: Anteromedial

A-C: Anterocentral

A-L: Anterolateral

C-M: Centromedial

C-C: Centrocentral

C-L: Centrolateral

P-M: Posteromedial

P-C: Posterocentral

P-L: Posterolateral

BHBK: Bent hip bent knee

EHEK: Extended hip extended knee

DP: Dorsiflexion/Plantarflexion

PS: Pronation/Supination

IE: Internal/External rotations

PTTL: posterotibiotalar ligament

Technical and statistical abbreviations

GRF: Ground reaction force

ROM: Range of motion

FE: Finite element

PTO: Principal trabecular orientation

RDA: Random transform analysis

MicroCT (μ CT): Micro-computed tomography

keV: electron kilovolts

μ m: micrometer

kV: kilovolt

μ A: microamp

ROI: Region of interest

VOI: Volume of interest

ANOVA: Analysis of variance

DFA: Discriminant function analysis

Equations

Eq1: $V = \frac{3}{4}\pi r^3$

CHAPTER 1: INTRODUCTION

Reconstructing past behaviour in fossil primates has important implications for understanding evolutionary history, environment, diet and phylogenetic relationships of past and present species (Fleagle 2013). The most commonly used source of information in studies of past behaviour is the examination of external morphology of fossil remains (Lovejoy & Heiple 1973, Stern & Susman 1991, Berger & Tobias 1996, Asfaw *et al* 1999, White *et al* 2009, Berger *et al* 2010, Kivell 2011a,b DeSilva *et al* 2013). The external morphology of hominoid bones has been well-studied in an effort to further understand the unique morphologies of critical fossil specimens (Latimer *et al* 1987, DeSilva 2009a, b, Fleagle 2013, Prang 2015). Although external morphology provides functional information, it encompasses features that are influenced by both genetic and non-genetic factors, and therefore make it challenging to determine which aspects are functionally driven for reconstructing fine details of behaviour, especially in fossil hominins (Lieberman 1997, Su 2011).

The shape and size of articular facets have been found to strongly correlate with joint mobility, as investigated by various authors (e.g., Ruff 1988, Ruff & Runstead 1992, Ruff *et al* 1994, Currey 2002). However, even the articular facets of bone are constrained by the need for congruence with articulating bones and the interdependence of all of the components of a particular joint that allow it to function effectively (Ruff & Runstead 1992, Lieberman *et al* 2001, Currey 2002). In order to reconstruct locomotion using only skeletal elements, it is important to understand which aspects of bony morphology are more sensitive to loading (i.e. stress) during life. Internal bone structure, rather than external bone shape and size, is considered a better reflection of how a bone was used during the life of an individual (Ruff & Runstead 1992, Lieberman 1997). This is arguably true for documenting how joints are loaded during habitual activities (Su 2011, Su *et al* 2013, Zeininger *et al* 2016, Ryan & Shaw 2012, Su & Carlson 2017). The concept of a bone functional adaptation can help move beyond the challenges that come with analyses of fragmentary fossil morphology and the longstanding palaeanthropological debates founded on differing functional interpretations of external morphology (Ruff *et al* 2006).

The advancement of technology such as microcomputed tomography (MicroCT) and its non-invasive abilities has allowed scientists to expand existing lines of evidence on which locomotor reconstructions can be based to include internal bone structure of rare hominin fossils. This is particularly useful to improving the current understanding of hominin

evolution when studying key transitional species. MicroCT has the capability to produce high resolution images with voxel sizes small enough to visualize typical trabecular struts, which has been a challenge faced by medical CT scan technology in the past.

The concept of bone functional adaptation (see Chapter 2) has been supported by empirical evidence using experimental manipulation of applied loads on animal models (Biewener *et al* 1996, Pontzer *et al* 2006, Barak *et al* 2011). Early studies on trabecular bone functional adaptation in primates focussed on the proximal femur, primarily testing the hypothesis that differences in habitual locomotor behaviours, presumably resulting in different hip kinematics, are reflected in differences in femoral head trabecular structure (Fajardo & Müller 2001, MacLatchy & Müller 2002, Ryan & Ketcham 2002a,b, 2005, Ryan & Van Rietbergen 2005, Ryan & Kovitz 2006, Ryan & Walker 2010, Ryan & Shaw 2013). A challenge faced in the analysis of comparative trabecular structure, as a means of reconstructing locomotion, is identifying homologous regions in species that exhibit a wide range of variation in external morphological features.

In order to use trabecular structure to infer locomotor abilities in extinct fossil hominins, it is important to determine whether or not it is effective at distinguishing locomotor behaviour between species. This study aimed to quantify and analyse trabecular structure in extant humans, hominoids and an outgroup of baboons in order to determine if functional signals were present in the ankle. The distal tibia was chosen due to its response to changes in posture and locomotion (see Chapter 2) and it is a robust bone that has preserved in multiple species in the hominin fossil record.

1.1. Hypotheses for the current study.

Four main hypotheses were tested in this dissertation based on the trabecular structure in the primate ankle:

- Trabecular architecture deep to the tibial plafond of primates is effective at distinguishing species characterized by divergent locomotor behaviours.
- Trabecular structure deep to the tibial plafond in primates mirrors known kinematics of extant species and will therefore reflect loading conditions imposed by posture and locomotion.
- Internal structure of the medial malleolus differs among primate species reflecting presumed responses to differing kinematic behaviour

- Trabecular structure in the distal tibiae of fossil hominins from Sterkfontein Member 4 is more reflective of human-like (biped) than ape-like (quadruped) habitual locomotion.

1.2. Predictions for interspecific and intraspecific trabecular structure in the primate tibial plafond.

The first goal of this study was to test the hypothesis that trabecular structure in the distal tibial plafond differs between taxa based on differences in locomotor loading. Initial predictions of structural differences were made based on previous studies of external morphology, trabecular bone architecture, kinematics and joint loading in extant primate species (See Chapter 2) (Table 1.1.).

Table 1.1 Interspecific predictions for trabecular parameters for distal tibia and medial malleolus of extant non-human primates species used in this dissertation.

Property*	Prediction (Distal tibia)	Prediction (Medial malleolus)
BV/TV	<i>Gorilla>Pan>Pongo>Papio>Homo</i>	<i>Gorilla>Pan>Pongo>Papio>Homo</i>
Tb.Th	<i>Gorilla>Homo>Papio>Pan>Pongo</i>	<i>Papio >Homo>Gorilla>Pan>Pongo</i>
Tb.Sp	<i>Homo>Papio>Pongo>Pan>Gorilla</i>	<i>Homo>Papio >Gorilla>Pan >Pongo</i>
Conn.D	<i>Papio> Pongo> Pan> Homo>Gorilla</i>	<i>Homo>Papio >Gorilla>Pan >Pongo</i>
DA	<i>Homo>Papio>Gorilla>Pan>Pongo</i>	<i>Homo>Papio >Gorilla>Pan >Pongo</i>
SMI	<i>Homo>Papio>Gorilla>Pan>Pongo</i>	<i>Homo>Papio >Gorilla>Pan >Pongo</i>
BS/BV	<i>Homo>Papio>Gorilla>Pan>Pongo</i>	<i>Homo>Papio>Gorilla>Pan>Pongo</i>

*BV/TV=bone volume fraction, Tb.Th= trabecular thickness, Tb.Sp= trabecular separation, Conn.D= connectivity density, DA=degree of anisotropy, SMI= structural model index, BS/BV= bone surface to bone volume ratio.

The second goal of this dissertation was to evaluate whether or not internal structure of the primate distal tibia evidences a locomotor signal that mirrors known ankle kinematics in extant species (see Chapter 2).

Bipedal walking is taken as the habitual form of locomotion in *H. sapiens*, the only extant species that demonstrates obligate bipedality. The gait cycle of *H. sapiens* is presumed to be more loaded during stance phase where a characteristic mediolateral weight shift on a support limb is observed during the last portion of stance phase immediately prior to toe off. This pattern of presumed loading was used to generate predictions of internal structural patterns (i.e. increased local strength mirroring the timing of a weight-shift during stance). A mediolateral weight shift has been proposed to determine talar trochlear trabecular structure (Su & Carlson 2017). Whether the opposing articular surface on the distal tibia undergoes the

same loading pattern, resulting in similar trabecular structural patterns in the talar trochlea and the distal tibia as with the talus, remains to be assessed. In order to examine this possibility, nine subregions deep to the plafond surface of the distal tibia were subjected to trabecular quantification. It is expected that in *H. sapiens*, the anteromedial, centrolateral and posteromedial regions will demonstrate increased bone strength relative to other VOIs, if such a pattern exists (Fig 1.1A).

Kinematic-based predictions for all non-human primates were derived similarly (Fig 1.1B-E). Based on observations of extreme dorsiflexion in the ankle when climbing (DeSilva 2009), as well as the suggested widened anterior rim of the plafond, it is predicted that the anterior and lateral regions of the primate ankle joint will demonstrate stronger trabecular structure in order to support increased loading during climbing bouts. Specific kinematics of extant species are further discussed in Chapter 2.

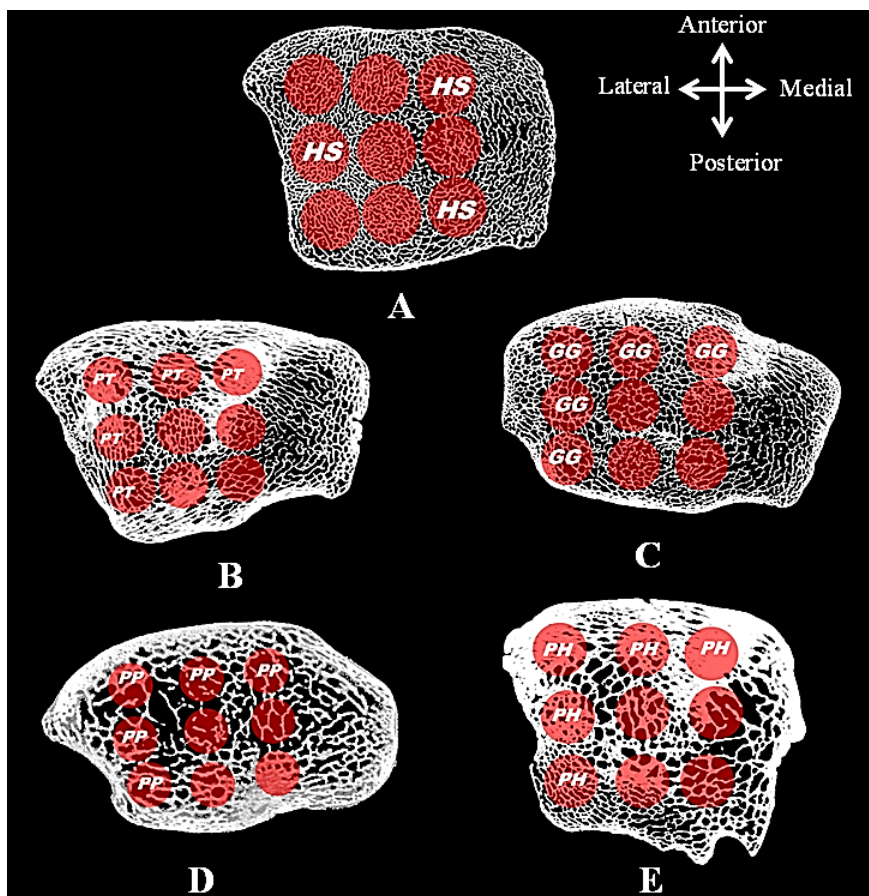


Figure 1.1. Transverse slice through the distal tibia in A) *Homo*, B) *Pan*, C) *Gorilla*, D) *Pongo* and E) *Papio*. The nine volumes of interest sampled in the present study (red circles) in relation to the articular surface of the distal tibial plafond. Areas of high loading in each species are marked respectively: *Homo* (HS), *Pan* (PT), *Gorilla* (GG), *Pongo* (PP) and *Papio* (PH).

1.3. Predictions for interspecific and intraspecific trabecular structure in the primate medial malleolus.

The third goal of this study was to provide the initial quantification of trabecular structure in the hominoid medial malleolus. The medial malleolus acts as a supporting structure in order to mediolaterally stabilise the ankle during locomotion (see Chapter 2). Trabecular structure in the medial malleolus of primate species (i.e. interspecific variation) is expected to resemble predictions in the tibial plafond, as non-human primates are expected to demonstrate generally stronger trabecular structure (i.e. higher BV/TV, Tb.Th, lower Tb.Sp and Conn.D) than modern humans (Table 1.1.).

External morphology of the medial malleolus in non-human primates, particularly hominoids, indicates a relatively stronger anterior region (i.e. more robust morphology as reinforcement) than posterior region. Since non-human primates use an inverted ankle when climbing (DeSilva 2009a,b DeSilva *et al* 2013), their joint position coincides with a body weight shift, albeit a less dramatic one than humans exhibit, that causes the reaction resultant force to travel through the medial malleolus. Landing on an inverted foot during the beginning of stance phase would increasingly load the lateral portion of the tibiotalar joint, which would change the force directed through the medial malleolus, resulting in a shear force (DeSilva *et al* 2013). Therefore, extant non-human primates sampled in this study are hypothesised to exhibit greater disparity between the anterior presumably highly-loaded subregion of the medial malleolus and the posterior presumably less-loaded subregion (DeSilva 2009, DeSilva *et al* 2013). The more gracile medial malleolus of *H. sapiens*, on the other hand, is expected to demonstrate similar levels of strength in anterior and posterior regions, in order to stabilise the less habitually dorsiflexed ankle during walking and running.

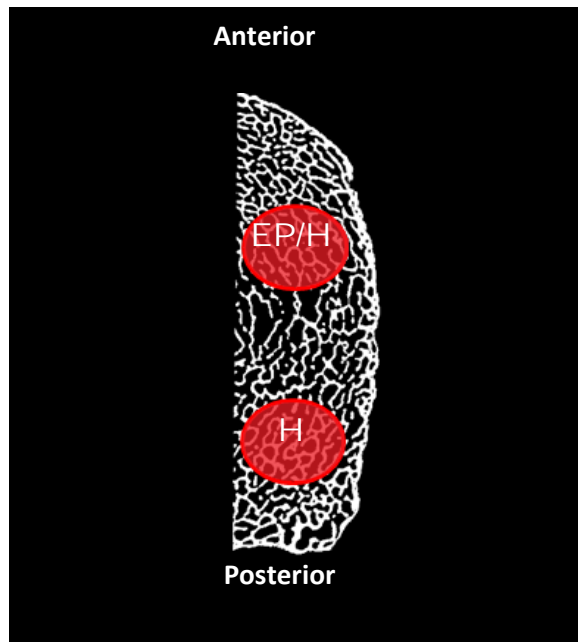


Fig 1.2. Transverse slice through the medial malleolus. The two volumes of interest (VOIs) sampled within the medial malleolus are situated anteriorly and posteriorly. It is predicted that extant non-human primates (EP) will show relatively greater structural bone strength in the anterior VOI as opposed to the posterior VOI whereas *Homo* (H) would demonstrate similar loading in the anterior and posterior volumes.

1.4. Predictions for the trabecular structure in the distal tibia of *Australopithecus africanus*.

The final goal of this study was to infer locomotor behaviour of *Australopithecus africanus* specimens from Sterkfontein Member 4 (South Africa) by analysing trabecular structure in the distal tibia relative to a comparative framework of extant primates that vary in habitual locomotor behaviours. The first goal of this study was to verify the accuracy of trabecular structure in distinguishing species, while the second goal was to compare these structural similarities/differences with ankle locomotor kinematics of extant primates (emphasizing hominoids). Achieving these two goals would strengthen arguments for incorporating trabecular bone in interpretations of fossil hominin locomotor behaviour. Based on previous analyses of trabecular fabrics in *A. africanus*, it is predicted that this hominin may exhibit a unique mosaic of human-like and ape-like trabecular characteristics (Barak *et al* 2013b, Zeininger *et al* 2016, Su & Carlson 2017).

Only a single fossil specimen (StW 358) preserves a full medial malleolus, which externally appears less robust than medial malleoli of extant non-human primates. It was, therefore, predicted that the medial malleolus in *A. africanus* (StW 358) was not exposed to habitual dorsiflexion, nor to the inversion demonstrated by hominoids during climbing. Instead, StW

358 was predicted to reflect trabecular structure similar to the *H. sapiens* condition characterized by relatively similar loading anteriorly and posteriorly.

1.5. Significance of the study.

Studies of trabecular bone functional adaptation have received mixed support in their utility for the reconstruction of locomotor behaviour in fossil hominins. Although trabecular bone is similar to external bone morphology in being a product of both genetic and non-genetic influences, such as hormones or diet (Beamer *et al* 1996, Devlin & Lieberman 2007, Judex & Carlson 2009, Devlin *et al* 2010, Havill *et al* 2010, Barak *et al* 2011, Raichlen *et al* 2015), the high plasticity of trabecular fabrics, and the ability of trabecular bone to respond and adapt to mechanical stimuli, makes it an important source of inferred functional information that can be used to reconstruct past behaviour. In order to integrate trabecular bone in structure-based interpretations of hominin past behaviour, it is important to understand the nature of variation within species that demonstrate divergent locomotor behaviours, as well as the extent to which trabecular bone is effective in distinguishing between forms of divergent locomotion. The ankle joint features centrally in the gait of all primate species, and thus it is a valuable indicator of locomotor ability; it has also proven to be sensitive to subtle variation in posture and loading, making it ideal for studying trabecular structure.

CHAPTER 2: LITERATURE REVIEW

The unique form of locomotion - obligate bipedalism - exhibited by modern *H. sapiens* is important in distinguishing the species, as well as its adaptive niche, from the extant great apes. The ability to walk habitually upright is thus considered one of the defining attributes of the hominin lineage. Bipedality, however, appears to have evolved independently and numerous times in many vertebrate lineages including extinct taxa such as dinosaurs (Thulborn 1984, Thulborn & Gillette 1989, Jones *et al* 2000). Extant vertebrate taxa are a product of this gait experiment resulting in some form of bipedal locomotion among animals as diverse as birds (Abourachid 2000), lizards (Snyders 1952, Snyders 1962) and various mammals, including rodents (Djawdan 1993) and marsupials (Thompson *et al* 1980). Amongst all of these forms, the upright walking and running of modern humans, however, often receives extra attention due to our evolutionary history and the implications bipedalism has for the advanced development of our species (Lovejoy 2005).

2.1. Experimental evidence for bone functional adaptation.

The most convincing evidence of trabecular adaptation in response to loading is in the *in vivo* experimental analyses that directly tests trabecular bone responses to controlled behavioural activities (Lanyon 1974, Biewener *et al* 1996, Pontzer *et al* 2006, Chang *et al* 2008, Polk *et al* 2008, Barak *et al* 2011, Harrison *et al* 2011). These *in vivo* experiments are often conducted on juvenile animals because bone is both actively modelling and remodelling during this time (Pearson & Lieberman 2004). Finite element (FE) analysis has been used as an effective tool in successfully quantifying and validating mechanical properties and functional significance of trabecular bone (Hollister *et al* 1994, Kabel *et al* 1999, Ulrich *et al* 1999, Ryan & van Rietbergen 2005, Nguyen *et al* 2013).

Many of the initial experimental studies focussed on the mammalian calcaneus due to its predictable loading environment. The calcaneus typically does not touch the ground during locomotion of non-primate mammals, but experiences a regular bending load from the Achilles tendon during ankle extension (Lanyon 1973, 1974, Skerry & Lanyon 1995, Biewener *et al* 1996, Skedros *et al* 2004, 2012, Sinclair *et al* 2013). These studies concluded that trabeculae underlying the Achilles tendon were aligned with compressive and tensile principal directions of stress (Lanyon 1974, Biewener *et al* 1996).

Experimental studies conducted to test the response of trabecular bone to different loading regimes are usually conducted within one species in a controlled fashion. More recently, *in vivo* experiments have expanded on this work to test how variation in the direction and magnitude of external loads affect trabecular structure (Pontzer *et al* 2006, Chang *et al* 2008, Harrison *et al* 2011, Barak *et al* 2011). Radin *et al* (1982) compared the effects of changes in loading impulse magnitude, but not loading orientation in the distal femora of sheep that walked on a stiff concrete surface with sheep that walked on a compliant wood chip surface. Their results showed that trabecular fabrics became more longitudinally oriented (anisotropic) in response to the harder concrete surface. Biewener *et al* (1996) measured *in vivo* principle compressive strains and trabecular architecture in the calcaneus of potoroos hopping on a treadmill, as a control group, and potoroos with the Achilles tendon removed, as the experimental group. Their results showed that primary trabecular orientation is aligned according to the measured principle strains in the calcaneus, and that trabecular organization was less organised in the animals with the Achilles tendon removed. This study is limited, however, as removal of a tendon such as the Achilles is not a natural occurrence and could have resulted in a pathological response.

Pontzer *et al* (2006) compared the orientation of spongiosa (very fine trabeculae just below the chondral surface) in the distal femora of Guinea fowl running on a level treadmill (control) and on an inclined treadmill (20°). This study concluded that the experimental birds running on the inclination had a 13.7° more flexed knee joint in midstance when peak forces occur, and that the predominant orientation of spongiosa was 13.6° more acute relative to the long axis of the bone in the inclined runners. A limitation to this project was that the spongiosa respond differently than normal trabecular bone, and that the random transform analysis (RDA) used in the study to quantify trabecular bone was only capable of quantifying trabecular orientation in 2D.

Experimental studies were also significant in demonstrating that the ankle (tibiotalar joint), and more specifically the distal tibia, is ideal to study when examining trabecular patterns as its internal structure has been proven to be very sensitive to subtle variations in ankle angles. The correspondence between trabecular orientation and applied loads was tested rigorously by Barak *et al* (2011) in mammalian trabecular bone by using Dorset sheep (*Ovis aries*). They tested the hypothesis that trabecular bone beneath articular surfaces of the sheep tarsal joint adjusts its orientation in response to a biologically normal shift in peak compressive force trajectory. A control group of sheep, as well as the experimental group of sheep (7°

incline), were run daily at a trot speed on a treadmill for 15 minutes. The inclined plane caused the tarsal joint to extend by 3-4.5°. This change in orientation was designed to expose the joints to loading directions that were different enough to yield statistically detectable effects on trabecular orientation, but not so different as to change joint function. These experimental studies are of particular importance for studies in which trabecular bone structure and orientation are analysed in extinct taxa to predict their locomotor behaviour.

The result of a combination of various experimental studies concluded that bone functional adaptation requires both a minimum magnitude and duration of loading to affect trabecular growth and remodelling (Rubin & Lanyon 1985, Skerry & Lanyon 1995, Biewener *et al* 1996, Barak *et al* 2011), and that it can vary based on the specific skeletal element examined (Carlson *et al* 2008, Wallace *et al* 2014). There are opposing experimental studies that have shown that relatively short periods of external loading can dramatically affect changes in trabecular structure, if the orientation or magnitude is unusual compared with normal daily activities (Simkin *et al* 1989, Smith *et al* 1989, Bassey & Ramsdale 1994). Thus, adaptation can be driven by infrequent loading, but still dynamic behaviours, rather than habitual loading (Burr 1990). Laboratory experiments offer unique insights into trabecular structure as the magnitude and direction of the load transmitted through the joint can be controlled and measured, and therefore used in establishing a clear difference in trabecular architecture due to habitual loading.

2.2. A review of trabecular structure and bone functional adaptation.

The concept of bone adaptation and remodelling in response to an external load is commonly referred to as Wolff's Law (Wolff 1896, Cowin 2001, Pearson & Lieberman 2004, Ruff *et al* 2006). Wolff was not the first to observe the structural properties of trabecular bone, however, as Julius Ward (1838) compared the distinct trabecular patterns of the human femoral neck to that of a support bracket for a street lamp, i.e., the origin of Ward's Triangle. Roux (1881) first recognized that bone cells were capable of responding to local mechanical stresses and that organisms had the ability to adapt their bony structure to new environments. More recently, this concept has been refined and renamed using terms such as the "Mechanostat" (Frost 1987) and the "mechanical adaptability hypothesis" (Martin *et al* 1998), or "bone functional adaptation" (Roux 1881, Cowin *et al* 1985, Lanyon & Rubin 1985, Ruff *et al* 2006).

Wolff's Law is actually a series of observations that imply the following conclusion: bone adapts its external shape and internal structure in response to the mechanical forces it is required to support (Wolff 1896, Huiskes *et al* 2000). This theory was partially based on previous observations by von Meyer (1867), namely that trabecular bone in the proximal femur resembled stress trajectories in overhead cranes. This theory has since been analysed by various authors including Koch (1917), who demonstrated graphically the principal static stresses in the proximal femur and led to the conclusion that trabecular architecture corresponds in a predictable manner to the calculated stress distribution within the bone. Although the mathematics of Wolff's Law has been challenged and many of the original assumptions refuted, or deemed too variable to be considered a "law" (Bertram & Swartz 1991, Pearson & Lieberman 2004, Wallace *et al* 2014, Lieberman *et al* 2004), experimental studies have consistently documented some sort of relationship between trabecular struts and applied loads (Pontzer *et al* 2006, Barak *et al* 2011).

The biomechanical signal that drives the adaptation process is associated with either microdamage in the bone, or strain in the mineralised bone tissue. It is assumed that functional adaptation produces anatomical structures that distribute their material optimally (Pauwels 1980) to in turn optimize load transmission throughout joint motion (Frost 1990, Heegaard *et al* 1999, Conconi *et al* 2015). Trabecular bone has frequently been observed to respond epigenetically in human clinical studies (Pauwels 1980), and is considered to have high environmental plasticity. It is this predictive responsiveness that has led to the hypothesis that orientation and structure of trabeculae within a bone indicate direction and magnitude of habitual loads over the lifespan of an individual, respectively (Ryan & Ketcham 2002a,b, 2005, Fajardo *et al* 2007, Su 2011, Ryan & Shaw 2012, 2013, 2015).

In vivo experimental studies of trabecular remodelling have demonstrated the presence of a basic genetic blueprint of trabecular structure, which can subsequently be changed by variation in load and habitual activities of an individual (Biewener *et al* 1996, Pontzer *et al* 2006, Chang *et al* 2008, Cunningham & Black 2009, Barak *et al* 2011, Harrison *et al* 2011). This variation is true for both external and internal bone morphology; however, variation in the internal cortical and trabecular structure reflects more directly how a bone or joint was loaded during life, as it is more responsive to the predominant directions of mechanical stress (Lieberman 1997, Ruff *et al* 2006). Trabecular bone has a lower apparent density than cortical bone and therefore exhibits a greater surface area exposed to an increased number of bone cells that make it more metabolically active in comparison to more densely packed

cortical bone (Huiskes *et al* 2000, Jacobs 2000, Currey 2002). Trabecular bone also remodels at a faster rate than cortical bone with an annual turnover rate of 25% in comparison to 2-3% observed in cortical bone (Eriksen 1986, 2010). The higher rate of remodelling and response to variations in magnitude and direction of load in trabecular bone indicates its comparatively greater sensitivity to function (Jacobs 2000, Carter & Beaupre 2001).

Trabecular matrix is most easily recognised at the epiphyses of long bones, as well as in the centrum of vertebrae, and is encased by a thin shell of cortical or subchondral bone. The general function of trabecular bone is to provide strength while optimally reducing mass, ultimately transferring external load away from the joint toward more densely packed cortical bone (Currey 2002, Barak *et al* 2008). The plasticity of this bone structure has been pivotal in understanding the effect of biomechanical stress (Ruff *et al* 2006). The shape of individual trabeculae varies over the lifetime of an individual in response to biomechanical loading.

The relative amount of trabecular bone (BV/TV) and its degree of uniformity in alignment (i.e., anisotropy) are the most biomechanically informative aspects of trabecular architecture (Goldstein *et al* 1993, Odgaard 1997). The primary indicator of trabecular organisation and structure are measured using the degree of anisotropy (DA) and trabecular shape (BS/BV). These indices examine the structure of individual trabeculae, and the patterns they form on a macrostructural level. Plate-like trabeculae (Fig 2.1) are indicative of higher load-bearing whilst rod-like trabeculae are seen as weaker and in response to a smaller biomechanical force (Su 2011). Strut orientation can be described as anisotropic (ordered along a plane) or isotropic (randomly distributed in all directions), where direction is inferred using DA. When trabecular struts are oriented perpendicular to each other, they form a lattice with cross braces that stabilize the overall network and support surrounding cortical bone (Currey 2002). Since trabeculae remodel and orient themselves by removing bone from one side and depositing bone to the other side until the direction of the trabecular strut is aligned in the direction of the principle strain, these factors make trabecular bone sensitive to external loading (Currey 2002). Other descriptive parameters such as trabecular thickness or separation are quantified in an effort to better understand heterogeneity in trabecular strength and/or the optimization of its structure (Kivell 2016).

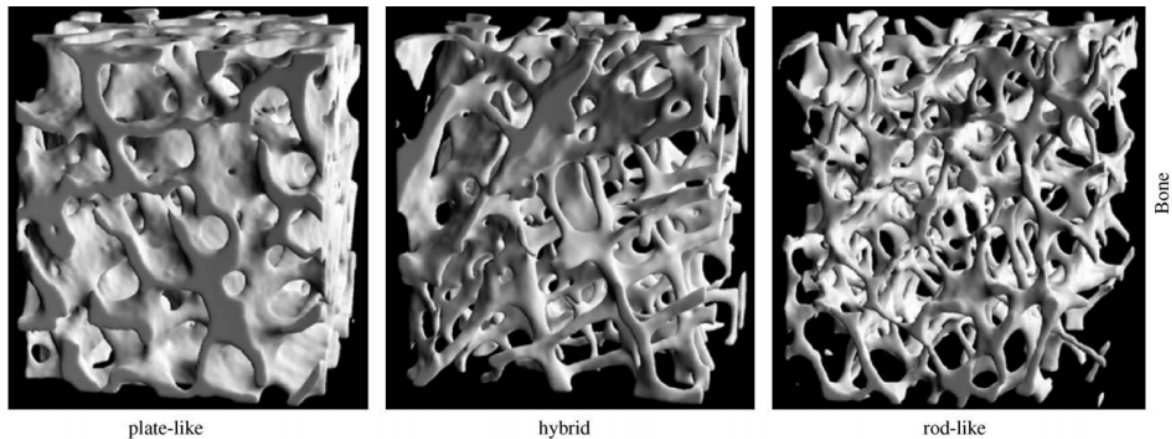


Figure 2.1. The macro-structure of trabecular bone. From Mathieu *et al* (2006).

2.3. Kinematics of extant non-human primates.

Kinematics and the functional morphology of nonhuman primates are two research fields that provide crucial information that can be used to establish morphological predictions in early hominin locomotor modes (Kimura 1996, Crompton *et al* 2003, Crompton *et al* 2008). The various postures and locomotor modes exhibited by primates have been summarised by Hunt (1992). These aid in classifying locomotion and biomechanics in primates for comparative studies, and serve as a template for comparative kinematic studies on extant primate positional and locomotor behaviour. Kinematic data on joint posture and loading during primate locomotor and manipulative behaviours are essential for accurately interpreting the functional significance of variation of trabecular structure across extant and fossil primates.

The outgroup used in this study was *Papio hamadryas*, which is a cercopithecoid that walks on a semiplantigrade foot, such that the heel is raised above the substrate during locomotion (Gebo 1992). Old World Monkeys (*Cercopithecidae*), to which Hamadryas baboons belong, are terrestrial quadrupedal digitigrade walkers (Berillon *et al* 2010, Rose 1977). *Papio* are known to climb, during which the midfoot flexes, although they exhibit significantly less dorsiflexion during climbing than hominoids (Hirasaki *et al* 1993, DeSilva 2009). *Papio* have also been observed spontaneously walking bipedally (Hunt 1992, Rose 1977). However, their morphology is similar to extant hominoids in that their foot is supinated during climbing and quadrupedal walking (Berillon *et al* 2010). Studies on Olive baboons (*P. anubis*) have demonstrated that baboons maintain a plantarflexed ankle throughout stance phase of terrestrial locomotion (Rose 1977).

The Asian apes, more than any other members of the *Hominidae* family, are restricted to an arboreal habitat (Thorpe & Crompton 2006). Although all extant apes, except for modern humans, live predominantly in forests (Dohlinow & Fuentes 1999), orangutan locomotion is most restricted to tree canopies whereas chimpanzees and gorillas are morphologically capable of a more terrestrial lifestyle. Orangutan locomotion, however, has only been very broadly described. Sugardjito & Van Hooff (1986) provided a broad ranging description of the locomotion of Sumatran orangutan positional behaviour, grouping 48% of their locomotion as quadramous scrambling. This was later refined by Cant (1987a,b) using a small sample size of only two adult females. Studies by Thorpe & Crompton (2006) demonstrated that orangutans possess a highly complex range of positional forms. DeSilva (2009) noted that *Pongo* hyperflexes their foot during vertical climbing bouts, similar to African apes. However, unlike African apes, *Pongo* is rarely terrestrial and therefore could load their ankle in a wider range of positions, including plantarflexion, when navigating vertical substrates arboreally (Tuttle & Cortright 1988, Thorpe & Crompton 2006).

The more terrestrial non-human apes (*Pan* and *Gorilla*) engage more frequently in quadrupedal knuckle-walking as the dominant form of locomotion (Elftman & Manter 1935, Hunt 1992). These species are also known to engage in bipedal walking for short bouts of time (Elftman & Manter 1935, Hunt 1992, 1994 Sockol *et al* 2007). The definitive heel strike of modern humans is not observed in bipedal walking chimpanzees, which instead contact the ground often simultaneously with the heel and the lateral midfoot in a locomotor term known as “inverted heelstrike plantigrady” (Elftman & Manter 1935, Vereecke *et al* 2003), and push off using a highly dorsiflexed ankle (bonobos: D’Áout *et al* 2004). Chimpanzees exhibit a bent hip bent knee gait (BHBK) when bipedal, which has been shown to be energetically inefficient compared to modern human bipedal gait (Sockol *et al* 2007). Humans bear more weight on the calcaneus during heel strike than the African apes, as shown in plantar pressure measurements (Elftman & Manter 1935, Wunderlich 1999, Vereecke *et al* 2003). African apes walking quadrupedally demonstrate a more lateral center of pressure over the duration of a foot contact in stance of terrestrial quadrupedal locomotion (Elftman & Manter 1935, Vereecke *et al* 2003). African apes are also known to engage in climbing vertical substrates, and are able to dorsiflex the ankle joint to 45° during stance phase of climbing behavior (DeSilva 2009, Holowoka & O’Neill 2013, DeSilva *et al* 2013). A similar degree of dorsiflexion would result in soft tissue failure and severe injury in modern humans (Begeman

& Prasad 1990). As a result, African apes are interpreted as having a greater range of motion about the ankle joint.

2.4. Trabecular bone functional adaptation in extant non-human primates.

Beddoe (1978) pioneered 2D studies on trabecular morphology in the femur and vertebrae of rhesus macaques and the talus and calcaneus of lemur species (Ward & Susman 1979). This was later expanded upon by Rafferty (1996) and Rafferty & Ruff (1994) by examining the femur and humerus of a sample of prosimian and anthropoid primates. The behavioural and mechanical flexibility (Wainwright *et al* 2008) that characterizes extant primates means that external morphology does not always reflect or predict behaviour. The outcomes of these various studies showed that species loading their joints primarily in one direction, or repetitively, (e.g. humans) have more anisotropic trabecular structure (i.e., more uniform trabecular orientation) than species with a more generalized locomotor repertoire (e.g. chimpanzees and orangutans) (Barak *et al* 2011). These studies are often small and therefore variation among species due to age, sex, environment (natural or captive), level of activity and previous loading history as well as body size could impact results (Barak *et al* 2011). Several comparative studies of primate trabecular bone across individuals or species have revealed variation in trabecular structure that fits well with predictions of differences in habitual mechanical loading during locomotion (Fajardo & Muller 2001, Ryan & Ketcham 2002a,b, 2005, Ryan & Shaw 2012, Scherf *et al* 2013, Tsegai *et al* 2013, Matarazzo *et al* 2015, Zeininger *et al* 2016, Su & Carlson 2017).

Although most trabecular studies of extant primates have focussed on the proximal femur and humerus (Rafferty & Ruff 1994, Rafferty 1996, MacLatchy & Muller 2002, Ryan & Ketcham 2002a,b, 2005, Ryan & van Rietbergen 2005, Fajardo *et al* 2007, Scherf 2007,2008, Saporin *et al* 2011, Ryan & Shaw 2013, Scherf *et al* 2013), other skeletal elements such as the mandible (Ryan *et al* 2010), bones of the wrist (Schilling *et al* 2014), calcaneus (Maga *et al* 2006, Zeininger *et al* 2016), talus (DeSilva & Devlin 2012, Su *et al* 2013, Su & Carlson 2017) and thoracic vertebrae (Cotter *et al* 2009, Oxnard & Yang 1981, Oxnard 1997) have been studied.

These studies have extended beyond hominoids and anthropoid primates to include extant strepsirrhines, where arguably clearer functional signals have been observed probably because of their more unique locomotor habits, e.g., vertical clinging and leaping (MacLatchy

& Müller 2002, Ryan & Ketcham 2002a, 2005). Ryan & Ketcham (2002a, 2005) found that non-leaping taxa (*Galago*, *Avahi*, *Tarsius*) have more anisotropic trabeculae compared to leaping taxa such as *Cheirogaleus*, *Loris*, *Perodictus* and *Otolemur*, which was reasoned to be reflective of the more stereotypical loading conditions in the non-leaping taxa. Ryan & Ketcham (2002a) also noted high levels of intraspecific variation in all taxa, suggesting that trabecular structure was responsive to subtle differences in individual behaviour. A similar study on a smaller sample was conducted by MacLachy & Müller (2002) using *Perodicticus* and *Galago* and yielded similar findings. These studies on strepsirrhines suggest that more stereotypical loading of the joints is typical in comparison to anthropoid primates (Demes *et al* 1994, Hirasaki *et al* 2000, Schmitt & Hanna 2004).

One of the first 3D analyses of non-human hominoid trabecular structure was conducted by Fajardo & Müller (2001) in gibbons, spider monkeys, rhesus macaque and baboon species. The authors investigated how differences in trabecular architecture of the proximal humerus and femur varied with arboreal and terrestrial behaviour. The study concluded that variation in the degree of anisotropy correlated with locomotor differences, in that the more arboreal gibbons and spider monkeys had more isotropic trabecular structure than the macaque and the baboon. The arboreal species are assumed to have had a more variable loading condition of the humerus and femur than the terrestrial species (i.e. more stereotypical loading condition). However, a more extensive analysis on a larger sample studied by Fajardo *et al* (2007) found a high degree of overlap in trabecular parameters including BV/TV and DA across quadrupedal (*Colobus*, *Macaca*, *Papio*) and climbing/suspensory (*Ateles*, *Symphalangus*, *Alouatta*) taxa. Many other authors have found the absence of a clear correlation between trabecular structure and predicted loading differences based on locomotion (Viola 2002, Scherf 2008, Ryan *et al* 2010, Ryan & Walker 2010, DeSilva & Devlin 2012, Shaw & Ryan 2012, Schilling *et al* 2014).

2. 5. Human gait kinematics.

The bipedal gait cycle of extended hip extended knee (EHEK) walkers can be divided into two phases known as stance phase and swing phase. Typically heel strike (initial contact) occurs at the beginning of stance, during which the foot is typically slightly supinated both in the rearfoot and forefoot. The foot is then driven passively by the ground reaction force (GRF) into pronation (i.e. a triplanar motion consisting of eversion, abduction and dorsiflexion occurring simultaneously) of the subtalar joint during the subsequent mid-stance

phase of walking (Barak *et al* 2013b). During a normal gait cycle, stance phase can be split into three sub-phases based on the sagittal motion of the ankle; a) the heel rocker; b) the ankle rocker and c) the forefoot rocker (Dawe & Davis 2011) (Fig 2.2). The heel rocker phase begins at heel strike, where the ankle is in a slight plantarflexed position pivoting around the calcaneus until the end of the heel rocker phase when the foot is flat on the ground. During this sub-phase, the dorsiflexors are eccentrically contracting to lower the foot to the ground. The ankle rocker phase is where the ankle moves from plantarflexion to dorsiflexion during which the shank (tibia and fibula) rotates forward around the ankle in the sagittal plane allowing forward progression of the body. During forefoot rocker phase, the foot rotates around the ankle joint, starting when the calcaneus lifts off the ground evident by the ankle beginning to plantarflex and continuing until maximum plantarflexion is achieved at toe-off, where power generation is achieved for the leg to initiate swing phase.

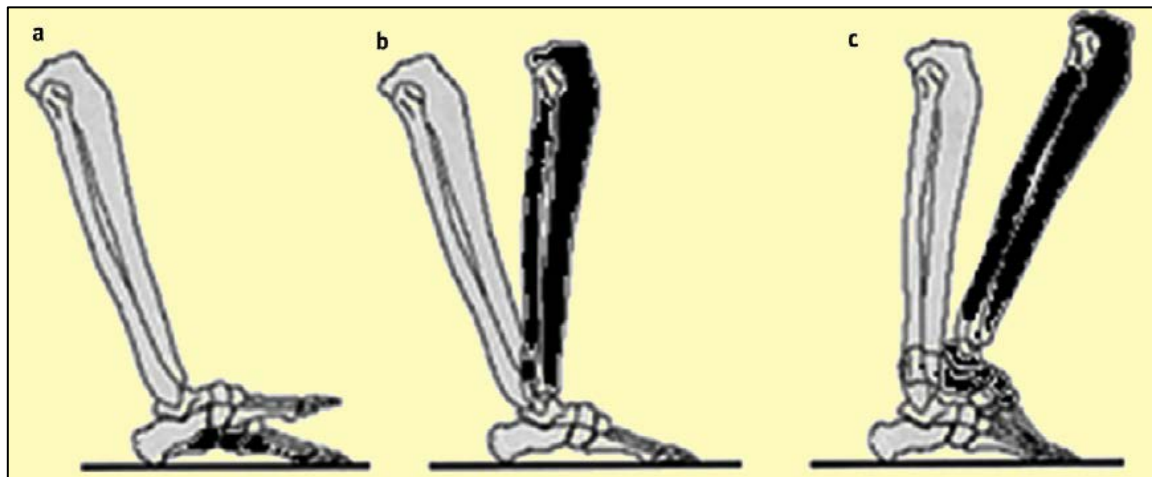


Figure 2.2. Image depicting the three subphases of stance phase, A- first rocker (heel rocker), B- second rocker (ankle rocker), C- third rocker (forefoot rocker). After Dawe & Davis (2011).

During swing phase, the ankle dorsiflexes, which enables the foot to clear the ground and avoid stumbling/tripping, before returning to slight plantarflexion at heel strike. This flexion motion is complemented by motion at the subtalar joint, with approximately 15° of eversion/inversion. For the majority of individuals, inversion occurs at heel-strike, and progresses to eversion during mid-stance phase, allowing the heel to rise and push off into swing.

2. 6. Trabecular bone functional adaptation in modern humans

The majority of studies on trabecular bone morphology are on humans, and usually within the context of medical research. For example, focus is often on obtaining a better understanding

of bone-related diseases, such as osteoporosis and osteopenia (Eriksen 1986, Simkim *et al* 1987, Smith *et al* 1989, Dempster 2000). However, attention has recently grown in the field of determining bone functional adaptations in humans from an evolutionary perspective. Within humans, more mobile, foraging populations show significantly greater BV/TV and thicker trabeculae in their proximal femur than that of less mobile, agricultural populations (Ryan & Shaw 2015).

Ontogenetic studies in modern humans also reveal the nature of trabecular structure as individuals grow. A distinctive trabecular pattern of the adult proximal femur is apparent between the ages of one and two years, when human infants develop independent walking and the femur becomes weight-bearing in a human-like way (Townesley 1948, Ryan & Krovitz 2006, Cunningham & Black 2009). Raichlen *et al* (2015) have recently followed on this work and suggested that subtle changes in trabecular structure of the human distal tibia reflect increased biomechanical stability during bipedalism that is gained between the ages of one and eight.

Human trabecular studies have been extended to include athletes of varying professions. Harrison *et al* (2011) concluded that elite athletes who engage in irregular-impact loading of the femur, such as squash and soccer players, showed higher trabecular bone density in *in vivo* magnetic resonance than those who engaged in high-magnitude, but vertical loading conditions (e.g. power-lifting), and 20% higher trabecular bone density than non-athletes. High density (thicker and more closely packed) trabecular structures were observed in the knee of gymnasts and Olympic fencers compared to control groups (Modlesky *et al* 2008a, Chang *et al* 2008). Trabecular structure is also proven to be severely underdeveloped in children with cerebral palsy that exhibit abnormal gait (Modlesky *et al* 2008b). A decrease in bone density is also observed in non-gravitational environments, such as seen in astronauts returning from prolonged bouts of space travel (Jee *et al* 1983, Bikle & Holloran 1999).

2.7. The role of the ankle in human gait.

The ankle joint plays a fundamental role in human locomotion at nearly every step of the gait cycle and supports weight throughout walking (Gage *et al* 1995, Leardini *et al* 2000). This complex comprised of the lower leg and the foot forms a kinematic linkage that allows the lower limb to interact with the ground (Brockett & Chapman 2016).

The ankle 'complex' is composed of three distinct joints: the subtalar, tibiotalar and talocalcaneonavicular joint (Sarrafiian 1993). The talocrural joint, the primary focus of this study is located at the superomedial part of the ankle joint and is formed by the articulation between the inferior articular surface of the tibia (including the malleolar articular surface on the lateral aspect of the medial malleolus of the tibia) with the superior and medial surfaces of the trochlea of the talus (Fig 2.3). The main structural component of this joint examined for the purpose of this study is the distal tibia. The distal tibia is formed by five surfaces: inferior, anterior, posterior, lateral and medial, which is prolonged distally by the medial malleolus (Fig 2.4). The inferior surface is concave anteroposteriorly and slightly convex transversely (mediolaterally), creating a dome-like articulation with the talus.



Figure 2.3. Osteological components of the tibiotalar complex. A- distal tibia, B- fibula, C- talus adapted from Gray's Anatomy (2009).

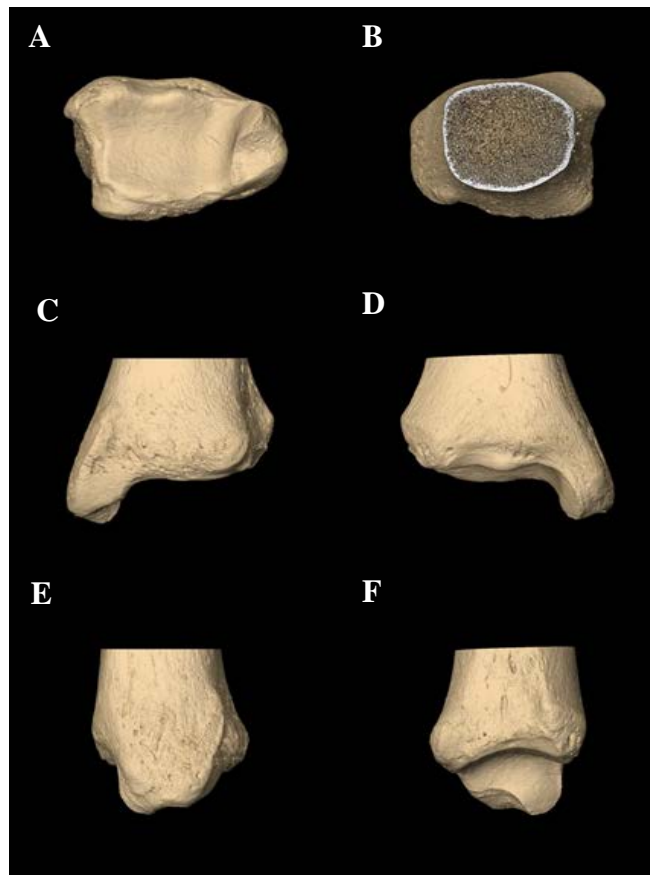


Figure 2.4. Morphology of the distal tibia. A) Inferior aspect, tibial plafond (articulating surface with talus). B) Superior aspect. C) Anterior aspect. D) Posterior aspect. E) Medial aspect of distal tibia, showing medial malleolus projection. F) Lateral aspect.

Stability of the ankle joint is important as ankle injuries are among the most common reported in emergency rooms (Leardini *et al* 2000). The joint itself withstands high compressive and shear forces during gait, with structural integrity maintained by bony and ligamentous structure. When compared to other joints, such as the hip or knee, the ankle is far less susceptible to processes such as osteoporosis, unless associated with previous trauma (Brocket & Chapman 2016).

According to McCullough and Burge (1980), stability of the ankle is determined by passive and dynamic factors. Passive stability depends on the anatomy and limitation of movement due to hard tissue ankle structure. It involves mechanical interactions between bony articular surfaces and reflects both the integrity of these structures and their mechanical properties (Sarrafian 1993, Leardini *et al* 2000). Active stability of the tibiotalar joint is provided through three groups of ligaments: the anterior tibiofibular ligament, the posterior tibiofibular ligament and the interosseous tibiofibular joint (Nordin & Frankel 2001, Brocket & Chapman 2016). The medial aspect of the ankle joint is supported by the medial collateral ligaments

(deltoid ligaments), which are integral in resisting eversion motion and valgus stress within the joint (Sarrafian 1993, Alexander & Bennett 1987). The deltoid ligament is large and strong and is fan-shaped over the medial part of the ankle joint. It originates on the medial side of the medial malleolus and inserts on the navicular, talus and calcaneus. This ligament comprises the anterior and posterior tibiotalar parts, as well as the tibionavicular and tibiocalcaneal parts. Maximally stable position of the ankle (i.e., close-packed position) is in dorsiflexion (Nordin & Frankel 2001). When not weight-bearing, side-to-side stability of the ankle is provided by medial and lateral malleoli, and the collateral ligaments (Nordin & Frankel 2001). The malleoli act to constrain the talus range of motion such that the joint primarily functions as a hinge joint, and thus contributes to plantar and dorsiflexion motion of the foot.

Primary osteokinematic movements at the ankle joint (i.e. movement of a bone as described with muscle actions and ranges of motion) are dorsiflexion and plantar flexion in the sagittal plane about a mediolateral axis (DP) (Barnett & Napier 1952, Yamaguchi *et al* 2009, Brockett & Chapman 2016). Pronation and supination (PS) are rotations that occur in the frontal plane about an anteroposterior axis (AP) (Brockett & Chapman 2016) (Fig 2.5). Internal (medial) and external (lateral) rotations (IE) occur in the transverse plane about a vertical axis. The axis of rotation of the ankle runs through medial and lateral malleoli, which are slightly offset from each other in coronal and transverse planes (Inman 1976, DeSilva 2009).

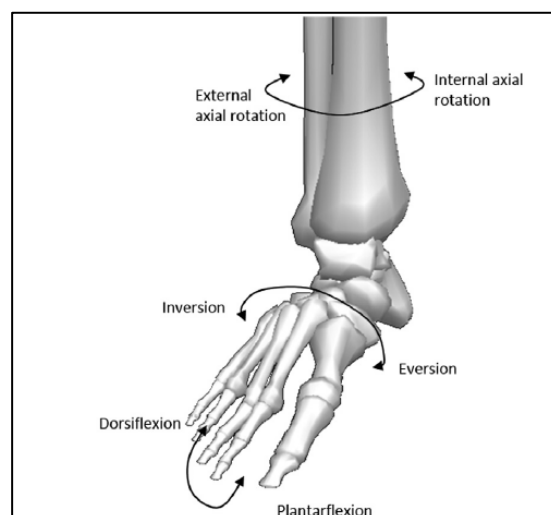


Figure 2.5. Diagram illustrating relative osteokinematic movements of the ankle joint complex. Adapted from Brockett & Chapman (2016). Figure adapted from Visual 3D (C-Motion, Rockville, Maryland).

Ankle range of motion (ROM) has been shown to vary significantly between individuals due to geographical and cultural differences based on their activities of daily living (Grimston *et al* 1993). Arthrokinematic movement (i.e. movements that occur at the articular surface of a bone as it moves about the joint axis of the X, Y and Z planes) of the ankle joint can be described as either open chain (i.e. during movement without weight-bearing) or closed chain (i.e. weight-bearing movement) (Grimston *et al* 1993, Sarrafian 1993).

For the purposes of gait kinematics, closed chain movement is considered whereby the ankle bears weight. This is the movement of the tibia on a fixed talus. In closed chain pronation, dorsiflexion is the result of anterior rotation of the tibia coupled with an anterior glide of the tibia over the talar trochlea, and an internal rotation of the tibia and inversion produced by lateral glide of the tibia, which is slight due to joint compression (Grimston *et al* 1993, Sarrafian 1993). Closed chain supination, which involves plantarflexion, is the result of posterior rotation of the tibia coupled with posterior glide of the tibia, and an external rotation of the tibia and eversion produced by medial glide of the tibia/fibula, which is slight to none due to joint compression.

2.8. Trabecular bone functional adaptation in the hindfoot of fossil hominins.

The confounding nature of external bony morphology in fossil hominoids has caused debate among paleoanthropologists, particularly surrounding the validity of reconstructing past behaviour (Madar *et al* 2002, Susman 2004, Begun & Kivell 2011) and the impact on species and phylogenetic relationships. Assumptions about trabecular bone and its mechanosensitivity in response to mechanical loading have been fundamental in many palaeontological and bioarcheological studies of fossil specimens (Ruff *et al* 2006). Trabecular analyses are non-invasive and can provide additional information on functional morphology (in conjunction with studies on cortical bone and the external morphology), which can be useful in cases where specimens possess a mosaic of external features. Fossil hominins, for example, demonstrate a “mosaic” of features, combining human-like and ape-like characteristics with their own unique features, sometimes demonstrating both primitive and derived features within a single skeletal element. With regards to the retention of primitive features, some scientists attribute this to phylogenetic inertia or retentions from a more arboreal ancestor that were either in the process of being lost or were selectively neutral and largely non-functional (Lovejoy *et al* 1973, Latimer & Lovejoy 1989). Scientists that aim to reconstruct behaviour

as a whole consider these primitive features as functionally useful, namely as an adaptive trait retained under stabilising selection (Stern 1975, Rose 1991, Stern & Susman 1991).

Previous trabecular studies on the bones of the hindfoot include the calcaneus, talus and distal tibia. The calcaneus was examined in a comparative framework by Zeininger *et al* (2016) with three main hypotheses. The first hypothesis was that in modern humans, the dorsal and plantar calcaneocuboid joint (CCJ) and the talcocrural joint (TCJ) show evidence of predictable habitual loading (Fig 2.6). The second is that within the comparative extant primate sample (*Pan troglodytes*, *Gorilla gorilla*, *Gorilla beringei* and *Papio ursinus*), only the dorsal CCJ shows evidence of predictable loading. Specifically, the prediction was made that based off of observed locomotor preferences, trabecular properties across the dorsal and plantar CCJ in modern humans would be similar, but there would be dissimilarity in non-human primates. In addition, a fossil calcaneus StW 352 from Member 4 of Sterkfontein (South Africa) attributed to *A. africanus* was examined to evaluate joint loading patterns in an extinct hominin species in order to address the evolution of these properties.

The results of this study demonstrated a higher elongation index, bone volume fraction, trabecular thickness and trabecular number in the dorsal CCJ compared to the plantar TCJ, while non-humans did not always exhibit predictable loading differences between the two regions. *H. sapiens* exhibited the most anisotropic and rod-like struts oriented in line with principal load axes and therefore a less variable and more predictably loaded TCJ compared to the other groups. The authors used multivariate analyses to show that the StW 352 dorsal CCJ best matched the pattern observed in *P. ursinus*, while the plantar CCJ best matched the pattern observed in *G. beringei*, and the TCJ best matched the pattern observed in *G. gorilla*. The authors suggested that these patterns indicated the StW352 calcaneus experienced more variable loading of the CCJ and TCJ joints compared to those of modern humans, but less variable loading than those exhibited by the extant primate samples. Therefore, this species is interpreted as having a large range of foot movements compared to modern humans, but not as large a range as modern non-human primates. In other words, locomotor kinematics of the StW 352 individual, as exhibited by the calcaneus, were somewhat unlike those of living hominoids or humans.

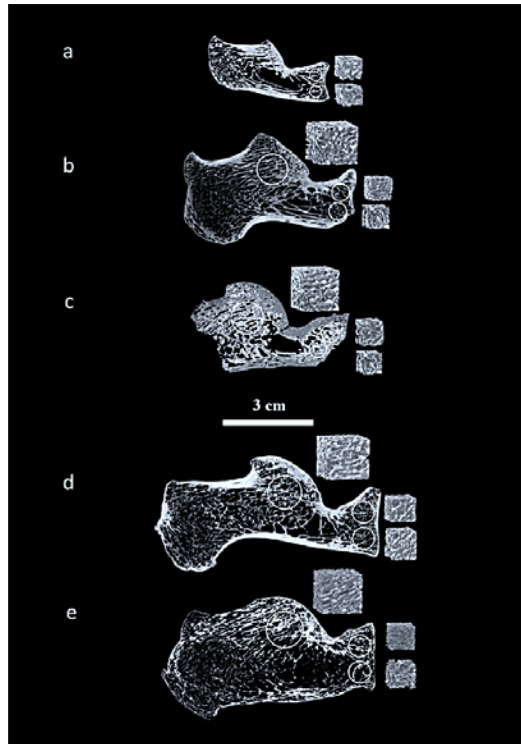


Figure 2.6. Volume of interest (VOI) locations (white circles), (a) *P. ursinus*, (b) *P. troglodytes*, (c) StW 352, (d) *G. gorilla*, and (e) *H. sapiens* calcanei examined in Zeininger *et al* 2016.

The talus was studied by DeSilva & Devlin (2012) to investigate the hypothesis that talar trabecular microarchitecture reflected loading patterns in the primate ankle joint, and therefore, that talar trabecular morphology might be useful in inferring locomotor behaviour in fossil hominins. A comparative framework of extant great apes (*Pan*, *Gorilla*, and *Pongo*) *Papio sp.* and modern humans (*H. sapiens*) was used to evaluate seven fossils from the Plio-Pleistocene of South Africa attributed to *A. africanus* (StW 88, StW 102, StW 347, StW 363, StW 486), *H. erectus* (SKX 42695) and *Paranthropus robustus* (TM 1517). Four volumes of interest were selected from the talar body in order to quantify trabecular microarchitecture (anteromedial, anterolateral, posteromedial, posterolateral).

The authors found that humans demonstrated a high DA across the entirety of the talus, which was considered to be consistent with the compressive forces experienced during bipedal walking, but that the other observed patterns in trabecular parameters did not aid in distinguishing locomotor preferences between groups. Intraspecific analyses revealed no regional differences in trabecular architecture unique to bipedal humans. Trabecular thickness, number, spacing and connectivity density had the same regional relationship in the talus of humans, chimpanzees, gorillas and baboons, which the authors interpreted as suggesting a deeply conserved architecture in the primate talus (DeSilva & Devlin 2012).

Due to the lack of statistical support for the predicted functional differences, the authors concluded that trabecular architecture may not simply reflect the loading environment in the talus, and that it may be a limited tool when trying to infer locomotor behaviour in fossil hominins. The fossils examined in this study, however, were analyzed using low resolution medical CT image scans (with the parameters 120keV and 1mm thickness), meaning the requisite spatial resolution of the image data was not high enough to view and analyse individual trabeculae. The voxel size required to adequately visualize among the thinnest trabecular struts is approximately 30 μ m, while the highest obtainable spatial resolution using medical CT is ~200 μ m (Scherf 2008).

A subsequent study by Su *et al* (2013) focused on the talus of an early Pleistocene hominin (KNM-ER 1464) from the Koobi Fora Formation, which has been attributed to *P. boisei*. This fossil was investigated using a comparative framework of extant primates (*Pan*, *Gorilla*, *Pongo* and modern humans). This study focused primarily on orientation and shape of trabeculae using degree of anisotropy and elongation index. Modern human tali were found to have relatively anisotropic and elongated trabeculae on the lateral aspect, which was unique when compared to the fossil hominin KNM-ER1464 talus and extant non-human primates. Trabecular anisotropy in the *P. boisei* talus most closely resembled the condition exhibited in African apes, except for high anisotropy in the posteromedial talus. Primary orientation of trabeculae in the anteromedial region of the fossil was significantly different to that of extant African apes, and more similar to that of modern humans in being directed parallel to the talar neck. Based on these findings, Su and colleagues (2013) suggested that the talus of *P. boisei* distributed weight to the midfoot in a human-like manner, but that the lateral aspect could be subjected to comparatively more variable loading conditions.

Su & Carlson (2017) extended this study to include *A. africanus* (StW486, StW 102, StW 363) and *P. robustus* (TM 1517), as well as incorporating baboons into the comparative sample of high resolution microCT scans. In their study, tali were divided into nine VOIs (Fig 2.7). The authors used discriminant function analyses on structural properties and found that TM 1517 (*P. robustus*) aligned with *Pan* and *Gorilla*, while other hominins mostly resembled baboons in structure. *Paranthropus* tali (KNM-ER 1464 and TM 1517) were unique in that their primary strut orientation resembled the human condition in the anterior-medial subregion, which was suggested to reflect a lateral to medial weight shift in the last half of stance phase. In these tali, strut orientation seemed to be positioned to distribute compressive loads medially and distally toward the talar head. This was not observed in the

A. africanus tali, which instead had a primary strut orientation that resembled more of an ape-like condition, with no evidence of a medial weight shift evident during the last half of stance phase. This study supported the hypothesis that trabecular strut orientation and shape can be used to distinguish species characterized by different locomotor behaviours and postural preferences.

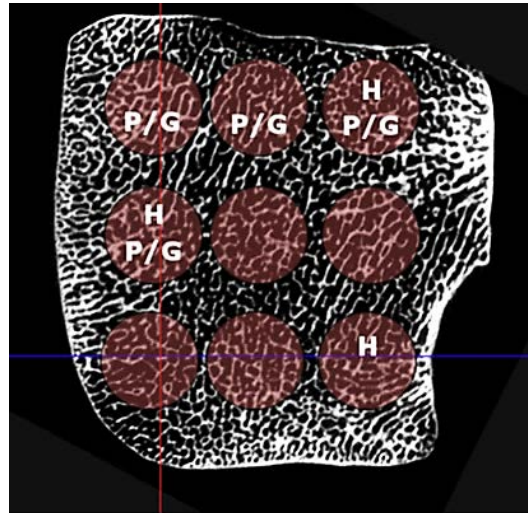


Figure 2.7. Adapted from Su & Carlson (2017). The nine volumes of interest sampled in the study in relationship to the articular surface of the trochlea. Highlighting predictions for human increased trabecular structural strength (H) and for chimpanzee and gorilla increased trabecular structural strength (P/G).

The distal tibia has been previously examined by Barak *et al* (2013b) using 2D principal trabecular orientation (PTO) of *A. africanus* fossils from Sterkfontein Member 4 (StW 358, StW 389) and a *Homo* specimen (StW 567) from Member 5 using two VOIs (Fig 2.8). This study yielded similar results to those of the Sterkfontein calcaneus and tali in that it demonstrated that early hominins primarily loaded their ankles in a relatively extended human-like posture, but still exhibited unique trabecular structure and organization, falling somewhat between patterns characterizing chimpanzee and human ranges. This resulted in strut orientation that was similar to humans, yet still distinctive within the hominin species. The australopith distal tibiae appear to have exhibited a human-like plantarflexion/dorsiflexion signal when compared to chimpanzees, suggesting that australopiths exhibited an efficient relatively human-like extended lower limb during bipedal gait.

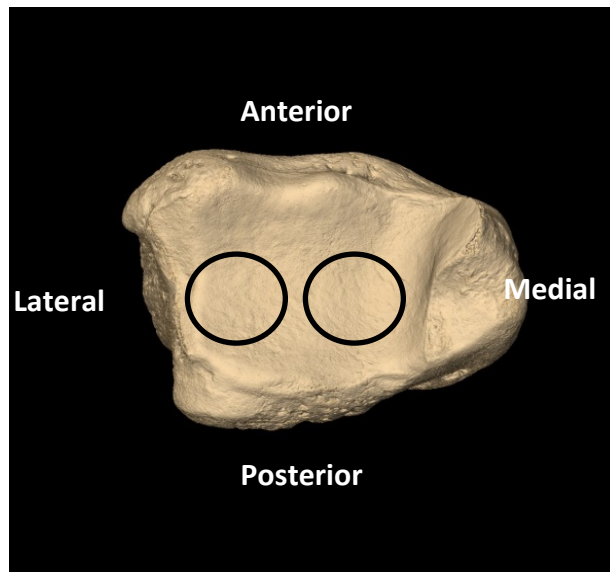


Figure 2.8. Representation of location of the lateral and medial VOIs in the distal tibia examined in Barak *et al* 2013b.

CHAPTER 3: MATERIALS AND METHODS

3.1. Materials.

3.1.1. Comparative sample

MicroCT data for the modern human specimens (*H. sapiens*) were kindly provided by Prof. Kristian Carlson and Dr. Tea Jashashvili. These specimens are housed at the Florisbad Collections at the Bloemfontein Museum (South Africa) (Table 3.1). The skeletal material was collected during archaeological excavations at different South African localities, namely Groot Brak River, Robberg Cave and Matjies River. Based on radiocarbon dating, these localities come from different periods of the Holocene between 5390 +/- 70 (Matjies River) at the oldest site and 2180 +/- 50 years (Groot Brak River) at the youngest site. Individuals in the modern human Holocene sample have been described as female according to museum records, except for SS3 (Matjies River) whose gender is unidentified, but is presumed male based on standard osteometric indicators of postcranial robusticity.

The extant non-human primate sample used in this study consisted of tibiae from adult chimpanzees (*Pan troglodytes troglodytes*), western lowland gorillas (*Gorilla gorilla gorilla*), Bornean orangutans (*Pongo pygmaeus*) and Hamadryas baboons (*Papio hamadryas sp.*) (Table 3.1) (Fig 3.1). MicroCT scan data from these individuals were kindly provided by Dr Anne Su (http://facultyprofile.csuohio.edu/csufacultyprofile/detail.cfm?FacultyID=A_SU) of Cleveland State University and were collected as part of her PhD dissertation work at Stony Brook University (Su 2011).

Several primate species were selected in order to sample a diversity of habitual locomotor repertoires. Adult females of each species were selected rather than adult males in order to minimize the potential effects of body size differences on structural results across the taxa (Table 3.2). Baboons have been included as a non-hominoid outgroup that habitually engages in terrestrial digitigrade quadrupedalism (Berillon *et al* 2010). In order to minimize the effect of body size differences in comparison with larger-bodied hominoids, male baboons were selected. It is acknowledged that sex could potentially affect trabecular bone structure (e.g. hormone differences and joint loading differences between sexes), but the effects on baboon versus hominoid comparisons are judged to be minimal based on the results of a recent study on calcaneal trabecular bone using pooled-sex baboons (Zeininger *et al* 2016). The relationship between variation in trabecular structure and body mass has been studied

extensively in extant primates in recent years (Scherf 2007,2008, Ryan & Shaw 2013, Barak *et al* 2013a). Generally larger primates have absolutely thicker and more widely-spaced trabeculae, but relative to body mass their trabecular struts are thinner and more tightly packed (Swartz *et al* 1998, Doube *et al* 2011, Ryan & Shaw 2013). Scaling of specific trabecular parameters with body mass varies, and depends on the bone and the taxonomic group (Cotter *et al* 2009, Ryan & Shaw 2013). Organisational properties such as DA have been shown to have no significant relationship with body mass (Doube *et al* 2011, Barak *et al* 2013a).

The age of individuals in the sample was assessed by examining epiphyseal fusion on all long bones of the skeleton. Comparative individuals were not included in the study if there was evidence of external damage or traumatic injury, bone degenerative diseases or any other systematic abnormalities. All specimens were dry-bone samples, and all were wild-shot except for the baboons that were wild born, subsequently caught, and then lived as captive animals (Coelho & Bramblett 1981).

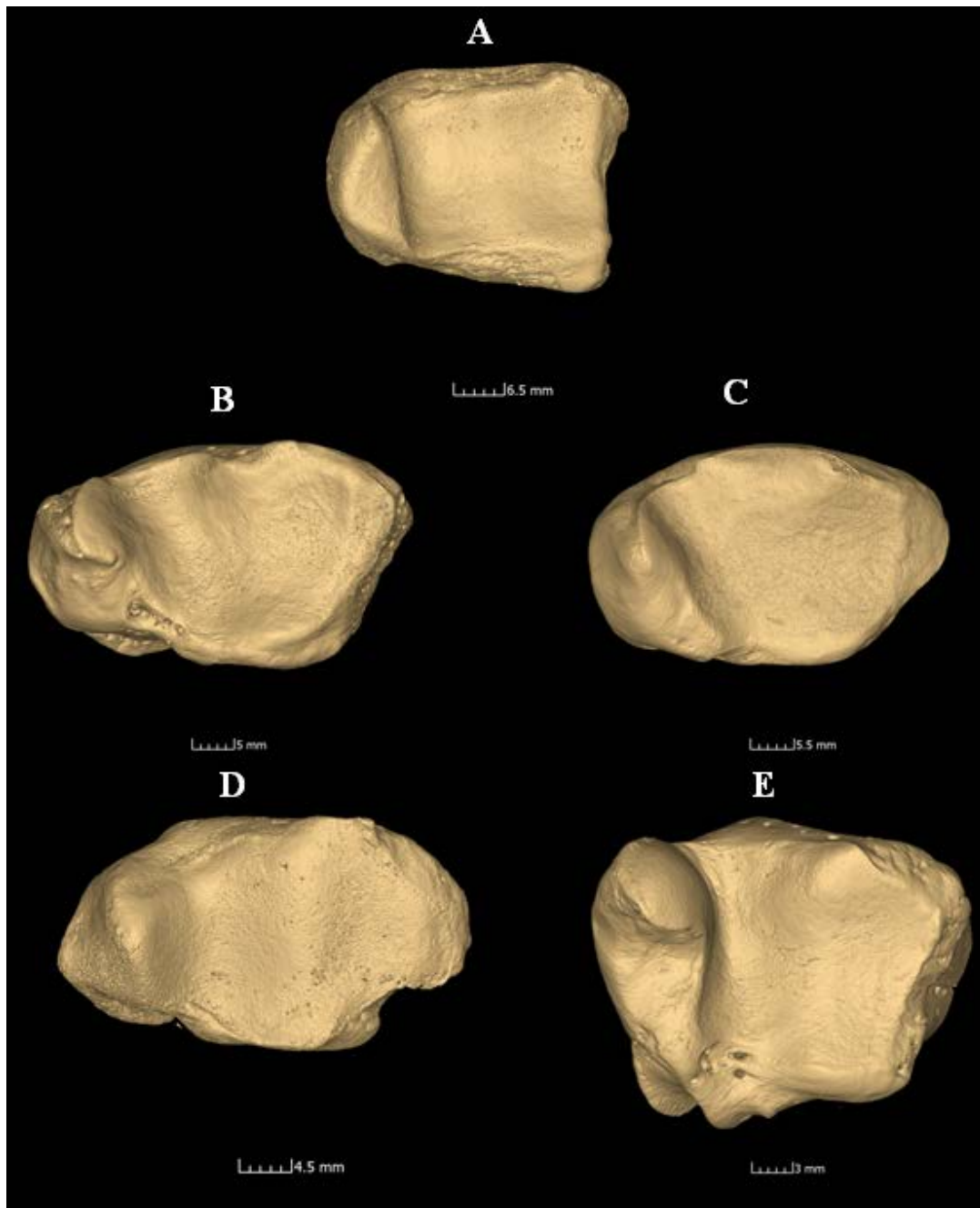


Fig 3.1. 3D reconstruction representative distal tibiae plafond of extant comparative species used in this study, A) *Homo sapiens*, B) *Pan troglodytes*, C) *Gorilla gorilla*, D) *Pongo pygmaeus*, and E) *Papio hamadryas*.

Table 3.1. Comparative primate species used in this study.

Species	Collections**	N tibia	N medial malleoli	Locomotor behaviour	References
<i>H. sapiens</i>	National Museum Bloemfontein (Florisbad Research Station)	7	7	Biped	Elftman & Manter 1935, Vereecke <i>et al</i> 2003
<i>P. troglodytes</i>	CMNH	11	4	Semi-arboreal plantigrade quadruped	Elftman & Manter 1935, Hunt 1992, Crompton <i>et al</i> 2008
<i>G. gorilla</i>	CMNH, AMNH, NMNH	10	5	Semi-arboreal plantigrade quadruped	Crompton <i>et al</i> 2008
<i>P. pygmaeus</i>	NMNH	10	10	Arboreal, quadrumanous	Thorpe & Crompton 2006
<i>P. hamadryas sp</i>	Bramblett (UT Austin)	11	7	Terrestrial semi-digitigrade quadruped	Berillon <i>et al</i> 2010

**AMNH= American Museum of Natural History, CMNH= Cleveland Museum of Natural History, NMNH= Smithsonian National Museum of Natural History

Table 3.2. Relative body weight according to sex in extant species sampled.

Species	Males		Females		References
	N	X (kg)	N	X (kg)	
<i>P. hamadryas</i>	41	16.9	39	9.9	Phillips- Conroy & Jolly 1981
<i>P. pygmaeus</i>	7	78.5	13	35.8	Markham & Groves 1990, Jungers 1997
<i>G. gorilla</i>	10	170.4	3	71.5	Jungers & Susman 1984
<i>P. troglodytes</i>	5	59.7	4	45.8	Jungers & Susman 1984
<i>H. sapiens</i>	405	47.9	319	42.2	Pennetti <i>et al</i> 1986

3.1.2. Fossil sample.

The fossil hominin specimens examined in this study are housed at the Evolutionary Studies Institute at the University of the Witwatersrand (Fig 3.2., Fig 3.3). Specimens StW 358, StW 389 and StW 515 have been described as originating from Sterkfontein Member 4, and are attributed to *A. africanus* (Berger & Tobias 1996, McHenry & Berger 1998, Kuman & Clarke 2000, Pickering *et al* 2004, DeSilva 2009b). Specimen StW 567 (right distal tibia) has been described as originating from Sterkfontein Member 5, and is attributed to *H. erectus*, or to an indeterminate *Homo sp.* and aged at 1.4 -1.7MY (Kuman & Clarke 2000, Pickering *et al* 2004, DeSilva 2009b). Complexity in stratigraphic dating of the Sterkfontein cave system

associated with infills (Kuman & Clarke 2000, Stratford *et al* 2012, 2013) has resulted in difficulty in distinguishing the boundary between Members 4 and 5, creating a challenge when assigning fossils to specific members. Revision of the stratigraphy at Sterkfontein indicates that Member 4 australopithecine breccias (2.8-2.6 Ma) extend into what was previously thought to be Member 5 (Kuman & Clarke 2000). Therefore, the Sterkfontein sample analysed in this present study (StW 358, StW 389, StW 515 and StW 567) is now considered to consist of Member 4 specimens attributed to *Australopithecus* (Fig 3.2., Fig 3.3). Although it has been noted in previous publications that there could be more than one species present in Member 4, there were no *a priori* morphological reasons to separate the postcranial sample, and thus all Member 4 specimens have been grouped into *A. africanus* for analyses (McHenry & Berger 1998, Kimbel & Rak 1993).

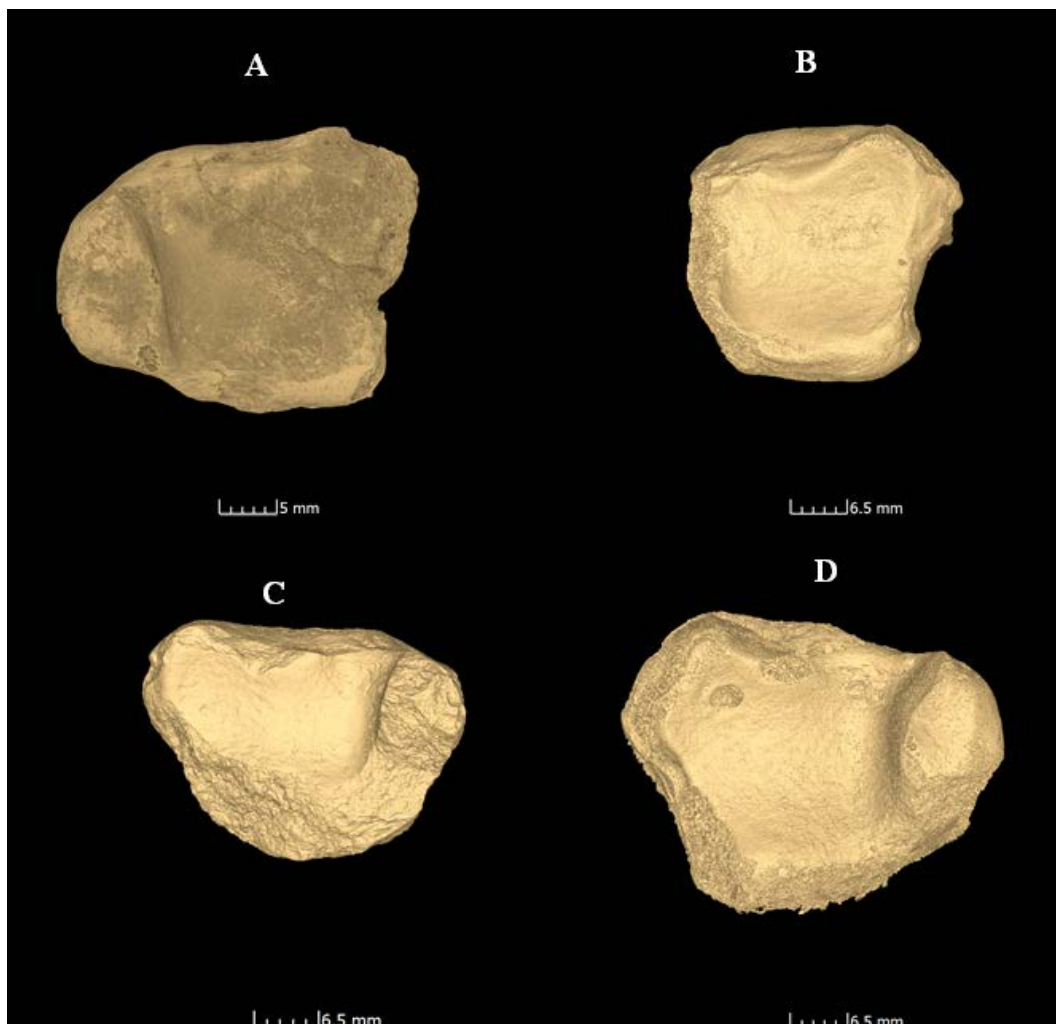


Fig 3.2. 3D reconstruction of fossil tibiae used in this study showing the tibial plafond, A) StW 358, B) StW 389, C) StW 515 and D) StW 567.

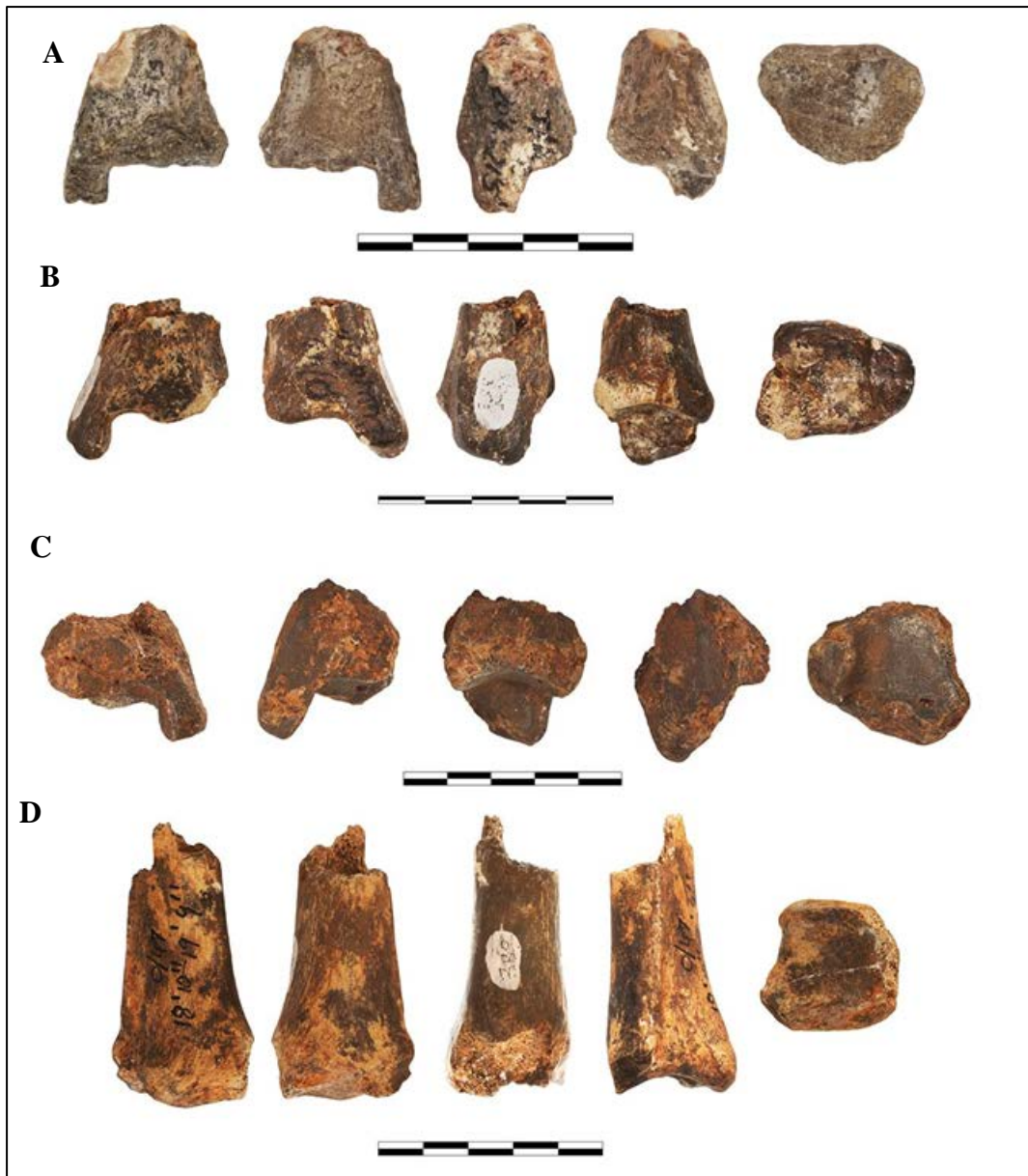


Figure 3.3. Hominin fossil distal tibiae from Sterkfontein Member 4 attributed to *A. africanus* examined in this study, A) StW 515, B) StW 358, C) StW 567, D) StW 389. Photographs courtesy of Dr Bernhard Zipfel and Roshna Wunderlich.

3.2. Methods.

3.2.1. Data collection.

Fossil tibiae were scanned at the Microfocus X-ray CT facility at the Palaeosciences Centre at the University of the Witwatersrand (Evolutionary Studies Institute, www.wits.ac.za/microct). A Nikon Metrology XTH 225/320 LC dual source industrial CT system was used and the relevant acquisition parameters included: 80-95 kV, 110-122 μ A, isometric voxel size ranging from 25 μ m to 31 μ m, using an aluminium filter (1.8mm thickness), beam hardening of 3, 2000 frames at an average of 5200 projections.

All comparative non-human specimens were scanned individually using a commercial μ CT system (eXplore Locus, SP, GE Healthcare Pre-Clinical Imaging, London, On, Canada) housed within the Department of Biomedical Engineering at the Cleveland Clinic Foundation (Su 2011). This system is advantageous, as it has a long specimen bed able to accommodate full length of the tibia. The GE eXplore Locus uses volumetric conebeam CT technology and allows for the entire sample to be imaged in one rotation. The long axis of the tibia was oriented parallel to the scanner bed during image acquisition in order to orient the distal articular surface perpendicular to the bed. Specimens were scanned at a spatial resolution setting of 45 μ m, which is small enough to produce morphometric results that are similar to traditional histological methods (Müller *et al* 1996). The source energy voltage was set to a maximum 80 kVp and the x-ray current was set to 450 μ A. The pixel matrix size was 1024x1024 and yielded a field of view of 47.1 mm and an isometric voxel size of 0.0448 mm. Each image was reconstructed from 720 views with an exposure time of 400 ms (Su 2011).

For each specimen, raw image data were imported into VG Studio MAX 3.0 (Volume Graphics GmbH, Heidelberg, Germany) in order to orient the bones in standardized positions for the purpose of analyses. Distal tibiae of fossil specimens and the comparative sample were oriented such that in the sagittal plane the anterior and posterior rims of the articular surface were level, and in the coronal and transverse planes the mediolateral axis was level (Fig 3.4). Reoriented volumes were then exported as a stack of 16-bit TIFF format image files for further processing. Analysis of the high resolution CT data took place at the Virtual Image Processing Lab (VIP Lab) at the Evolutionary Studies Institute, University of the Witwatersrand.

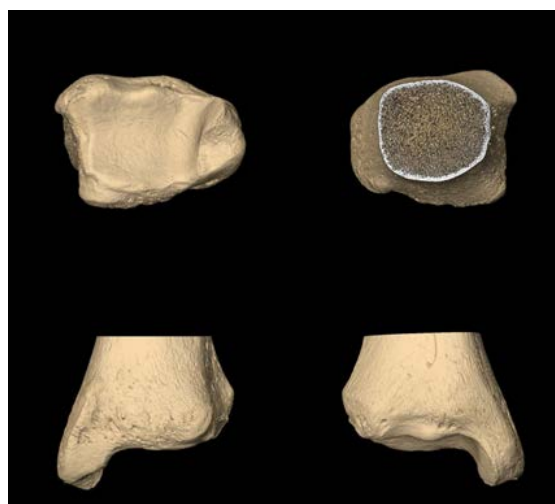


Figure 3.4. Standardized anatomical positions for distal tibiae in VG Studio MAX 3.0.

3.2.2. Image segmentation.

Fossil image data, as well as the modern human comparative data, required an additional segmentation step to remove matrix/sediment infill within the bone (i.e. between struts). Image stacks that required additional segmentation were imported into VG Studio MAX 3.0, where the region-growing tool was used in the segmentation panel. A threshold for distinguishing bone from non-bone was individually selected for each specimen. The brush tool was used and a minimum threshold was set in order to manually include any trabecular struts that were not selected by the thresholding option. Once bone material was sufficiently highlighted as a separate region of interest (ROI), the ROI was extracted as a new volume of interest (VOI). Subsequent to extracting a cleaned fossil VOI, fossil and human archaeological samples were exported as 16-bit TIFF stacks for division into volumes of interest (VOIs) in Avizo Lite 9.0.0 software.

3.2.3. Division into volumes of interest (VOIs).

Aligned distal tibiae image stacks were imported into Avizo Lite 9.0.0 (FEI, Visualization Sciences Group) where a 3D generated isosurface was produced in order to crop the whole bone into two separate areas of interest: the tibial plafond and the medial malleolus. This was performed using the crop editor tool in Avizo Lite 9.0.0. Once each area was cropped, separate 16-bit TIFF image stacks were exported for each one. This process was repeated for all extant comparative species and fossils in the sample.

The tibial plafond was subsequently segmented into a 3x3 grid of 9 anatomically-aligned regions: anteromedial, antero-central, anterolateral, centromedial, centro-central, centrolateral, posteromedial, postero-central, and posterolateral (Fig 3.5, Fig 3.6) in order to account for locomotor signals across the anteroposterior axis as well as the mediolateral axis in order to coincide with known kinematic data. Maximum linear mediolateral and anteroposterior dimensions of the isolated tibial plafond were digitally measured using the 2D linear measurement tool in Avizo Lite 9.0.0. These dimensions were divided into thirds, such that each region was defined as a square with dimensions of 1/3 of the mediolateral length (Y dimension) and 1/3 of the anteroposterior length (X dimension). An image stack was then cropped using the crop editor in Avizo Lite 9.0.0 to exclude air and cortical bone superficial to the trabecular mesh. Depth of each cropped area (i.e. the Z dimension) was set equal to the X and Y dimensions, resulting in cubic volumes. Once a cubic trabecular VOI was isolated, the volume editor and ellipse tools were used to generate a best-fit spherical volume with

diameters equal to the cubic VOI X, Y and Z dimensions (Fig 3.7). Areas outside of the spherical VOI (e.g. edges) were eliminated because of their known propensity to create artifacts in quantified variables (Ketcham & Ryan 2004).

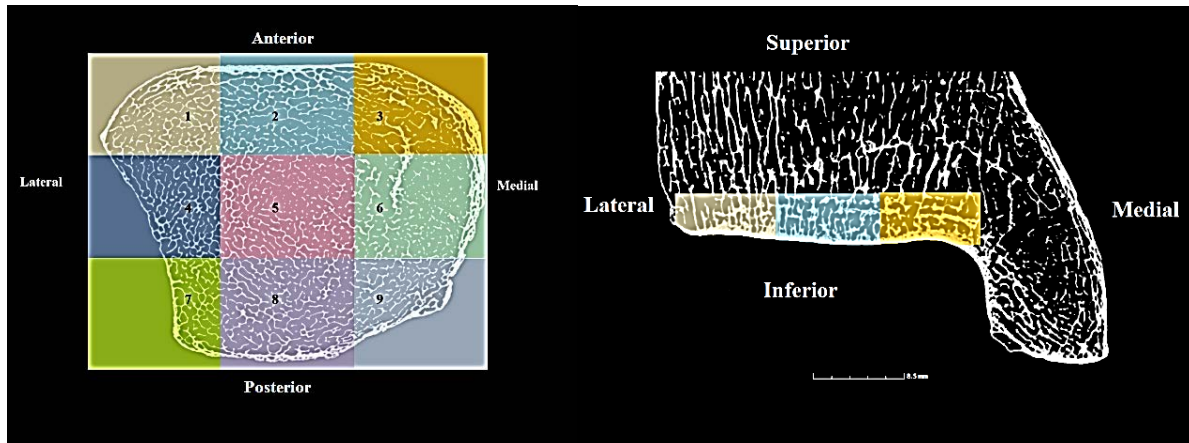


Figure 3.5. Orientation of tibial plafond and division into nine volumes of interest (not to scale).

From within the medial malleolus, two VOIs (anterior and posterior) were segmented, where each volume was defined using half of the anteroposterior length (Fig 3.6). As with VOIs beneath the tibial plafond, the cropping tool in Avizo Lite 9.0.0 was used to define and isolate individual VOIs within the medial malleolus. Each volume was exported as a 16-bit TIFF stack for analyses.

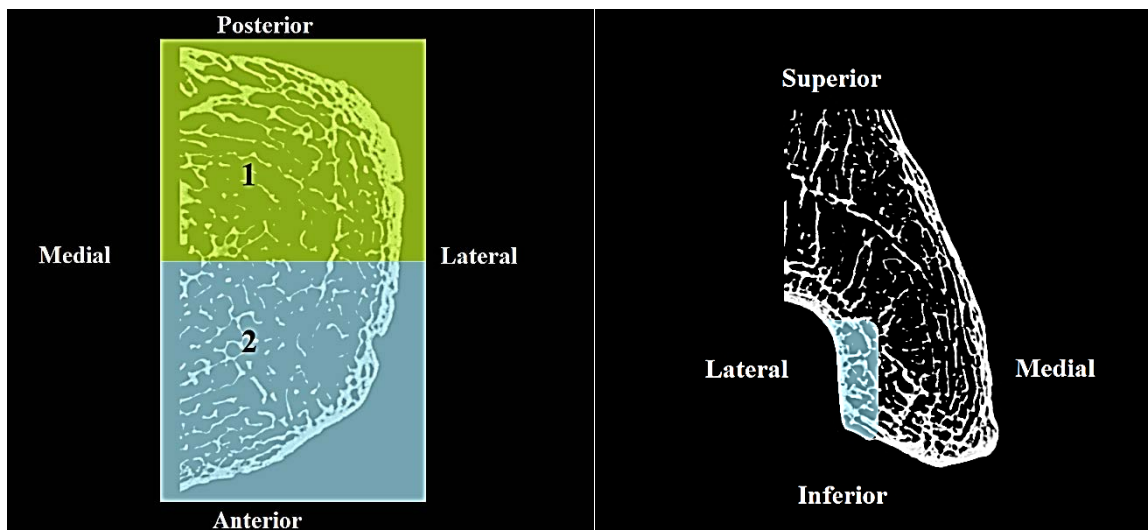


Figure 3.6. Orientation of medial malleolus and division into nine volumes of interest (images not to scale).



Fig 3.7. Visual representation of a spherical trabecular volume as analysed in this study.

3.2.4. Thresholding and quantification of trabecular parameters

All 16-bit TIFF image stacks of cropped spherical VOIs were then imported into ImageJ (ImageJ 1.50i, Java 1.6.0_20, <https://imagej.nih.gov/ij/>). Initially, all stacks were batch converted to 8-bit TIFF stacks for analyses using the BoneJ plugin (BoneJ 1.4.1, bonej.org, Doube *et al* 2010) for ImageJ and subsequently smoothed using a Gaussian filter to reduce noise. Each image stack was binarised into bone and non-bone using the median greyscale value for each image stack. The 8-bit binarised image stacks were then used for the purpose of quantifying the trabecular properties. Output variables computed by BoneJ and reported in this study are listed in Table 3.3. Total volume of the spherical volumes was calculated manually using Eq. 1, as the BoneJ plugin calculates total cubic volume of the binarised image stack rather than total volume of the sphere.

$$V = \frac{3}{4}\pi r^3 \text{ (Eq. 1)}$$

3.3. Statistical analyses.

All comparative analyses were performed using JMP (Version 13, SAS Institute Inc, Cary, NC, 1989-2007). Morphological (structural) and organizational variables were quantified firstly using descriptive statistics in order to quantitatively explore statistical testing. In addition, boxplots were used to visualize the extent of variation exhibited by extant species

and fossil individuals. Horizontal lines inside boxes indicate median values, ends of boxes indicate 25th and 75th percentiles, and whiskers indicate minimum and maximum values, except for outliers that are denoted by closed circles. All variable distributions were checked for normality using Shapiro-Wilks test. When distributions differed significantly from a normal distribution, they were log-transformed. A one way analysis of variance (ANOVA) with post-hoc pairwise comparison tests (Tukey-HSD) was performed to statistically assess predicted differences in trabecular architecture between regions within a specific taxon (i.e. intraspecific patterns), and to statistically assess predicted differences in individual VOIs between taxa (i.e. interspecific patterns). Statistical significance was set at $p=0.05$ for all tests (Table A1, Table A2).

In addition, a multivariate discriminant function analysis (DFA) was performed to test the ability of a combination of trabecular parameters to discriminate between species differing in habitual locomotor behaviour, this was achieved through a canonical correlation analysis that determined the successive function and canonical roots. The eigenvalues are interpreted as the proportion of variance accounted for by the correlation between the respective canonical variates. The canonical correlation is the result of the square root of the eigenvalue and is an overall index of the canonical correlation between two sets of variables. Prior to this, a Pearson's Correlation test was performed to eliminate the possibility of oversampling a particular parameter (e.g., including two covarying parameters) (Table A3). The chosen variables were representative of structure (BV/TV and Tb.Sp), orientation (DA) and shape (BS/BV) (Table 4.14).

Table 3.3. Trabecular parameters quantified in the present study.

Parameter	Symbol	Description	References
Bone volume fraction	BV/TV	Characterised as a fundamental measurement of the architectural properties of trabecular bone. It is the dimensionless ratio of the number of bone voxels present in the VOI relative to the total number of voxels in the VOI. TV is calculated manually using $V = \frac{3}{4}\pi r^3$ (Eq.1)	Parfitt 1983, Odgaard 1997, Hildebrand <i>et al</i> 1999, Odgaard 2009, Doube <i>et al</i> 2010
Trabecular thickness	Tb.Th	Mean thickness of the trabecular struts in a given VOI, based on the intersections between a superimposed grid of lines and bone voxels.	Parfitt 1983, Odgaard 1997, Hildebrand <i>et al</i> 1999,
Trabecular separation	Tb.Sp	Mean width of the spaces between adjacent trabeculae in a given VOI.	Odgaard 1997, Dougherty & Kunzelmann 2007, Odgaard 2009, Doube <i>et al</i> 2010
Connectivity density	Conn.D	Number of interconnected trabeculae per unit volume (taken as a proxy for trabecular number)	Odgaard & Gunderson 1993, Kabel <i>et al</i> 1999, Odgaard 2009, Doube <i>et al</i> 2010
Degree of anisotropy	DA	Describes the trabecular orientation in 3D space calculated using the mean intercept length (MIL). The more anisotropic the structure, the greater the preference of strut orientation in a certain magnitude. Lower DA denotes isotropic struts, demonstrating a symmetry of structure and orientation equally in multiple directions.	Harrigan & Mann 1984, Odgaard 1997, Odgaard <i>et al</i> 1997, Odgaard 2009
Structural Model Index	SMI	A dimensionless measure of the relative proportion of plate-like vs rod-like structures in a given VOI. Values typically range from 0 (idealised plates) to 3 (idealised rods). Negative values indicate a more concave structure.	Hildebrand & Ruegsegger 1997, Salmon <i>et al</i> 2015
Bone surface density	BS/BV	The ratio of trabecular bone surface area relative to total trabecular bone volume in a given VOI.	Salmon <i>et al</i> 2015

CHAPTER 4: RESULTS

4.1. Interspecific comparison of trabecular structure in the distal tibia of humans, extant non-human primates and australopiths from South Africa.

4.1.1. Structural patterns in BV/TV, Tb.Th, Tb.Sp and Conn.D across extant species.

Average BV/TV across the extant comparative sample was generally lowest in *Homo* (5 out of 9 VOIs), including at VOI1-VOI3 (A-M, A-C and A-L) (Table 4.1, Fig 4.1). Average BV/TV of *Papio*, on the other hand, was highest in 7 of 9 VOIs: all those in the anterior (VOI1-VOI3) and posterior regions (VOI7-VOI9), as well as the central VOI4. Humans exhibited the highest average BV/TV at the other 2 of 9 VOIs: VOI5 (C-C) and VOI6 (C-L). The central region was lowest in average BV/TV across all extant species, except for *Homo* where VOI6 (C-L) was the highest average BV/TV observed across the tibial plafond. *Homo* demonstrates the highest variation in BV/TV within a single species compared to the extant non-human primates since humans tend to exhibit the largest standard deviations (largest at 7 of 9 VOIs) (Table 4.1, Fig 4.1). Statistically significant differences in BV/TV between species occurred at the lateral VOIs (Table 4.1). BV/TV in VOI3 (A-L) in *Homo* was significantly lower than that in *Papio* and *Pongo*. BV/TV in VOI6 (C-L) in *Homo* was significantly greater than those in *Papio*, *Pongo* and *Gorilla*.

The average thickest trabeculae in the distal tibia were usually observed in *Pongo* (8 of 9 VOIs), including all three of the anterior and all three of the central VOIs (Table 4.2, Fig 4.2). There was a general trend of an increasing ML gradient in the anterior region in thickness across all extant species (L>C>M), except in *Papio* (C>M>L). *Homo* also exhibited the second lowest average Tb.Th in each of the anterior VOIs (VOI1-VOI3). Again, *Homo* exhibited an overall higher variation in individuals of the same species in comparison to the extant non-human primates in thickness, exhibiting the highest standard deviations in all 9 VOIs. Statistically significant differences in thickness occurred mostly in the anterior region (VOI1, VOI3) where *Pongo* demonstrated significantly greater thickness than *Pan* and *Homo* in VOI1, *Pan* and *Papio* in VOI2 and *Homo* and *Pan* in VOI3 (Table 4.2). In addition, *Gorilla* demonstrated significantly thicker struts than *Papio* in VOI3. Average Tb.Th in the posterior volumes was highest in *Pongo* in 2 of 3 VOIs, being significantly higher in thickness than both *Pan* and *Homo* at VOI7 (P-M) (Table 4.2, Fig 4.2). The central region

yielded no significant differences in Tb.Th between extant species, though *Pongo* exhibited the generally highest average thickness in all three central volumes.

Homo demonstrated an overall higher average Tb.Sp across most of the distal tibia in comparison to the extant non-human primates (6 of 9 VOIs), including all three anterior volumes, while *Gorilla* exhibited the highest average separation in the remaining 3 VOIs (2 central and 1 posterior) (Table 4.3, Fig 4.3). *Pongo* demonstrated an increase in Tb.Sp in the central and posterior regions. *Papio* usually exhibited the lowest average spacing across the extant comparative sample (7 of 9 VOIs), while *Pan* and *Pongo* each exhibited the lowest average spacing in one VOI. *Gorilla* demonstrated the overall highest variation in individuals of the same species with higher standard deviations in 4 of 9 VOIs, including all posterior volumes. *Homo* exhibited the second highest amount of variation (3 of 9 VOIs). Tb.Sp in the distal tibia of extant species exhibited statistically significant differences across all 9 volumes in the distal tibia of extant primates (Table 4.3, Fig 4.3). *Homo* demonstrated significantly higher separation than all extant non-human primates: each anterior subregion (VOI1, VOI2, and VOI3) and two of the three posterior subregions (VOI8 and VOI9) (Table 4.3). The central region yielded fewer post-hoc pairwise significant comparisons, being reduced to only those between the significantly higher *Homo* and the lower *Papio* (VOI4 and VOI5). *Homo* was also greater than *Pan* and *Pongo* in VOI6. There were additional significant differences observed between non-human primate species: *Gorilla* demonstrated higher Tb.Sp than *Papio* across all 9 VOIs, and higher Tb.Sp than *Pan* in 3 VOIs (VOI5, VOI6 and VOI7).

Homo exhibited the most connected struts on average (5 of 9 VOIs), followed closely by *Pan* (3 of 9 VOIs), while *Gorilla* exhibited the least connected struts on average (4 of 9 VOIs) followed closely by *Pongo* (3 of 9 VOIs) (Table 4.4, Fig 4.4). Average Conn.D was usually lowest in the central region across all species compared to their anterior and posterior regions, except in *Gorilla*, which demonstrated the lowest connectivity in the anterior region. Across the ML direction, Conn.D was generally lowest on average laterally in extant non-human primates, and lowest on average in the medial volumes in *Homo*. The most variation among individuals of the same species was observed in *Pan* (7 out of 9 VOIs). Conn.D in the distal tibia was similar to Tb.Th in that statistically significant group differences occurred mostly in the anterior region (VOI1—VOI3) and P-M (VOI7) (Table 4.4, Fig 4.4). In VOI1, *Pan* was significantly higher in Conn.D than all extant species, except *Papio*. Conn.D in VOI2 (A-C) was significantly higher in *Papio* than *Gorilla* and *Pongo*, while Conn.D was also significantly higher in *Homo* than *Gorilla*. Conn.D in VOI3 was significantly smaller in

Gorilla compared to *Papio*, *Pan* and *Homo*. *Papio* was also significantly greater in Conn.D than *Pongo* in VOI3 (Fig 4.4).

4.1.2. Structural patterns in DA, SMI and BS/BV across extant species.

Papio usually exhibited the most anisotropic struts on average (8 of 9 VOIs), while *Homo* usually exhibited the most isotropic struts on average (7 of 9 VOIs) (Table 4.5). There were statistically significant differences in DA across all VOIs in the distal tibia (Table 4.5, Fig 4.5). DA in VOI1 (A-M) was significantly lower in *Homo* than any other extant non-human primate species, suggesting greater isotropy in *Homo* in this subregion. In VOI2 (A-C), *Homo* was again significantly lower in DA compared to *Gorilla* and *Pongo*. In VOI3 (A-L), *Homo* was significantly lower than *Papio* in DA.

Homo exhibited the lowest overall average SMI in the distal tibia (7 of 9 VOIs), except along two medial VOIs (VOI1 and VOI7). *Homo* was lower in average SMI than *Pongo* and *Pan* in VOI4 and lower on average than all extant non-human primate species in VOI5 and VOI6. *Homo* tends to demonstrate more plate-like SMI compared to the extant non-human primates, which tend to demonstrate more rod-like trabeculae. There were statistically significant differences in SMI in the anterior and central region between extant species (Table 4.6, Fig 4.6). SMI in *Pan* was significantly higher and more spherical than all other species in VOI2, and greater than *Homo* in VOI3-VOI6.

Papio demonstrated the highest average BS/BV (6 of 9 VOIs) followed by *Pan* (2 of 9 VOIs) and *Homo* (1 of 9 VOIs) (Table 4.7). *Gorilla* consistently exhibited the lowest average BS/BV (9 of 9 VOIs) (Table 4.7). *Homo* exhibited the greatest amount of intraspecific variability among individuals (highest standard deviation at 8 of 9 VOIs). BS/BV in extant primates exhibited statistically significant differences between species across all volumes in the distal tibia (Table 4.7, Fig 4.7). *Papio* demonstrated significantly higher BS/BV, especially in the anterior volumes compared to the other comparative species.

4.2. Trabecular properties of *A. africanus* specimens in comparison to extant species sampled.

4.2.1. Structural patterns in BV/TV, Tb.Th, Tb.Sp and Conn.D in *A. africanus*.

In general, BV/TV in *A. africanus* was higher than *Homo* and fell within the ape-like range of variation (Table 4.1, Fig 4.1). BV/TV in the anterior region of the fossils was generally

lowest in StW 515 across all preserved VOIs sampled for that individual (VOI1-VOI4) (Fig. 4.1). The lowest recorded BV/TV in a fossil specimen was observed in VOI1 (A-M) of StW 515. BV/TV in StW 567 was higher in medial and central VOIs than lateral VOIs, and was highest in the anterior region (VOI2:A-C). StW 389 had generally lower BV/TV than StW 358 and StW 567, but similar BV/TV to StW 515, with its highest BV/TV in the posterior region ($P > A > C$). StW 389 exhibited the highest BV/TV in the central regions (VOI2, VOI5), while in its posterior region the highest BV/TV was more laterally positioned (VOI9: P-L). BV/TV of StW 358 was highest laterally in the anterior and central VOIs ($L > C > M$), while in the posterior region BV/TV was highest medially ($M > C > L$).

As with BV/TV, the fossil sample exhibited substantial variability in Tb.Th. In the fossils, Tb.Th overlapped with both human-like ranges and non-human primate like ranges of strut thickness. Average strut thickness in StW 515 was lowest of the fossil sample in all volumes (VOI1-VOI9), and fell below the range of all extant comparative species in observed strut thickness (Table 4.2, Fig 4.2). StW 358 demonstrated generally thicker struts on average than the other fossil specimens, with the thickest struts observed laterally (VOI3, VOI6, VOI9). Average strut thickness of StW 358 was within the range of observed extant non-human primate strut thickness, except in VOI5, VOI6 and VOI7 where its average thickness was greater than that observed in any of the comparative species, this could be due to segmentation of trabeculae. StW 358 also exhibited a laterally increasing gradient in the anterior and central regions ($L > C > M$), while in the posterior region the thickest struts were in the medial VOI (VOI7). StW 389, on the other hand, demonstrated general thickness within the observed *Homo* range of variation, with its thickest struts observed in central VOIs as opposed to lateral VOIs (VOI2, VOI4, and VOI7) (Table 4.3, Fig 4.3). Tb.Th in StW 567 was greatest anteriorly at VOI1 (A-M), generally thickest in the central VOIs in the anterior and posterior region (VOI5, VOI8), and fell within the range of variation of extant hominoids, most closely to more terrestrial species (e.g., *Pan* and *Gorilla*). The central region of StW 567 demonstrated generally thicker struts compared to its anterior and posterior regions.

Tb.Sp in the fossil hominin sample was highest generally in central VOIs (VOI3, VOI6, VOI9) rather than medial or lateral VOIs (VOI2, VOI5, and VOI8) (Table 4.3, Fig 4.3). All fossils demonstrated lower separation than found in the modern human sample, but all were within the observed non-human primate range. StW 567 was lowest in Tb.Sp in the central and medial VOIs of its anterior and posterior subregions of (VOI1, VOI2, VOI7, VOI8). StW 358 demonstrated its lowest separation laterally (VOI3, VOI6, VOI9). StW 358 also

exhibited the lowest separation in its anterior region (VOI1: A-M), and was generally lower in the medial and central VOIs overall.

Conn.D in the fossil sample was highly variable (Table 4.4, Fig 4.4). StW 358 demonstrated a generally low Conn.D, falling within the non-human primate range of distribution. StW 567 also demonstrated a generally low Conn.D across all volumes, but usually fell within the observed *Homo* distribution. StW 389 had a relatively high Conn.D compared to the other fossil samples, and in fact was higher than the ranges observed in any of the modern comparative species. StW 515 also demonstrated high Conn.D, falling outside of the distribution of Conn.D found in extant comparative species similar to StW 389.

4.2.2. Structural patterns in DA, SMI and BS/BV in *A. africanus*.

DA in the fossil sample demonstrated greater variation in the anterior region than central and posterior regions (Table 4.5, Fig 4.5). DA in the anterior region fell within the observed *Homo* distribution in medial and central VOIs (VOI1 and VOI2). In VOI3 (A-L), StW 515 and StW 567 exhibited DAs that fell below of any of the values observed in the extant species. The lowest DA in the anterior region was exhibited by StW 567. StW 358 and StW 389, on the other hand, exhibited DAs that fell within the observed *Gorilla*, *Homo*, *Pan* and *Pongo* ranges of variation. StW 389 demonstrated its highest DA in VOI1, while StW 358 exhibited its highest DA in VOI2 and StW 515 in VOI5. StW 567 had the lowest observed DA in the central region among the fossil specimens sampled, and in this region fell within the observed *Gorilla* and *Homo* distributions.

The australopith fossils exhibited highly variable SMI, mostly overlapping with the observed *Homo* distribution (Table 4.6, Fig 4.6). They tended to exhibit SMIs that decreased from medial to lateral (M>C>L), thus becoming more rod-like in more medial VOIs. SMI was lowest in StW 358 in all VOIs, extending into negative SMI, the only specimen examined to do so, indicating a trabecular fabric composed of concave structures. The highest SMI was observed in StW 515 for all regions (VOI1-VOI9). BS/BVs in all fossil VOIs, except VOI3, VOI8 and VOI9, were within the observed human range of variation and tended to fall at the higher end of the observed non-human primate ranges of variation (Table 4.7, Fig 4.7).

Table 4.1: Bone volume fraction (BV/TV) mean and standard deviation of structural variables by region, along with results of analysis of variance (p=0,05). Symbols indicate posthoc pairwise comparisons between groups, *Pongo* (□), *Pan* (○), *Gorilla* (●), *Papio* (◇), *Homo* (Δ), *A. africanus*.

Region	<i>Papio</i> ◇	<i>Pongo</i> □	<i>Gorilla</i> ●	<i>Pan</i> ○	<i>Homo</i> Δ	<i>A. africanus</i>	ANOVA	
	n=10	n=10	n=11	n=10	n=7	n=4	F	P
A-M	0,412(0,161)	0,399(0,159)	0,342(0,083)	0,359(0,052)	0,258(0,153)	0,327 (0,25)	1,837	0,139
A-C	0,464(0,09)	0,409(0,152)	0,348(0,133)	0,287(0,109)	0,35(0,223)	0,352(0,268)	2,235	0,081
A-L	0,506(0,064)○Δ	0,5(0,074)Δ	0,401(0,066)	0,373(0,15)◇	0,343(0,143)◇□	0,517(0,29)	4,739	0,003
C-M	0,33(0,147)	0,224(0,076)	0,27(0,078)	0,27(0,03)	0,29(0,201)	0,453(0,38)	1,024	0,406
C-C	0,305(0,116)	0,196(0,108)	0,268(0,0762)	0,243(0,071)	0,321(0,23)	0,444(0,248)	1,515	0,215
C-L	0,208(0,144)○Δ	0,268(0,075)Δ	0,305(0,072)Δ	0,331(0,075)◇	0,433(0,208)◇□●	0,492(0,294)	3,968	0,008
P-M	0,452(0,103)	0,326(0,12)	0,343(0,079)	0,363(0,126)	0,324(0,19)	0,462(0,262)	1,8	0,146
P-C	0,424(0,112)	0,35(0,139)	0,368(0,090)	0,432(0,072)	0,334(0,159)	0,412(0,28)	1,327	0,275
P-L	0,414(0,143)	0,388(0,085)	0,366(0,069)	0,401(0,091)	0,309(0,149)	0,463(0,2)	1,166	0,339

Table 4.2: Trabecular thickness (Tb.Th) mean and standard deviation of structural variables by region, along with results of analysis of variance (p=0,05). Symbols indicate posthoc pairwise comparisons between groups, *Pongo* (□), *Pan* (○), *Gorilla* (●), *Papio* (◇), *Homo* (Δ), *A. africanus*.

Region	<i>Papio</i> ◇	<i>Pongo</i> □	<i>Gorilla</i> ●	<i>Pan</i> ○	<i>Homo</i> Δ	<i>A. africanus</i>	ANOVA	
	n=10	n=10	n=11	n=10	n=7	n=4	F	P
A-M	0,256(0,051)	0,282(0,041)○Δ	0,263(0,027)	0,217(0,03)□	0,218(0,069)□	0,225(0,079)	3,999	0,008
A-C	0,268(0,042)	0,318(0,036)○	0,283(0,036)	0,232(0,042)□	0,256(0,073)	0,213(0,067)	4,98	0,002
A-L	0,248(0,039)□●	0,321(0,034)◇Δ○	0,3(0,027)◇	0,266(0,033)□	0,262(0,064)□	0,235(0,087)	5,772	0,0008
C-M	0,224(0,052)	0,257(0,038)	0,243(0,029)	0,223(0,035)	0,243(0,062)	0,216 (0,058)	1,088	0,374
C-C	0,235(0,055)	0,27(0,036)	0,243(0,026)	0,231(0,039)	0,254(0,057)	0,29(0,065)	1,313	0,281
C-L	0,253(0,063)	0,28(0,025)	0,269(0,023)	0,267(0,058)	0,266(0,072)	0,289(0,099)	0,369	0,829
P-M	0,263(0,034)	0,299(0,037)Δ○	0,264(0,035)	0,239(0,038)□	0,22(0,056)□	0,262(0,075)	4,977	0,002
P-C	0,267(0,035)	0,291(0,033)	0,28(0,032)	0,263(0,044)	0,236(0,061)	0,269(0,062)	2,176	0,088
P-L	0,266(0,051)	0,283(0,042)	0,292(0,03)	0,269(0,036)	0,225(0,074)	0,261(0,107)	2,534	0,054

Table 4.3: Trabecular spacing (Tb.Sp) mean and standard deviation of structural variables by region, along with results of analysis of variance (p=0,05) .

Symbols indicate posthoc pairwise comparisons between groups, *Pongo* (□), *Pan* (○), *Gorilla* (●), *Papio* (◇), *Homo* (Δ), *A. africanus*.

Region	<i>Papio</i> ◇ n=10	<i>Pongo</i> □ n=10	<i>Gorilla</i> ● n=11	<i>Pan</i> ○ n=10	<i>Homo</i> Δ n=7	<i>A. africanus</i> n=4	ANOVA F	P
A-M	1,766(0,184)Δ●○	1,985(0,472)Δ	2,391(0,380)◇Δ	2,347(0,282)◇Δ	2,914(0,351)◇□○●	1,894(0,347)	13,346	<0,0001
A-C	1,797(0,167)Δ●○	1,911(0,183)Δ●○	2,505(0,181)◇□Δ	2,435(0,185)◇Δ□	3,02(0,408)◇□○●	1,934(0,318)	40,92	<0,0001
A-L	1,231(0,216)Δ○●	1,406(0,205)□○●	2,054(0,334)◇□Δ	2,057(0,318)◇□Δ	2,67(0,283) ◇□○●	1,734(0,402)	37,017	<0,0001
C-M	2,074(0,138)●Δ○□	2,46(0,153)●◇	2,989(0,257)◇□○	2,489(0,173)●◇	2,767(0,355)◇	2,067(0,087)	25,151	<0,0001
C-C	2,154(0,099)●Δ○□	2,509(0,18)●◇	2,954(0,302)◇□○	2,52(0,252)●◇	2,77(0,376)◇	2,215(0,275)	14,635	<0,0001
C-L	1,741(0,304)Δ●	1,953(0,246)Δ	2,332(0,450)◇	1,947(0,217)Δ	2,703(0,289)◇○□	1,897(0,402)	9,667	<0,0001
P-M	2,048(0,117)●	1,794(0,31)●Δ	2,573(0,452)○□◇	1,767(0,294)●Δ	2,387(0,296)○□	1,898(0,026)	12,632	<0,0001
P-C	2,04(0,244)Δ●	2,168(0,255)Δ	2,454(0,473)Δ◇	2,098(0,298)Δ	2,921(0,287)◇○□●	2,115(0,419)	9,762	<0,0001
P-L	1,429(0,18)Δ	1,388(0,334)Δ	1,783(0,48)Δ	1,44(0,39)Δ	2,524(0,206)□◇○●	1,892(0,128)	14,705	<0,0001

Table 4.4: Connectivity Density (Conn.D) mean and standard deviation of structural variables by region, along with results of analysis of variance (p=0,05).

Symbols indicate posthoc pairwise comparisons between groups, *Pongo* (□), *Pan* (○), *Gorilla* (●), *Papio* (◇), *Homo* (Δ), *A. africanus*.

Region	<i>Papio</i> ◇ n=10	<i>Pongo</i> □ n=10	<i>Gorilla</i> ● n=11	<i>Pan</i> ○ n=10	<i>Homo</i> Δ n=7	<i>A. africanus</i> n=4	ANOVA F	P
A-M	3,674(0,897)●□	2,133(0,842)○◇	2,084(1,106)○◇	4,101(1,209)●□Δ	2,521(1,047)○	4,025(3,828)	8,167	<0,0001
A-C	2,547(0,913)●□	1,672(1,04)◇	1,644(1,01)◇Δ	2,917(1,234)	3,145(1,094)●	10,133(6,996)	6,872	0,0002
A-L	3,943(1,031)●□	2,488(0,944)◇	1,663(0,924)◇○Δ	3,155(1,051)●	3,141(1,082)●	9,913(7,307)	7,552	0,0001
C-M	3,026(1,425)	1,664(1,116)	2,721(1,305)	3,029(1,149)	2,664(0,829)	4,605(3,311)	2,164	0,089
C-C	2,207(1,04)	1,405(1,261)	2,178(1,323)	2,564(1,33)	2,995(0,765)	2,251(2,246)	2,126	0,094
C-L	1,665(0,929)	1,983(0,625)	1,712(0,944)	2,074(0,967)	2,926(0,964)	2,897(2,537)	2,543	0,053
P-M	3,067(1,071)	1,959(0,65)	2,389(0,905)	3,508(1,137)	3,325(1,025)	3,014(1,918)	4,426	0,004
P-C	2,075(1,041)	2,389(0,939)○Δ	2,154(1,201)	3,355(1,155)□	3,372(0,717)□	2,712(2,766)	3,474	0,015
P-L	1,972(0,845)	2,175(1,081)	1,723(1,239)	2,367(1,242)	3,049(0,974)	4,18(2,816)	1,726	0,162

Table 4.5: Degree of anisotropy (DA) mean and standard deviation of structural variables by region, along with results of analysis of variance (p=0,05).

Symbols indicate posthoc pairwise comparisons between groups, *Pongo* (□), *Pan* (○), *Gorilla* (●), *Papio* (◇), *Homo* (Δ), *A. africanus*.

Region	<i>Papio</i> ◇ n=10	<i>Pongo</i> □ n=10	<i>Gorilla</i> ● n=11	<i>Pan</i> ○ n=10	<i>Homo</i> Δ n=7	<i>A. africanus</i> n=4	ANOVA F	P
A-M	0,74(0,055)Δ	0,689(0,08)Δ	0,717(0,09)Δ	0,722(0,074)Δ	0,517(0,117)◇○●□	0,477(0,093)	9,152	<0,0001
A-C	0,669(0,048)	0,721(0,106)Δ	0,724(0,073)Δ	0,647(0,128)	0,545(0,12)●□	0,432(0,171)	4,488	0,004
A-L	0,774(0,062)Δ○	0,688(0,098)	0,679(0,079)	0,652(0,085)◇	0,61(0,097)◇	0,499(0,18)	4,593	0,004
C-M	0,779(0,074)●□○Δ	0,613(0,112)◇	0,561(0,081)◇	0,634(0,041)◇	0,649(0,062)◇	0,559(0,064)	10,794	<0,0001
C-C	0,74(0,069)□	0,604(0,103)◇	0,637(0,112)	0,69(0,081)	0,65(0,076)	0,623(0,04)	3,295	0,0193
C-L	0,816(0,062)Δ●	0,74(0,099)	0,687(0,097)◇	0,762(0,08)	0,679(0,094)◇	0,624(0,046)	3,920	0,008
P-M	0,765(0,054)Δ	0,74(0,126)	0,676(0,091)	0,714(0,105)	0,607(0,099)◇	0,605(0,08)	3,308	0,019
P-C	0,81(0,043)Δ●○	0,745(0,085)Δ	0,682(0,086)◇	0,7123(0,089)Δ◇	0,59(0,063)◇□○	0,619(0,037)	9,432	<0,0001
P-L	0,869(0,046)Δ□●	0,698(0,121)◇	0,741(0,086)◇	0,78(0,123)	0,685(0,086)◇	0,526(0,050)	5,394	0,001

Table 4.6: Structural Model Index (SMI) mean and standard deviation of structural variables by region, along with results of analysis of variance (p=0,05).

Symbols indicate posthoc pairwise comparisons between groups, *Pongo* (□), *Pan* (○), *Gorilla* (●), *Papio* (◇), *Homo* (Δ), *A. africanus*.

Region	<i>Papio</i> ◇ n=10	<i>Pongo</i> □ n=10	<i>Gorilla</i> ● n=11	<i>Pan</i> ○ n=10	<i>Homo</i> Δ n=7	<i>A. africanus</i> n=4	ANOVA F	P
A-M	2,63(0,508)	3,016(0,627)	2,724(0,607)	3,023(0,459)	2,946(1,561)	1,617(1,66)	0,533	0,712
A-C	2,508(0,707)○	2,406(0,492)○	2,486(0,44)○	3,603(0,819)Δ□●◇	2,258(1,334)○	1,352(1,432)	4,762	0,003
A-L	2,626(0,524)Δ	2,617(0,402)Δ	2,41(0,389)	2,569(0,623)Δ	1,683(0,928)◇□○	0,795(1,573)	3,683	0,011
C-M	2,83(0,363)	3,439(0,592)Δ	3,013(0,585)	3,174(0,489)Δ	2,201(0,953)□○	1,503(1,13)	4,874	0,003
C-C	2,8(0,591)Δ	3,377(0,508)Δ	2,89(0,524)Δ	3,088(0,58)Δ	1,712(0,932)□○●◇	0,189(1,313)	8,133	<0,0001
C-L	3,136(0,584)Δ	2,998(0,388)Δ	2,682(0,364)Δ	3,117(0,483)Δ	1,368(1,4)◇○□●	0,283(1,389)	9,237	<0,0001
P-M	2,256(0,529)	2,7(0,504)	2,744(0,587)	2,878(0,544)	2,578(1,269)	0,442(1,64)	1,152	0,345
P-C	2,3(0,472)	2,457(0,318)	2,642(0,571)	2,605(0,492)	2,159(1,27)	0,441(1,338)	0,873	0,488
P-L	2,72(0,587)	2,971(0,607)	2,931(0,634)	3,05(0,474)	2,214(1,394)	0,55(2,282)	1,589	0,195

Table 4.7: Bone surface to bone volume ratio (BS/BV) mean and standard deviation of structural variables by region, along with results of analysis of variance (p=0,05). Symbols indicate posthoc pairwise comparisons between groups, *Pongo* (□), *Pan* (○), *Gorilla* (●), *Papio* (◇), *Homo* (Δ), *A. africanus*.

Region	<i>Papio</i> ◇ n=10	<i>Pongo</i> □ n=10	<i>Gorilla</i> ● n=11	<i>Pan</i> ○ n=10	<i>Homo</i> Δ n=7	<i>A. africanus</i> n=4	ANOVA F	P
A-M	5,104(0,687)●Δ	4,129(1,321)●	2,185(0,553)◇○□	4,57(0,873)●	3,361(2,198)◇	3,98(0,625)	9,838	<0,0001
A-C	4,984(0,599)●○□	3,68(0,445)◇	2,561(0,831)◇Δ	3,636(1,048)◇	3,915(1,77)●	4,992(0,86)	8,237	<0,0001
A-L	5,776(0,564)●Δ□○	4,226(0,553)◇●	2,695(0,521)◇○□Δ	4,288(0,601)●◇	3,736(0,364)◇●	5,665(1,712)	44,464	<0,0001
C-M	4,523(0,997)●□	2,839(0,708)◇	1,594(1,034)◇○Δ	3,715(0,379)●	3,538(1,814)●	4,495(0,507)	12,069	<0,0001
C-C	3,861(0,813)●	2,614(0,906)	1,559(0,838)◇Δ○	3,5278(0,686)●	3,611(1,778)●	4,232(0,269)	9,149	<0,0001
C-L	3,804(0,764)●	3,393(0,455)●	2,033(0,637)Δ◇○□	3,7(0,453)●	4,549(1,808)●	4,441(0,447)	10,659	<0,0001
P-M	4,674(0,945)●	3,629(0,588)●	2,174(0,571)○◇Δ□	4,838(0,849)●	4,146(1,848)●	4,683(0,267)	12,619	<0,0001
P-C	4,441(0,951)●	3,803(0,541)●	2,418(0,725)○◇Δ□	4,578(0,6)●	3,954(1,416)●	4,512(0,494)	10,7647	<0,0001
P-L	4,684(0,782)●	3,892(0,554)●	2,329(0,602)◇○Δ□	4,261(0,764)●	3,916(1,294)●	6,75(3,326)	13,398	<0,0001

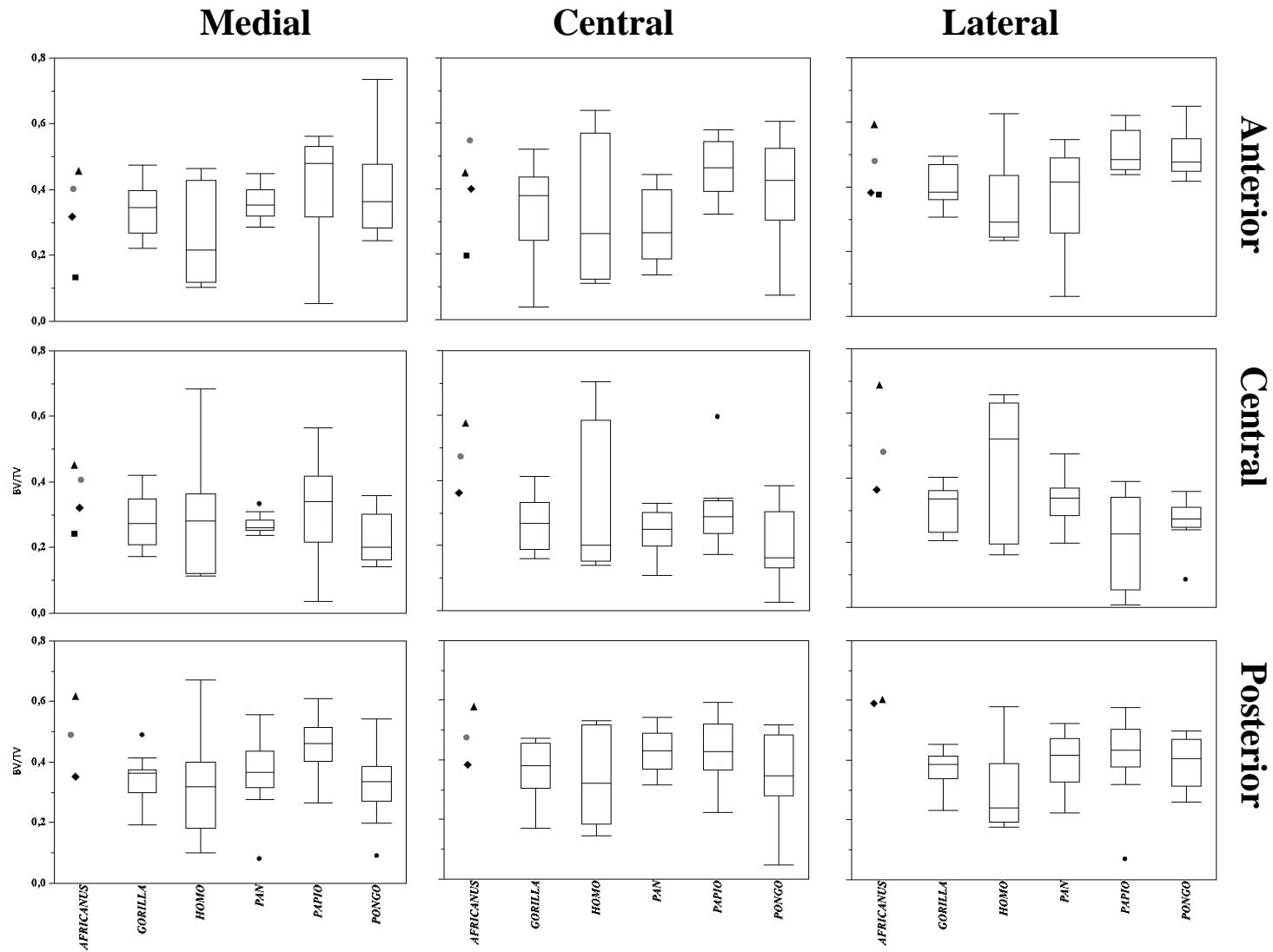


Figure 4.1. Boxplots indicating bone volume fraction (BV/TV) by subregion across groups. *Africanus* specimens represented by symbols (▲ StW 358, ◆ StW 389, ■ StW 515 and ● StW 567).

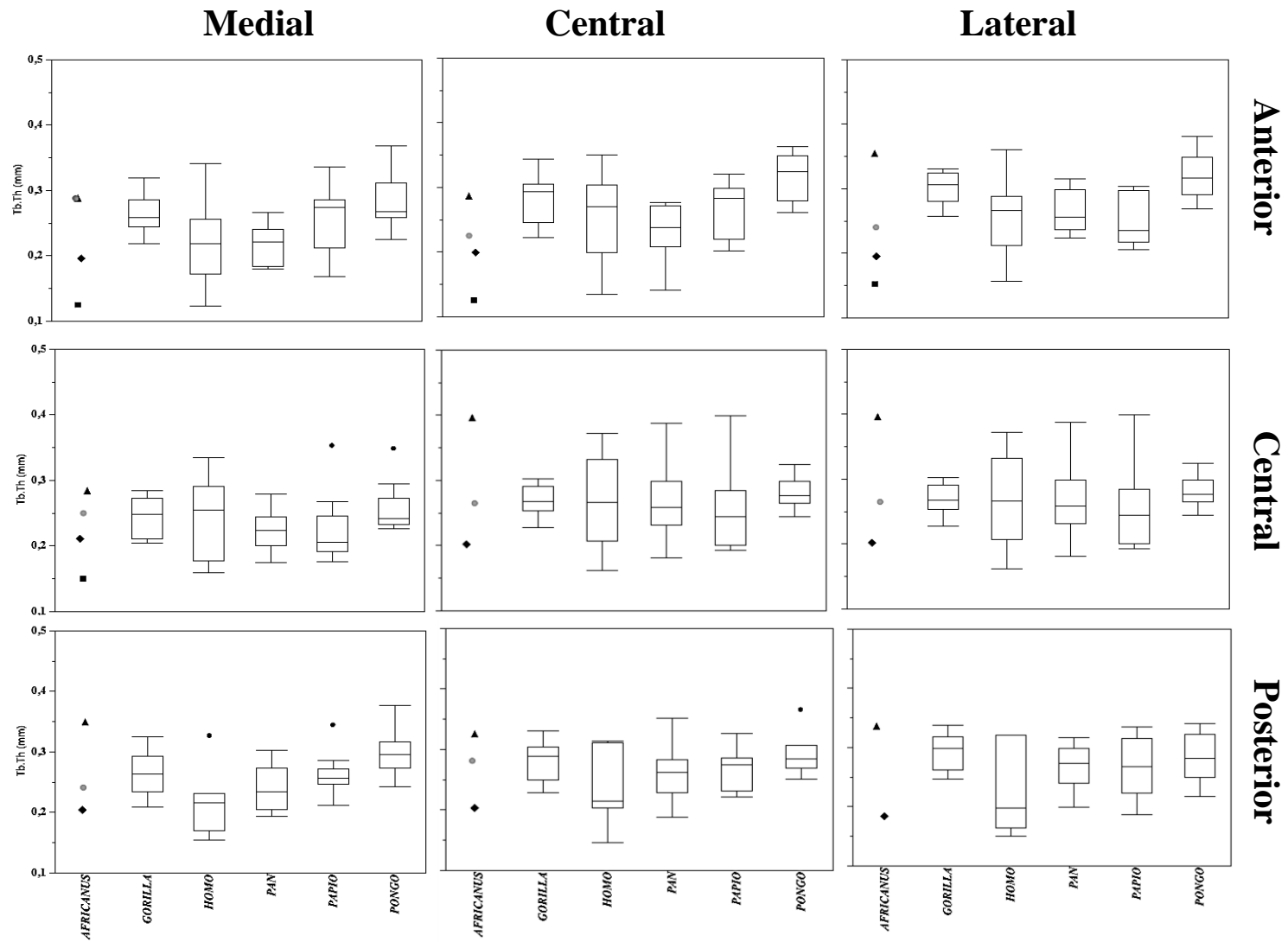


Figure 4.2. Boxplots indicating trabecular thickness (Tb.Th) by subregion across groups. *Africanus* specimens represented by symbols (▲ StW 358, ◆ StW 389, ■ StW 515 and ● StW 567).

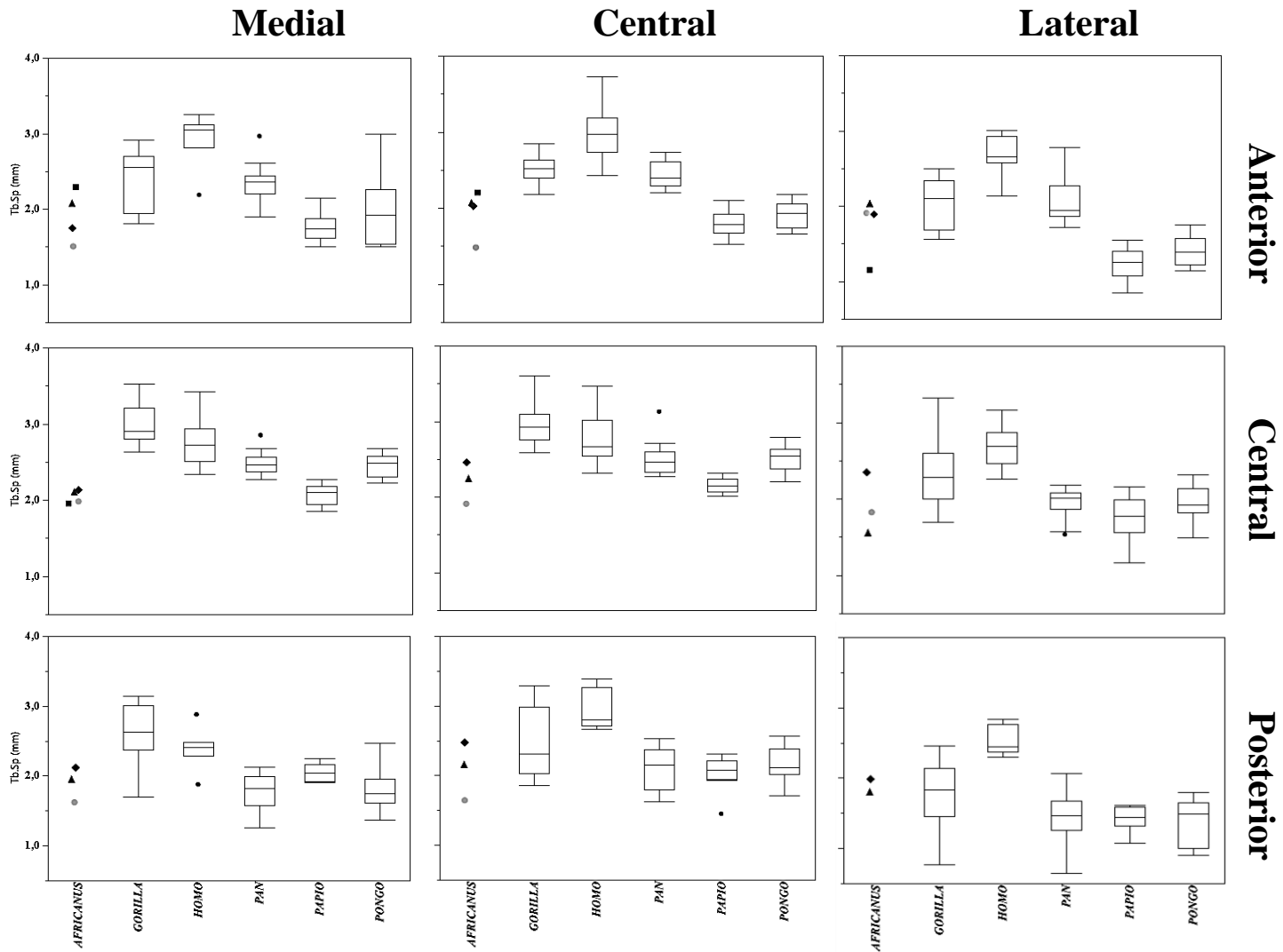


Figure 4.3. Boxplots indicating trabecular spacing (Tb.Sp) by subregion across groups. *Africanus* specimens represented by symbols (▲StW 358, ◆ StW 389, ■StW 515 and ●StW 567).

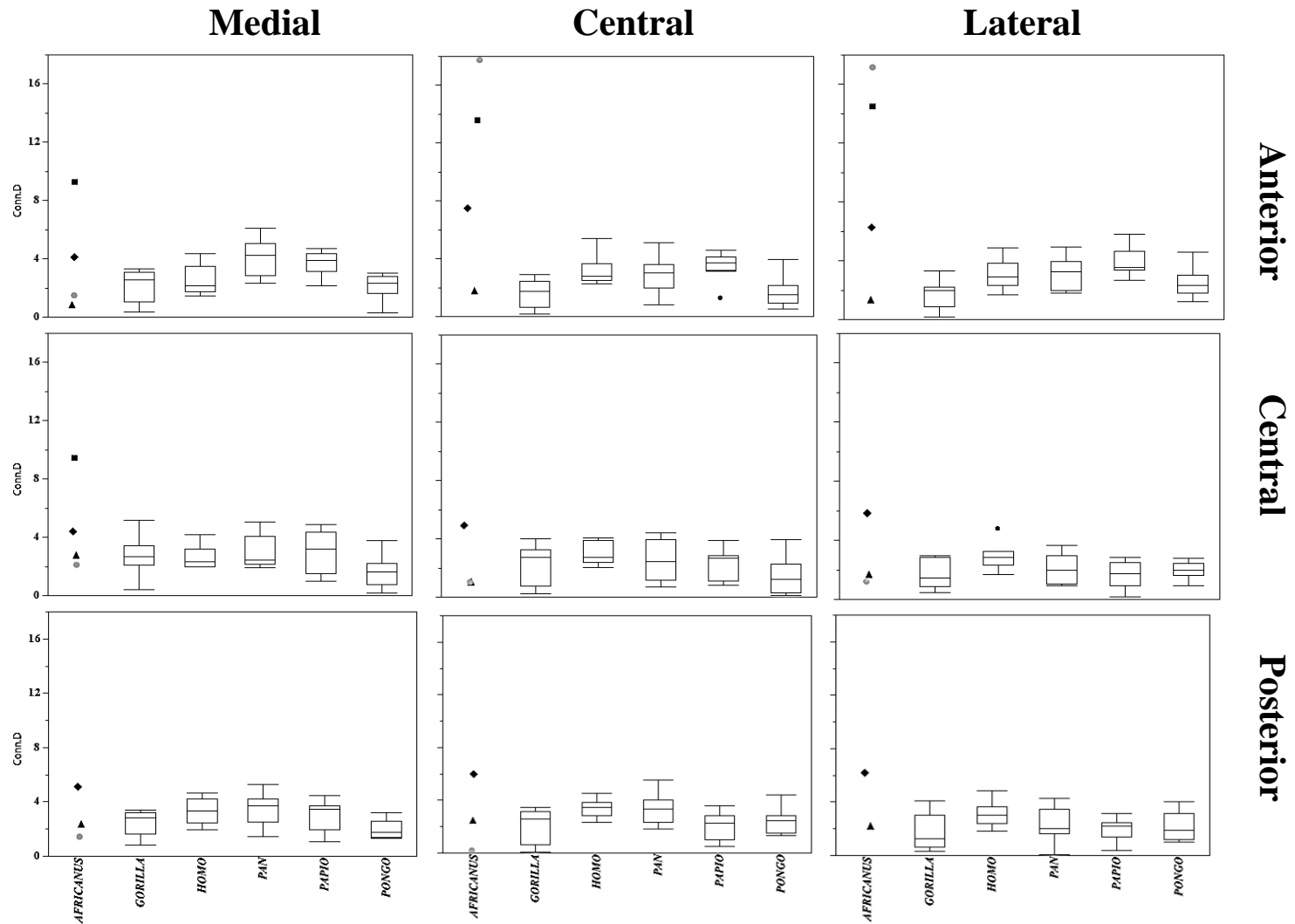


Figure 4.4. Boxplots indicating connectivity density (Conn.D) by subregion across groups. *Africanus* specimens represented by symbols (▲ StW 358, ◆ StW 389, ■ StW 515 and ● StW 567).

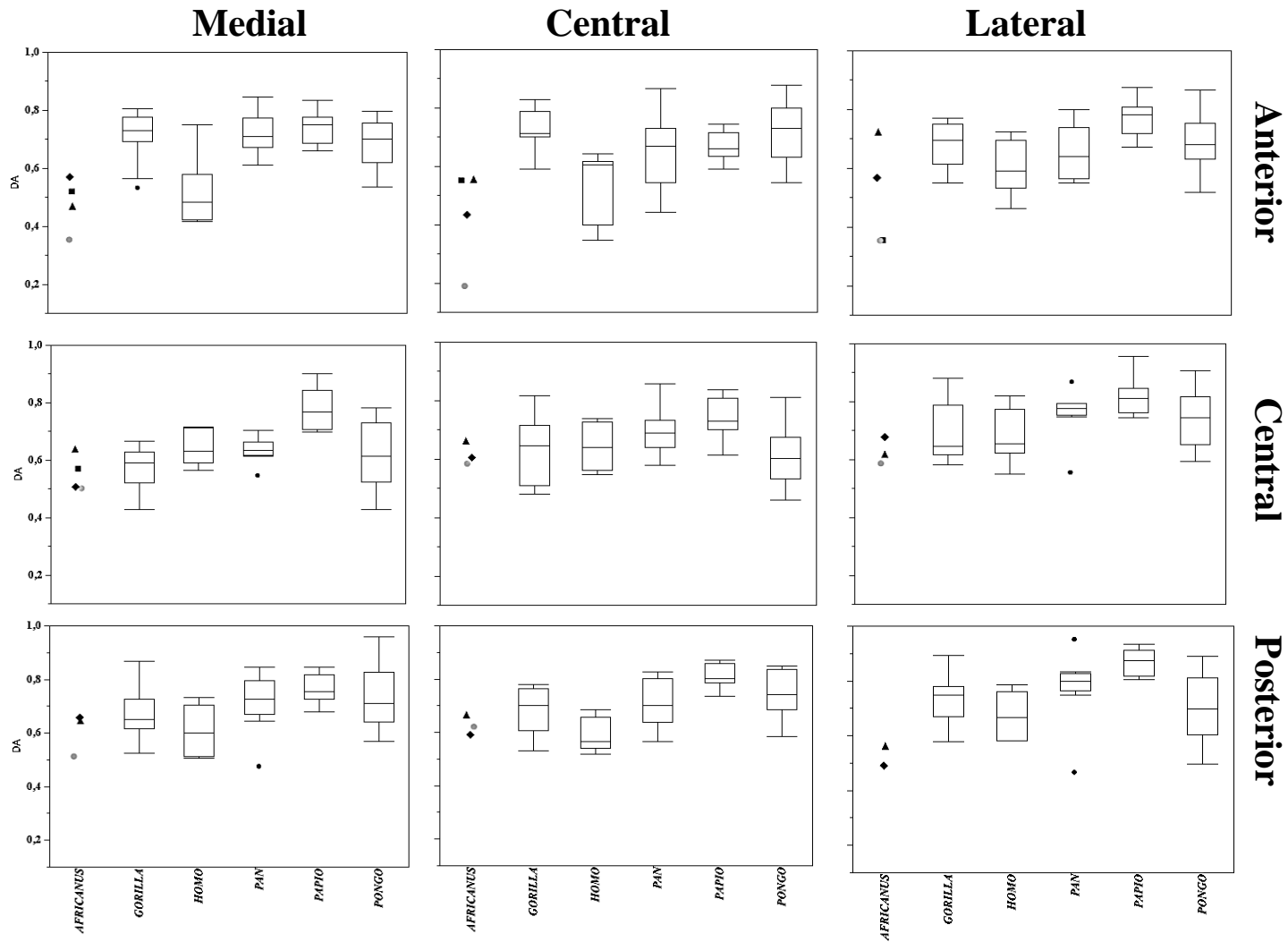


Figure 4.5. Boxplots indicating degree of anisotropy (DA) by subregion across groups. *Africanus* specimens represented by symbols (▲ StW 358, ◆ StW 389, ■ StW 515 and ● StW 567).

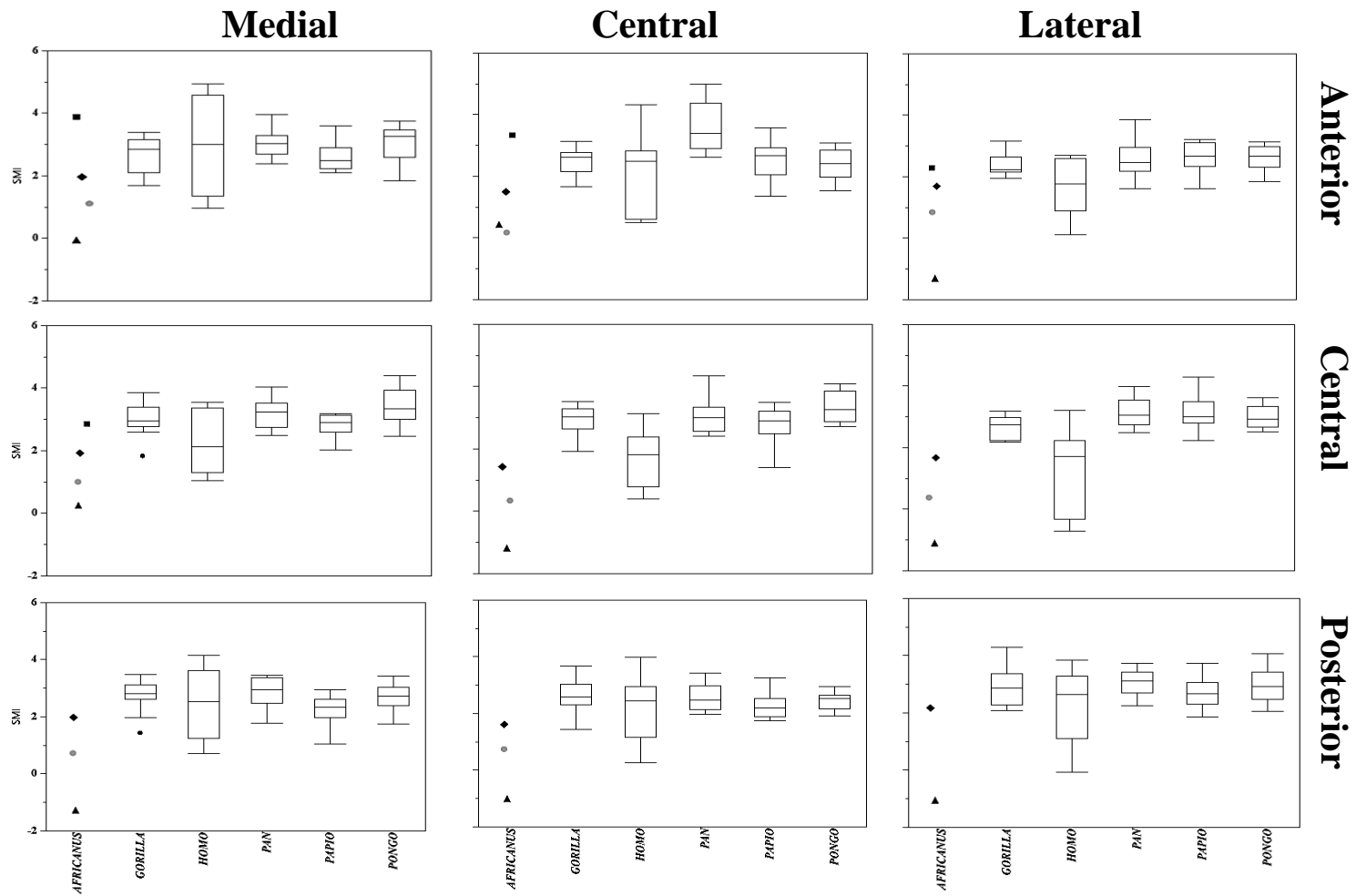


Figure 4.6. Boxplots indicating structural model index (SMI) by subregion across groups. *Africanus* specimens represented by symbols (▲ StW 358, ◆ StW 389, ■ StW 515 and ● StW 567).

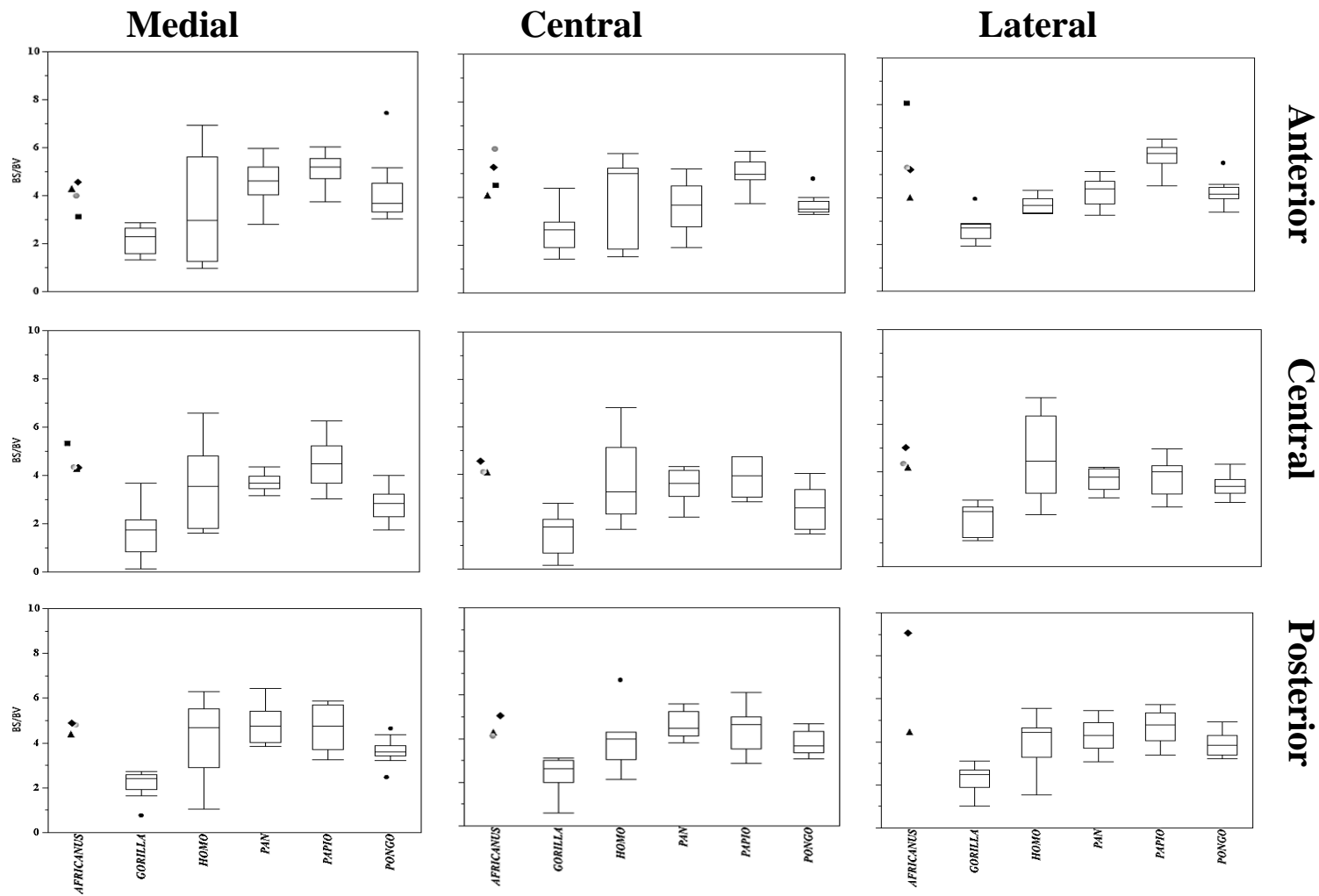


Figure 4.7. Boxplots indicating bone surface to bone volume ratio (BS/BV) by subregion across groups. *Africanus* specimens represented by symbols (▲ StW 358, ◆ StW 389, ■ StW 515 and ● StW 567).

4.3. Intraspecific variation in trabecular properties of the distal tibia in humans and extant non-human primates.

4.3.1. Trabecular analyses of the distal tibia in *Homo sapiens* (modern human hunter-gatherers).

Table 4.8. Summary of analysis of variance for trabecular parameters in the distal tibia of modern *H.sapiens* (* parameters with statistically significantly differences between VOIs in the distal tibia).

ANOVA Summary Homo (n=7)					
Parameter	DF	Sum of squares	Mean square	F Ratio	Prob>F
BV/TV	8	0,125	0,016	0,585	0,861
Tb.Th	8	0,015	0,002	0,546	0,817
Tb.Sp*	8	2,555	0,319	2,845	0,010
Conn.D	8	6,502	0,813	0,710	0,681
DA*	8	0,185	0,023	2,706	0,014
SMI	8	12,956	1,619	1,042	0,417
BS/BV	8	4,716	0,589	0,252	0,978

4.3.1.1. BV/TV, Tb.Th, Tb.Sp, and Conn.D structural patterns in *H. sapiens* (modern hunter-gatherers).

Comparisons of BV/TV between VOIs in the modern human sample yielded no statistically significant differences (Table 4.8, Fig 4.8A), although a general pattern of higher average BV/TV was observed in the anterior and posterior regions than the central regions. BV/TV was highest on average at VOI2 (A-C) in the anterior region, at VOI6 (C-L) in the central region and VOI8 (P-C) in the posterior region. In the anterior region, average strut thickness mirrored the increasing lateral trend observed in average BV/TV in the anterior and central volumes (L>M>C), except in the posterior region where the thinnest struts on average were observed in the lateral volume (C>M>L) (Table 4.8, Fig 4.8B).

Comparisons of average Tb.Th between VOIs of modern *Homo* did not reveal any statistically significant differences across regions in the distal tibia (Table 4.8)), although there is a trend of decreasing thickness in the posterior region compared to the anterior and central regions (Fig 4.8B). The average thickest struts in the anterior region were observed at VOI3 (A-L), in the central region at VOI6 (C-L), and the posterior region at VOI8 (P-C).

The anterior and central regions demonstrated a similar pattern in average Tb.Sp where $C > M > L$. The posterior region differed in average Tb.Sp where $C > L > M$ (Table 4.8, Fig 4.8C). The central region exhibited a lower average Tb.Sp overall when compared to the anterior region. The lowest observed average Tb.Sp was at VOI7 (P-M), and the highest at VOI2 (A-C) (Fig 4.8C).

Comparisons of average Conn.D in modern *Homo* did not reveal any statistically significant differences (Table 4.8, Fig 4.8D), although the central VOIs (VOI4-VOI6) demonstrated a trend of lower average connectivity when compared to the anterior and posterior regions (highest). The mean highest connectivity in the anterior region was observed at VOI2 (A-C), in the central region at VOI5 (C-C) and the posterior region at VOI8 (P-C) and coincided with highest Tb.Sp in the respective regions.

4.3.1.2. DA, SMI and BS/BV structural patterns in *Homo sapiens* (modern hunter-gatherers).

There is a posteriorward trend towards increased DA, such that VOIs generally exhibit higher average DA values in the posterior region (Table 4.8, Fig 4.9A). Central VOIs have less variation in DA across the region when compared to the variation observed in the different VOIs in the anterior and posterior regions. There is also a lateralward trend towards increased DA, such that VOIs generally exhibit higher DA values in the lateral than the central and medial subregions (Table 4.8, Fig 4.9A) ($L > C > M$). The lateral region exhibited the highest average DA at VOI3 (A-L), VOI6 (C-L) and VOI9 (P-L). DA was significantly greater in VOI6 (C-L) and VOI9 (P-L) than VOI1 (A-M).

Comparisons between SMI and BS/BV of VOIs in modern *Homo* were not statistically significant in the distal tibia (Table 4.8, Fig 4.9B, C). Average SMI is generally lowest in the central regions and highest in the anterior regions ($A > C > P$). The highest average SMI in the anterior region was observed at VOI1 (A-M), the central region at VOI4 (C-M) and in the posterior region at VOI7 (P-M) (rod-like). Average BS/BV was highest at VOI2 (A-C) in the anterior region, at VOI6 (C-L) in the central region and VOI8 (P-M) in the posterior region. SMI in the central volumes of *Homo* was more rod-like than in the anterior and posterior VOIs.

4.3.2 Trabecular analyses of distal tibia in *P. troglodytes* (common chimpanzee).

Table 4.9. Summary of analysis of variance for trabecular parameters in the distal tibia of *P. troglodytes* (* parameters with statistically significantly differences between VOIs in the distal tibia).

ANOVA Summary <i>Pan</i> (n=10)					
Parameter	DF	Sum of squares	Mean square	F Ratio	Prob>F
BV/TV*	8	0,215	0,027	4,582	0,0001
Tb.Th*	8	0,025	0,003	2,751	0,097
Tb.Sp*	8	10,687	1,336	18,025	<0,0001
Conn.D	8	37,977	2,747	2,895	0,069
DA	8	0,205	0,026	2,958	0,059
SMI	8	7,739	0,967	2,062	0,057
BS/BV*	8	14,508	1,813	4,366	0,0002

4.3.2.1. *BV/TV, Tb.Th, Tb.Sp, and Conn.D structural patterns in P. troglodytes* (common chimpanzee).

Trabecular bone in the distal tibiae of *Pan* demonstrated significant differences in average BV/TV, Tb.Th, Tb.Sp, and BS/BV (Table 4.9). Average BV/TV in *Pan* is lower in the central regions in comparison to the anterior and posterior regions (highest) (Fig 4.10A). The highest average BV/TV in the anterior and central regions was observed laterally at VOI3 (A-L) and VOI6 (C-L) and in the posterior region at VOI8 (P-C). The only statistically significant pairwise post-hoc difference involved VOI2 (A-C), which was significantly lower than the more posterior VOI8 (P-C).

There was a general increasing gradient from medial to lateral in Tb.Th in *Pan*, (L>C>M) (Fig 4.10B). The mean thickness is similar throughout the bone except for the central region (VOI4-6), where a slight decrease in average thickness is observed (Table 4.9, Fig 4.10B). VOI6 was significantly greater than VOI4 in strut thickness.

The central region demonstrated a higher mean Tb.Sp than the anterior and posterior regions (A>C>P) (Table 4.9, Fig 4.10C). A decreasing medial lateral gradient was observed in the anterior, central and posterior regions where the lateral regions demonstrated a lower average Tb.Sp (Fig 4.10C) (L>C>M). Statistically significant differences within a region were

observed in the posterior and central regions where the central VOIs were significantly higher in spacing than the lateral VOIs (VOI5>VOI6, VOI8>VOI9).

Conn.D is higher on average in the posterior region compared to the anterior and central regions in *Pan* and exhibited a lateralward decrease, such that medial regions exhibited a higher connectivity (M>C>L) (Table 4.9, Fig 4.10D). The trabecular architecture of *Pan* is characterized by a high bone volume consisting of fewer, thicker struts that are densely packed across the lateral aspect of the distal tibiae.

4.3.2.2. DA, SMI and BS/BV structural patterns in *P. troglodytes* (common chimpanzee).

Average DA was highest in the anterior region at VOI1 (A-M), in the central region at VOI6 (C-L) and in the posterior region at VOI9 (P-L), the highest DA was observed at VOI9 (P>A>C). DA was generally higher in the posterior region compared to the anterior and central. However, there were no statistically significant differences in average DA over the entire 9 VOIs (Table 4.9, Fig4.11A).

The posterior region was lowest in SMI (C>A>P), although the difference was not significant (Table 4.9, Fig 4.11B). All trabeculae were rod-like, except in VOI2 (A-C) where they were relatively more spherical. Medial VOIs exhibited a lower mean SMI in the posterior region (L>M>C), while in the anterior and central regions the latter VOIs were greater in SMI than the medial and lateral volumes (C>M>L). No statistically significant differences were observed in SMI of any VOIs.

All VOIs in the central region had lower average BS/BV than in the anterior and posterior regions (P>A>C). Average BS/BV was highest in the medial volumes (M>C>L) in the posterior region, in the anterior and central region the central VOI exhibited a lower BS/BV than the lateral (M>L>C) (Fig 4.11C).

4.3.3. Trabecular analyses of distal tibia in *G. gorilla* (western lowland gorilla).

Table 4.10. Summary of analysis of variance for trabecular parameters in the distal tibia of *G. gorilla* (* parameters with statistically significantly differences between VOIs in the distal tibia).

ANOVA Summary <i>Gorilla</i> (n=11)					
Parameter	DF	Sum of squares	Mean square	F Ratio	Prob>F
BV/TV*	8	0,112	0,014	3,314	0,002
Tb.Th*	8	0,033	0,004	5,017	<0.0001
Tb.Sp*	8	14,247	1,783	11,991	<0,0001
Conn.D	8	9,623	1,203	1,305	0,251
DA*	8	0,253	0,032	3,992	0,0004
SMI	8	3,290	0,436	1,549	0,152
BS/BV*	8	7,126	0,891	3,362	0,002

4.3.3.1 BV/TV, Tb.Th, Tb.Sp, and Conn.D structural patterns in *G. gorilla* (western lowland gorilla).

A general trend of increasing medial to lateral average BV/TV was observed across the tibial plafond, as medial VOIs exhibit a lower BV/TV than the lateral except in the posterior region where C>L>M (Fig 4.12A). The central region exhibited the lowest average BV/TV when compared to the posterior and anterior regions. BV/TV in *Gorilla* exhibited statistically significant differences between the anterior and central regions (Table 4.10, Fig 4.12A) where VOI3 (A-L) was significantly greater than VOI4 (C-M) and VOI5 (C-C) in the central region of the distal tibia.

Lateral VOIs exhibited the thickest trabecular struts on average, thus exhibiting a lateralward trend (Fig 4.12B). Average Tb.Th in the anterior region was slightly higher than in the posterior region (Table 4.10, Fig 4.12B). In the anterior region, VOI2 (A-C) was significantly greater than VOI4 (C-M), VOI3 (A-L) was also significantly greater than VOI5 (C-C), while VOI9 (P-L) demonstrated significantly thicker struts than VOI4 (C-M).

Average Tb.Sp in the central region was highest when compared to anterior and posterior regions, while the anterior region exhibited the lowest overall Tb.Sp (Fig 4.12C). Average Tb.Sp exhibited a decreasing lateralward trend, such that the lateral regions demonstrated the lowest Tb.Sp at VOI9 (P-L) (Table 4.10, Fig 4.12C). Some anterior and central VOIs differed significantly as VOI3 (A-L) demonstrated a significantly lower separation than the central

VOI4 (C-M) and VOI5 (C-C). The same observation was made between some of the central and posterior regions, as VOI9 (P-L) was statistically significantly lower in separation than VOI4 (C-M) and VOI5 (C-C). In the central region, VOI4 and VOI5 (C-M, C-C) were significantly higher in Tb.Sp than the lateral VOI6 (C-L), similar to the posterior region where VOI8 (P-C) was significantly greater in Tb.Sp than VOI9 (P-M) (Fig 4.12C).

Average Conn.D showed little variation from anterior to posterior (Table 4.10, Fig 4.12D), but exhibited slightly greater connectivity in the central and posterior regions as opposed to the anterior. Lateral regions in particular, on the other hand, exhibited some differences from anterior to posterior. For example, the central-lateral VOI6 (C-L) is statistically significantly greater than the posterior-lateral VOI9 (P-L). A general lateralward decrease in the central and posterior regions (L>C>M) was observed (Table 4.10, Fig 4.12D).

4.3.3.2 DA, SMI and BS/BV structural patterns in *G. gorilla* (western lowland gorilla).

Central regions were lower in average DA than the anterior and posterior regions (Table 4.10, Fig 4.13A); the lowest average DA recorded was at VOI4 (C-M). Average DA in the central and posterior regions was highest at the lateral VOIs (i.e. VOI6 (C-L) and VOI9 (P-L)) (Table 4.10, Fig 4.13A). The anterior VOIs were significantly greater than the central VOIs (VOI1, VOI2>VOI4), and two of the posterior VOIs (VOI8, VOI9) were also significantly higher in DA than VOI4 (C-M).

SMI in *Gorilla* yielded no statistically significant differences across the tibial plafond, although the anterior and central regions were similar in having a higher SMI at the medial VOIs (VOI1, VOI4) (Table 4.10, Fig 4.13B), and were mostly rod-like in structure.

BS/BV in *Gorilla* was generally low (< 4) compared to other taxa (Fig 4.13C). The central VOIs were lower in average BS/BV than those in the anterior and posterior regions. Anterior and central regions exhibited a lateralward increase in BS/BV where VOI3, VOI6>VOI1, VOI4, however, in the posterior region a different trend was apparent (i.e., C>L>M) (Table 4.10, Fig 4.13C). Two anterior VOIs (VOI2, VOI3) were statistically higher in BS/BV than two central VOIs (VOI4, VOI5).

4.3.4. Trabecular analyses of distal tibia in *P. pygmaeus* (Bornean orangutan).

Table 4.11. Summary of analysis of variance for trabecular parameters in the distal tibia of *P. pygmaeus* (* parameters with statistically significantly differences between VOIs in the distal tibia).

ANOVA Summary <i>Pongo</i> (n=10)					
Parameter	DF	Sum of squares	Mean square	F Ratio	Prob>F
BV/TV*	8	1,129	0,142	6,929	<0,0001
Tb.Th*	8	0,061	0,008	3,691	0,001
Tb.Sp*	8	12,029	1,504	20,728	<0,0001
Conn.D	8	8,398	1,045	1,403	0,207
DA*	8	0,223	0,028	2,551	0,016
SMI*	8	11,087	1,386	5,473	<0,0001
BS/BV*	8	88,374	11,047	6,208	<0.0001

4.3.4.1. BV/TV, Tb.Th, Tb.Sp, and Conn.D structural patterns in *P. pygmaeus* (Bornean orangutan).

Average BV/TV in the anterior VOIs of the distal tibia were higher than those of the posterior, while VOIs of the central region exhibited the lowest overall average BV/TV (A>P>C) (Table 4.11, Fig 4.14A). The lateral regions across the ML axis in the anterior and posterior regions demonstrated an increasing lateral gradient (L>C>M) in BV/TV except in the central region where L>M>C (Fig 4.14A).

Tb.Th demonstrated generally thicker struts on average in the anterior regions compared to the central and posterior regions (A>P>C) (Table 4.11, Fig 4.14B). Although not significantly different, there was a trending increasingly lateral gradient in trabecular thickness across the ML axis (L>C>M) except in the posterior region where an increasingly medial gradient was observed (M>C>L) (Fig 4.14B). Significant differences in thickness occurred between the anterior and central regions where VOI1 and VOI3>VOI4 and VOI5.

Average Tb.Sp was greater in the central regions across the AP axis (C>A>P) (Table 4.11, Fig 4.7C). The medial and central regions exhibit higher separation than the lateral regions (VOI2>VOI3 and VOI4, VOI5>VOI6 and VOI8>VOI9). The lowest average separation in the ML axis occurs at the lateral regions (VOI3, VOI6, VOI9) (Fig 4.14C). The central region is significantly higher in separation than the posterior region (VOI4-VOI6 > VOI7-VOI9).

Conn.D yielded no statistically significant differences between regions in the distal tibia although the central regions demonstrated lower average connectivity than the anterior and posterior regions and was higher in the lateral VOIs (VOI3, VOI6, VOI9) than in the medial and VOIs (VOI1, VOI4, VOI7) (Table 4.11, Fig 4.14D).

4.3.4.2. DA, SMI and BS/BV structural patterns in *Pongo pygmaeus* (Bornean orangutan).

DA values across the distal tibia are higher on average in the anterior and posterior regions ($P > A > C$) (Table 4.11., Fig 4.15A). Average DA in the anterior and posterior VOIs were highest in the central VOI (VOI2 and VOI5) (Fig 4.14A), the central region differed as the highest DA was observed in the lateral VOI (VOI6).

Average SMI in the distal tibia of *Pongo* was generally higher in the central region across the AP axis ($C > A > P$) (Table 4.11, Fig 4.15B). SMI across the ML axis in the anterior and central regions were highest on average at the medial VOIs (VOI1, VOI4), in the posterior region SMI was highest at the lateral VOI (VOI9) (Fig 4.15B) and were approaching solid spherical state. The central VOIs (VOI4, VOI5) were significantly greater in SMI than the anterior VOIs (VOI2, VOI3). The central VOIs were also significantly higher than the posterior VOIs (VOI4, VOI5 $>$ VOI7, VOI8) and were generally rod-like in shape (Fig 4.15B).

Average BS/BV in *Pongo* was lowest in the central regions across the AP axis ($A > P > C$). There was a trending increasingly lateral gradient across the ML axis as the lateral VOIs (VOI3, VOI6, VOI9) demonstrated a higher average BS/BV than the medial VOIs (VOI1, VOI4, VOI7). The anterior region demonstrated significantly higher BS/BV than the central region (VOI2, VOI3 $>$ VOI5, VOI6) (Fig 4.15C).

4.3.5. Trabecular analyses of distal tibia in *P. hamadryas* (Hamadryas baboon).

Table 4.12. Summary of analysis of variance for trabecular parameters in the distal tibia of *P. hamadryas* (* parameters with statistically significantly differences between VOIs in the distal tibia).

ANOVA Summary <i>Papio</i> (n=10)					
Parameter	DF	Sum of squares	Mean square	F Ratio	Prob>F
BV/TV*	8	0,437	0,055	4,288	0,0003
Tb.Th	8	0,022	0,003	1,266	0,273
Tb.Sp*	8	5,116	0,64	20,561	<0,0001
Conn.D*	8	57,158	7,145	6,258	<0,0001
DA*	8	0,254	0,032	9,469	<0,0001
SMI	8	5,939	0,742	2,474	0,019
BS/BV*	8	19,836	2,48	6,061	<0,0001

4.3.5.1. BV/TV, Tb.Th, Tb.Sp, and Conn.D structural patterns in *P. hamadryas* (Hamadryas baboon).

All structural parameters quantified in the *Papio* sample were significantly different except average Tb.Th and average SMI (Table 4.12). The lowest average BV/TV observed across the AP axis was in the central region (A>P>C) (Table 4.12, Fig 4.16A). Average BV/TV in the anterior region was highest laterally (VOI3), while in the central and posterior regions average BV/TV was higher medially (VOI4, VOI7) (Table 4.12, Fig 4.16A). The anterior regions were significantly higher in average BV/TV than the central regions (VOI2, VOI3>VOI4-VOI6) (Table 4.12, Fig 4.16A).

Tb.Th was not significantly different across the tibial plafond although the average thickness is consistent along the tibial plafond, slightly increasing in the anterior and posterior regions (P>A>C) (Table 4.12, Fig 4.16B).

Along the AP axis, the anterior region demonstrated the lowest average Tb.Sp (Table 4.12, Fig 4.16C). Tb.Sp across the ML axis demonstrated a decreased average separation in the lateral regions (VOI3, VOI6, VOI9), the lowest at which occurred in the anterior region (VOI3), in general (M>C>L) (Table 4.12, Fig 4.16C). The central VOIs had significantly higher average separation than all of the anterior VOIs (VOI4-VOI6>VOI1-VOI3). The central region also had significantly higher average separation than the posterolateral VOI

(VOI4, VOI5>VOI9). There were also significant differences within VOIs in the same region in *Tb.Sp* (VOI1 and VOI2>VOI3), (VOI5>VOI6) and (VOI7 and VOI8>VOI9).

Conn.D across the AP axis was highest in the anterior regions (A>C>P) (Table 4.12, Fig 4.16D). Conn.D in the central and posterior VOIs demonstrated a trending decreasing connectivity density across the ML axis (M>C>L) in the anterior region the lateral VOI was highest in connectivity (L>M>C) (Table 4.12, Fig 4.16D). The anterior regions demonstrated significantly higher connectivity than the central region (VOI1-VOI3>VOI5, VOI6). The VOIs in the anterior region also demonstrated significantly higher Conn.D than VOIs in the posterior region (VOI1-3>VOI8, VOI9).

4.3.5.2. DA, SMI and BS/BV structural patterns in *P. hamadryas* (*Hamadryas baboon*).

Average DA across the tibial plafond in *Papio* is generally high compared to other taxa (>0.6). Across the AP axis, there is an increasing posterior gradient (P>C>A) (Table 4.12, Fig 4.17A). Across the ML axis the lateral VOIs are highest in average DA, in the central and anterior regions the central VOIs are higher than that of the medial (L>M>C), in the posterior region, the central VOI has a greater DA than the medial (L>C>M) (Table 4.12, Fig 4.17A). The posterior region had significantly higher DA than all of the volumes in the anterior region (VOI7-VOI9>VOI1-VOI3). The central region was also significantly higher in average DA in two posthoc comparisons (VOI4, VOI6> VOI2). There were also significant differences between VOIs in the anterior regions (VOI3>VOI2) and posterior region (VOI9>VOI7).

Trabeculae were mostly rod-like across *Papio* distal tibia. Average SMI was lowest in the posterior region and highest in the central region generally (C>A>P) (Table 4.12, Fig 4.17B). Significant differences in SMI occur between the central and posterior regions where VOI6>VOI7 and VOI8. Average BS/BV is lowest at the central region across the AP axis (A>P>C) (Table 4.12, Fig 4.17C). Average BS/BV was highest in the lateral VOIs in the anterior and posterior region (L>M>C), in the central region the medial VOI was highest in BS/BV (M>C>L). The anterior region (VOI1-VOI3) was significantly higher in average BS/BV than the central VOIs (VOI4-VOI6). The anterolateral VOI (VOI3) was significantly greater in BS/BV than all of the posterior VOIs (VOI7-VOI9).

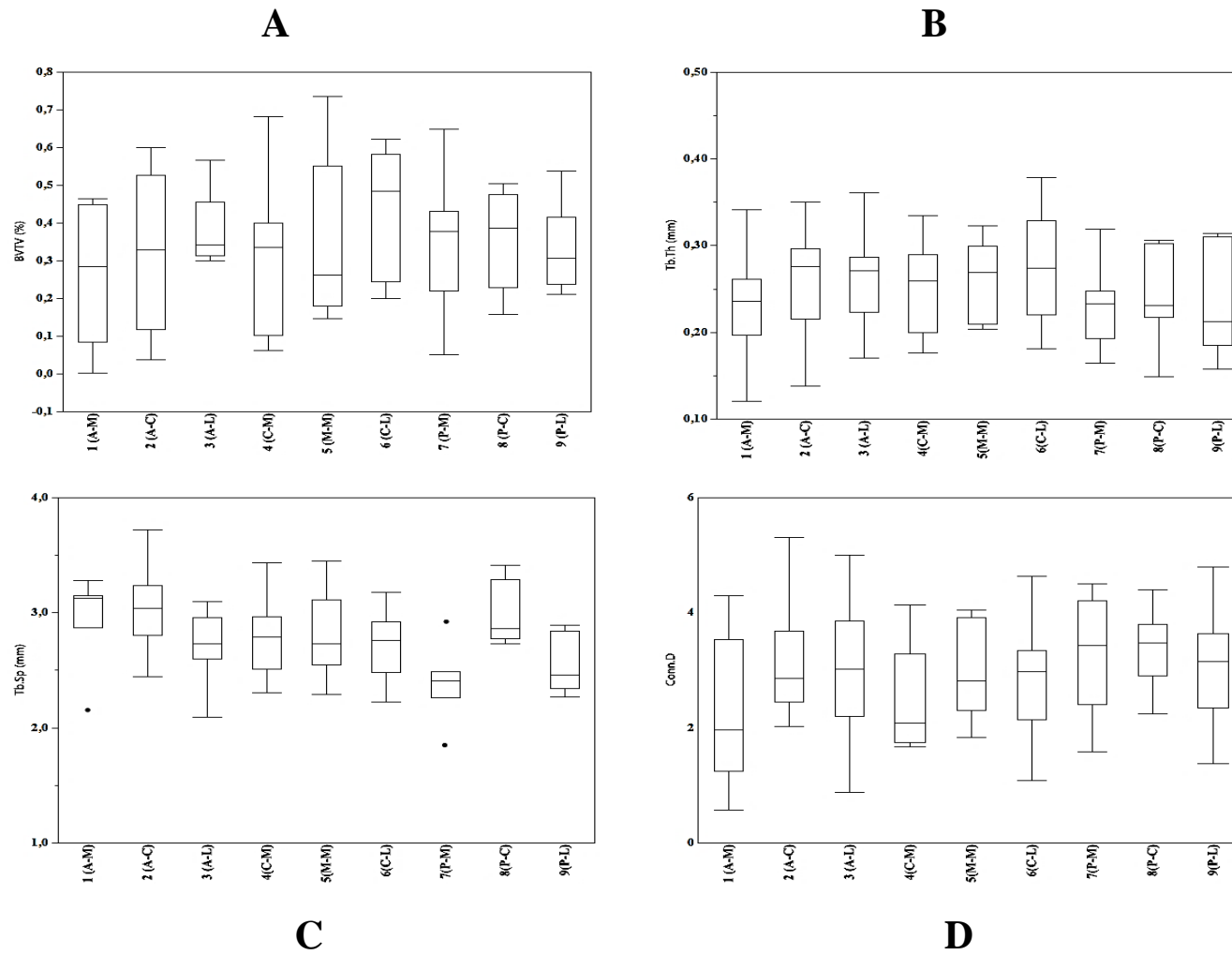


Figure 4.8. Boxplots indicating A) bone volume fraction (BV/TV), B) trabecular thickness (Tb.Th), C) trabecular spacing (Tb.Sp) and D) connectivity density (Conn.D) by subregion in *H. sapiens*.

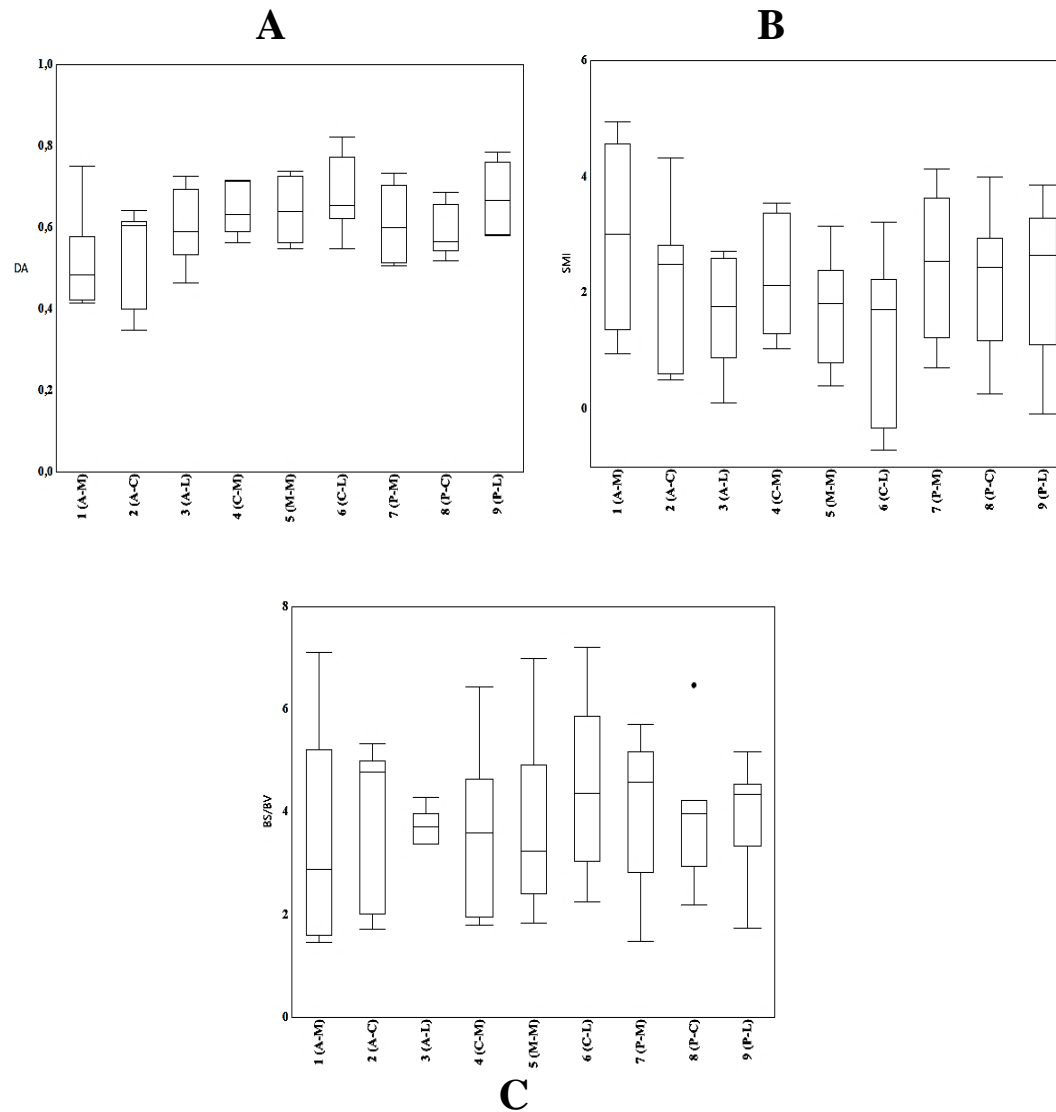


Figure 4.9. Boxplots indicating A) degree of anisotropy (DA), B) structural model index (SMI) and C) bone surface to bone volume ratio (BS/BV) by subregion in *H. sapiens*.

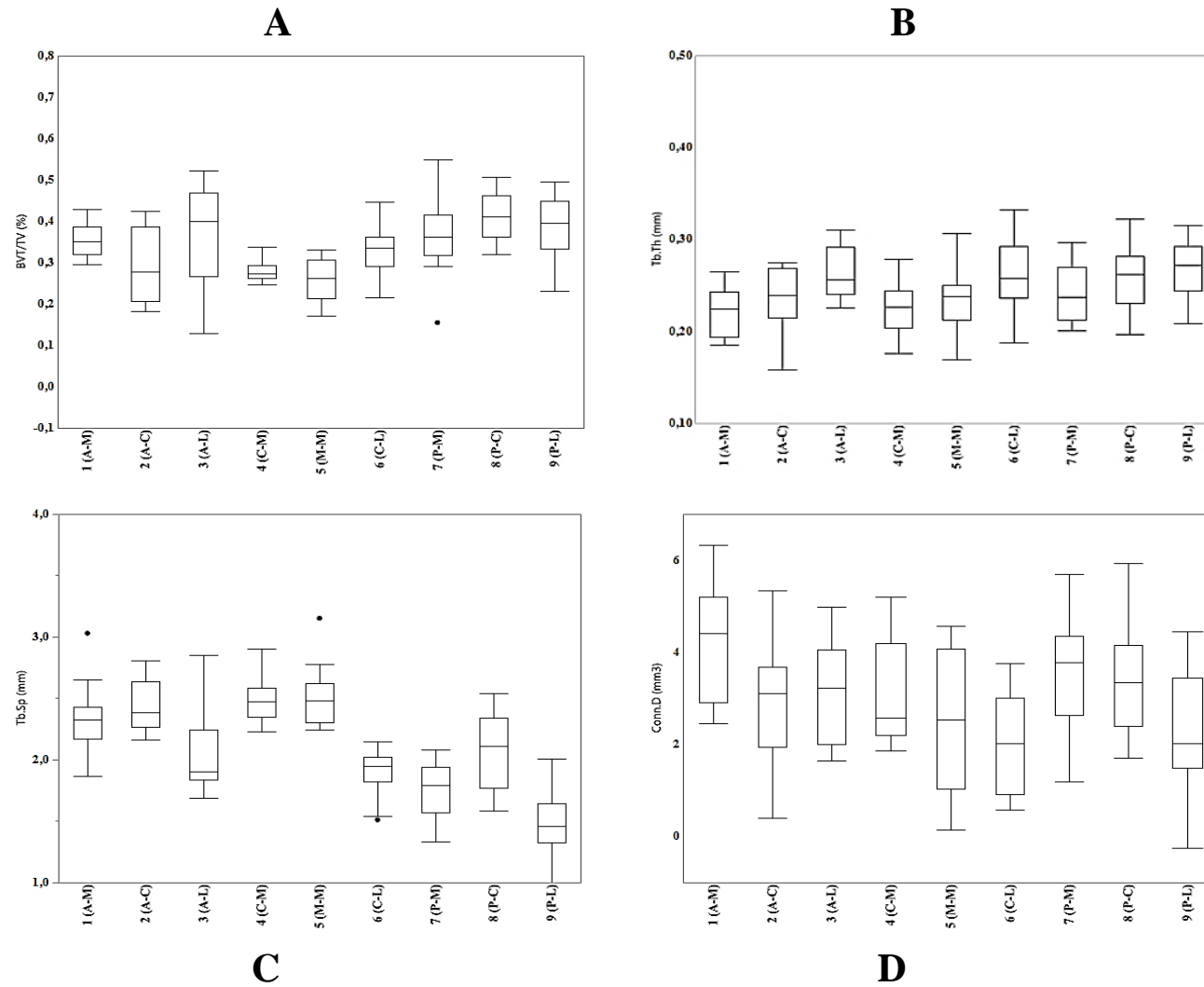


Figure 4.10. Boxplots indicating A) bone volume fraction (BV/TV), B) trabecular thickness (Tb.Th), C) trabecular spacing (Tb.Sp) and D) connectivity density (Conn.D) by subregion in *P. troglodytes*.

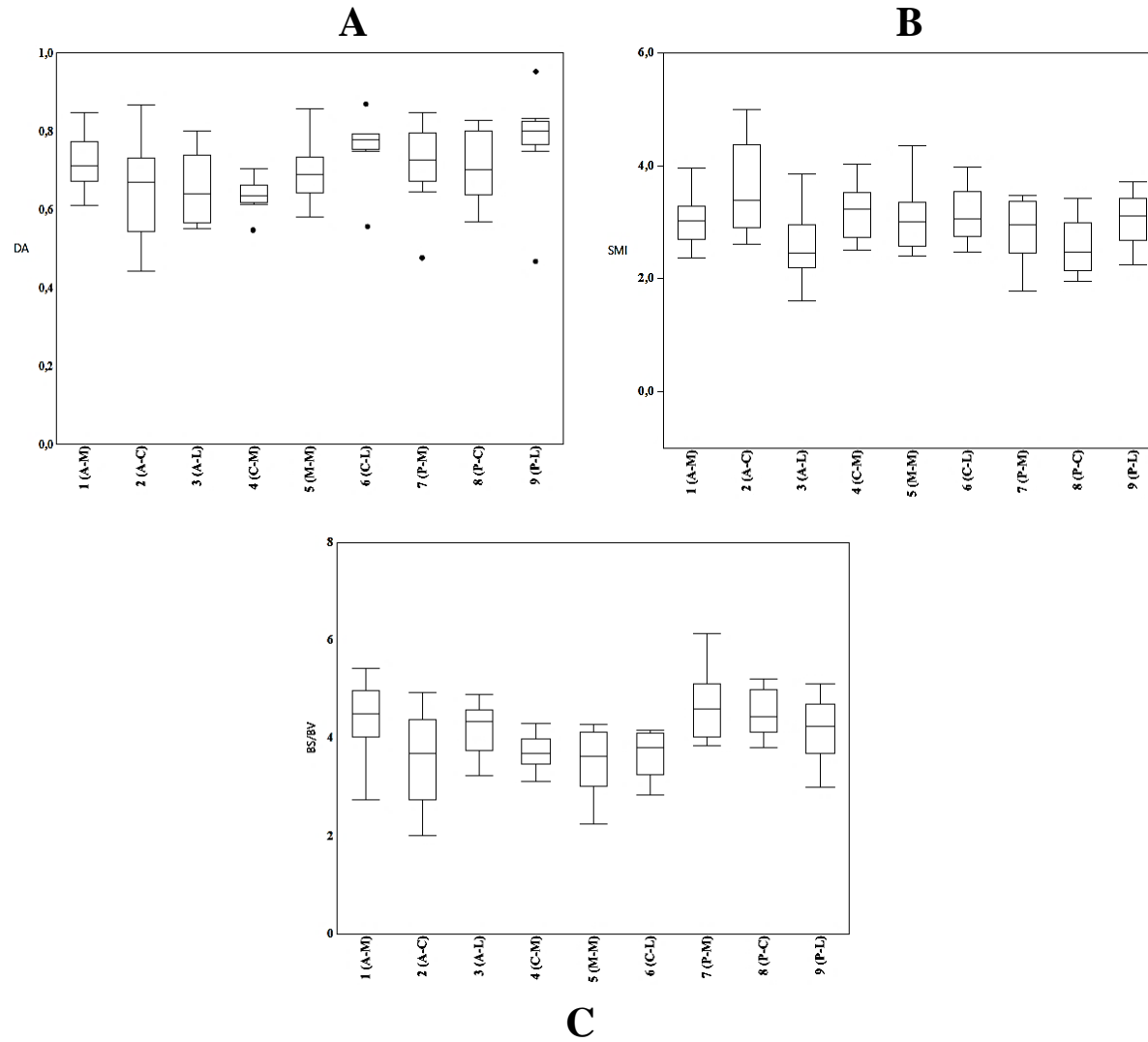


Figure 4.11. Boxplots indicating A) degree of anisotropy (DA), B) structural model index (SMI) and C) bone surface to bone volume ratio (BS/BV) by subregion in *P. troglodytes*.

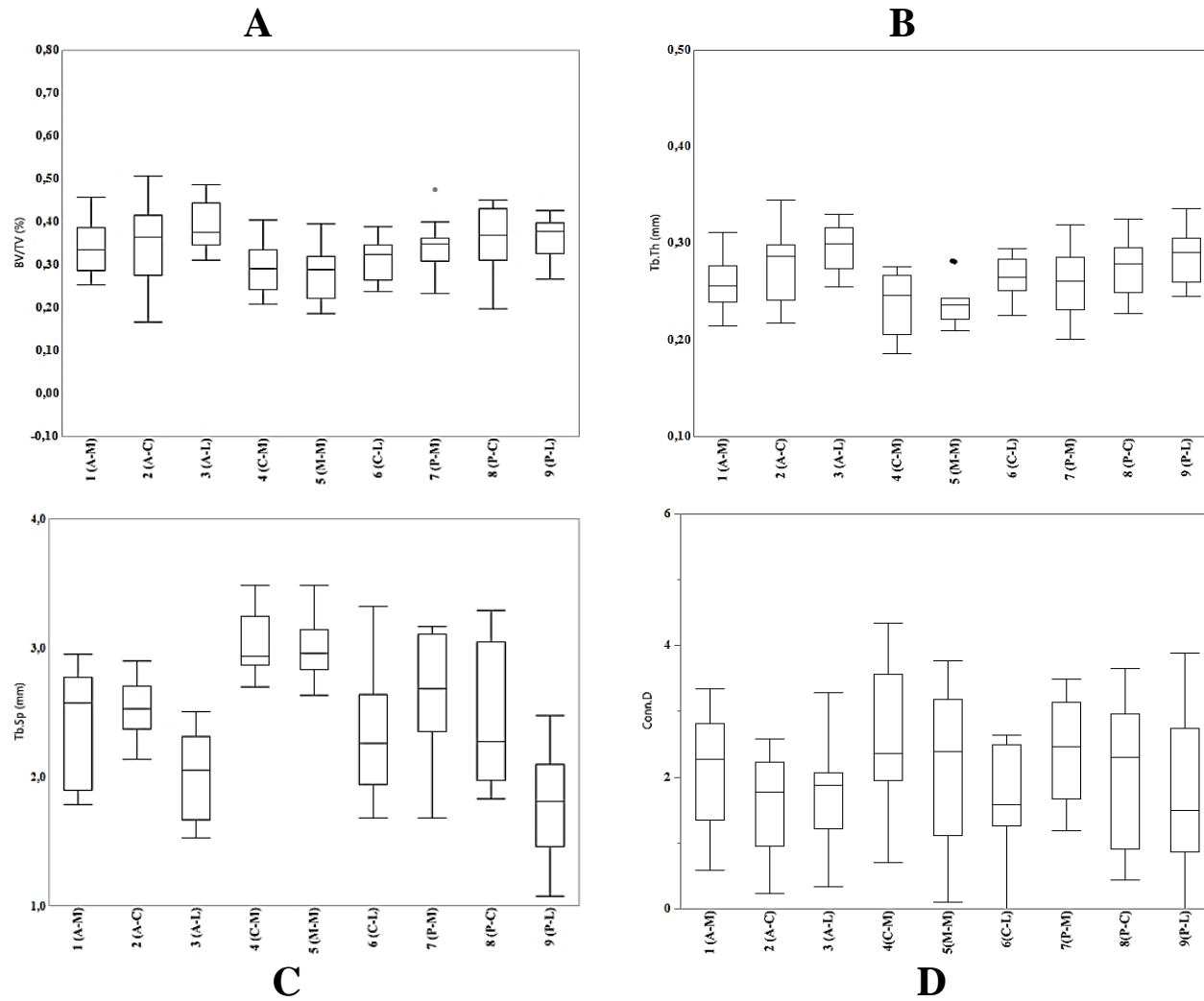


Figure 4.12. Boxplots indicating A) bone volume fraction (BV/TV), B) trabecular thickness (Tb.Th), C) trabecular spacing (Tb.Sp) and D) connectivity density (Conn.D) by subregion in *G. gorilla*.

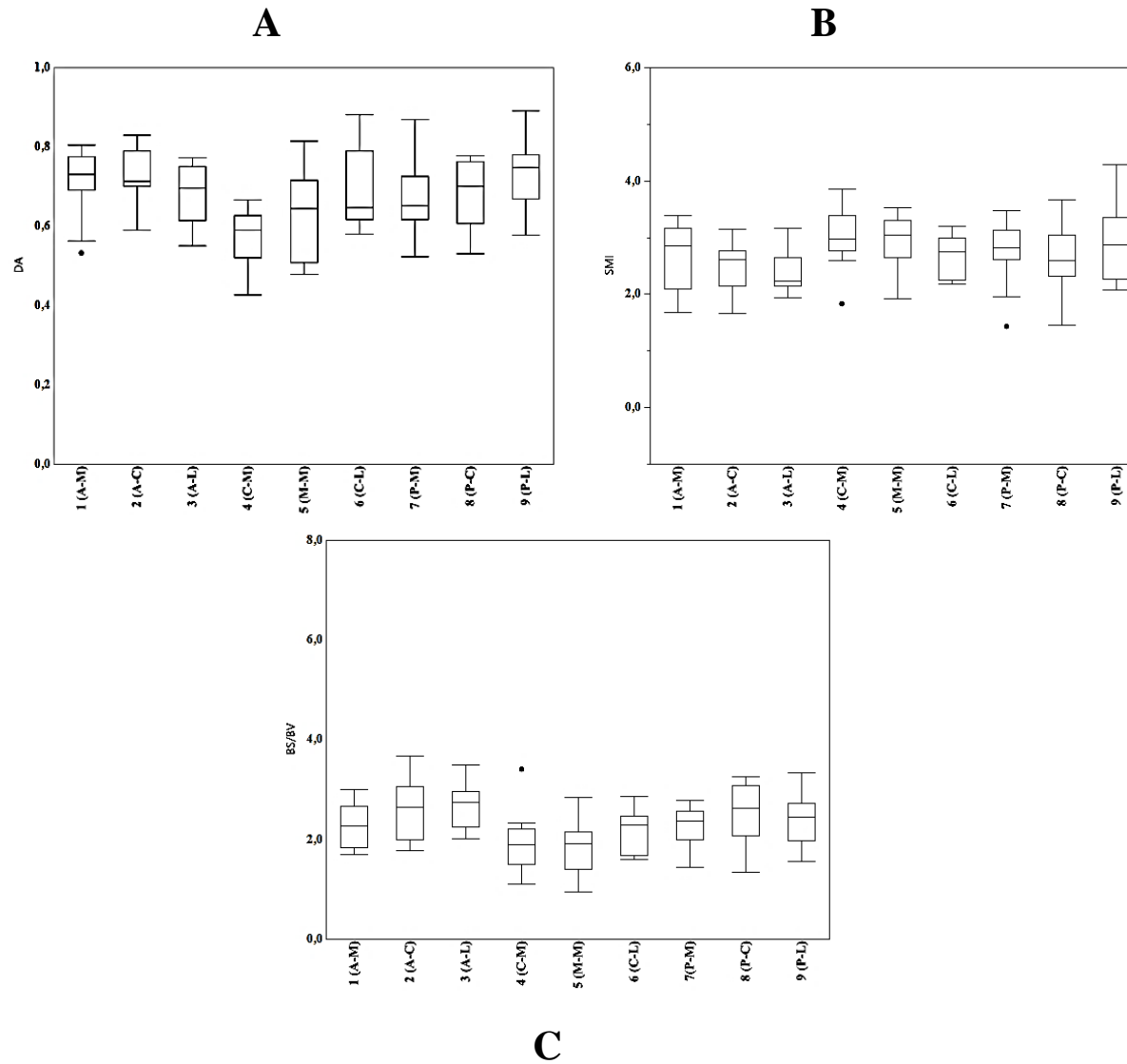


Figure 4.13. Boxplots indicating A) degree of anisotropy (DA), B) structural model index (SMI), C) bone surface to bone volume ratio (BS/BV) by subregion in *G. gorilla*.

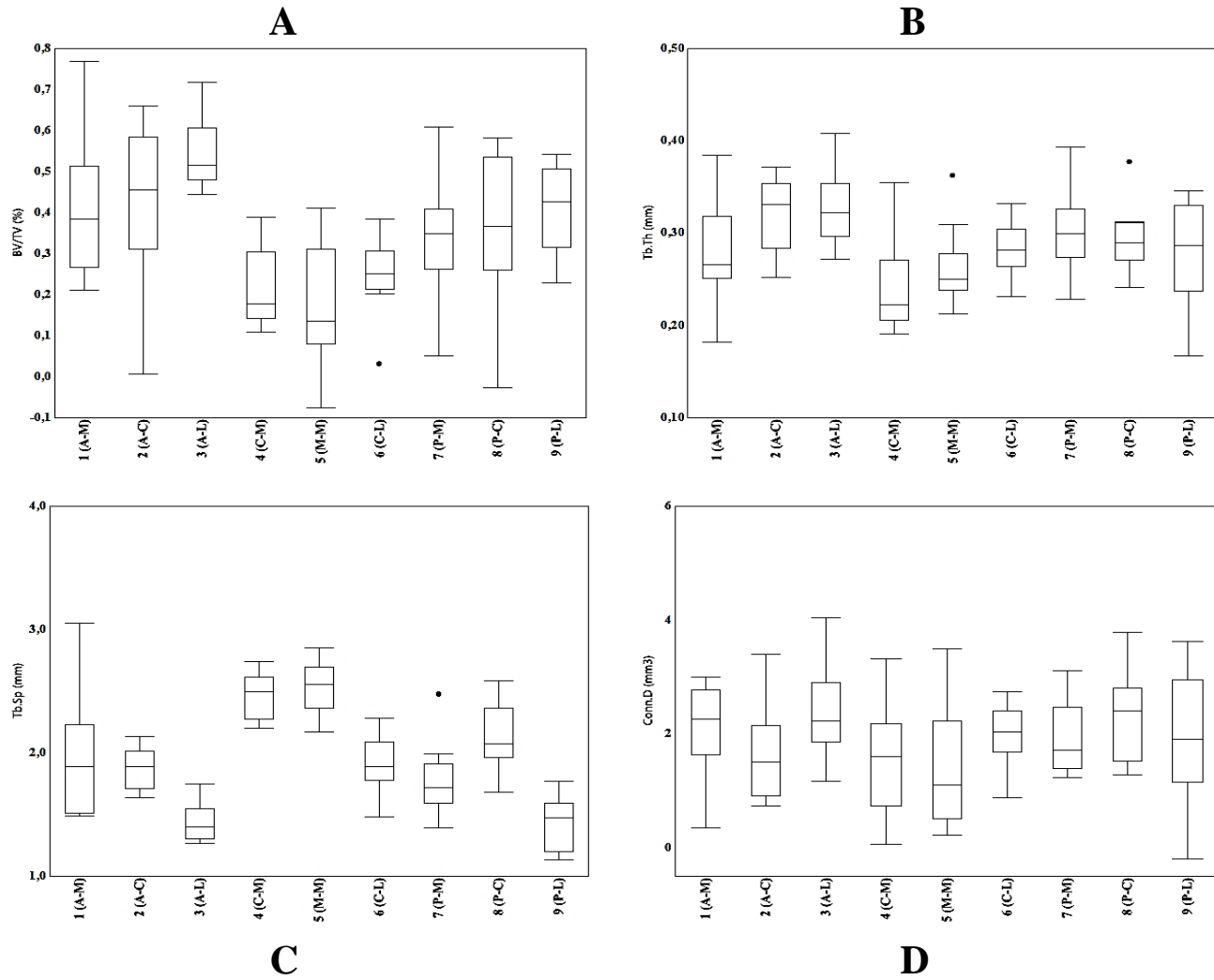


Figure 4.14. Boxplots indicating A) bone volume fraction (BV/TV), B) trabecular thickness (Tb.Th), C) trabecular spacing (Tb.Sp) and D) connectivity density (Conn.D) by subregion in *P. pygmaeus*.

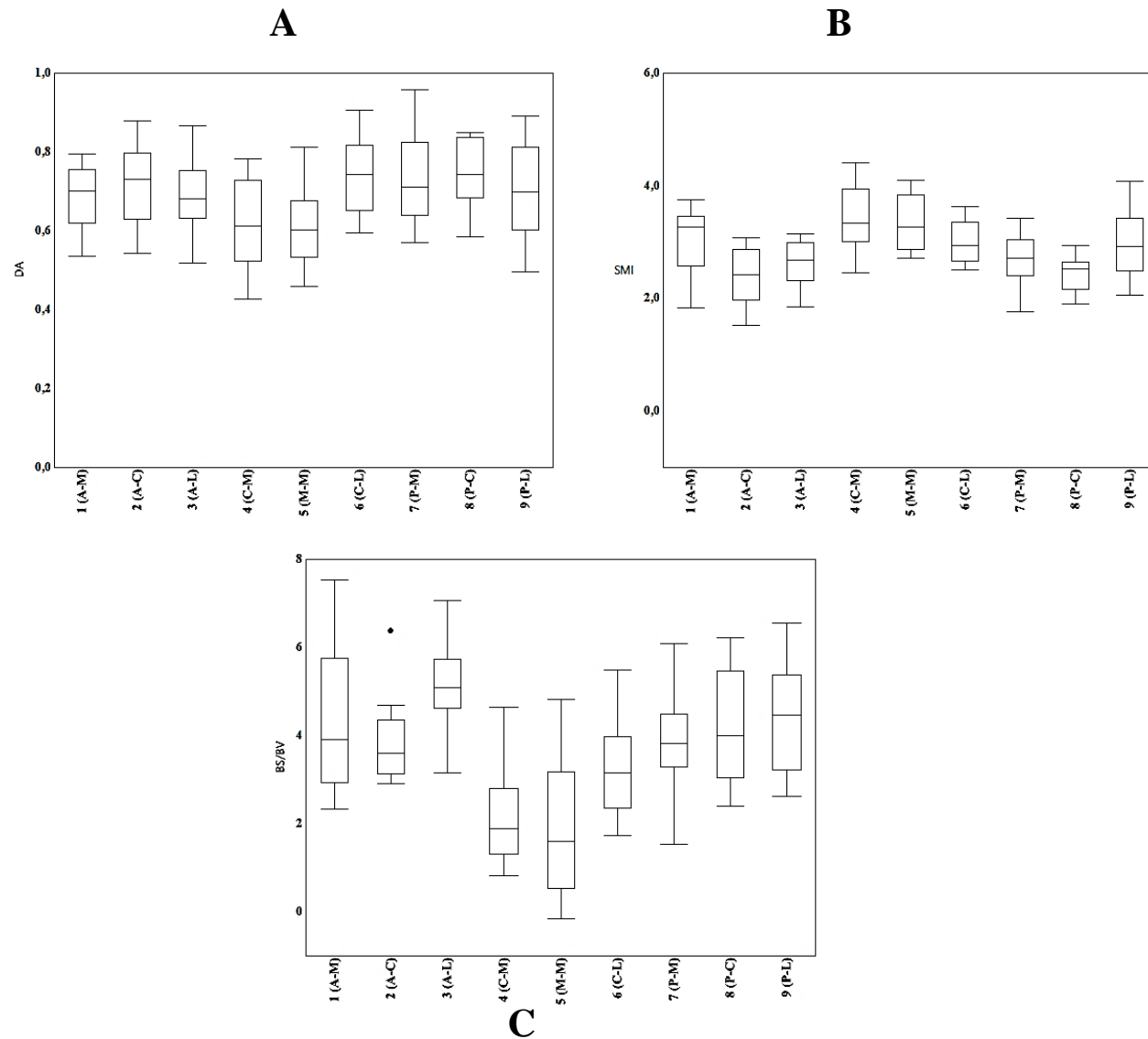


Figure 4.15. Boxplots indicating A) degree of anisotropy (DA), B) structural model index (SMI) and C) bone surface to bone volume ratio (BS/BV) by subregion in *P. pygmaeus*.

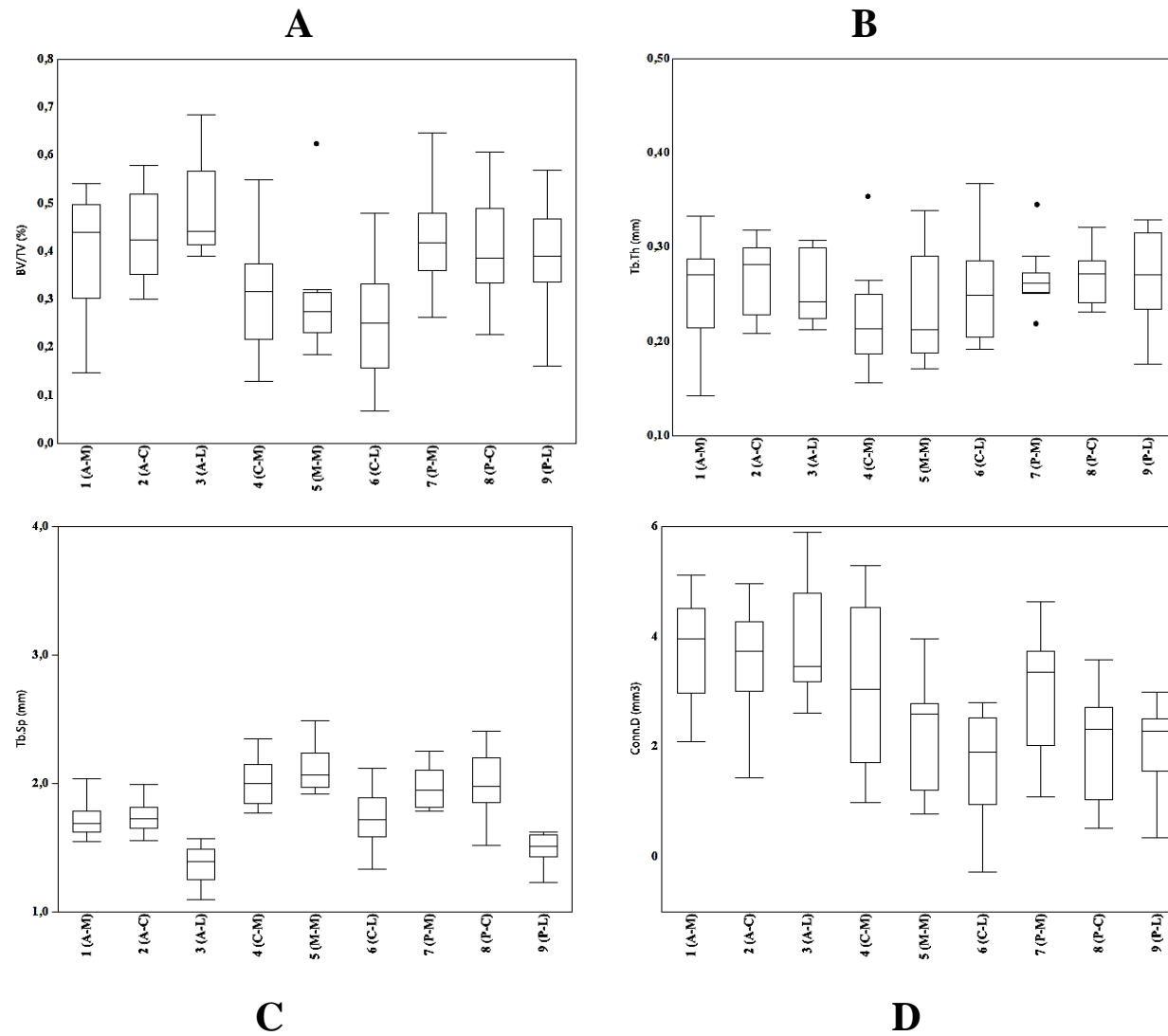


Figure 4.16. Boxplots indicating A) bone volume fraction (BV/TV), B) trabecular thickness (Tb.Th), C) trabecular spacing (Tb.Sp) and D) connectivity density (Conn.D) by subregion in *P. hamadryas*.

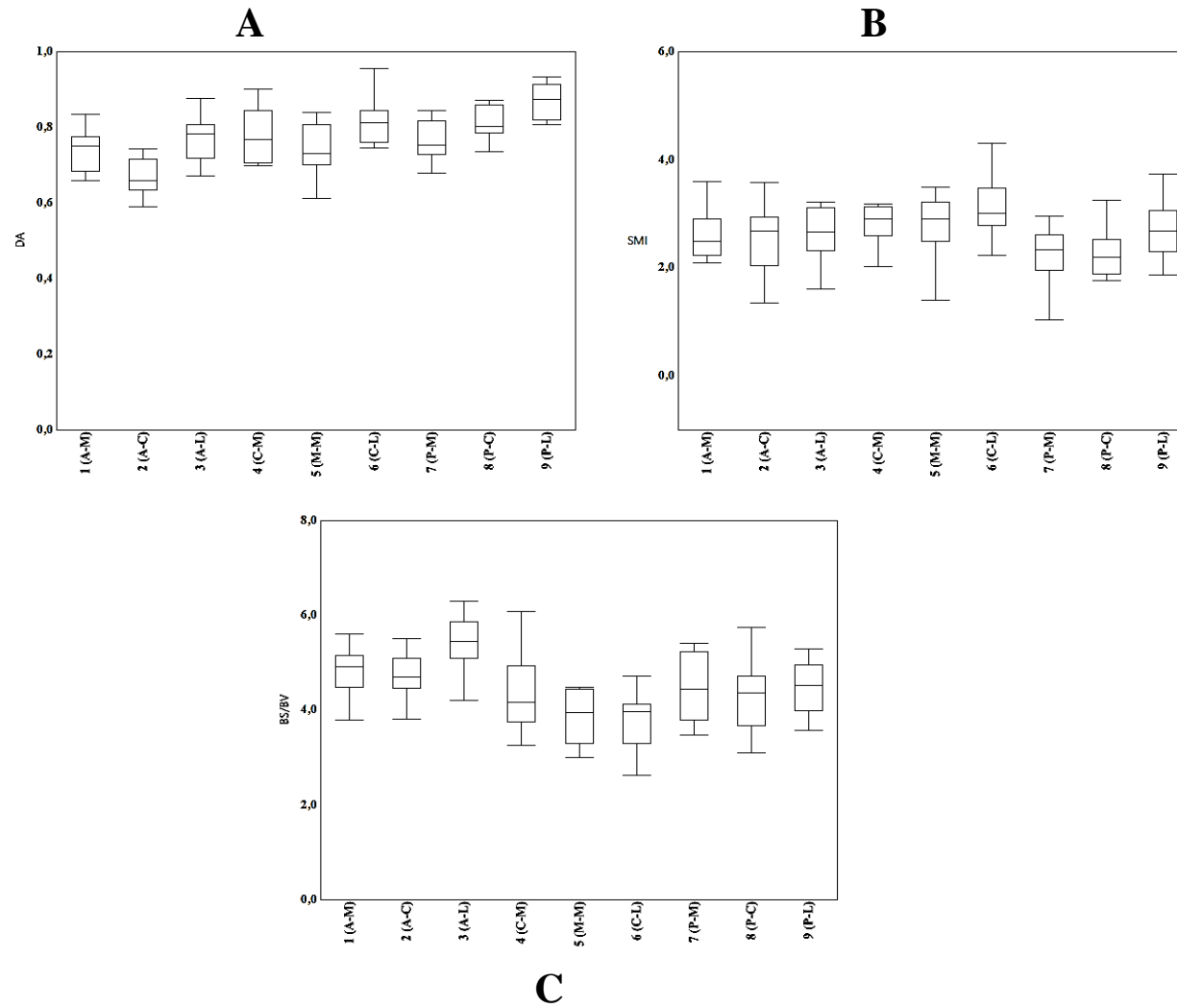


Figure 4.17. Boxplots indicating A) degree of anisotropy (DA), B) structural model index (SMI) and C) bone surface to bone volume ratio (BS/BV) by subregion in *P. hamadryas*.

4.4. Interspecific comparison of trabecular structure in the medial malleolus of humans, extant non-human primates and australopiths from South Africa.

4.4.1. Structural patterns in BV/TV, Tb.Th, Tb.Sp and Conn.D in extant species.

Homo demonstrated the lowest average BV/TV (Table 4.13, Fig 4.18) in both the anterior and posterior VOIs in comparison to those of the extant non-human primates. The highest average BV/TV in the anterior VOI was demonstrated by *Papio* and by *Gorilla* in the posterior VOI. The posterior VOI demonstrated a lower average BV/TV than the anterior in all species sampled, except in *Gorilla* where the posterior had a higher average BV/TV. *Papio* demonstrated the greatest variation (i.e. highest standard deviation) in the anterior VOI and *Gorilla* in the posterior VOI (Table 4.13).

The average thinnest struts were observed in *Homo* across the medial malleolus in both the anterior and posterior VOIs compared to the non-human primates (Table 4.13, Fig 4.19). The mean thickest struts in the anterior VOI were observed in *Papio*, while in the posterior VOI the mean thickest struts were observed in *Gorilla*. Intraspecific variation was highest in *Papio* in the anterior VOI and *Gorilla* in the posterior VOI. In the posterior VOI, there is a general decrease in average strut thickness compared to the anterior VOI across all species, except in *Gorilla*, which demonstrates a slight increase in average thickness in the posterior VOI.

Homo exhibited the highest average Tb.Sp of all the species in the anterior and posterior VOIs (Table 4.13, Fig 4.20). *Homo* also demonstrated the greatest variation among individuals of the same species in both the anterior and posterior VOIs. *Papio* exhibited the lowest average spacing overall in both the anterior and posterior VOIs (i.e. lowest Tb.Sp). The anterior VOI demonstrated higher average Tb.Sp than the posterior in *Homo* and *Gorilla*. The posterior VOI demonstrated higher Tb.Sp than the anterior VOI in *Pan*, *Pongo* and *Papio*.

Average Conn.D in *Homo* was highest in the anterior VOI and in *Pan* in the posterior VOI. *Papio* exhibited the lowest average Conn.D in both the anterior and posterior VOIs (Table 4.13, Fig 4.21). Intraspecific variation was highest in *Homo* across both VOIs (Table 4.13) and lowest in *Papio*. The anterior VOI was higher in average Conn.D than the posterior in *Homo*, *Pongo* and *Papio*. The posterior VOI was higher in average Conn.D than the anterior in *Pan* and *Gorilla*.

4.4.2. Structural patterns in DA, SMI and BS/BV in extant species.

Average DA in the anterior VOI was generally higher than the posterior VOI across all extant species, except *Pongo* (Table 4.13, Fig 4.22). The highest overall average DA was exhibited by *Papio* in both regions, while in the anterior VOI *Pongo* exhibited the lowest average DA, and in the posterior volume *Gorilla* exhibited the lowest average DA. Intraspecific variation was highest in *Pongo* in the anterior and posterior VOIs. *Homo* also demonstrated higher intraspecific variation in the posterior VOI.

The highest average SMI in the medial malleolus was generally exhibited by *Homo* in both the anterior and posterior VOIs (Table 4.13, Fig 4.23). Variation among individuals in the species was low in SMI, except in the *Gorilla* posterior VOI. *Pongo* also exhibited a high average SMI - approaching spherical state. *Pan* and *Papio* tended to have a similar average SMI in both anterior and posterior VOIs.

Average BS/BV in the medial malleolus was generally higher in the anterior VOI in comparison to the posterior VOI across all species (Table 4.13, Fig 4.24). The highest average BS/BV in the anterior and posterior VOIs was observed in *Pan* and the lowest in *Homo* (Table 4.13, Fig 4.24). Average BS/BV was higher in the anterior VOI in *Homo*, *Pan*, *Pongo* and *Papio*, and higher in the posterior VOI in *Gorilla*. Intraspecific variation in the anterior VOI was less than that of the posterior VOI in all extant non-human primates, although *Homo* exhibited higher levels of intraspecific variation in the posterior VOI.

4.5. Trabecular properties of the *A. africanus* medial malleolus in comparison to extant species sampled.

4.5.1. Structural patterns in BV/TV, Tb.Th, Tb.Sp and Conn.D in medial malleolus of *A. africanus*.

A. africanus individuals exhibited a high range of variation in BV/TV in the medial malleolus (Table 4.13, Fig 4.18). In the anterior VOI, StW 567 exhibited a lower BV/TV in comparison to StW 358 and StW 515. StW 567 fell within the *Homo* range of BV/TV, while StW 358 fell within the *Pan* and *Papio* range of BV/TV, and StW 515 was within the range of *Papio* sample. The only fossil specimen represented in the posterior VOI is StW 358, which exhibited a decrease in BV/TV in the posterior VOI (0,257) in comparison to the anterior VOI (0,563), corresponding with patterns observed in all extant species sampled (except

Gorilla) (Fig 4.18). BV/TV of the posterior VOI in StW 358 falls within the range of modern *Homo*, *Gorilla* and *Pongo*.

StW 567 demonstrated the thinnest trabeculae, and was not within the range of any extant sampled species (closest to *Homo*-like). Strut thickness of StW 358 and StW 515, on the other hand, fell within the range of extant non-human hominoids. The fossil sample demonstrated high intraspecific variation in trabecular thickness in the anterior volume (Table 4.13, Fig 4.19). The posterior VOI of StW 358 exhibited strut thickness that fell within the *Homo* and *Gorilla* range of distribution.

Tb.Sp in the anterior VOI of *A. africanus* was within the extant hominoid range (Table 4.13, Fig 4.20). The highest Tb.Sp within the fossil group was observed in the anterior VOI of StW 358 (1,949). There was a general posteriorward decrease in thickness in StW 358 (1,949 to 1,758) similar to the extant sample.

There was a high amount of variation within *A. africanus* Conn.D in the anterior VOI (Table 4.13, Fig 4.21). StW 515 and StW 567 fossil specimens, on the other hand, exhibited a very high connectivity falling outside the range of any extant species in the anterior VOI (Fig 4.21). The lowest connectivity in the anterior VOI was observed in StW 358, which fell within the range of *Homo*, *Gorilla* and *Pan*. In the posterior VOI, StW 358 fell within the *Homo* range in connectivity, demonstrating a higher connectivity than any of the extant non-human primates.

4.5.2. Structural patterns in DA, SMI and BS/BV in medial malleolus of *A. africanus*.

A. africanus individuals demonstrated variation in DA of the anterior VOI that overlapped with the ranges of *Gorilla*, *Homo* and *Pongo* (Table 4.13, Fig 4.22). The highest DA observed in the anterior VOI was in StW 358, which fell within *Homo*, *Gorilla* and *Pongo* ranges of distribution. StW 515 and StW 567, on the other hand, grouped together and had a more *Pongo*-like distribution. In the posterior VOI, StW 358 fell within the range of both *Homo* and *Pongo*.

The highest SMI in the anterior VOI was exhibited by StW 567, which fell within the *Homo* range of distribution. StW 515 and StW 358 exhibited SMI values that were not within the range of any of the extant sampled species. In the posterior VOI, StW 358 exhibited a SMI value that fell in the range of *Homo* and *Pongo* (Table 4.13, Fig 4.23).

The fossil sample demonstrated a generally high BS/BV in the anterior VOI (above 5) (Table 4.13, Fig 4.24). StW 567 exhibited the lowest BS/BV among the fossils, falling within the range of the extant sample. StW 358 and StW 515, on the other hand, demonstrated a BS/BV that was not within the range of any of the extant species sampled. In the posterior VOI, StW 358 had a BS/BV value that was lower than the value in its anterior VOI. The posterior VOI in StW 358 fell within the range of values exhibited by *Gorilla* and *Pan*.

Table 4.13. Summary statistics (mean and standard deviation) of trabecular parameters in the medial malleolus of extant hominoids and *A. africanus*.

Parameter	<i>Homo</i> (n=7)		<i>Pan</i> (n=4)		<i>Gorilla</i> (n=4)	
	Anterior	Posterior	Anterior	Posterior	Anterior	Posterior
BV/TV	0,216(0,069)	0,145(0,068)	0,494(0,045)	0,405(0,074)	0,43(0,031)	0,458(0,167)
Tb.Th	0,183(0,023)	0,161(0,02)	0,298(0,05)	0,259(0,03)	0,29(0,025)	0,4(0,242)
Tb.Sp	2,091(0,342)	2,031(0,322)	1,931(0,293)	2,006(0,218)	2,121(0,05)	1,934(0,252)
Conn.D	4,778(2,179)	3,343(2,495)	3,309(1,346)	3,507(1,075)	2,182(0,966)	2,301(0,89)
DA	0,604(0,072)	0,52(0,134)	0,714(0,062)	0,632(0,068)	0,587(0,118)	0,465(0,06)
SMI	3,771(0,64)	4,584(0,886)	2,031(0,648)	2,735(0,407)	2,178(0,318)	2,799(0,82)
BS/BV	3,718(0,958)	2,806(1,063)	4,761(0,472)	4,458(0,537)	4,05(0,468)	4,192(0,829)
Parameter	<i>Pongo</i> (n=10)		<i>Papio</i> (n=6)		<i>Africanus</i> (n=4)*	
	Anterior	Posterior	Anterior	Posterior	Anterior (n=3)*	Posterior (n=1)*
BV/TV	0,341(0,064)	0,298(0,061)	0,578(0,075)	0,401(0,078)	0,477(0,196)	0,257
Tb.Th	0,281(0,068)	0,27(0,054)	0,386(0,049)	0,322(0,022)	0,238(0,064)	0,171
Tb.Sp	1,766(0,213)	1,853(0,259)	1,388(0,178)	1,532(0,171)	1,761(0,146)	1,758
Conn.D	2,541(1,117)	2,073(0,943)	1,132(0,35)	1,281(0,62)	5,765(1,777)	6,089
DA	0,522(0,121)	0,536(0,167)	0,75(0,093)	0,638(0,126)	0,459(0,094)	0,331
SMI	3,443(0,707)	3,481(0,568)	1,897(0,432)	2,469(0,524)	0,9(2,186)	3,637
BS/BV	3,7(0,513)	3,34(0,64)	4,114(0,312)	3,593(0,633)	5,255(0,702)	4,779

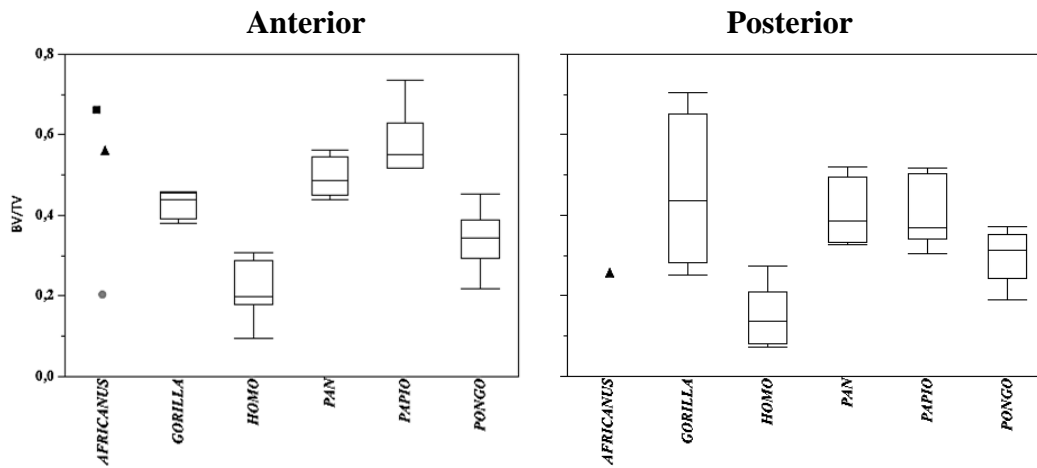


Figure 4.18. Boxplots indicating bone volume fraction (BV/TV) in the medial malleolus by subregion across species. *Africanus* specimens represented by symbols (▲StW 358, ■StW 515 and ●StW 567).

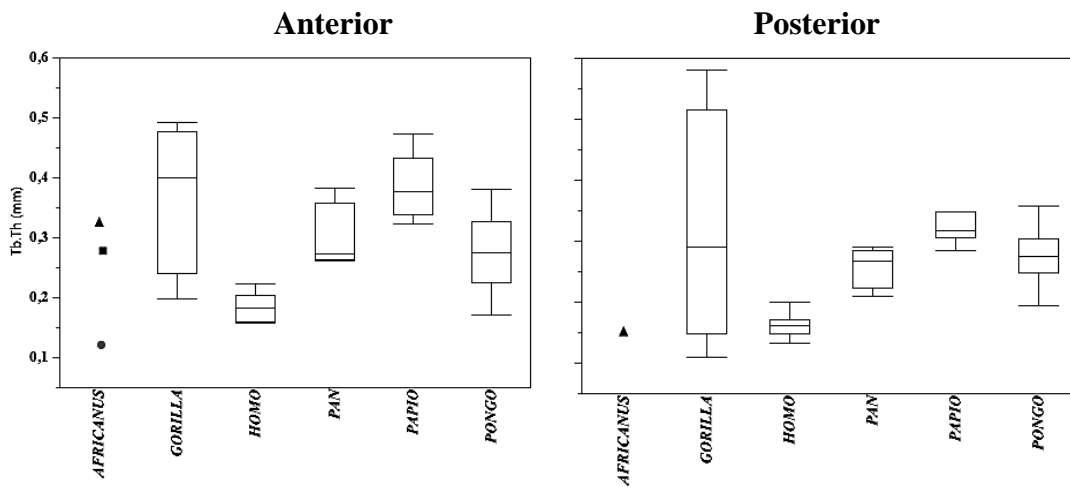


Figure 4.19. Boxplots indicating mean trabecular thickness (Tb.Th) in the medial malleolus by subregion across species. *Africanus* specimens represented by symbols (▲StW 358, ■StW 515 and ●StW 567).

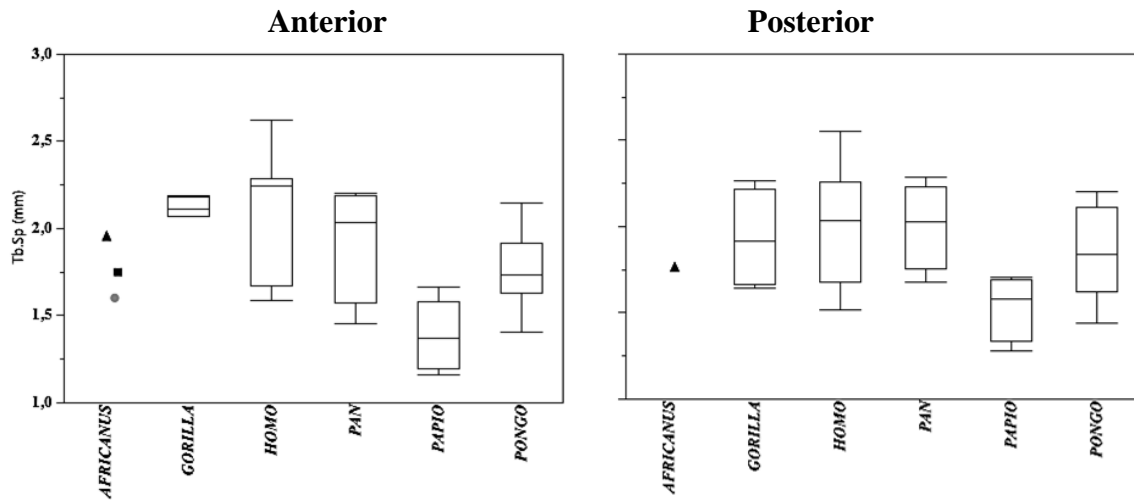


Figure 4.20. Boxplots indicating trabecular spacing (Tb.Sp) in the medial malleolus by subregion across species. *Africanus* specimens represented by symbols (▲StW 358, ■StW 515 and ●StW 567).

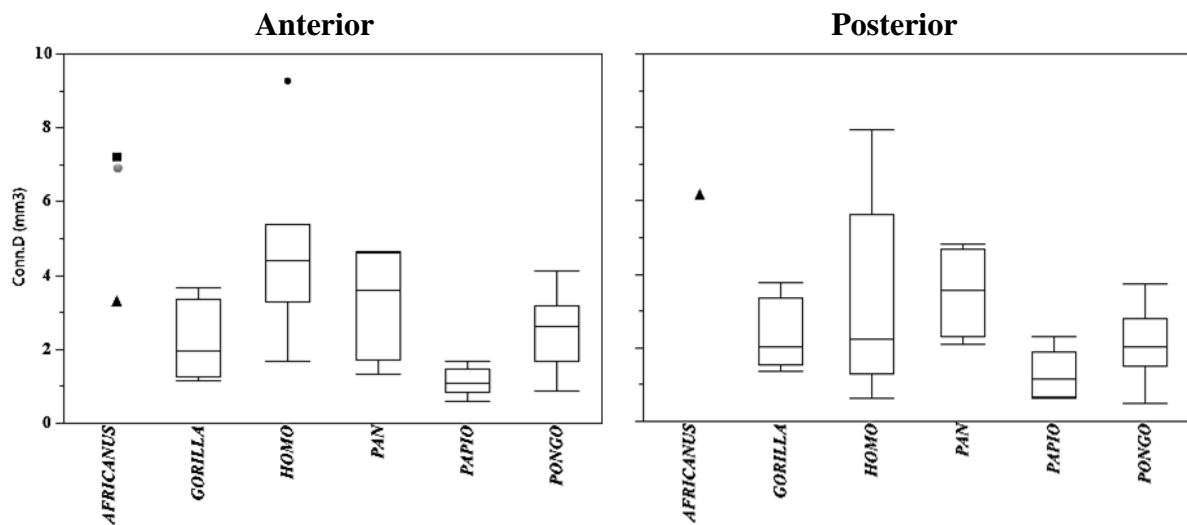


Figure 4.21. Boxplots indicating connectivity density (Conn.D) in the medial malleolus by subregion across species. *Africanus* specimens represented by symbols (▲StW 358, ■StW 515 and ●StW 567).

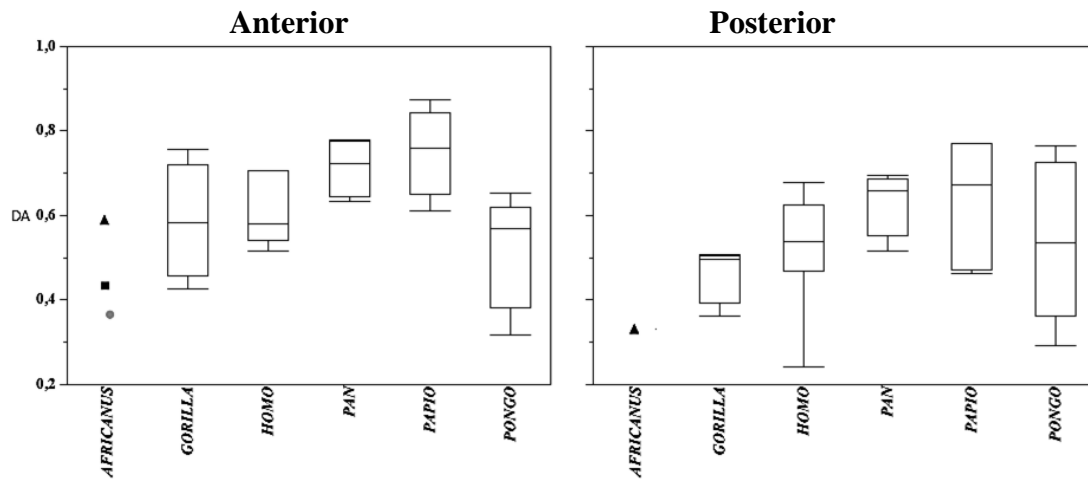


Figure 4.22. Boxplots indicating degree of anisotropy (DA) in the medial malleolus by subregion across species. *Africanus* specimens represented by symbols (▲StW 358, ■StW 515 and ●StW 567).

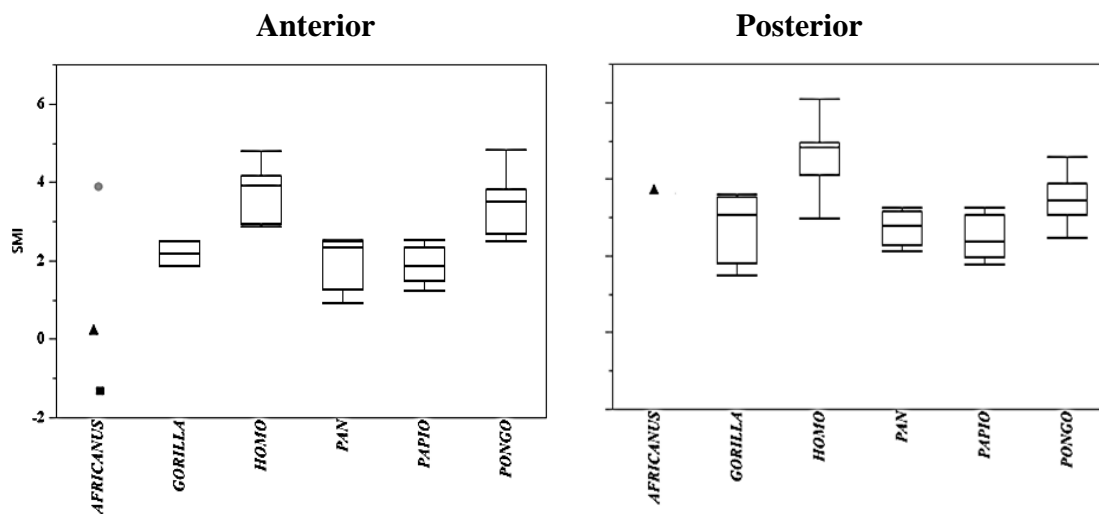


Figure 4.23. Boxplots indicating structural model index (SMI) in the medial malleolus by subregion across species. *Africanus* specimens represented by symbols (▲StW 358, ■StW 515 and ●StW 567).

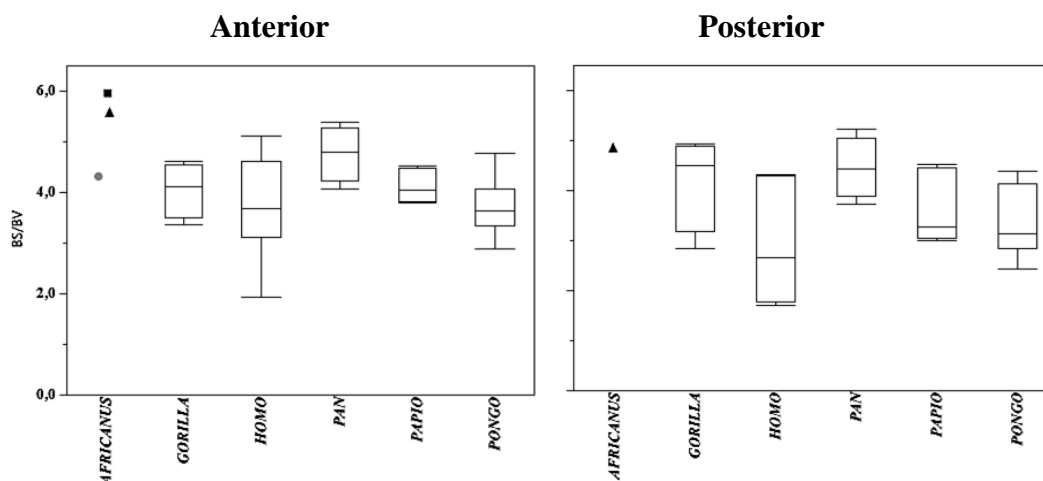


Figure 4.24. Boxplots indicating bone surface to bone volume ratio (BS/BV) in the medial malleolus by subregion across species. *Africanus* specimens represented by symbols (▲StW 358, ■StW 515 and ●StW 567).

4.6. Intraspecific variation in trabecular properties of the medial malleolus in humans and extant non-human primates.

4.6.1. Trabecular analyses of the medial malleolus in *H. sapiens* (modern human hunter-gatherers).

Average BV/TV in the anterior VOI was generally higher than the posterior VOI in *Homo* (Fig 4.25A). There is little variation within individuals of the sample. Average Tb.Th is slightly higher in the anterior VOI compared to the posterior VOI; the posterior VOI demonstrated a higher degree of variation among the sample in Tb.Th (Fig 4.25B). Average Tb.Sp in *Homo* is slightly higher in the anterior VOI (Fig 4.25C). Average Conn.D is higher in the anterior VOI in comparison to the posterior VOI, which also has a larger range of variation (Fig 4.25D).

Average DA in the anterior VOI of the human medial malleolus was higher than the posterior VOI, which demonstrated higher variability within individuals in the sample (Fig 4.16A). Average SMI in the medial malleolus was higher in the posterior VOI (solid spherical) compared to the anterior VOI (rod-like) (Fig 4.26B). Average BS/BV in the anterior VOI is higher than the posterior VOI, while the variation in both volumes is high within individuals of the species (Fig 4.26C).

4.6.2. Trabecular analyses of the medial malleolus in *P. troglodytes* (common chimpanzee).

Average BV/TV in *Pan* was generally higher in the anterior VOI than the posterior VOI, while the latter had a higher amount of variation (Fig 4.27A). The lowest observed BV/TV

was 0,327 in the posterior VOI. The average thickest struts were observed generally in the anterior VOI compared to the posterior VOI (Fig 4.27B). Tb.Sp in the medial malleolus of *Pan* is higher on average in the posterior VOI compared to the anterior VOI (Fig 4.27C). The anterior VOI also demonstrates higher variation among individuals in the sample in Tb.Sp. Conn.D in *Pan* is the most variable parameter measured in the trabecular structure in the medial malleolus (Fig 4.27D). The anterior VOI has a slightly higher average Conn.D than the posterior VOI.

Average DA in *Pan* was higher in the anterior VOI than the posterior VOI (Fig 4.28A). The posterior VOI demonstrated higher intraspecific variation. The highest observed DA was 0,778 in the anterior VOI, while the lowest was 0,517. Average SMI in the posterior VOI was higher than in the anterior VOI (rod-like) of the medial malleolus (Fig 4.28B). The anterior VOI is slightly higher on average in BS/BV compared to the posterior VOI, and has a lower range of variation in individuals (Fig 4.28C).

4.6.3 Trabecular analyses of medial malleolus in *G. gorilla* (western lowland gorilla).

The posterior VOI was generally higher in average BV/TV than the anterior VOI in *Gorilla* which exhibited very low variation between individuals in BV/TV (Fig 4.29A). Tb.Th was similar to BV/TV, as it was highest on average in the posterior VOI. The posterior VOI also demonstrated higher variation than the anterior VOI in Tb.Th (Fig 4.29B). Mean Tb.Sp in the anterior volume of *Gorilla* showed little variation between individuals in the species (Fig 4.29C). Spacing in the anterior VOI was higher than in the posterior VOI. Average Conn.D in the medial malleolus of *Gorilla* was slightly higher in the posterior VOI than the anterior VOI (Fig 4.29D). Both anterior and posterior VOIs demonstrate high levels of variation between individuals in the species in connectivity.

Average DA in the anterior VOI was higher and more variable among individuals than the posterior VOI (Fig 4.30A). SMI in *Gorilla* was higher, on average and more variable among individuals in the posterior VOI compared than the anterior VOI (Fig 4.30B). Average BS/BV was generally high in both the anterior and posterior VOIs, although the posterior VOI was slightly higher and demonstrated more intraspecific variation (Fig 4.30C).

4.6.4. Trabecular analyses of the medial malleolus in *P. pygmaeus* (Bornean orangutan).

Average BV/TV in *Pongo* is generally higher in the anterior VOI than the posterior VOI (Fig 4.31A). The average Tb.Th in the anterior and posterior VOIs is similar, although the anterior VOI is slightly higher in strut thickness and exhibits more intraspecific variation (Fig 4.31B). Tb.Sp in *Pongo* was slightly higher in the posterior VOI than in the anterior VOI on average (Fig 4.31C). Conn.D in the posterior VOI was slightly lower than in the anterior VOI on average (Fig 4.31D).

Average DA of *Pongo* is slightly higher in the posterior VOI compared to the anterior VOI (Fig 4.32A). The posterior VOI also demonstrates a greater variation among individuals than does the anterior VOI. Average SMI and BS/BV in the anterior and posterior VOIs in *Pongo* are similar, although the anterior VOI is slightly higher than the posterior VOI in both SMI and BS/BV (Fig 4.32B,C).

4.6.5. Trabecular analysis medial malleolus in *P. hamadryas* (Hamadryas baboon).

BV/TV in *Papio* is higher in the anterior VOI compared to the posterior VOI with no overlap (Fig 4.33A). While BV/TV in the anterior VOI is above 0,5, the posterior VOI is consistently below 0,5. Variation within individuals in the species is slightly higher in the posterior VOI compared to the anterior VOI. Tb.Th in the anterior VOI of *Papio* is higher than in the posterior VOI (Fig 4.33B). The thickest struts occur in the anterior VOI, which also exhibits the higher amount of intraspecific variation. Tb.Sp and Conn.D in the anterior VOI are higher than in the posterior VOI (Fig 4.33C,D).

DA in the anterior VOI was higher and exhibited a lower amount of intraspecific variation (Fig 4.34A). DA was generally high in the anterior VOI, being above 0,6 and nearing 0,9. By comparison, the posterior VOI was slightly lower, ranging from 0,4 to 0,7. Average SMI in the anterior VOI (rod-like) was lower than in the posterior VOI; the posterior VOI had SMI values that extended beyond 3, which was not observed in the anterior VOI (solid sphere) (Fig 4.34B). Average BS/BV is higher in the anterior VOI compared to within the posterior VOI (Fig 4.34C).

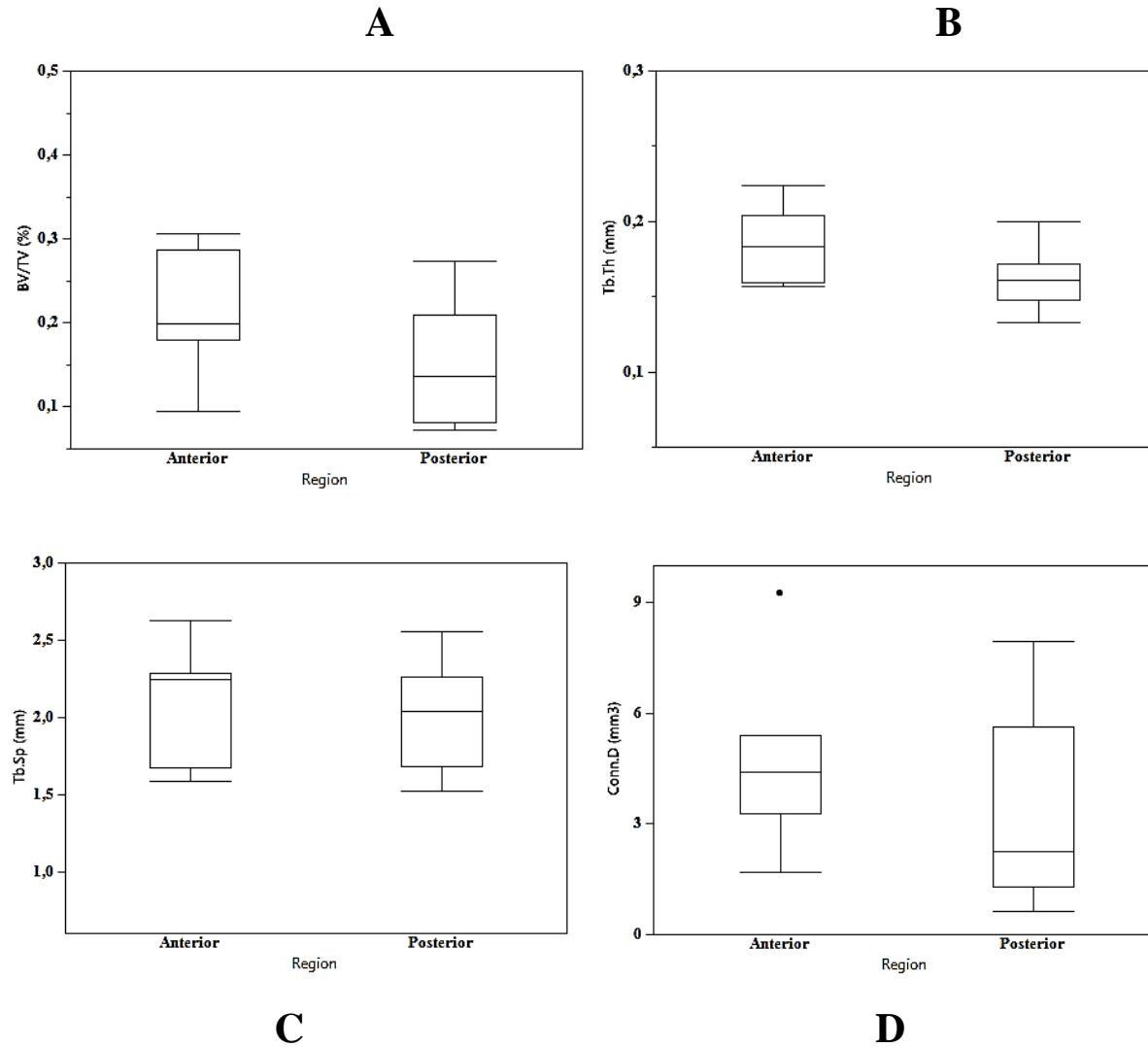


Figure 4.25. Boxplots indicating A) bone volume fraction (BV/TV), B) trabecular thickness (Tb.Th), C) trabecular spacing (Tb.Sp) and D) connectivity density (Conn.D) by subregion in the medial malleolus of *H. sapiens*.

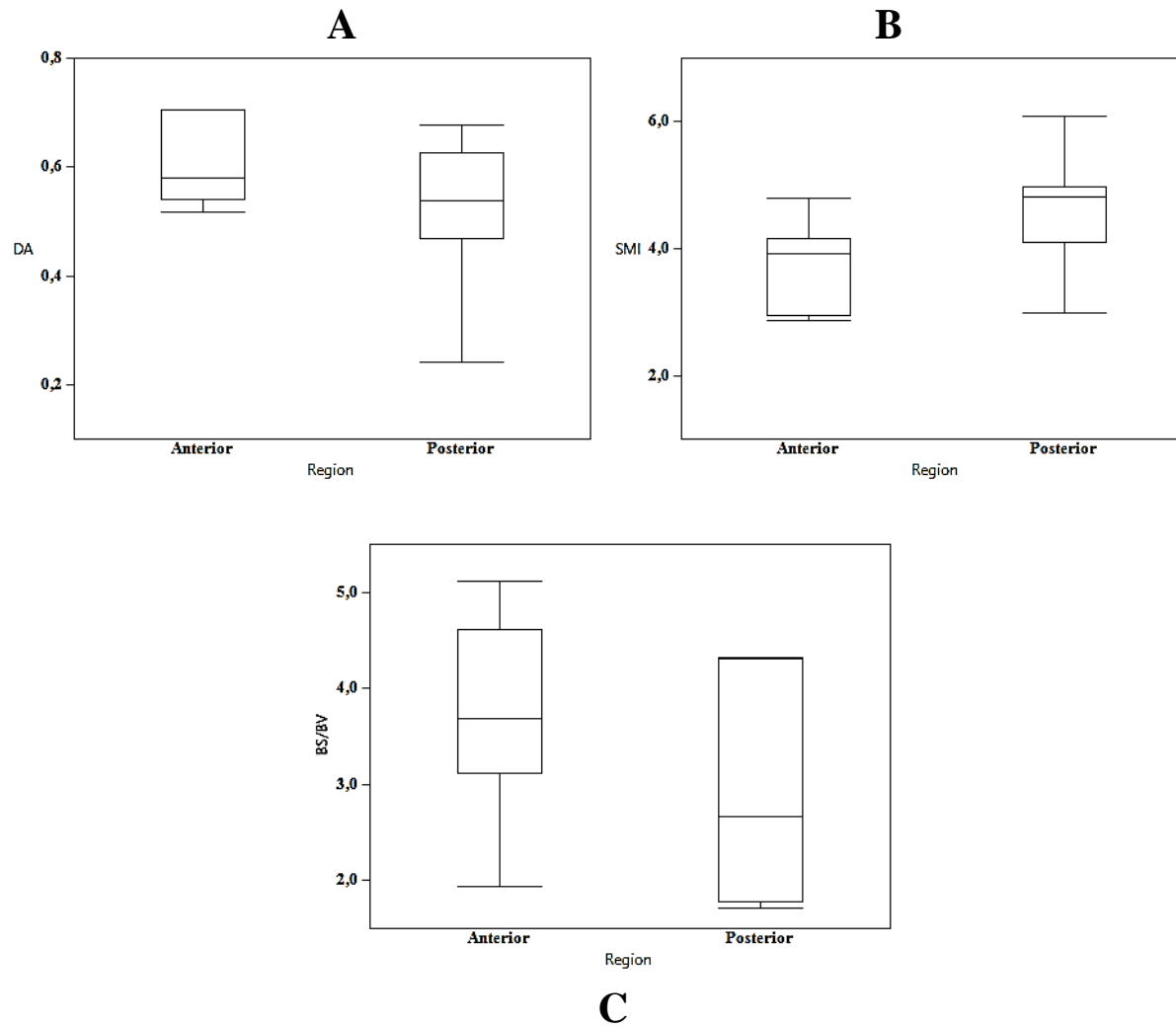


Figure 4.26. Boxplots indicating A) degree of anisotropy (DA), B) structural model index (SMI) and C) bone surface to bone volume ratio (BS/BV) by subregion in the medial malleolus of *H. sapiens*.

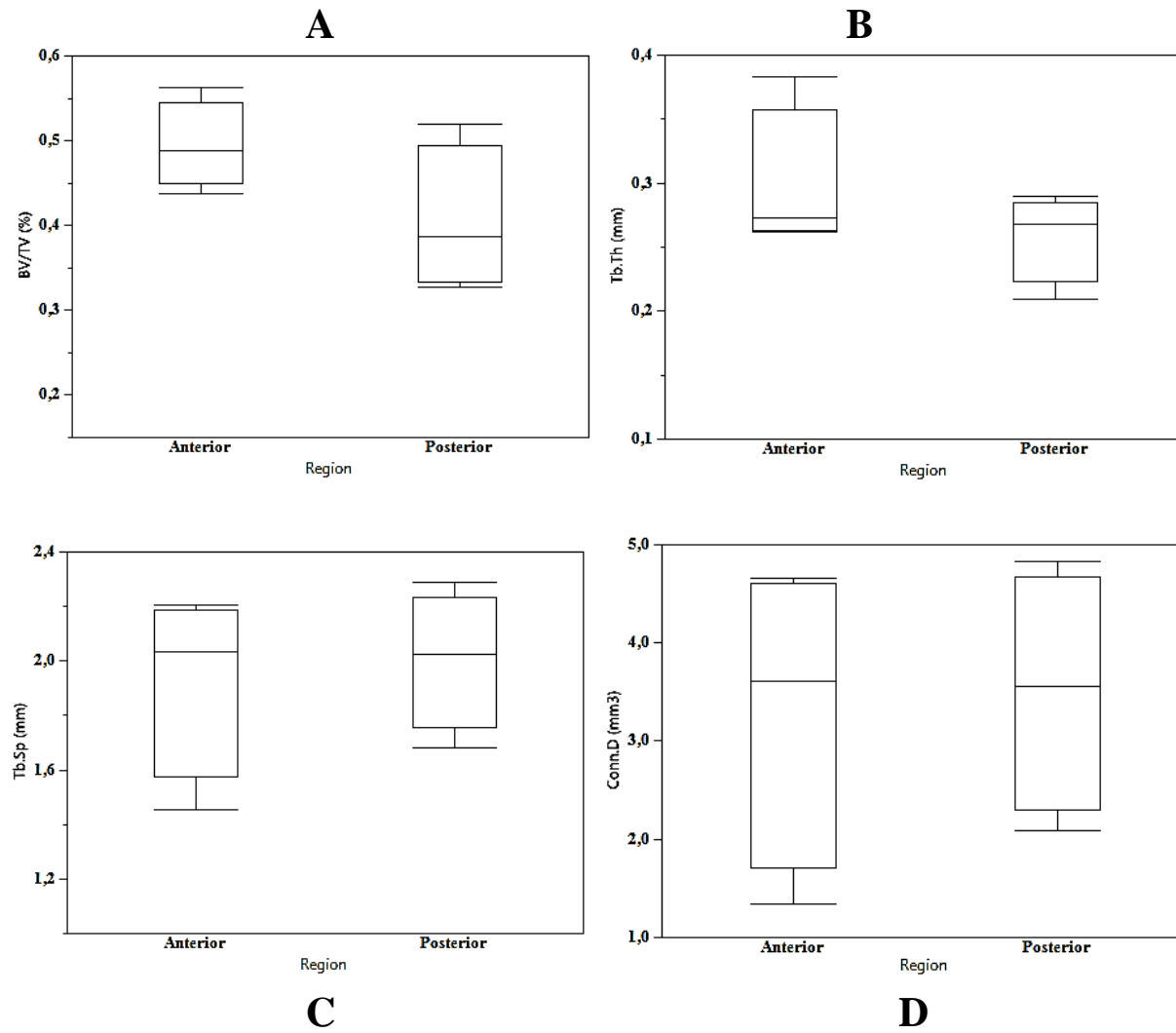


Figure 4.27. Boxplots indicating A) bone volume fraction (BV/TV), B) trabecular thickness (Tb.Th), C) trabecular spacing (Tb.Sp) and D) connectivity density (Conn.D) by subregion in the medial malleolus of *P. troglodytes*.

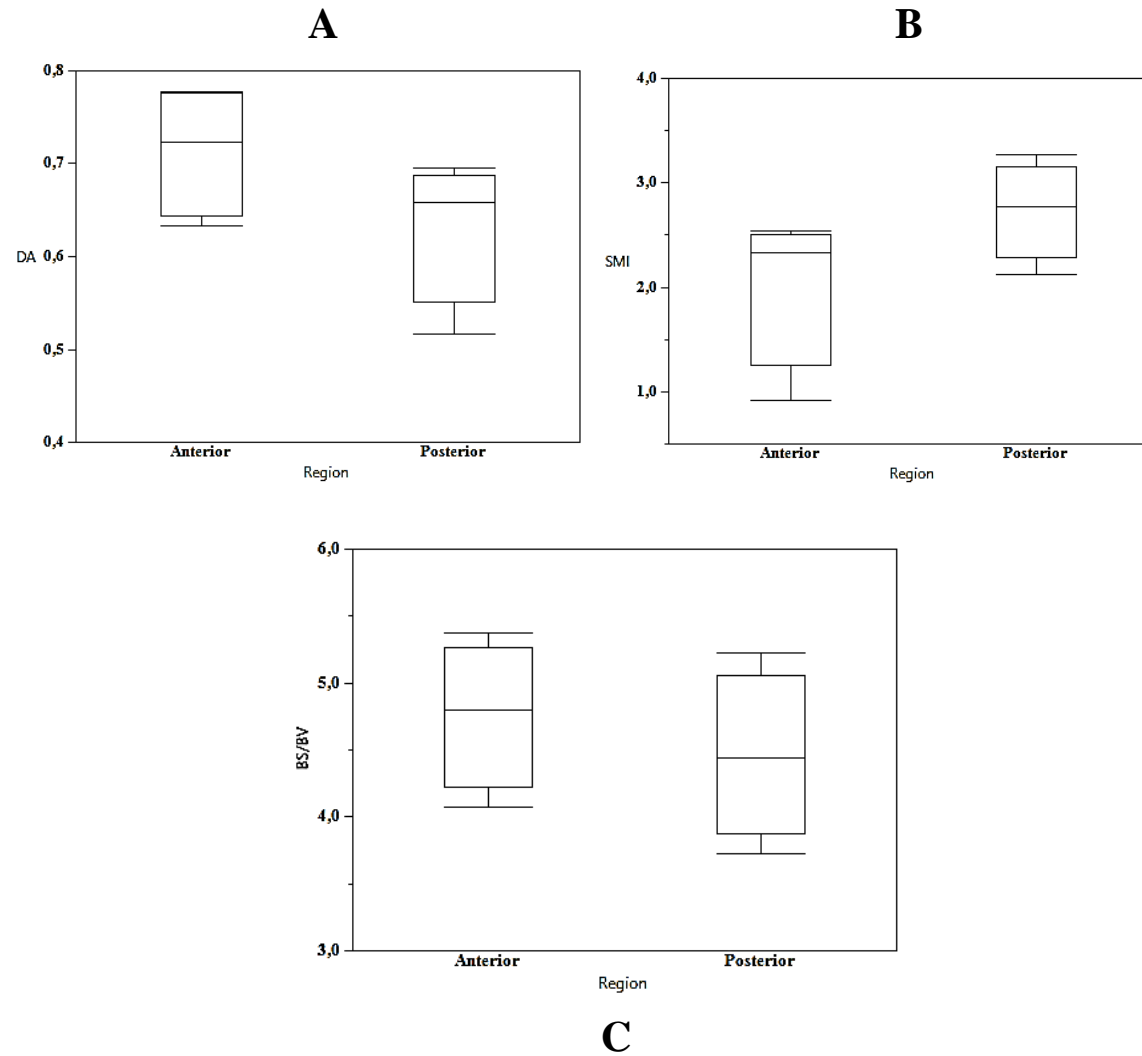


Figure 4.28. Boxplots indicating A) degree of anisotropy (DA), B) structural model index (SMI) and C) bone surface to bone volume ratio (BS/BV) by subregion in the medial malleolus of *P. troglodytes*.

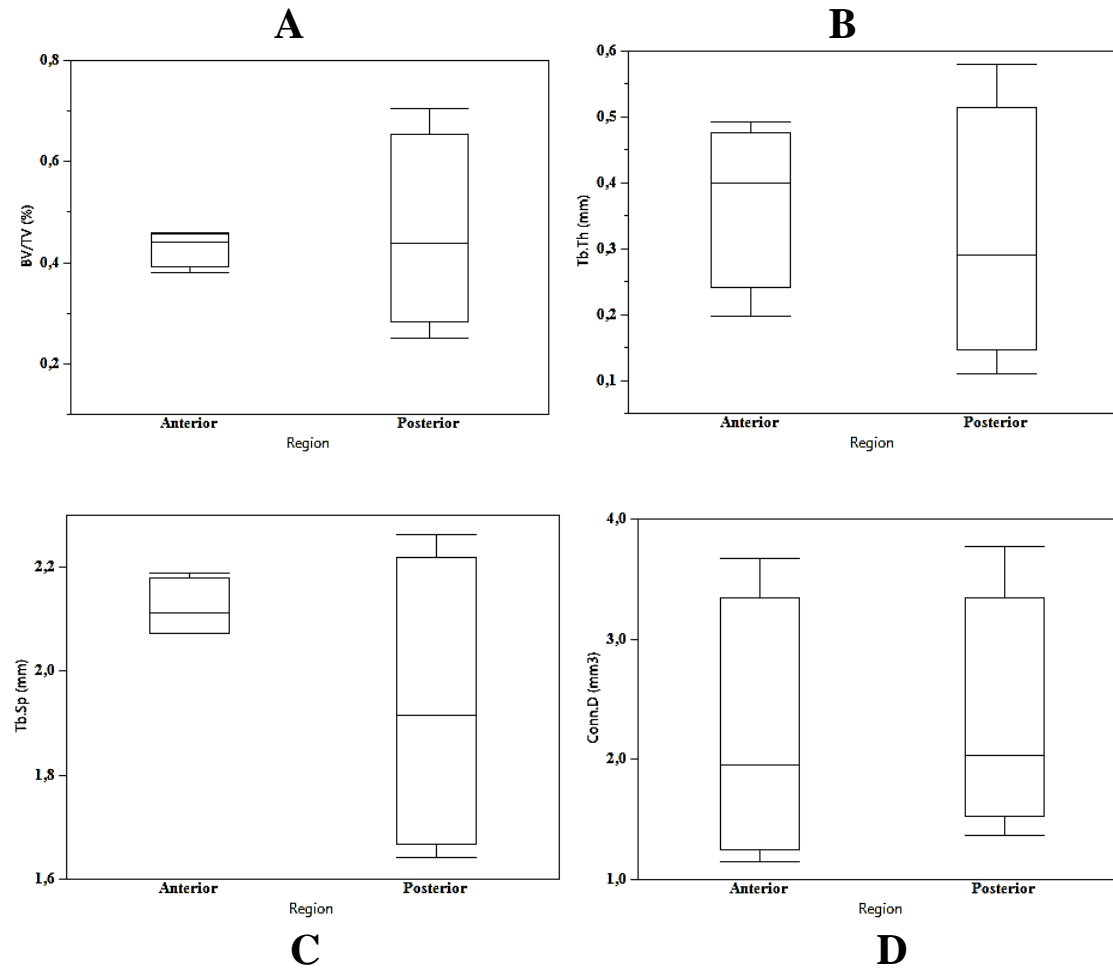


Figure 4.29. Boxplots indicating A) bone volume fraction (BV/TV), B) trabecular thickness (Tb.Th), C) trabecular spacing (Tb.Sp) and D) connectivity density (Conn.D) by subregion in the medial malleolus of *G. gorilla*.

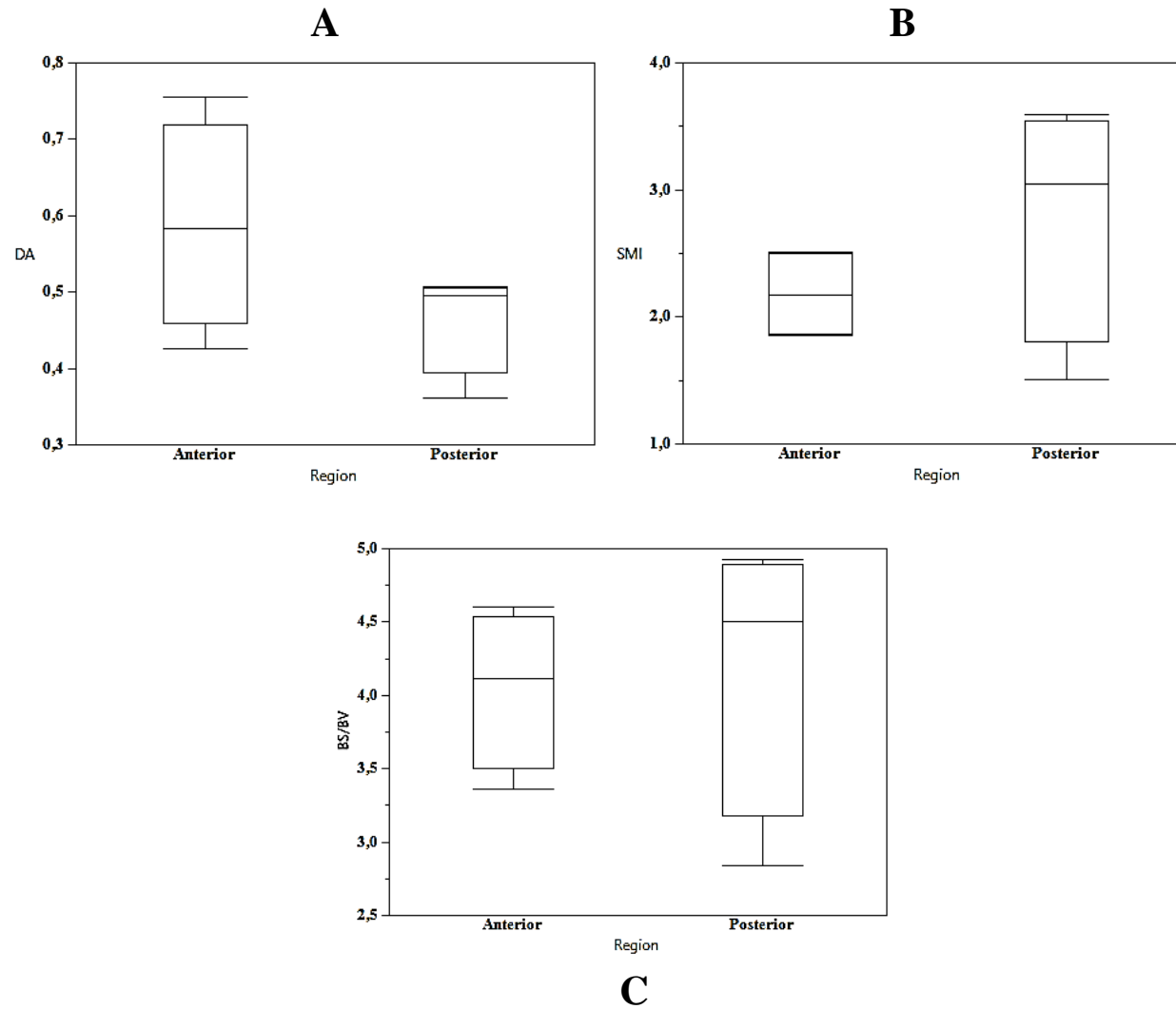


Figure 4.30. Boxplots indicating A) degree of anisotropy (DA), B) structural model index (SMI) and C) bone surface to bone volume ratio (BS/BV) by subregion in the medial malleolus of *G. gorilla*.

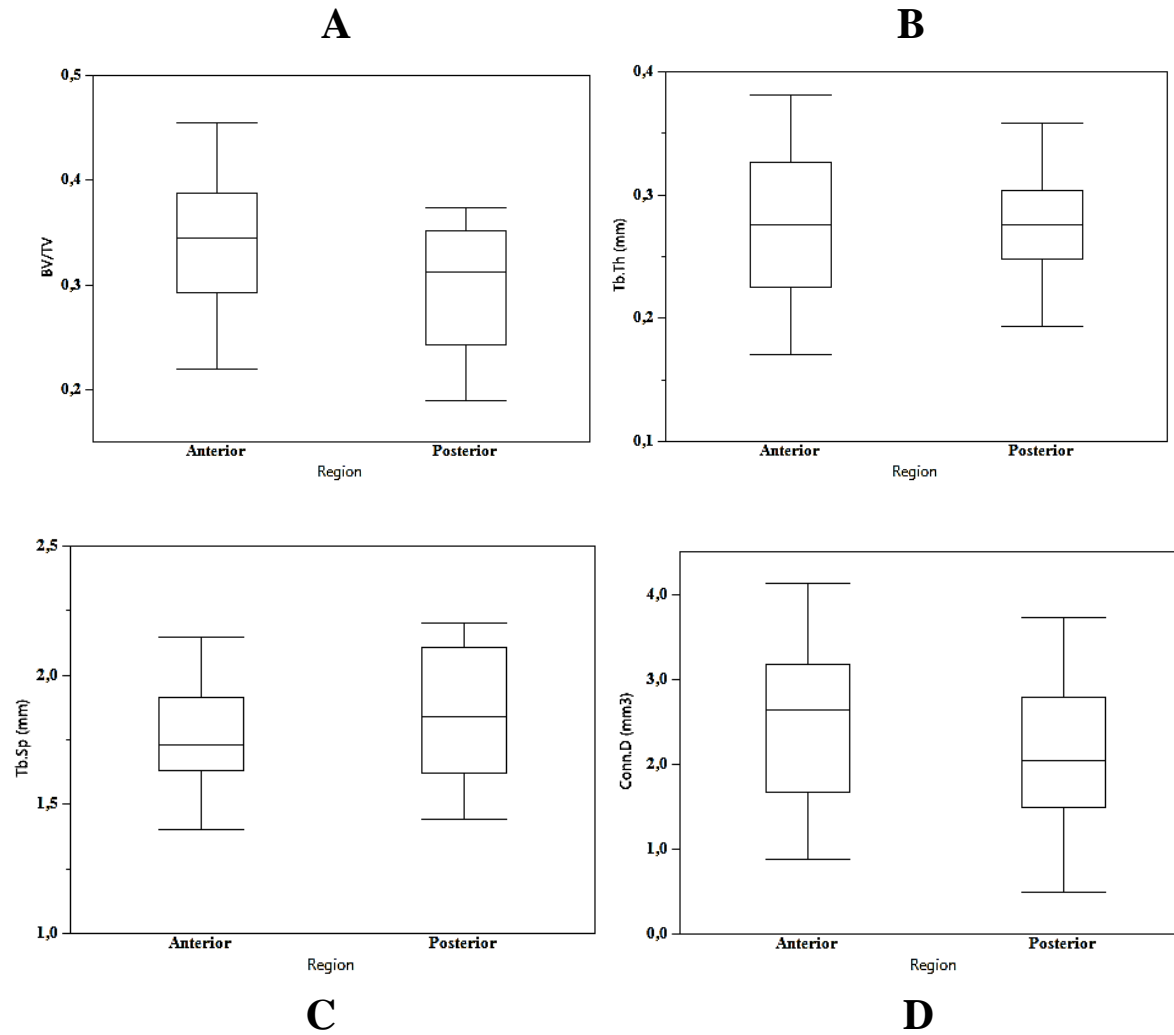


Figure 4.31. Boxplots indicating A) bone volume fraction (BV/TV), B) trabecular thickness (Tb.Th), C) trabecular spacing (Tb.Sp) and D) connectivity density (Conn.D) by subregion in the medial malleolus of *P. pygmaeus*.

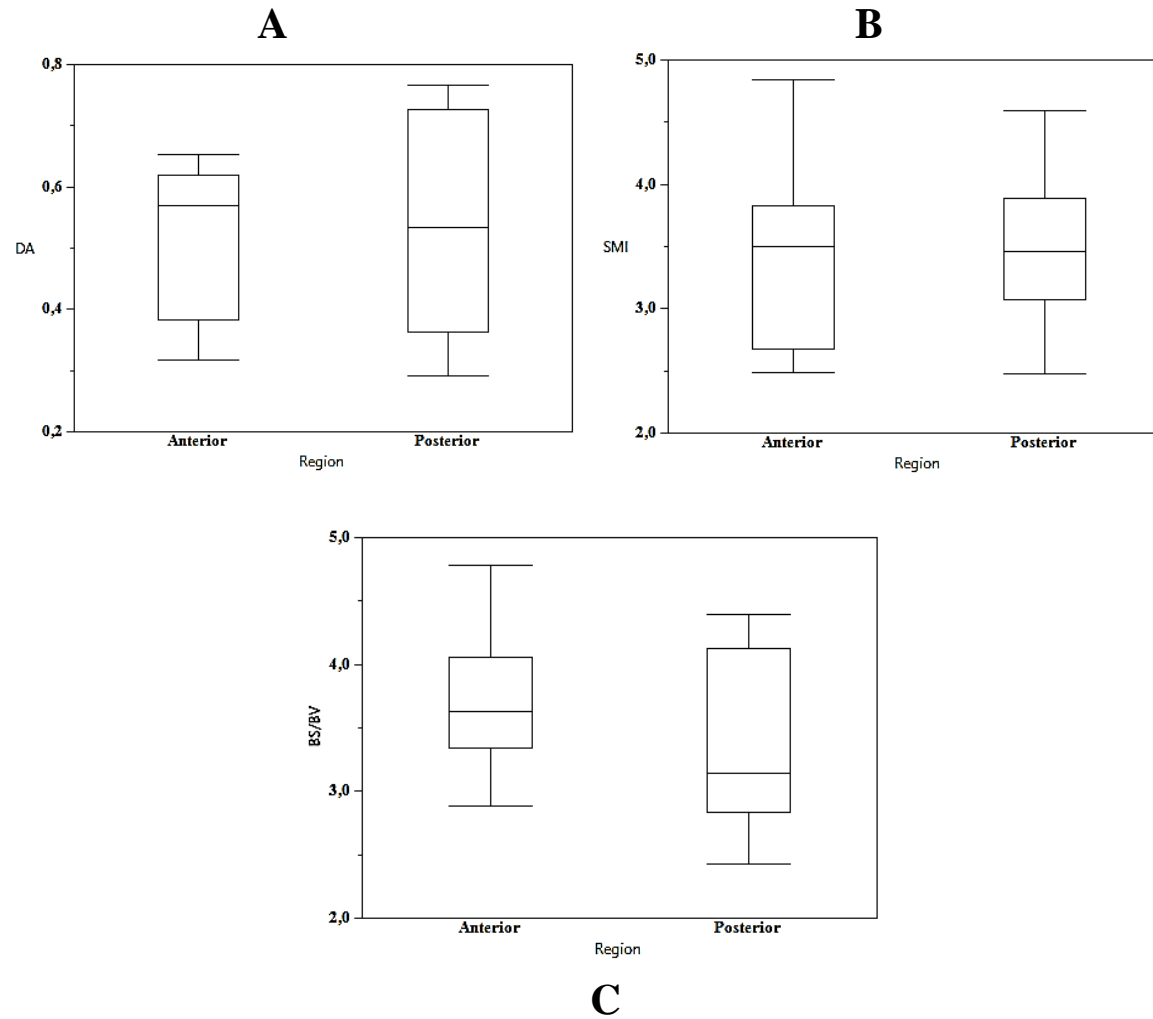


Figure 4.32. Boxplots indicating A) degree of anisotropy (DA) B) structural model index (SMI) and C) bone surface to bone volume ratio (BS/BV) by subregion in the medial malleolus of *P. pygmaeus*.

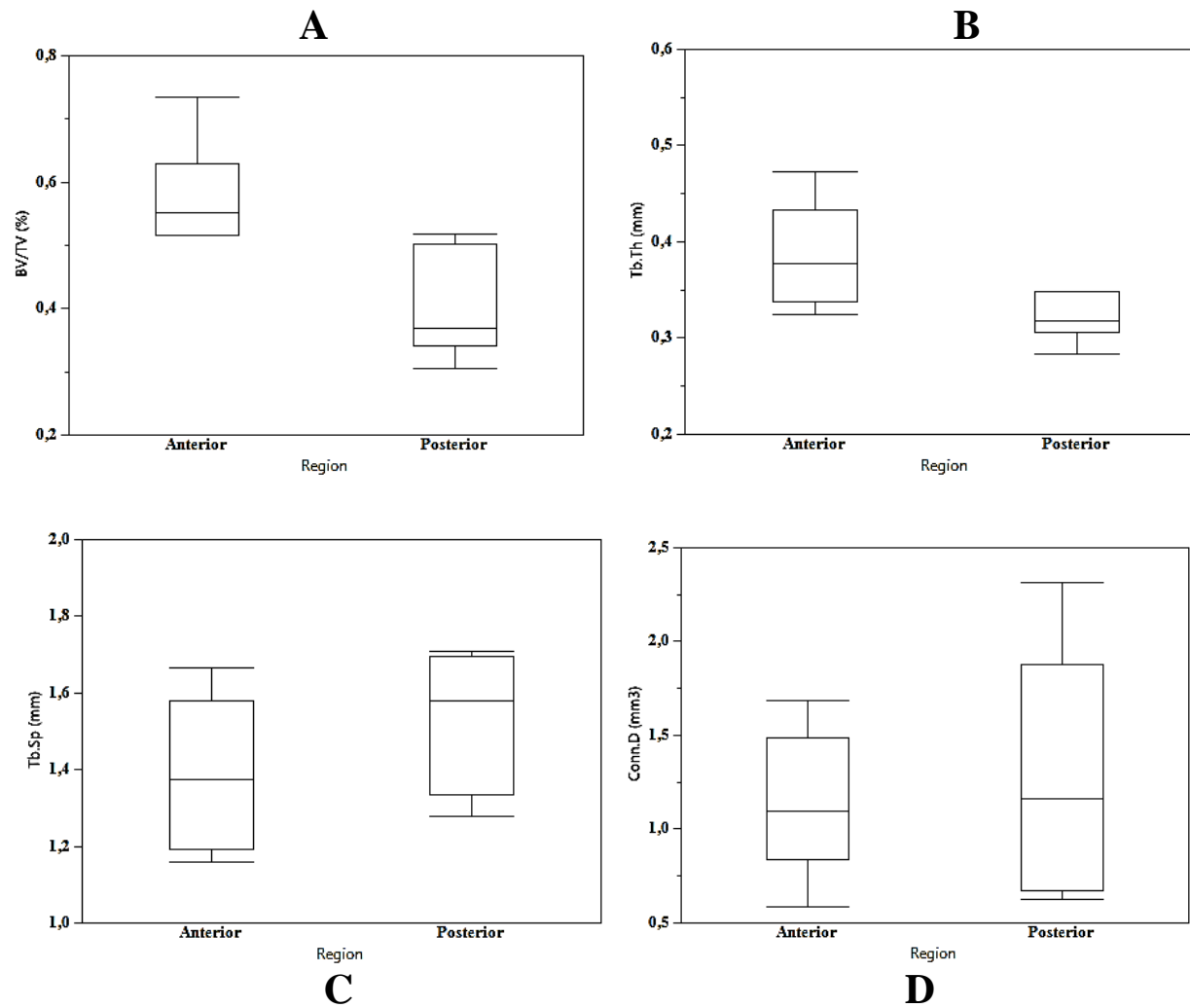


Figure 4.33. Boxplots indicating A) bone volume fraction (BV/TV), B) trabecular thickness (Tb.Th), C) trabecular spacing (Tb.Sp) and D) connectivity density (Conn.D) by subregion in the medial malleolus of *P. hamadryas*.

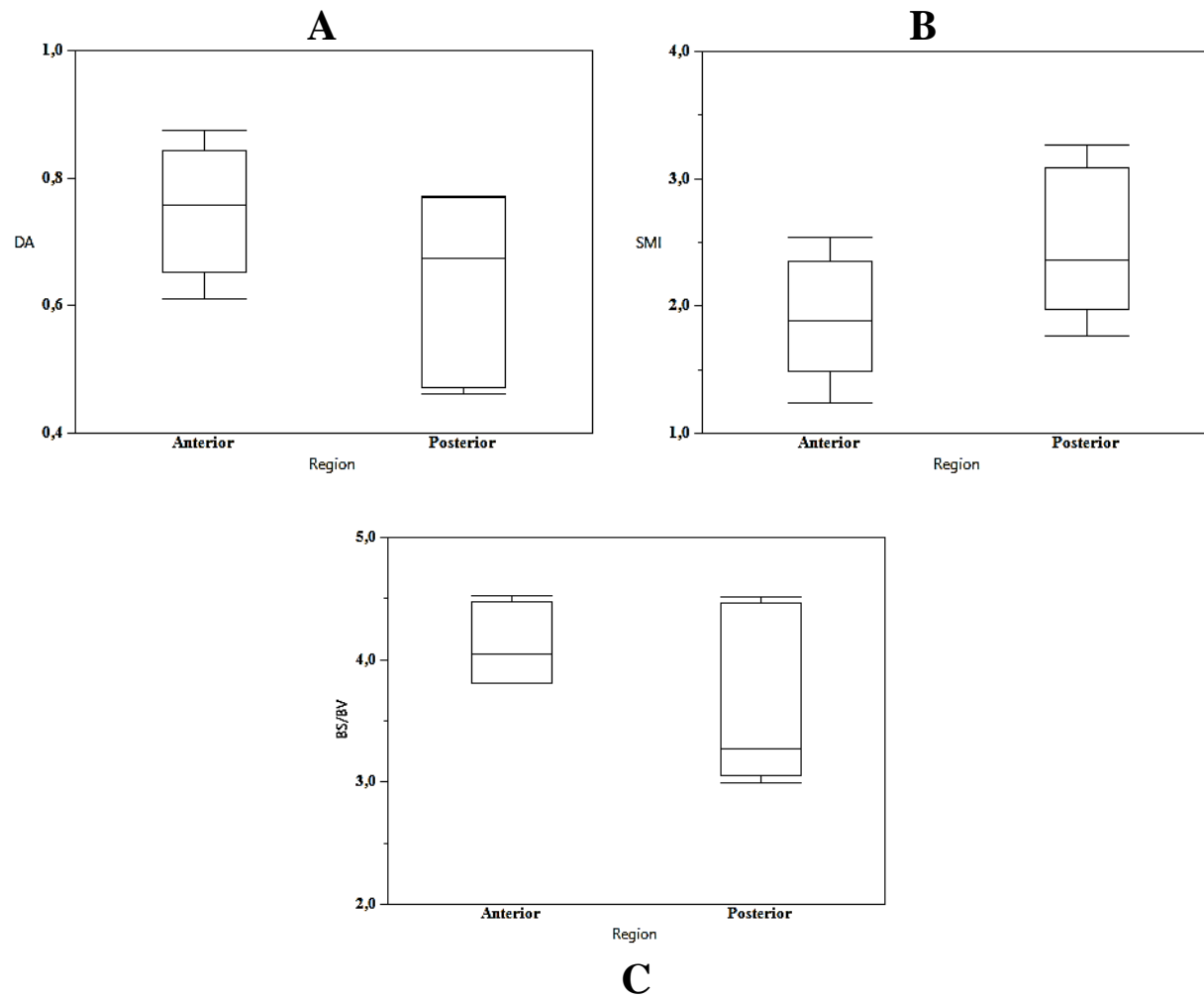


Figure 4.34. Boxplots indicating A) degree of anisotropy (DA), B) structural model index (SMI) and C) bone surface to bone volume ratio (BS/BV) by subregion in the medial malleolus of medial malleolus of *P. hamadryas*.

4.7. Discriminant Function Analysis of extant species.

Assessment of structural properties deep to the distal tibia plafond revealed that the first discriminant function (DF1) accounts for between 58.30% and 89% of the variance among extant groups (depending on the VOI). The DF1 usually separated terrestrial digitigrade quadrupeds (baboons) at one extreme from bipeds (humans) at the other (Table 4.15, Fig 4.35). Across the x axis, DF1 typically reflects higher BV/TV, lower Tb.Sp and higher DA in *Papio*, while in humans it typically reflects lower BV/TV, higher Tb.Sp and lower DA (Table 4.15, Fig 4.35). Overlap between species (e.g., *Pan* and *Pongo*) is observed in all 9 VOIs. In fact, these two species were the most common misclassified by the DFA. In the central regions, there is greater overlap between species in the sample, particularly *Homo*, *Pongo* and *Pan*.

The second discriminant function (DF2) accounts for between 6% and 33% of the variance among the extant groups (depending on the VOI) (Table 4.15, Fig 4.35). DF2 typically reflects higher BS/BV and Tb.Sp from positive to negative, clustering *Homo* at the positive extreme (i.e. high BS/BV and high Tb.Sp) in most VOIs and *Gorilla* (i.e. low BS/BV and low Tb.Sp) at the negative extreme in most VOIs. Predicted group classifications are presented in Table 4.14. The DFA has a stronger ability to distinguish between species in the anterior region, as is indicated by the fewer misclassifications that occurred in this VOI. The overall least successful VOI in the DFA was the central most region C-C (VOI 5), which had approximately 20% misclassification rates (Table 4.14).

Projecting fossil specimens into discriminant space revealed that StW 358 plotted within *Pan* and *Pongo* clusters in all VOIs of the anterior region (Fig 4.35, row 1). StW 515 and StW 389, on the other hand, clustered with *Homo* in VOI1 (A-M) and StW 567 plotted closer to *Homo* within the DFA, although it falls just outside of the *Homo* cluster. In the A-C (VOI2) volume, all fossil specimens fall outside the DF space of the extant groups, except StW 358, which falls within *Pongo*. StW 389, StW 515 and StW 567 plot more closely to the extant non-human primate clusters than the *Homo* cluster. In the A-L volume (VOI3), StW 567 falls within the *Homo* cluster. By comparison, StW 389 and StW 515 fall outside the DF space of the extant samples. Both, however, are closer to non-human primate clusters than the modern human cluster. StW 358 falls within the *Pan* cluster

In the central region (Figure 4.35, row 2), there is greater overlap between extant species, especially *Pan*, *Homo* and *Pongo*. In the C-M region (VOI4), *Gorilla* and *Papio* are at

opposing ends of discriminant function space while *Pan*, *Pongo* and *Homo* overlap in the center. StW 358 and StW 515 plotted between *Pan* and *Papio* clusters, while StW 567 falls just outside of the *Papio* cluster. StW 389 falls far outside clusters of the extant species in VOI4. The fossils plotted outside clusters of extant species in the central VOI (C-C, VOI5). StW 358 and StW 389 were closest to *Pongo* and *Papio* clusters with a negative DF2, while StW 567 plotted closer to the *Pan* cluster and maintained a positive DF2. In the lateral volume (C-L, VOI6), StW 358 and StW 389 fall within the *Homo* cluster, while StW 567 falls outside clusters of extant species and demonstrates a negative DF1, but falls closest to *Pan*, *Pongo* and *Papio* clusters.

In the posterior region (Fig 4.35, row 3), there was noticeable overlap among extant hominoids, except for *Gorilla* which was unique partially due to very low BS/BV affecting the DF2. In the fossils, StW 389 falls within the *Homo* cluster in P-M (VOI7) and P-C (VOI8) VOIs, while StW 358 falls within the *Pongo* cluster in both P-M (VOI7) and P-C (VOI8) VOIs. StW 567 plotted outside of the clusters of the extant species in the P-M VOI (VOI7), but falls within the *Pan/Pongo* combined cluster in the P-C VOI (VOI8). In the posterolateral VOI, two fossils (StW 358 and StW 389) fall outside the clusters of any extant species, although StW 358 falls relatively closer to the extant non-human comparative sample. StW 389 demonstrated a high DF2, probably caused by the high BS/BV in the P-L VOI (VOI9).

Table 4.14. Predicted group membership summary for discriminant function analyses

VOI	Count	Number misclassified	% misclassified	2log likelihood
A-M	48	4	8,33	25,767
A-C	48	3	6,25	14,225
A-L	48	4	8,33	17,352
C-M	48	2	4,167	15,196
C-C	48	10	20,83	37,825
C-L	48	6	12,5	33,803
P-M	48	6	12,5	22,69
PC	48	8	16,67	34,846
P-L	48	9	18,75	35,08

Table 4.15. Summary of discriminant function analysis of the distal tibia.

Region	Function	Wilks' Lambda	p value	Eigenvalue	% of variance	Cumul %	Canonical Corr
A-M	1	0,092	<0,0001	2,986	66,874	66,874	0,866
	2	0,368	<0,0001	1,295	29,018	95,891	0,751
	3	0,844	0,125	0,174	3,889	99,78	0,385
	4	0,99	0,52	0,009	0,22	100	0,099
A-C	1	0,077	<0,0001	5,109	82,914	82,914	0,914
	2	0,468	0,0002	0,969	15,732	98,646	0,702
	3	0,922	0,488	0,075	1,212	99,858	0,264
	4	0,991	0,543	0,009	0,142	100	0,093
A-L	1	0,041	<0,0001	5,436	71,028	71,028	0,919
	2	0,265	<0,0001	1,952	25,502	96,53	0,813
	3	0,781	0,033	0,191	2,501	99,031	0,401
	4	0,931	0,081	0,969	0,963	100	0,263
C-M	1	0,09	<0,0001	5,292	89,001	89,001	0,917
	2	0,567	0,0042	0,380	6,396	95,396	0,525
	3	0,783	0,0343	0,261	4,387	99,783	0,455
	4	0,987	0,4604	0,013	0,217	100	0,113
C-C	1	0,123	<0,0001	2,981	77,437	77,437	0,865
	2	0,488	0,0004	0,561	14,564	92	0,599
	3	0,761	0,0206	0,288	7,484	99,485	0,473
	4	0,981	0,3611	0,02	0,515	100	0,139
C-L	1	0,147	<0,0001	2,023	63,816	63,816	0,818
	2	0,444	<0,0001	1,049	33,072	96,887	0,715
	3	0,909	0,4	0,086	2,712	99,599	0,281
	4	0,987	0,464	0,013	0,401	100	0,112
P-M	1	0,153	<0,0001	2,711	79,939	79,939	0,855
	2	0,569	0,0044	0,537	15,829	95,768	0,591
	3	0,874	0,223	0,143	4,23	99,998	0,354
	4	0,99	0,961	0,0008	0,0017	100	0,007
P-C	1	0,139	<0,0001	2,133	64,591	64,591	0,825
	2	0,437	<0,0001	1,061	32,13	96,721	0,717
	3	0,902	0,354	0,099	3,016	99,736	0,301
	4	0,991	0,544	0,009	0,264	100	0,264
P-L	1	0,127	<0,0001	2,067	58,303	58,303	0,821
	2	0,389	<0,0001	1,413	39,854	98,156	0,765
	3	0,939	0,61	0,065	1,825	99,982	0,247
	4	0,99	0,866	0,0006	0,019	100	0,026

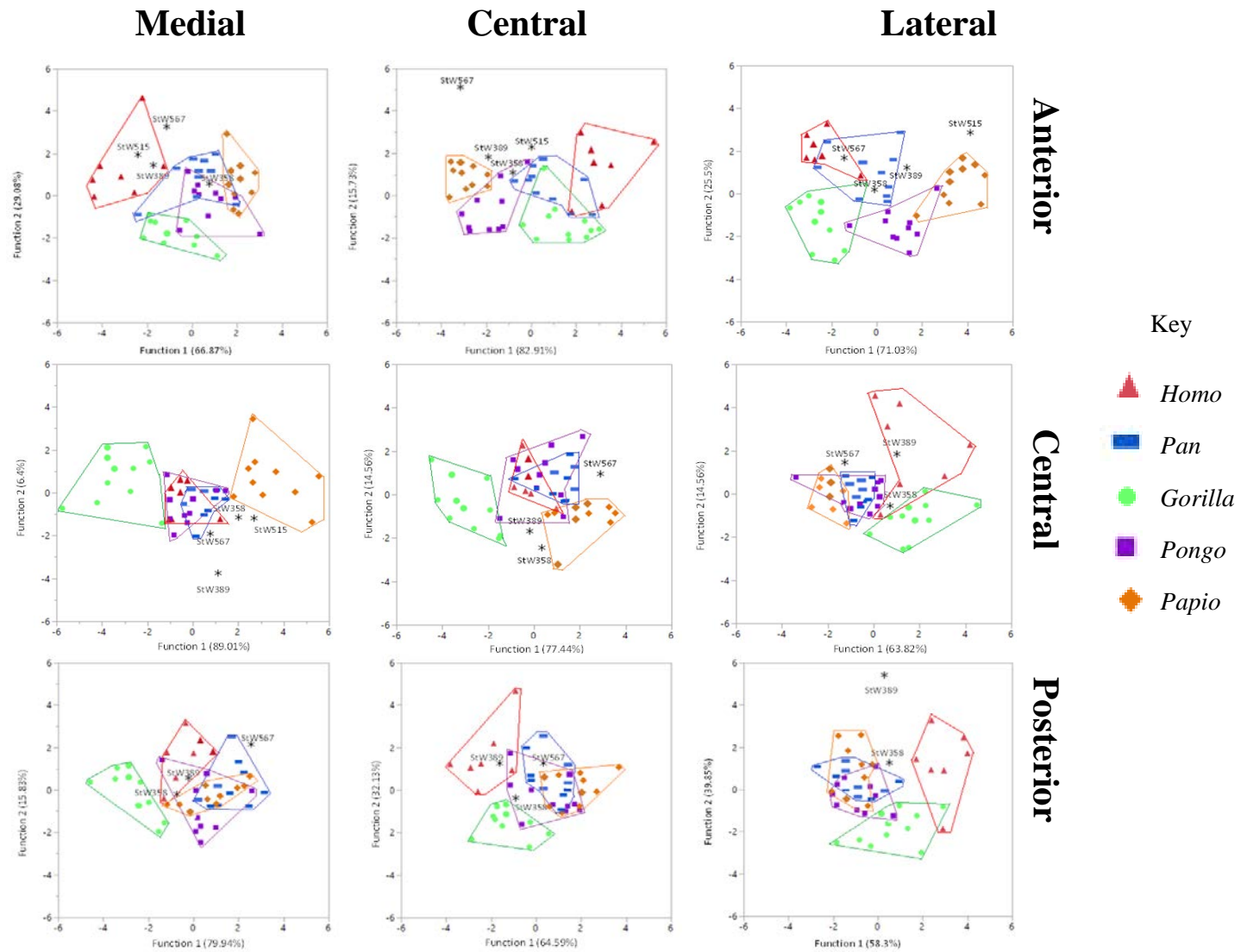


Figure 4.35. Plots of Discriminant Function 1 versus Discriminant Function 2 of individuals in groups summarizing scalar values by subregions. Rows represent anterior, central and posterior regions of distal tibia, respectively. Columns represent medial, central and lateral subregions from left to right, respectively

CHAPTER 5: DISCUSSION AND CONCLUSION

The primary aim of this dissertation was to investigate the relationship between skeletal form of the distal tibia and locomotor loading in extant and fossil species. The results of this study support the previous identification of a locomotor signal in trabecular fabrics of the distal tibia of hominoids and *A. africanus* (i.e., see Barak *et al* 2013b), and expanded upon it to develop a more detailed understanding of functional signals in trabecular fabrics beneath articular surfaces of the tibial plafond and the medial malleolus. Specifically, this study tested whether trabecular structure in the primate distal tibia was able to differentiate extant primate species based on habitual locomotor and postural behaviours. The first null hypothesis that trabecular structure does not distinguish species was rejected based on multivariate DFA.

The second hypothesis tested the relationship between trabecular structure in the primate distal tibia and known kinematic data from these extant species. The null hypothesis that trabecular structure was not reflective of kinematic data was rejected for all extant species with which associated kinematic data are available (*Homo*, *Pan*, *Gorilla*). Kinematic data on free-ranging *Pongo* and *Papio* are limited, and thus behavioural-based predictions are generalised as similar to African apes. The findings of this study suggest that areas of strengthened bone in the distal tibia correlate with areas of presumed high loading resulting from posture and locomotor behaviour in *Homo*, *Pan* and *Gorilla*. Distinct loading conditions associated with obligate bipedality (i.e., those in modern *Homo*) are observed in trabecular structure deep to the plafond of the distal tibia and differ from patterns observed in extant non-human hominoids that demonstrate an anterolateral strengthened trabecular fabric associated with extreme dorsiflexion during climbing bouts.

The third hypothesis tested whether or not trabecular structure in the medial malleolus contained a functional signal based on inferences drawn from ankle kinematics of the extant species (see DeSilva *et al* 2009, 2013). Sample size was not sufficient to conduct statistical testing of this hypothesis, but preliminary findings of this study suggest that a possible functional signal may distinguish trabecular fabrics of the anterior versus posterior region of the medial malleolus. Anterior regions of the medial malleolus are more reinforced in extant non-human primates that have been observed to demonstrate relatively high frequencies of arboreal (mostly climbing) behaviours. The results of this study therefore tentatively indicate a potential loading difference incurred during (a possible variety) of arboreal behaviours where the foot is in an inverted position against a vertical substrate in extant non-human

primates (DeSilva *et al* 2013). The examination of internal structure of the medial malleolus could potentially be used in studies of fossil hominins such as *A. sediba* that possess a seemingly externally robust medial malleolus, which could potentially indicate a greater weight-bearing resistance that would be especially useful during inversion of the ankle during vertical climbing bouts.

The fourth hypothesis tested whether trabecular structure in *A. africanus* distal tibiae was human-like or ape-like. Based on differences in trabecular structure of the tibial plafond, the results of this study suggest that the *A. africanus* distal tibiae sample was comprised of two different morphs, both appearing in Member 4. One morph appears to be more baboon-like in structure, while the other demonstrates the characteristic mosaic of human-like and ape-like features attributed to other anatomical regions of *A. africanus*. This result highlights the importance of combining external morphological studies with internal structural studies in fossil hominins so as to accurately reconstruct behaviour.

5.1. Trabecular architecture in the primate distal tibia differs between species.

Results of the discriminant function analysis (DFA) demonstrated that anterior VOIs as a whole had the lowest percentage of misclassified specimens among the three regions (anterior, central, posterior) when considering BV/TV, Tb.Sp, DA and BS/BV (Table 4.14). This coincides with kinematic-based predictions that across the primate species examined in this study, the anterior region would be best at differentiating the loading patterns experienced by the primate species examined in this study. The central most VOI (VOI5) exhibited the highest percent of misclassified specimens among all VOIs, which was the VOI predicted to have minimal kinematic based loading differences across species.

Specific predictions of trabecular parameter differences between species were partially met (see Chapter 1). As predicted, BV/TV was generally lowest in *Homo*, although this difference was not statistically significant beyond the lateral region where *Pan* and *Papio* had significantly greater BV/TV than *Homo*. Irrespective of VOI location, low BV/TV in *Homo* coincides with recent work on the gracilisation of more sedentary populations of humans in the Holocene (Chirchir *et al* 2015).

While it was predicted that Tb.Th would be greater in larger-bodied primates, this was not observed. Rather, *Pongo* generally demonstrated the thickest struts in the distal tibia (*Pongo*>*Gorilla*>*Pan*>*Papio*>*Homo*). Increased thickness of orangutan trabeculae was

interpreted as an adaptation to support the varying postural and locomotor strategies exhibited by orangutans. Recent studies have demonstrated a high degree of intraspecific variation in trabecular structure of other skeletal elements, such as the metacarpals, in taxa such as *Pongo* (Tsegai *et al* 2013), and in humans in the humerus and femur (Ryan & Shaw 2012, 2015, Saers *et al* 2016).

Predictions outlined in Chapter 1 specifically regarding Tb.Sp and Conn.D parameters were partially met as modern humans demonstrated the highest separation among the extant taxa. Tb.Sp differed significantly among species, and was one of the more consistent parameters capable of distinguishing species. The high Tb.Sp and low Conn.D of modern humans was interpreted as a mechanism for balancing bone strength, while keeping the skeleton as light as possible. The lowest Tb.Sp and highest Conn.D was observed in *Papio*, resulting in a mechanically strong bone composed of numerous thin and densely packed trabeculae. The African apes (*Gorilla* and *Pan*) tend to mirror humans in strengthening the bone using fewer, thicker, slightly more separated struts compared to the Asian apes and the cercopithecoids, this also was observed in the calcaneus and talus (Zeininger *et al* 2016, Su & Carlson 2017).

Predictions regarding DA were not met in this study. High DA values were observed in the talus of humans relative to non-human hominoids (Su & Carlson 2017). It was predicted that due to the limited locomotor repertoire of modern humans (i.e., predominantly bipedal locomotion), and their less mobile ankle joint, they also would exhibit higher DA. Opposite the prediction, modern humans generally demonstrated the lowest DA of all of the extant species in the present study.

Predictions regarding BS/BV were not met in this study, as *Papio* consistently demonstrated the highest BS/BV of the extant species (*Papio*>*Pan*>*Pongo*>*Homo*>*Gorilla*), except in the posterior VOIs where *Homo* demonstrated higher BS/BV than any of the *Pongo* and *Gorilla*. High BS/BV in the more arboreal *Pan* and *Pongo* is interpreted as reflecting stronger struts over a variety of postural and locomotor styles. Interestingly, *Pan* and *Pongo* can be characterized as the two most versatile species in terms of locomotor repertoire compared to the other extant species (Hunt 1992, Thorpe & Crompton 2006). High BS/BV in *Papio* was unexpected, and further studies on kinematics of *Papio* would be useful to fully examine effects of its digitigrade posture and potentially restricted ankle movements on shape of trabeculae. The observed posteriorward increase in BS/BV in *Homo* is consistent with other studies that have observed the posterior region of *Homo* to be more reinforced in internal

bone studies (Hvid *et al* 1985, Lai *et al* 2005). This posterior reinforcement in humans in comparison to other non-human primates in this study is interpreted as a reflection of the definitive heel strike at touch down exhibited by modern humans when walking.

5.2. Trabecular architecture in non-human primates is reflective of known kinematics.

5.2.1. Trabecular structure in extant non-human hominoids.

Based on behavioural studies of chimpanzees and gorillas, it was predicted that the African hominoids examined in this study would share similar locomotor repertoires and therefore exhibit similar trabecular structure in the distal tibia, although *Pan* is more arboreal than larger-bodied *Gorilla*. This prediction was not supported, however, based on findings of the DFA whereby chimpanzee trabecular structure were mistaken for orangutans and baboons (76.47% of misclassified chimpanzees) more often than gorillas and humans (23.53% of misclassified chimpanzees), and gorillas occupied a discriminant function space that was separate from the other extant species sampled across all volumes except for a slight overlap in the central and lateral volumes in the anterior and posterior regions. *Gorilla* was also misclassified the least number of times in the DFA compared to the extant species including humans (1.92% of total misclassifications). Chimpanzees and orangutans were the two species with the highest percentage of misclassified specimens in the DFA (65.38% of total misclassifications, each 32.69% respectively), which were mostly in the central and posterior region.

General predictions that chimpanzees and lowland gorillas would demonstrate higher loading in the anterior and lateral regions of the distal tibia were partially met. The lateral and anterior regions in gorilla tibiae demonstrated higher BV/TV, Tb.Th and BS/BV, along with lower Tb.Sp and Conn.D. These indicate substantial bone volume composed of fewer, thicker plate-like trabecular struts that were relatively anisotropic in distribution. A predominant anterior loading regime was predicted based on vertical climbing behaviour and the extreme dorsiflexion associated with it that has been observed in modern chimpanzees and to a lesser extent, gorillas, during this locomotor mode. The prediction was not met in the chimpanzees included in this study, however, as their posterior region demonstrated general greater strength than their anterior region although this difference was not significant (as determined by BV/TV). Vertical climbing in the chimpanzee locomotor budget varies based on localities, as Doran (1993) found that chimpanzees in the Tai forest (*Pan troglodytes verus*) spent 11% of their total locomotor activities climbing and Hunt (1989, 1991, 1992) found that

chimpanzees at Gombe and Mahale (*Pan troglodytes schweinfurthii*) spent only 5.5% of their total locomotor budget climbing. Although the chimpanzees examined in this study were obtained from different museums (Table 3.1), the lack of clear anterior loading associated with vertical climbing in the distal tibia could be attributed to differences in locomotor budgets of individuals within the study sample. This observation also serves as a potential indicator that general arboreality and not specifically vertical climbing, is important in the remodelling and strengthening of the internal and external structure of the ankle in non-human primates.

Chimpanzees are more versatile than gorillas in their range of locomotor behaviours, in part due to lesser constraints imposed by a large body size (Hunt 1992, 1994). Due to their large body sizes, gorillas are often constrained by tree size and structure when climbing (Jungers & Susman 1984, Cant 1987a,b, 1992), although female western lowland gorillas are known to climb more than males (Remis 1995, 1999). The restrictions on locomotion imposed by a large body size in *Gorilla* could be a contributing factor to the relatively well separated cluster occupied by *Gorilla* in the DFA, as well as the lack of misidentifications. The locomotor behaviour of gorillas in general have been understudied, (Schaller 1963, Doran 1997) and therefore in order to understand the role of the ankle in gorilla locomotion it is important to expand upon kinematic data concerning climbing.

Chimpanzees are able to dorsiflex their ankle to 45° ($\pm 7.5^{\circ}$) during vertical climbing bouts, and also substantially invert and abduct their foot (DeSilva 2009). This joint capability brings the chimpanzee body close to the vertical substrate, reducing climbing metabolic costs associated with increased muscular activity needed to counter the downward torque acting on their large body about the fixed pedal grasp of the trunk. Chimpanzees are also able to walk bipedally for short bouts of time using a compliant bent hip bent knee (BHBK) gait, which differs from the extended hip extended knee (EHEK) gait typical in humans; the former has mostly been observed in wild chimpanzees gathering and transporting important resources such as fruits (Hunt 1992, Thorpe & Crompton 2006, Pontzer *et al* 2014). During chimpanzee bipedal gait, initial contact is simultaneously made with the heel and the lateral aspect of the midfoot, i.e., inverted heel-strike plantigrady (Elftman & Manter 1935, Vereecke *et al* 2003, DeSilva *et al* 2013). This may be a factor in the more laterally strengthened tibial plafond, as it may reflect the high lateral loading imposed by body weight during both quadrupedal and bipedal strides. The generally high amount of misclassifications in *Pan* (more with other non-

human primates than modern humans) is attributed to the generalised locomotor repertoire of chimpanzees, and the intraspecific variation of individuals within a population.

The orangutan is the most arboreal of the great apes, having retained morphology suited for a lifestyle in tree canopies. Predictions regarding the orangutan distal tibia were partially met in this study (see Chapter 1). Similar to other extant great apes, orangutans exhibited increased anterior strength in the tibial plafond (high BV/TV, high Tb.Th, low Tb.Sp, high BS/BV). As orangutans are predominantly arboreal, safety to reduce injury when climbing is important. While it remains undocumented, orangutans may have had a similar maximum dorsiflexion angle at the ankle joint as chimpanzees ($45.5^\circ + 7.1^\circ$) during their navigation of an arboreal environment in order to remain close to the vertical substrate.

Interestingly, distribution of DA across the tibial plafond in orangutans used in this study is similar in distribution as modern humans, demonstrating a higher DA at the antero-central (VOI2), centrolateral (VOI3) and posterocentral (VOI8) VOIs. Previous studies of the locomotion and postural behaviour of orangutans have concluded that they possess a complex, diverse spectrum of locomotor modes (Thorpe & Crompton 2006). Although the locomotor repertoire of orangutans is dominated by orthograde and pronograde suspensory postures, often associated with feeding accounting for 24% of their locomotor behaviour, Thorpe & Crompton (2006) also noted that bipedal walking accounted for 7.3% of overall locomotion, of which 5.5% was hand-assisted. Therefore, based on the trabecular structure and the directedness in its distribution across the whole bone, it is assumed that most of the weight still goes through the two lower limbs on the compliant substrate (i.e. tree branches). Although foot posture and substrate compliancy differ, orangutans have been observed to more fully extend their hindlimb during bipedal scrambling, which was also observed on irregularly-placed and variously angled supports. Cant (1987a) also noted that bipedal behaviour was observed, but he did not record it because it was hand-assisted, and therefore presumably better classed as orthograde clamber.

High DA across the distal tibia of orangutans, higher often than *Homo* hunter-gatherers, and a distribution that is similar in pattern to *Homo* DA, calls for more investigation into the biomechanics of the orangutan bipedality. This is potentially important in understanding the role of the orangutan in modelling the evolutionary origin of bipedality from an arboreal last common ancestor.

Externally, the non-human hominoid medial malleolus is more robust and mediolaterally thicker than that observed in humans. High loads experienced by the anterior region are presumed to occur during foot inversion associated with climbing bouts in free-ranging great apes. DeSilva *et al* (2013) have argued that when the ape foot is inverted against a vertical substrate (e.g., a tree trunk), the reaction force should pass anteriorly through the medial malleolus, resulting in a reinforced anterior region. Although African apes are more terrestrial than the Asian apes, Doran (1996) stated that climbing is second only to terrestrial quadrupedalism in terms of the frequency of locomotor behaviours of African apes. Although findings were tentative, there is a potential indicator of increased bone strength and anisotropy in the anterior region of the medial malleolus in chimpanzees and orangutans. The gorillas used in this sample did not exhibit great differences in trabecular structure in the anterior and posterior regions of the medial malleolus, although preliminary findings of this study indicate a slightly stronger posterior region in the gorilla medial malleolus. Vertical climbing in lowland gorillas was estimated to compose 19.7% of their total locomotor budget, more so than chimpanzees (6.5%) and slightly less than orangutans (20.6%) (Hunt 2004). The lack of a clear functional signal across the AP axis in the medial malleolus of *Gorilla* could be due to the small sample size.

5.2.2. Trabecular structure in the distal tibia of digitigrade quadrupedal *Papio*.

Predictions regarding trabecular structure of the baboon distal tibia were partially met in this study. Anterior and lateral regions were predicted to be strongest, similar to conditions observed in other non-human primates. The lateral region demonstrated a higher BV/TV, Tb.Th, and BS/BV, as well as a low Tb.Sp and Conn.D. This suggests a dense trabecular fabric composed of fewer, thicker, plate-like struts. The posterior region rather than the anterior region, however, generally demonstrated comparatively more strengthened trabecular structure. The DFA revealed that the cercopithecoid *Papio* was misclassified 23.08% across the 9 VOIs, mostly in the posterior region (66.67% of misclassified *Papio* across 9 VOIs) where *Papio* was misclassified as *Pan* and *Pongo*. The lack of clear groupings predominantly in the posterior region is attributed to offloading in the posterior region of the primate distal tibia as the majority of locomotor imposed loading is assumed to be anterolaterally directed.

Plantigrady in cursorial animals is rarely observed (Hildebrand & Goslow 1998). Instead, digitigrady or unguligrade gaits are adopted to maximize length of the limb, which is a key determinant of the energetic costs associated with locomotion (Hildebrand & Goslow 1998,

Pontzer 2007). In the comparative sample, *Papio* represents the digitigrade primate. Cercopithecoids rarely vertically climb and when they do, they are kinematically different from the methods practiced by hominoids and atelines (Hunt 1992, Hirasaki, 2000, Gebo 1992, Isler 2003, 2004, 2005, DeSilva 2009). Published data and ankle flexion calculated from video of climbing bouts in wild baboons and geldas (Hirasaki *et al* 1993, Isler 2003, 2004, 2005, DeSilva 2009) support the idea that cercopithecoid monkeys do not experience extreme dorsiflexion at the ankle, but instead dorsiflex in the midfoot region during climbing.

The posterior tibiotalar ligament (PTTL), which originates in the intercollicular groove in the medial malleolus, has been hypothesized to act as an important dorsiflexion restrictor in the human ankle (DeSilva 2009). Hominoids and atelines, by comparison, have a weakly developed intercollicular groove, and the attachment of their respective PTTLs is close to the ankle axis of rotation, which limits the role of these ligaments as ankle stabilizers. In contrast, the intercollicular groove in terrestrial cercopithecoids, like that of modern humans, is significantly larger and positioned away from the axis of rotation, changing the role of the PTTL to one that restricts dorsiflexion. These results suggest that *Papio* has a more limited range of motion of the ankle compared to that of the extant nonhuman great apes, but not as restrictive as the modern human ankle. This could also potentially account for the stereotypical loading of the distal tibia that is reflected in the extreme high DA values observed across the distal tibia in *Papio* in comparison to the sampled hominoids.

The unique digitigrade posture during quadrupedalism has contributed to loading conditions that are both ape-like (lateral loading) and human-like (posterior loading) in *Papio*. External morphology of the baboon medial malleolus differs from that of extant hominoids and ateline primates that exhibit a mediolaterally wide anterior surface of the distal tibia (i.e. adapted for the efficient distribution of forces through the ankle during positions of extreme dorsiflexion) and an anteroposteriorly reduced tibial metaphysis which could allow for an increased range of dorsiflexion (DeSilva 2009). The medial malleolus of hominoids is also significantly thicker mediolaterally than in the cercopithecoid monkeys, consistent with kinematic data demonstrating the medial loading of the midfoot during climbing observed by DeSilva (2009). Predictions regarding the high anterior loading (indicated by strengthened trabecular bone in the anterior region of the medial malleolus) in the sampled *Hamadryas* baboons were met with caution as the baboons were wild shot and subsequently kept in captivity, therefore making predictions regarding behaviour, substrate and activity levels difficult. Moreover, the high anterior loading observed in this species should not be attributed to a climbing

adaptation as they do not vertically climb, but instead scramble on inclined branches to access higher areas of the crowns.

5.3. Trabecular architecture in modern human hunter-gatherers is highly variable and isotropic

It was predicted that due to the limited range of motion in the human ankle, as well as the stereotypical loading imposed by habitual bipedality, the modern human sample of hunter-gatherers would exhibit higher DA than the extant non-human primates. This was rejected as modern humans generally exhibited the lowest DA values across the tibial plafond in comparison to the other sampled taxa. High DA values were observed in the talus of humans relative to non-human hominoids (Su & Carlson 2017) and therefore were expected to be similar in the tibial plafond. The results of the multivariate DFA revealed that human trabecular fabrics occupied a different discriminant function space compared to the extant non-human primates in the anterior and posterior region, with the most overlap occurring in the central region, although bipedal humans still demonstrated a low percentage of misclassifications (9.62%) and all of these were in the central region (VOI4, VOI5).

Individuals in the human sample examined in this study were misclassified only in the central regions where the overlap occurred with *Pan* and *Pongo* (75% of total misclassified humans), and once with *Papio* in VOI5. The central VOI's (VOI4 and VOI5) were not associated with kinematic predictions in the extant primate species, and therefore the misclassification was attributed to a lack of a clear distinctive loading conditions in the central most region.

Along the AP axis, it was predicted that the posterior region of the ankle would exhibit stronger bone properties relative to the anterior and central, which was confirmed in this study since the posterior region demonstrated higher BV/TV and Tb.Th, lower Tb.Sp and Conn.D. This was supported by previous work on internal structure of trabecular bone in the human distal tibia that found that the posterior portion is not only stronger but also has an increased bone volume density, trabecular number, thickness and highly anisotropic struts relative to the anterior portion of the distal tibia (Hvid *et al* 1985, Lai *et al* 2005). This increased posterior strengthening has been interpreted by authors as an internal bony adaptation to the reduction in the contact area of the distal tibia, and thus results in an increase in internal stress during contact between the tibia and talus during plantarflexion (Kura *et al* 1998).

Similar anterior and posterior trabecular structure in the human medial malleolus is interpreted as adaptive for ankle support (High BV/TV and Tb.Th, low Conn.D, Tb.Sp), as both regions would need to be strong in order to support and stabilise the ankle during the full stance phase of walking and running. The medial malleolus in humans primarily serves as a support structure in order to mediolaterally stabilise the ankle during locomotion, both through the robust nature of the bone and by its attachment points for ligamentous reinforcements (i.e. the deltoid ligament on the medial aspect).

During bipedalism, particularly running gaits, humans support their entire body weight on a single lower limb, thus requiring strong stable lower limb joints (e.g., the ankle). The medial malleolus is characterised in humans as possessing a mediolaterally wide proximal base, a convex medial surface, a slightly concave articular surface that is continuous with the articular surface of the distal tibial plafond and an anterior and posterior colliculus that are each separated from one another by an intercollicular groove. The anterior colliculus is a narrower, slender anterior portion that extends distally below the level of the posterior colliculus with a convex medial surface that serves as an attachment for the superficial portion of the deltoid ligament. The posterior colliculus is comparatively broader, although it contains the smaller portion of the articular surface. It has a shallow sulcus on its posterior surface for the attachment of the tendon sheaths of *m. tibialis posterior* and *m. flexor digitorum longus*. The intercollicular groove, and the distal surface for the posterior colliculus, serve as the attachment of the deep posterior talotibial ligament (Kelikan & Saraffian 2006).

Low DA values in the modern human sample analysed in this study are attributed to the foraging, highly active nature of hunter-gatherers. Studies on trabecular structure in the lower limb of modern human populations with varying lifestyles were conducted by Saers *et al* (2016) who found a significant correlation between inferred mobility level and trabecular structure in all volumes of interest along the lower limb. The largest possible single cubic VOI that included trabeculae were sampled in the joint was taken from beneath the talar surface. This study also revealed a lower DA in the distal tibia of hunter-gatherers (Black Earth) in comparison to more sedentary groups of humans (Norris Farms and Kerma).

Bone tissue repairs microdamage and remodels/models in response to mechanical loading (Frost 2003), whereby bone is added under high dynamic strain (Sugiyama *et al* 2010). Therefore, bone structure should reflect an individual's mechanical homeostasis to a certain

extent. In this study, walking was taken as the habitual locomotor mode of humans to which trabecular bone is functionally adapted, although running could result in minor kinematic differences accompanied by greater load magnitudes that could be potentially informative in studies of trabecular structure (Daoud *et al* 2012). Velocity during running is greater than walking and therefore it is assumed that the ankle loads would be greater too, which could potentially influence trabecular structure, especially in highly active persistence runners.

However, the hunter-gatherer sample analysed in this study demonstrated DA values that were even lower than those of extant non-human primates, suggesting a high isotropy in the trabecular structure of the distal tibiae. This highly isotropic trabecular structure has been attributed to the unshod conditions of the hunter-gatherers coupled with probable high substrate variability on the coastal plains of the western and southern cape of South Africa. During most of human evolutionary history, the foot to ground interaction has involved a bare foot interacting with a natural but highly variable substrate (Willems *et al* 2016). Hunter-gatherers are generally adapted for endurance running and are often partially shod or unshod (Trinkaus 2005, Williams *et al* 2016). The hunter-gatherer humans used in this study were assumed to be unshod based on anthropological, ethnological and palaeontological data (as most pre-pastoralists were during the Holocene) (Hausman 1982, Roberts 1989, Sealy & Pfeiffer 2000, Roberts & Berger 1997, Stock & Pfeiffer 2001, Zipfel & Berger 2007) and occupied open air cave deposits, which are surrounded by uneven, rocky substrates.

Due to the lack of a mediating factor on shock absorbance (i.e., footwear) during barefoot (or minimally shod) running and walking on different types of substrates, combined with the high activity levels, low DA in modern human hunter-gatherers could suggest favouring of isotropically distributed trabeculae in order to compensate for the variable loading conditions across the tibial plafond. The difference in population groups could potentially explain the differences in observations of the talus by Su & Carlson (2017), as the human sample used were from 20th century Americans from the Hamann-Todd Collection at the Cleveland Museum of Natural History.

Although the human sample size and composition is small, and therefore only tentative conclusions can be reliably drawn, there is a pattern of grouping of individuals according to locality, resulting in the higher variation in the human sample. Mobility in ancient hunter-gatherer societies is interpreted as partially dependent on the abundance and distribution of resources in the environment at the time of occupation, and, therefore, foragers in areas

where resources are scantily distributed tend to be more mobile, directly impacting on the activity levels observed in nomadic hunter-gatherer populations (Kelly 1983, Donald & Mitchell 1994, Binford 2001). The advantage of a coastal population includes richness and reliability of marine foods, which meant less need to be mobile in order to secure food resources (Bailey & Parkington 1988, Bailey & Milner 2002). Although all three hunter-gatherer populations represented by the study sample were of coastal distribution, subtle variation in the diet of the populations based on stable isotope analysis reveal that the hunter-gatherers at Matjies River Rock Shelter had eaten more mixed diets consisting of terrestrial food and low-trophic-level marine food such as shellfish (Sealey & Pfeiffer 2000, Sealey 2006). The Robberg population, located only 14km east of Matjies River, demonstrated stable isotope $\delta^{15}\text{N}$ values indicative of high-trophic-level sea foods (including seal meat consumption) in both men and women. This suggests that Matjies River individuals probably exhibited higher activity levels than Groot Brak and Robberg Cave individuals.

5.4. Trabecular structure in the distal tibia of *A. africanus* indicates the possibility of two potentially different morphs in Sterkfontein Member 4

The external morphology of hominin species such as *A. africanus* is often described as a mosaic of primitive ape-like characteristics and derived human-like characteristics. Results of this study revealed that the amount of variability expressed in the fossil specimens (most notably in BV/TV, Conn.D and SMI) was well above the observed intraspecific variation in the extant comparative samples, suggesting the possibility of one hypervariable morph or two potentially different morphs in Sterkfontein Member 4 (Table A4).

All of the hominin distal tibiae sampled were more ape-like in bone volume fraction (BV/TV) and trabecular separation (Tb.Sp) across all nine VOIs. Trabecular thickness (Tb.Th) was more varied, however, StW 389 and StW 515 were more human-like (i.e. thinner struts) and StW 358 and StW 567 were more ape-like (i.e. generally thicker struts). The hominins were also unique in Conn.D compared to the extant primate taxa, exhibiting high variation in strut connectivity. StW 389 and StW 515 fell well above the observed connectivity in extant taxa, while StW 358 and StW 567 were *Gorilla*-like in connectivity. All hominins demonstrate highly anisotropic trabeculae (i.e. higher than modern humans, but within the range of extant non-human primates), except StW 567 which often exhibited low DA, even lower than that observed in modern human hunter-gatherer populations.

The results of the DFA demonstrated the unique internal structure of the australopith ankle, as the fossil hominins often fell within the discriminant function space of the more generalised locomotor species (i.e. *Pan* and *Pongo*), or completely outside of the morphospace of the extant species used in this study. This unique structure, therefore, can be interpreted as exhibiting a gait that is perhaps kinematically unlike that observed in any of the living primate species that were compared in the study.

5.4.1. A potentially second morph in Sterkfontein represented by StW 389 and StW 515 from Sterkfontein Member 4.

StW 389 and StW 515 demonstrated a generally lower BV/TV and Tb.Th coupled with uniquely high Conn.D. Human-like strut thickness was observed in the anterior region of StW 389 (VOI1-VOI3) as well as the posterior region (VOI8-VOI9) (Table A4). Although StW 515 was incomplete and only the anterior and the centromedial region could be analysed, the anteromedial VOI demonstrated human-like BV/TV, DA and SMI. This region is important kinematically, and is distinctively stronger in modern humans compared to extant non-human primates presumably as a result of mediolateral weight shift during bipedality. Connectivity density in StW 358 and StW 515 was unique and very high across all volumes (except VOI1 and VOI4 in StW 389).

This trabecular structure (high Conn.D, low BV/TV, Tb.Sp, Tb.Th) was not observed in the extant hominoids, but the combination of trends more closely resembles those in the structural properties of *Hamadryas* baboons. Whether or not this is due to sexual differentiation in the species is unclear and would require further analyses using pooled sex samples of extant species. This has been performed using baboons, which exhibited little difference between sexes in terms of trabecular structure (Zeininger *et al* 2016). Both of these fossil specimens (StW 389 and StW 515) exhibited high DA across the tibial plafond, particularly in the lateral region. Thus, this is interpreted as a potential second morph within distal tibia from Sterkfontein Member 4.

To date, *A. africanus* is one of two hominins recognized in Member 4 deposits of Sterkfontein (Kuman & Clarke 2000, Pickering & Kramers 2010). Interestingly, the presence of more than one hominin in Member 4 has also been supported by morphological studies of postcranial remains (Zipfel & Berger 2009, Zipfel *et al* 2010, DeSilva *et al* 2012). Due to the difficulties in delineating Member 4 and Member 5 deposits (Kuman & Clarke 2000, Stratford *et al* 2012, 2013), this unknown species represented by baboon-like internal

structure perhaps could be *A. prometheus* or another hominin taxon (i.e. *Paranthropus robustus*).

5.5. Unique trabecular structure of StW 358 from Sterkfontein Member 4.

External morphology of StW 358 demonstrates a lack of a swollen metaphysis and instead the anterior and posterior margins of the plafond are flat which is observed in extant non-human primates. StW 358 also demonstrated unique trabecular structure in comparison to the extant primate sample as well as the other sampled fossil specimens. BV/TV in StW 358 was uniquely high laterally (VOI3, VOI6, VOI9) and posteriorly in VOI8 and VOI9 (Table A4). This unique trabecular structure was also observed in thickness in the central and posterior regions (VOI5-VOI7) where struts were thicker than those observed in extant species as well as other fossil specimens. The most unique parameter measured was SMI in StW 358, which extended into the negative SMI, the only specimen sampled to do so, representing a fabric that consists of concavities. Most of the other trabecular parameters measured were non-human like in distribution, interestingly DA in the anteromedial and antero-central region of StW 358 was most similar to modern human hunter-gatherer sample. This is a kinematically important region, associated with medial loading during the mediolateral weight shift observed during bipedal gait, although the rest of the tibial plafond was represented by an overlapping human-like and ape-like DA distribution.

5.6. Trabecular structure of StW 567, a presumed *Homo sp.* from Sterkfontein Member 5.

Upon closer examination of StW 567, it was determined that the specimen was a sub-adult based on the fusion of the epiphyses as represented by growth plates in the 2D sagittal slices through the tibial plafond. When sampling for trabecular spheres, care was taken to only include trabeculae just beneath the joint surface and not across areas of growth plates. Based on the sub-adult status of the specimen and the presence of growth plates, assumptions were tentative regarding the trabecular structure. This specimen was included in the study conducted by Barak *et al* (2013b), which concluded that the species represented by StW 567 walked with an EHEK gait like modern humans. This specimen has been tentatively assigned to *Homo sp.* and is the only specimen from Member 5.

In StW 567, more anisotropically distributed trabeculae are found in the medial and central regions, indicative of more repetitive medial loading of the tibia during locomotion. This

specimen also demonstrates uniquely low DA in the anterior region and an overlap of human-like and non-human like DA over the rest of the VOIs sampled in the central and posterior regions. The other trabecular parameters measured were mostly overlapping and resembled both the human-like and nonhuman-like conditions, although the connectivity density was nonhuman-like across the VOIs sampled, except in VOI2 and VOI3 where the connectivity was unique to the specimen (Table A4). The unique distribution of DA, SMI, Conn.D and Tb.Sp in the anterior region of the distal tibia of StW 567 suggest a different loading regime in the anterior region that is not observed in humans and non-human primates today. The distribution of DA has been interpreted as reflecting abnormal gait within an individual, and possibly an early occurrence of hyperpronation in a hominin specimen, resulting in an exaggerated medial weight transfer during stance phase of bipedalism. Hyperpronation would result in initial contact on an inverted foot, which would result in high medially-directed forces on the tibiotalar joint. If trabecular structure reflects the same loading patterns as ankle kinematics would imply, then a higher loaded central region would be observed in the tibial plafond. The central region in these fossil specimens was relatively strengthened, which was not the case in any of the extant sample. Instead, the extant samples tended to exhibit the lowest presumed loads in the central region.

5.7. The distal tibia of StW 515 and links to the proximal StW514.

StW 515 (previously StW514b) was originally associated with StW514a, a proximal right tibial fragment (Berger & Tobias 1996), and demonstrated morphological features that distinguish it from the tibia of humans. Rather, this specimen had external morphological characteristics of a knee joint that was more mobile and ape-like. These include: a convex lateral condyle (Martin & Saller 1959), which is associated with greater rotational ability and more extreme flexion of the knee-joint; a straight posteromedial border of the lateral condyle (Tardieu 1983, Senut & Tardieu 1985); and a circular depression for the distal attachment of the semimembranosus, as opposed to the indistinct horizontal groove observed in humans (Aiello & Dean 1990).

Due to the relatively incomplete state of the StW 515 distal tibia, little work has been conducted on its external morphology in order to make functional inferences. The articular surface possesses a posterior tilt in the AP plane that has been associated with a habitually dorsiflexed ankle, although this has been disputed in terms of the importance in interpreting locomotor behaviour (Latimer *et al* 1987, Berger & Tobias 1996). External morphology of

the distal tibia and the fragmentary StW514 proximal tibia thought to be associated with this individual has raised questions as to whether or not it is in fact a hominin tibia. The discovery of “Little Foot” (*A. prometheus*) in Member 2 at Sterkfontein, and particularly the highly mobile first metatarsal of this species could be indicative of high mobility of the foot, and demonstrates a morph that does not appear to be incompatible with the tibia represented by StW514-515 (Berger & Tobias 1996). Based on findings of the internal trabecular structure in the distal tibia of StW 515 in this study, there is additional support for the idea of a more chimpanzee-like tibia represented by StW 515 and StW514.

5.8. Trabecular structure and the probability of climbing in *A. africanus* from Sterkfontein Member 4

The anterior region of StW 567 is unique compared to the other distal tibiae, StW 358 and StW 515, as it is the only specimen exhibiting human-like trabecular structure in the anterior region. This could be interpreted as more vertical loading in a more vertically oriented tibia (e.g., less climbing), unlike the condition exhibited in StW 358 and StW 515. StW 515, on the other hand, exhibited the lowest BV/TV, Tb.Th and Tb.Sp and a relatively high Conn.D (higher than observed in any extant species) and BS/BV. StW 515 also exhibited a very low DA (lower than any extant species). StW 515 stands out as the only fossil of the three that exhibits trabecular structure suggestive of a general incompatibility with climbing since the medial malleolus appears internally much less stronger than the non-human hominoids in the sample.

The only fossil specimen that possessed a fully intact medial malleolus was StW 358. It exhibited a non-human primate (i.e. chimpanzee-like) trabecular structure in the anterior malleolar region (high BV/TV, Tb.Th, DA, BS/BV and low Tb.Sp and Conn.D), although the posterior region fell within the human range of variation. Trabecular structure of the anterior region in StW 358 suggests higher anterior loading, as observed in the extant non-human primate sample. This may reflect an adaptation for foot inversion during climbing bouts. StW 358 demonstrated unique trabecular features in the posterior region, including low Conn.D and BS/BV coupled with low Tb.Sp and extremely low DA. This pattern suggests a loading condition unobserved in the extant sample, and although there is overlap with *Homo* to some degree in the posterior region, the general trabecular structure indicates a trabecular fabric composed of numerous thin densely-packed isotropic trabeculae. Skeletal adaptations associated with climbing abilities have been found in *A. anamensis* based on scapular

morphology (Green & Alemseged 2012), in the foot of *A. sediba* (DeSilva *et al* 2013), and the hand of *A. africanus* (Ricklan 1987). Internal structure of the medial malleolus also suggests that climbing was part of the locomotor repertoire of StW 358, which was the *Australopithecus sp.* from Sterkfontein Member 4 (Berger & Tobias 1996).

5.9. Limitations of this study and future work

The ability of trabecular bone to distinguish species based on their locomotor abilities has received mixed support, partially due to the difficulty in isolating functionally equivalent loaded regions across species with a differing external morphology. Positioning of VOIs is important in comparing the functional signals of anatomically and biomechanically equivalent loaded regions across a sample when morphology is complex and there is a large degree of morphological and size variation (Maga *et al* 2006, Kivell *et al* 2011a, b, Lazenby *et al* 2011). Size and location of the VOI could therefore directly impact the interpretation of whether or not a functional signal is present. Barak *et al* (2013b) examined the distal tibia using two VOIs located medially and laterally. Their study yielded statistically significant findings that support the reflection of clear plantarflexion and dorsiflexion signals in trabecular architecture. The current study expanded on this work by increasing the number of VOIs in order to examine trabecular bone structure in conjunction with published 3D kinematics.

Although efforts were made to reduce the effects of body size on the results by using an all-female sample across the primate taxa (except in *Papio* where males were included), trabecular parameters such as BV/TV and Tb.Th are closely correlated to body size in primate groups (Ryan & Shaw 2012). Intraspecific variation within extant species and the correlation of internal bone structure with kinematics is also important for the interpretation of loading and gait. Correction for body weight would therefore be potentially useful to conduct in order to deduce if structural differences are disproportionately reflective of body weight rather than function.

Although the sample size for this study was more sufficient for the extant apes, it would be beneficial to increase the human sample size and possibly introduce groups of humans with different activity levels or originating from different geographic localities in order to understand the factors affecting bone remodelling and functional adaptation in Holocene humans. The findings of this study could also be improved upon by obtaining locality information for extant non-human primate species, as it has been shown to impact differences

in locomotor budgets of chimpanzees (Doran 1996, Hunt 1994). The medial malleoli findings were also restricted by a small sample size. In order to statistically account for the presence of a locomotor signal, it is recommended that future work is conducted on a larger sample size of primates, and possibly introducing fossil hominin taxa such as *A. sediba* with unique external morphology.

Primary trabecular orientation has proven to be a strong indicator in distinguishing groups in the talus (Su & Carlson 2017), and it would therefore be an additional result to add support to the accuracy of trabecular structure in distinguishing extant species with divergent locomotor behaviour. This also would aid in the identification of whether or not a mediolateral weight shift is observed in the distal tibia of *A. africanus*.

Trabecular strut shape is often characterized by two different measurements. The first, SMI, measuring whether trabeculae are plate-like or rod-like, has had its accuracy disputed based on the underlying assumption that the entire bone surface is convex and that the curvature differential is positive at all points on the surface. Trabecular surfaces consist of intricate connections that suggest that a high proportion of the surface could be concave, which violates this first assumption and therefore renders SMI readings as negligible (Salmon *et al* 2015), this could possibly account for negative SMI observed in StW 358. BS/BV has been used as a second, alternative measurement for trabecular shape. Further studies should compare the results of SMI and BS/BV in order to conclude which is a better representation of trabecular shape for comparative purposes.

Another limitation faced by the current study is the absence of kinematic data available for certain extant primate species. This is especially true for orangutans, as the kinematic data available may not fully represent the entirety of the relevant high load conditions (e.g., some locomotor behaviours, particularly arboreal ones). It is important to understand the different types of locomotor behaviours, and the behaviour-specific kinematics involved in order to predict and test whether the bone is loaded beyond the remodelling threshold, and if it is not loaded beyond such a threshold, then presumably its structure would reflect something else besides load during gait, or a different locomotor behaviour.

Within primates, most trabecular studies have focussed on hominoids, in part because of their close relationship to humans and their potential informative value to inferring behaviour in fossil hominoids and hominins (Machiarelli *et al* 1999, DeSilva & Devlin 2012, Shaw & Ryan 2012, Barak *et al* 2013b, Scherf *et al* 2013, Su *et al* 2013, Tsegai *et al* 2013, Schilling

et al 2014, Raichlen *et al* 2015, Su & Carlson 2017). Studies of trabecular structure of hominins have been conducted mostly on australopithecines, most notably *A. africanus*. In order to understand variation and experimentation in gait in fossil hominins, it is important to reconstruct trabecular architecture in more species (e.g. *Paranthropus* and early *Homo*) and on multiple specimens (where possible) in order to appreciate the variation within the hominin fossil record. In order to understand the variation in trabecular structure of hominins in Sterkfontein Member 4, it is important to analyse trabecular structure of all hominin taxa present as a base for comparison. The study could therefore be expanded to include *A. prometheus* (StW 573) and trabecular information from *P. robustus*, in order to conclude if the structural properties observed in StW 389 and StW 515 are more similar than observed in *A. africanus*.

5.10. Conclusion.

This study has demonstrated that trabecular structure in the distal tibia may contribute as a reliable source of information when inferring joint loading and locomotor kinematics in fossil hominins. The study conducted by Barak *et al* (2013b) examined trabecular structure in two VOIs to assess anteroposterior differences in the distal tibia of primates in order to determine whether or not locomotor signals were present. This study expanded upon the findings of Barak *et al* (2013b) to include 9 VOIs in order to amplify locomotor signals associated with kinematics of extant species, particularly with regard to 3D joint movements. This allowed for the assessment of not only anteroposterior signals but also mediolateral signals (which proved to be statistically significant between *Homo* and *Pan* as well as *Homo* and *Papio*) in the distal tibia and resulted in greater precision in the sampling strategy.

The results of the multivariate DFA have highlighted the ability of trabecular structure to distinguish species based on locomotor type and how the ability to differentiate species fluctuates between regions. The anterior region was better than the central and posterior at differentiating between species; this generally resulted in humans on one extreme being characterized by a low BV/TV and fewer and thicker trabecular struts, and baboons on the other extreme being characterized by a high BV/TV and more numerous, thinner and more densely packed trabeculae. Often, the most incorrectly identified individuals were chimpanzees and orangutans, which supports the idea that species with more overlapping locomotor behaviours may exhibit trabecular structure that is more similar. The findings of

this study reiterate the importance of VOI location in comparative trabecular functional studies.

In general, non-human primates exhibited stronger trabecular structure in the anterior and lateral regions of the distal tibia, while humans demonstrated strengthened trabecular structure more posteriorly and medially across the tibial plafond. Hominoid trabecular structure was also different from that observed in the cercopithecoid outgroup, with the former exhibiting high BV/TV composed of fewer, thicker trabecular struts compared to the high BV/TV consisting of numerous, thin and densely packed trabeculae of the latter. Interestingly, the human sample analysed in this study demonstrated generally more isotropic struts compared to the non-human primate sample. This was unexpected as the bipedal gait of humans was predicted to demonstrate more stereotypical loading and therefore result in more anisotropic struts based on previous investigations.

Intraspecific studies are important in improving understanding of the developmental, mechanical and physiological influences on remodelling of trabecular bone. The intraspecific comparisons were used to assess the ability of trabecular structure to reflect kinematic data in primate species investigated here. The findings of this study conclude that aspects of trabecular structure are reflective of ankle kinematics in extant species. The trabecular structure in modern *Homo* was more medially strengthened in comparison to the lateral strengthening observed in the non-human primate sample (with the exception of *Pongo*). Ties between the medial strengthening and high anisotropy observed in *Pongo* and the locomotor behaviour and kinematics of this species require further investigation.

The modern human sample demonstrated more medial strengthening in the posterior region of the tibial plafond compared to the higher anterior strengthening in the extant non-human hominoid sample. This strengthened anterior region in primates has been attributed to the extreme dorsiflexion observed during bouts of vertical climbing. Anterior strengthening was also observed in the medial malleolus in climbing non-human hominoids as well as cercopithecoids. Although findings of the medial malleolus are tentative, they indicate a possible locomotor signal in loading conditions across the anteroposterior axis in hominoids.

The high intraspecific variation and the tendency of individuals from the same localities to cluster together in the *Homo* sample has been interpreted as a result of differences in activity levels in coastal hunter-gatherer populations (although the sample size did not allow for statistical testing between populations). Hunter-gatherers generally exhibit a more isotropic

trabecular structure compared to sedentary groups of modern humans (Saers *et al* 2016). It is therefore important to consider not only activity levels when selecting a sample of modern humans for comparative trabecular studies, but also substrate and the effects of footwear. In analysing trabecular structure of multiple groups of modern humans, navigating highly variable landscapes with or without shoes, it is possible to further the understanding around the role of activity levels, substrate and footwear on the internal trabecular structure in the ankle.

Several authors have investigated using trabecular bone in studies of fossil hominin locomotion (Macchiarelli *et al* 1999, DeSilva & Devlin 2012, Barak *et al* 2013b, Su *et al* 2013, Su & Carlson 2017). It is important to understand the nuances of trabecular responses to loading in order to examine gait and variation in the fossil record. Many aspects of external morphology may be constrained by phylogeny or function, and therefore the sensitivity of trabecular bone to mechanical loading in combination with high remodelling rates may provide a dynamic source of data.

The results of this study indicate that there are potentially two different morphs within the fossil sample from Sterkfontein Member 4 (i.e. StW 358, StW 389, StW 515 and StW 567). This was based on the trabecular structure of distal tibiae in the fossil specimens where StW 515 and StW 389 demonstrated structure that was more similar to cercopithecoids (i.e. trabecular structure that consists of numerous, thin, densely packed trabeculae) as opposed to the overlapping *Pan*- and *Homo*-like structure observed in StW 358 and StW 567. These fossil hominins demonstrated a unique trabecular structure in the distal tibia that could be interpreted as a bipedal gait with a greater range of motion about the ankle that is not observed in modern humans. This is further corroborated by findings in the medial malleolus of StW 358, which is anteriorly strengthened as seen in climbing non-human hominoids. The findings of this study therefore imply that climbing was still part of the *A. africanus* locomotor repertoire, although to a lesser extent than observed in modern non-human hominoids.

This study has demonstrated the usefulness of internal bone structure in corroborating external morphological analyses on fragmentary fossil hominin specimens. When external morphology may not be visible, or even if the shaft and metaphysis are largely missing, it may still be possible to extract functional information from internal properties provided the element can be oriented and sufficient contrast is available for segmenting the trabecular

fabric. This is especially valuable in sites such as Sterkfontein where multiple hominin species have been identified and many fragmentary remains have been discovered.

CHAPTER 6: REFERENCES

- Aiello, L.C. and Dean, M.C. 1990. An Introduction to Human Evolutionary Anatomy. London: Academic Press.
- Alexander, R. McN., Bennett, M.B. 1987. Some principles of ligament function, with examples from the tarsal joints of the sheep (*Ovis aries*). *Journal of Zoology*, 211: 487-504.
- Abourachid, A. 2000. Bipedal locomotion in birds: the importance of functional parameters in terrestrial adaptation in Anatidae. *Canadian Journal of Zoology*, 78(11): <https://doi.org/10.1139/z00-112>
- Asfaw, B., White, T., Lovejoy, O., Latimer, B., Simpson, S. and Suwa, G. 1999 *Australopithecus garhi*: a new species of early hominid from Ethiopia. *Science*, 284: 629–635 doi:10. 1126/science.284.5414.629
- Bailey, G. and Parkington, J. 1988. The archaeology of prehistoric coastlines. Cambridge University Press, London.
- Bailey, G. and Milner, N. 2002. Coastal hunter-gatherers and social evolution: marginal or central? Before Farming. *Liverpool University Press Online*, doi: 10.3828/bfarm.2002.3-4.1
- Barak, M.M., Weiner, S. and Shahar, R. 2008. Importance of the integrity of trabecular bone to the relationship between load and deformation in rat femora: an optical metrology study. *Journal of Materials Chemistry*, 18: 3855–3864.
- Barak, M.M., Lieberman, D.E. and Hublin, J.J. 2011. A Wolff in sheep's clothing: trabecular bone adaptation in response to changes in joint loading orientation. *Bone*, 49: 1141–1151.
- Barak, M.M., Lieberman, D.E. and Hublin, J.J. 2013a. Of mice, rats and men: trabecular bone architecture in mammals scales to body mass with negative allometry. *Journal of Structural Biology*, 183: 123–131.
- Barak, M.M., Lieberman, D.E., Raichlen, D., *et al.* 2013b. Trabecular evidence for a human-like gait in *Australopithecus africanus*. *PLoS ONE* 8, e77687.
- Barnett, C. and Napier, J. 1952. The axis of rotation at the ankle joint in man. Its influence upon the form of the talus and the mobility of the fibula. *Journal of Anatomy*; 86(Pt 1): 1.
- Bassey, E.J. and Ramsdale, S.J. 1994. Increase in femoral bone density in young women following high-impact exercise. *Osteoporosis International*, 4: 72–75.
- Beamer, W.G., Donahue, L.R., Rosen, C.J., and Baylink DJ. 1996. Genetic variability in adult bone density among inbred strains of mice. *Bone*, 18: 397-403.
- Beddoe, A.H. 1978. A quantitative study of the structure of trabecular bone in man, rhesus monkey, beagle and miniature pig. *Calcified Tissue International*, 25: 273–281.
- Begeman, P.C., and Prasad, P. 1990. Human ankle impact response in dorsiflexion. Proceedings of the 34th Stapp Car Crash Conference (Society of Automotive Engineers Inc, Warrendale, PA), No: 902308:39-54.

- Begun, D.R. and Kivell, T.L. 2011. Knuckle-walking in *Sivapithecus*? The combined effects of homology and homoplasy with possible implications for pongine dispersals. *Journal of Human Evolution*, 60:158–170.
- Berillon, G., Daver, G., D’Août, K., Nicolas, G., De La Villetanet, B., Multon, F., Digrandi, G. and Dubreuil, G., 2010. Bipedal versus quadrupedal hind limb and foot kinematics in a captive sample of *Papio anubis*: setup and preliminary results. *International Journal of Primatology*, 31: 159e180.
- Berger, L.R. and Tobias, P.V. 1996. A chimpanzee-like tibia from Sterkfontein, South Africa and its implications for the interpretation of bipedalism in *Australopithecus africanus*. *Journal of Human Evolution* 30, 343e348.
- Berger, L.R., de Ruiter, D.J., Churchill, S.E., *et al.* 2010. *Australopithecus sediba*: a new species of *Homo*-like australopith from South Africa. *Science*, 328: 195–204.
- Bertram, J.E.A. and Swartz, S.M. 1991. The ‘law of bone transformation’: a case of crying Wolff? *Biological Reviews*, 66: 245–273.
- Biewener, A.A., Fazzalari, N.L., Konieczynski, D.D., *et al.* 1996. Adaptive changes in trabecular architecture in relation to functional strain patterns and disuse. *Bone* 19, 1–8.
- Bikle, D.D. and Halloran, B.P. 1999. The response of bone to unloading. *Journal of Bone and Mineral Metabolism* 17, 233–244.
- Binford, L.R., 2001. *Constructing Frames of Reference*. University of California Press, Berkeley (CA)
- Brockett, C.L., and Chapman, G.J. 2016. Biomechanics of the ankle. *Journal of Orthopaedic Trauma* 30(3):232-238.
- Burr, D.B. 1990. Experimental overload and bone adaptation. In: *Bone Morphometry* (ed. Takahashi HE), pp. 140–148. Japan, Nishimura: Nishimura Co Ltd.
- Cant, J.G.H. 1987a. Positional behavior of female Bornean orangutans (*Pongo pygmaeus*). *American Journal of Primatology*, 12:71–90.
- Cant, J.G.H. 1987b. Effects of sexual dimorphism in body size on feeding postural behavior of Sumatran orangutans (*Pongo pygmaeus*). *American Journal of Physical Anthropology*, 74:143–148.
- Cant, J.G.H. 1992. Positional behaviour and body size of arboreal primates: a theoretical framework for field studies and an illustration of its application. *American Journal of Physical Anthropology* 88, 273–283.
- Carlson, K., Lublinsky, S. and Judex, S. 2008. Do different locomotor modes during growth modulate trabecular architecture in the murine hind limb? *Integrative and Comparative Biology* 48, 385–393.
- Carter, D.R. and Beaupre, G.S. 2001. *Skeletal Function and Form: Mechanobiology of Skeletal Development, Aging, and Regeneration*. Cambridge: Cambridge University Press.

- Chang, G., Pakin, S.K., Schweitzer, M.E., *et al.* 2008. Adaptations in trabecular bone microarchitecture in Olympic athletes determined by 7T MRI. *Journal of Magnetic Resonance Imaging* 27, 1089–1095.
- Chirchir, H., Kivell, T.L., Ruff, C.B., *et al.* 2015. Recent origin of low trabecular bone density in modern humans. *Proceedings of the National Academy of Science USA* 112, 366–371.
- Coelho Jr., A.M. and Bramblett, C.A., 1981. Sexual dimorphism in the activity of olive baboons (*Papio cynocephalus anubis*) housed in monosexual groups. *Archives of Sexual Behavior*. 10, 79e91.
- Conconi, M., Leardini, A. and Parenti-Castelli, V. 2015. Joint kinematics from functional adaptation: A validation on the tibio-talar articulation. *Journal of Biomechanics* 48: 2960–2967
- Cotter, M.M., Simpson, S.W., Latimer, B.M., *et al.* 2009. Trabecular microarchitecture of hominoid thoracic vertebrae. *The Anatomical Record*, 292: 1098–1106.
- Cowin, S.C. (ed.) 2001. Bone Biomechanics Handbook. 2nd edn. Boca Raton: CRC Press.
- Crompton, R.H., Vereecke, E.E. and Thorpe, S.K.S. 2008. Locomotion and posture from the common hominoid ancestor to fully modern hominins, with special reference to the last common panin/hominin ancestor. *Journal of Anatomy*, 212:501-543
- Cunningham, C.A. and Black, S.M. 2009. Anticipating bipedalism: trabecular organization in the newborn ilium. *Journal of Anatomy*, 214: 817–829.
- Currey, J.D. 2002. Bones: Structure and Mechanics. Princeton: Princeton University Press.
- Daoud, A.I, Geissler, G.J., Wang, F., Saretsky, J., Daoud, Y.A. and Lieberman, D.E. 2012. Foot Strike and Injury Rates in Endurance Runners: A Retrospective Study. *Medicine & Science in Sports & Exercise*, 44 (7): 1325-1334.
- D'Août, K., Vereecke E, Schoonaert, K. *et al.* 2004. Locomotion in bonobos (*Pan pansicus*): differences and similarities between bipedal and quadrupedal terrestrial walking, and a comparison with other locomotor modes. *Journal of Anatomy*, 204: 353–361.
- Dawe, E.J. and Davis, J. 2011. VI Anatomy and biomechanics of the foot and ankle. *Orthopaedics and Trauma*, 25(4): 279-286
- Demes, B., Larson, J., Stern, J., *et al.* 1994. The kinetics of primate quadrupedalism: 'hindlimb drive' reconsidered. *Journal of Human Evolution*, 26: 353–374.
- Dempster, D.W. 2000. The contribution of trabecular architecture to cancellous bone quality. *Journal of Bone and Mineral Research*, 15: 20–23.
- DeSilva, J.M., 2009. Functional morphology of the ankle and the likelihood of climbing in early hominins. *Proceedings of the National Academy of Science USA* 106, 6567e6572.
- DeSilva, J.M. and Devlin, M.J. 2012. A comparative study of the trabecular bony architecture of the talus in humans, non-human primates, and *Australopithecus*. *Journal of Human Evolution*, 63: 536–551.

- DeSilva, J.M., Proctor, D.J. and Zipfel, B. 2012. A complete second metatarsal (StW 89) from Sterkfontein Member 4, South Africa. *Journal of Human Evolution*, 63: 487-496.
- DeSilva, J.M., Holt, K.G., Churchill, S.E., Carlson, K.J., Walker, C.S., Zipfel, B and Berger, L.R. 2013. The lower limb and mechanics of walking in *Australopithecus sediba*. *Science* 340, 123299.
- Devlin, M.J., and Lieberman, D.E. 2007. Variation in estradiol level affects cortical bone growth in response to mechanical loading in sheep. *Journal of Experimental Biology*, 210: 602-613.
- Devlin, M.J., Cloutier, A.M., Thomas, N.A., Panus, D.A., Lotinun, S., Pinz, I., Baron, R., Rosen, C.J., and Bouxsein, M.L. 2010. Caloric restriction leads to high marrow adiposity and low bone mass in growing mice. *Journal of Bone and Mineral Research*, 25: 2078-2088.
- Djawdan, M. 1993. Locomotor Performance of Bipedal and Quadrupedal Heteromyid Rodents. *Functional Ecology*, 7. 195. 10.2307/2389887.
- Dohlinow, P. and Fuentes, A. 1999. The nonhuman primates. Mountainview, CA: Mayfield Publishing Co.
- Donald, L., and Mitchell, D. H. 1994. Nature and culture on the Northwest Coast of North America: The case of the Wakashan salmon resources. In Burch, E. S., Jr. and Ellanna, L. J. (eds.), *Key Issues in Hunter-Gatherer Research*, Berg, New York, pp. 95-117.
- Doran, D.M. 1993. Sex differences in adult chimpanzee positional behavior: the influence of body size on locomotion and posture. *American Journal of Physical Anthropology*, 91: 99-115.
- Doran, D.M. 1996. Comparative positional behavior of the African apes. In: McGraw, W.C., Marchant, L.F., Nishida, T. (eds.) *Great Ape Societies*. Cambridge: Cambridge University Press. pp. 213-224.
- Doran, D.M., 1997. Ontogeny of locomotion in mountain gorillas and chimpanzees. *Journal of Human Evolution*, 32: 323-344.
- Doube, M., Klosowski, M.M., Aganda-Carreras, I., *et al.* 2010. BoneJ: free and extensible bone image analysis in ImageJ. *Bone*, 47: 1076–1079.
- Doube, M., Klosowski, M.M., Wiktorowicz-Conroy, A.M., *et al.* 2011. Trabecular bone scales allometrically in mammals and birds. *Proceedings of the Royal Society B*. doi:10.1098/rspb.2011.0069.
- Elftman, H. and Manter, J., 1935. Chimpanzee and human feet in bipedal walking. *American Journal of Physical Anthropology*. 20, 69e79.
- Eriksen, E.F. 1986. Normal and pathological remodelling of human trabecular bone: three dimensional reconstruction of the remodelling sequence in normal and in metabolic bone disease. *Endocrine Reviews*, 7: 379–408.
- Eriksen, E.F. 2010. Cellular mechanisms of bone remodelling. *Reviews in Endocrine and Metabolic Disorders*, 11: 219–227.

- Fajardo, R.J. and Müller, R. 2001. Three-dimensional analysis of nonhuman primate trabecular architecture using micro-computed tomography. *American Journal of Physical Anthropology*, 115: 327–336.
- Fajardo, R.J., Müller, R., Ketcham, R., *et al.* 2007. Nonhuman anthropoid primate femoral neck trabecular architecture and its relationship to locomotor mode. *The Anatomical Record*, 290: 422–436.
- Fleagle, J.G. 2013. *Primate Adaptation and Evolution*, 3rd edn. New York: Academic Press.
- Frost, H.M. 1987. Bone ‘mass’ and the ‘mechanostat’: a proposal. *The Anatomical Record*, 219: 1–9.
- Frost, H.M. 1990. Skeletal structural adaptations to mechanical usage (SATMU): 1. Redefining Wolff’s law: the bone modelling problem. *The Anatomical Record*, 226: 403–413.
- Frost, H.M. 2003. Bone’s mechanostat: a 2003 update. *The Anatomical Record*, 275A:1081-1101.
- Gage, J.R., Deluca, P.A. and Renshaw, T.S. 1995. Gait analysis: principles and applications. *Journal of Bone and Joint Surgery (America)* 77-A(10): 1607-1623.
- Gebo, D.L. 1992. Plantigrady and foot adaptation in African apes- implications for hominid origins. *American Journal of Physical Anthropology*, 129(4): 499-511.
- Goldstein, S.A., Goulet, R. and McCubbrey, D. 1993. Measurement and significance of three-dimensional architecture to the mechanical integrity of trabecular bone. *Calcified Tissue International* 53(S1), S127–S133.
- Gray, H. 2009. *Gray’s anatomy: with original illustrations by Henry Carter*. Arcturus Publishing
- Green, D.J. and Alemseged, Z. 2012. *Australopithecus afarensis* scapular ontogeny, function, and the role of climbing in human evolution. *Science*, 338 (6106):514—517 DOI: 10.1126/science.1227123
- Grimston, S.K., Nigg, B.M., Hanley, D.A. and Engsberg, J.R. 1993 Differences in ankle joint complex range of motion as a function of age. *Foot and Ankle International*, 14: 215e22.
- Harrigan, T.P. and Mann, R.W. 1984. Characterization of microstructural anisotropy in orthotropic materials using a 2nd rank tensor. *Journal of Material Science* 19, 761e767.
- Harrison, L.C.V., Nikander, R., Sikio, M., *et al.* 2011. MRI texture analysis of femoral neck: detection of exercise load-associated differences in trabecular bone. *Journal of Magnetic Resonance Imaging*, 34: 1359–1366.
- Hausman, A.J. The biocultural evolution of Khoisan populations of Southern Africa. 1982. *American Journal of Physical Anthropology*; 58(4):315–30.
- Havill, L.M., Allen, M.R., Bredbenner, T.L., Burr, D.B., Nicoletta, D.P., Turner, C.H., Warren, D.M. and Mahaney, M.C. 2010. Heritability of lumbar trabecular bone mechanical properties in baboons. *Bone*, 46:835–840

- Heegaard, J.H., Beupre, G.S and Carter D.R. 1999. Mechanically modulated cartilage growth may regulate joint surface morphogenesis. *Journal of Orthopaedic Research*, 17: 509–517.
- Hildebrand, T. and Ruegsegger P. 1997. Quantification of bone microarchitecture with the structure model index. *Computational Methods in Biomechanics and Biomedical Engineering*; 1:15 – 23.
- Hildebrand, M. and Goslow, G. 1998. *Analysis of Vertebrate Structure*, 5th ed. Hoboken, NJ: Wiley
- Hildebrand, T., Laib, A., Muller, R., Dequeker, J. and Ruegsegger, P. 1999. Direct three-dimensional morphometric analysis of human cancellous bone: microstructural data from spine, femur, iliac crest, and calcaneus. *Journal of Bone and Mineral Research*, 14:1167 – 74.
- Hirasaki, E., Kumakura, H. and Matano, S. 1993. Kinesiological characteristics of vertical climbing in *Ateles geoffroyi* and *Macaca fuscata*. *Folia Primatologica*, 61: 148- 156.
- Hirasaki, E., Kumakura, H. and Matano, S. 2000. Biomechanical analysis of vertical climbing in the spider monkey and the Japanese macaque. *American Journal of Physical Anthropology*, 113: 455–472.
- Hollister, S.J., Brennan, J.M. and Kikuchi, N. 1994. A homogenization sampling procedure for calculating trabecular bone effective stiffness and tissue level stress. *Journal of Biomechanics*, 27: 433–444.
- Holowoka, N.B. and O’Neill, M.C. 2013. Three-dimensional moment arms and architecture of chimpanzee (*Pan troglodytes*) leg musculature. *Journal of Anatomy*, 223: 610-628.
- Huiskes, R., Ruimerman, R., van Lenthe, G.H., *et al.* 2000. Effects of mechanical forces on maintenance and adaptation of form in trabecular bone. *Nature*, 405: 704–706.
- Hunt, K.D. 1989. Positional behavior in *Pan troglodytes* at the Mahale Mountains and the Gombe Stream National Parks, Tanzania. Ph.D. Thesis. University of Michigan.
- Hunt, K.D. 1991. Mechanical implications of chimpanzee positional behaviour. *American Journal of Physical Anthropology*, 86: 521–536.
- Hunt, K.D. 1992. Positional behavior of *Pan troglodytes* in the Mahale Mountains and Gombe Stream National Parks, Tanzania. *American Journal of Physical Anthropology* 87, 83e105.
- Hunt, K.D. 1994. Body size effects on vertical climbing among chimpanzees. *International Journal of Primatology* 15, 855–865.
- Hunt, K.D. 2004. The special demands of great ape locomotion and posture. In: Russon, A.E., Begun, D.R. (eds.). *The Evolution of Thought*. Cambridge: Cambridge University Press. pp. 172-189.
- Hvid, I., Rasmussen, O., Jensen, N.C. and Nielsen S. 1985. Trabecular bone strength profiles at the ankle joint. *Clinical Orthopaedics* 306 – 312
- Inman, V.T. 1976. *The joints of the ankle*. Baltimore: Williams & Wilkins

- Isler, K. 2003. 3D-kinematics of vertical climbing in hominoids. Ph.D. Thesis. University of Zürich.
- Isler, K. 2004. Footfall Patterns, Stride Length and Speed of Vertical Climbing in Spider Monkeys (*Ateles fusciceps robustus*) and Woolly Monkeys (*Lagothrix lagotricha*). *Folia Primatologica*, 75: 133-149.
- Isler, K. 2005. 3-D kinematics of vertical climbing in hominoids. *American Journal of Physical Anthropology*, 126: 66-82.
- Jacobs, C.R. 2000. The mechanobiology of cancellous bone structural adaptation. *Journal of Rehabilitation Research & Development* 37, 209–216.
- Jee, W.S., Wronski, T.J., Morey, E.R., *et al.* 1983. Effects of spaceflight on trabecular bone in rats. *American Journal of Physiology*, 244: 310– 314.
- Jones, T., Farlow, J., Ruben, J., Henderson, D. and Willem, H. 2000. Cursoriality in bipedal archosaurs. *Nature*, 406: 716-8 doi: 10.1038/35021041.
- Judex, S. and Carlson, K.J. 2009. Is bone's response to mechanical signals dominated by gravitational loading? *Medicine & Science in Sports & Exercise* 41, 2037–2043.
- Jungers, W. L. and Susman, R. L. 1984. Body size and skeletal anatomy in the African apes. In (R. L. Susman, Ed.) *The Pygmy Chimpanzee: Evolutionary Biology and Behavior*. New York: Plenum Press.
- Kabel, J., van Rietbergen, B., Odgaard, A., *et al.* 1999. Constitutive relationships of fabric, density, and elastic properties in cancellous bone architecture. *Bone*, 25: 481–486.
- Kelikan, A.S. 2011. *Sarraffian's Anatomy of the Foot and Ankle. Descriptive, Topographic, Functional*. Lippincott Williams & Wilkins, Philadelphia.
- Kelly, R.L. 1983. Hunter–gatherer mobility strategies. *Journal of Anthropological Research*, 39 (3): 277– 306
- Ketcham, R.A. and Ryan, T.M., 2004. Quantification and visualization of anisotropy in trabecular bone. *Journal of Microscopy*. 213 (Pt 2), 158e171.
- Kimbel, W.H. and Rak, Y. 1993. The importance of species in paleoanthropology and an argument for the phylogenetic concept of the species category. In WH Kimbel and LB Martin (eds.): *Species, Species Concepts, and Primate Evolution*. New York: Plenum, pp. 461–484.
- Kimura, T. 1996. Centre of gravity of the body during the ontogeny of primate bipedal walking. *Folia Primatologica*, 66: 126–136.
- Kivell, T.L., Kibii, J.M., Churchill, S.E., *et al.* 2011a. *Australopithecus sediba* hand demonstrates mosaic evolution of locomotor and manipulative abilities. *Science*, 333: 1411–1417.
- Kivell, T.L., Skinner, M.M., Lazenby, R., *et al.* 2011b. Methodological considerations for analyzing trabecular architecture: an example from the primate hand. *Journal of Anatomy*, 218: 209–225.

- Kivell, T.L., Skinner, M.M., Lazenby, R.L., *et al.* 2012. Trabecular architecture of fossil hominin first metacarpals. *American Journal of Physical Anthropology*, 147(S54), 182.
- Kivell, TL. 2016. A review of trabecular bone functional adaptation: What have we learned from trabecular analyses in extant hominoids and what can we apply to fossils? *Journal of Anatomy*, 228: 569-594
- Koch, J.C. 1917. The laws of bone architecture. *American Journal of Anatomy*, 21:177–298.
- Kuman, K. and Clarke, R.J., 2000. Stratigraphy, artefact industries and hominid associations for Sterkfontein, Member 5. *Journal of Human Evolution* 38, 827e847.
- Kura, H., Kitaoka, H.B., Luo, Z and An, K. 1998. Measurement of surface contact area of the ankle joint. *Clinical Biomechanics*, 13(4):365-370.
- Lai, Y.M., Qin, L., Yeung, H.Y., Lee, K.K.H. and Chan, K.M. 2005. Regional differences in trabecular BMD and micro-architecture of weight-bearing bone under habitual gait loading—A pQCT and microCT study in human cadavers. *Bone*, 37: 274-282.
- Lanyon, L.E. 1973. Analysis of surface bone strain in the sheep during normal locomotion. *Journal of Biomechanics*, 6: 41–49.
- Lanyon, L.E. 1974. Experimental support for the trajectorial theory of bone structure. *The Journal of Bone and Joint Surgery* 56B, 160–166.
- Lanyon, L.E., Rubin, C.T. 1985. Functional adaptation in skeletal structures. In: Functional Vertebrate Morphology. (eds Hildebrand M, Bramble DM, Liem KF, Wake BD), pp. 1–25. Cambridge, Massachusetts: Belknap Press.
- Latimer, B., Ohman, J.C. and Lovejoy, C.O. 1987. Talocrural joint in African hominoids – Implications for *Australopithecus afarensis*. *American Journal of Physical Anthropology*, 74(2): 155-175.
- Latimer, B. and Lovejoy, C.O. 1989. The calcaneus of *Australopithecus afarensis* and its implications for the evolution of bipedality. *American Journal of Physical Anthropology*, 78: 369–386.
- Lazenby, R.A., Skinner, M.M., Kivell, T.L. and Hublin, J.J. 2011. Scaling VOI size in 3D μ CT studies of trabecular bone: a test of the over-sampling hypothesis. *American Journal of Physical Anthropology*, 144(2):196-203 doi: 10.1002/ajpa.21385.
- Leardini, A., O'Connor, J.J., Catani, F. and Giannini, S. 2000. The role of passive structures in the mobility and stability of the human ankle joint: a literature review. *Foot and Ankle International*, 21(7): 602-615.
- Lieberman, D.E. 1997. Making behavioral and phylogenetic inferences from hominid fossils: considering the developmental influence of mechanical forces. *Annual Review of Anthropology*, 26: 185– 210.
- Lieberman, D.E., Devlin, M.J. and Pearson, O.M. 2001. Articular area responses to mechanical loading: effects of exercise, age, and skeletal location. *American Journal of Physical Anthropology*, 116: 266–277.

- Lieberman, D.E., Polk, J.D. and Demes, B. 2004. Predicting long bone loading from cross-sectional geometry. *American Journal of Physical Anthropology*, 123: 156–171.
- Lovejoy, C.O., Heiple, K.G. and Burstein, A.H. 1973. The gait of *Australopithecus*. *American Journal of Physical Anthropology*, 38: 757–780.
- Lovejoy, C.O. 2005. The natural history of human gait and posture part 1. Spine and pelvis. *Gait and Posture*, 21: 95–112.
- Macchiarelli, R., Bondioli, L., Galichon, V., *et al.* 1999. Hip bone trabecular architecture shows uniquely distinctive locomotor behaviour in South African australopithecines. *Journal of Human Evolution*, 36: 211–232.
- MacLatchy, L. and Müller, R. 2002. A comparison of the femoral head and neck trabecular architecture of *Galago* and *Perodicticus* using micro-computed tomography (ICT). *Journal of Human Evolution*, 43: 89– 105.
- Madar, S.I., Rose, M.D., Kelley, J., MacLatchy, L. and Pilbeam, D. 2002. New *Sivapithecus* postcranial specimens from the Siwaliks of Pakistan. *Journal of Human Evolution*, 42: 705–752.
- Maga, M., Kappelman, J., Ryan, T.M., *et al.* 2006. Preliminary observations on the calcaneal trabecular microarchitecture of extant large-bodied hominoids. *American Journal of Physical Anthropology*, 129: 410–417.
- Markham, R. and Groves, C.P. 1990. Brief Communication: Weights of Wild Orang Utans. . *American Journal of Physical Anthropology* 81:1-3 doi: 10.1002/ajpa.1330810102
- Martin, R. and Saller, K. 1959. *Lehrbuch der Anthropologie*, Vol. 2, 3rd edn, Stuttgart: Gustav Fischer
- Martin, R.B., Burr, D.B. and Sharkey, N.A. 1998. *Skeletal Tissue Mechanics*. New York: Springer.
- Matarazzo, S.A. 2015. Trabecular architecture of the manual elements reflects locomotor patterns in primates. *PLoS ONE* 10, e0120436.
- McCullough, C.J. and Burge, P.D. 1980. Rotatory stability of the load-bearing ankle. An experimental study. *The Bone & Joint Journal*, 62-B(4):460-464.
- McHenry, H.M. and Berger, L.R., 1998. Body proportions in *Australopithecus afarensis* and *A. africanus* and the origin of the genus *Homo*. *Journal of Human Evolution*. 35, 1e22.
- Modlesky, C.M., Majumdar, S. and Dudley, G.A. 2008a. Trabecular bone microarchitecture in female collegiate gymnasts. *Osteoporosis International*, 19: 1011–1018.
- Modlesky, C.M., Subramanian, P. and Miller, F. 2008b. Underdeveloped trabecular bone microarchitecture is detected in children with cerebral palsy using high-resolution magnetic resonance imaging. *Osteoporosis International*, 19: 169–176.
- Müller, R., Hanhm M., Vogel, M., Delling, G. and Reugsegger, P. 1996. Morphometric analysis of noninvasively assessed bone biopsies: Comparison of high-resolution computed tomography and histologic sections. *Bone*, 18 (3): 215-220.

- Nordin, M. and Frankel, V. 2001. Basic biomechanics of the musculoskeletal system, vol. 3. Baltimore, MA: Lippincott Williams & Wilkins.
- Nguyen, N.H., Pahr, D.H., Gross, T., *et al.* (2013) The biomechanical role of trabecular bone in the siamang (*Symphalangus syndactylus*) manual proximal phalanx. *European Society for the study of Human Evolution* 3, 162.
- Odgaard, A. 1997. Three-dimensional methods for quantification of cancellous bone architecture. *Bone* 20, 315–328.
- Odgaard, A., Kabel, J., van Reitbergen, B., *et al.* 1997. Fabric and elastic principal directions of cancellous bone are closely related. *Journal of Biomechanics*, 30: 487–495.
- Odgaard, A. 2009. Quantification of cancellous bone architecture. In: Bone Mechanics Handbook, 2nd edn. (ed. Cowin SC), pp. 14–19. New York: Informa Healthcare USA.
- Odgaard, A. and Gundersen, H.J.G. 1993. Quantification of connectivity in cancellous bone, with special emphasis on 3-D reconstructions. *Bone*, 14: 173–182.
- Oxnard, C.E. and Yang, H.C.L. 1981. Beyond biometrics: studies of complex biological patterns. *Symposia of the Zoological Society of London*, 46: 127–167.
- Oxnard, C.E. 1997. From optical to computational fourier transforms: the natural history of an investigation of the cancellous bone structure of bone. In: Fourier Descriptors and their Applications in Biology. (ed. Lestrel P), pp. 379–408. Cambridge: Cambridge University Press.
- Parfitt, A.M., 1983. Stereologic basis of bone histomorphometry: theory of quantitative microscopy and reconstruction of the third dimension,. In: Recker, R.R. (Ed.), Bone histomorphometry: techniques and interpretation. CRC Press, Boca Raton, FL, pp. 53e87
- Pauwels, F. (ed.) 1980. Biomechanics of the Locomotor Apparatus: Contributions on the Functional Anatomy of the Locomotor Apparatus. Berlin: Springer.
- Pearson, O.M. and Lieberman, D.E. 2004. The aging of Wolff's 'law': ontogeny and responses to mechanical loading in cortical bone. *Yearbook of Physical Anthropology*, 47: 63–99.
- Pennetti, V., Sgaramella-Zonta, L., and Astolfi, P. 1986. General health of the African Pygmies of the Central African Republic. In: Cavalli-Sforza LL (ed) African Pygmies. Academic Press, New York, pp 127-138
- Phillips-Conroy, J.E. and Jolly, C.J. 1981. Sexual dimorphism in two subspecies of Ethiopian Baboons (*Papio Hamadryas*) and their hybrids. *American Journal of Physical Anthropology*, 56(2): 115-129.
- Pickering, R., Clarke, R.J. and Moggi-Cecchi, J.2004. Role of carnivores in the accumulation of the Sterkfontein Member 4 hominid assemblage: A taphonomic reassessment of the complete hominid fossil sample (1936–1999). *American Journal of Physical Anthropology*, 125: 1-15.
- Pickering, R., Kramers, J.D., 2010. Re-appraisal of the stratigraphy and determination of new U-Pb dates for the Sterkfontein hominin site, South Africa. *Journal of Human Evolution*, 59, 70e86.

- Polk, J.D., Blumenfeld, J. and Ahlumwalia, D. 2008. Knee posture predicted subchondral apparent density in the distal femur: an experimental validation. *The Anatomical Record* 291, 293–302.
- Pontzer, H., Lieberman, D.E., Momin, E., *et al.* 2006. Trabecular bone in the bird knee responds with high sensitivity to changes in load orientation. *Journal of Experimental Biology*, 209: 57–65.
- Pontzer, H., Raichlen, D.A. and Rodman, P.S. 2014. Bipedal and quadrupedal locomotion in chimpanzees. *Journal of Human Evolution*, 66:64-82.
- Prang, T.C. 2015. Rearfoot posture of *Australopithecus sediba* and the evolution of the hominin longitudinal arch. *Nature Scientific Reports*, <http://dx.doi.org/10.1038/srep17677>
- Radin, E.L., Orr, R.B., Kelman, J.L., Paul, I.L. and Rose, R.M. 1982. Effect of prolonged walking on concrete on the knees of sheep. *Journal of Biomechanics*, 15 (7): 487-492.
- Rafferty, K.L. 1996. Joint design in primates: external and subarticular properties in relation to body size and locomotor behaviour. PhD Dissertation, Johns Hopkins University.
- Rafferty, K.L. and Ruff, C.B. 1994. Articular structure and function in *Hylobates*, *Colobus*, and *Papio*. *American Journal of Physical Anthropology*, 94: 395– 408.
- Raichlen, D.A., Gordon, A.D., Foster, A.D., *et al.* 2015. An ontogenetic framework linking locomotion and trabecular bone architecture with applications for reconstructing hominin life history. *Journal of Human Evolution* 81, 1–12. <http://dx.doi.org/10.1016/j.jhevol.2015.01.003>.
- Remis, M. J. 1995. Effects of body size and social context on the arboreal activities of lowland gorillas in the Central African Republic. *American Journal of Physical Anthropology*, 97: 413–434
- Remis, M.J. 1999. Tree Structure and sex differences in arboreality among western lowland gorillas (*Gorilla gorilla gorilla*) at Bai Hokou, Central African Republic. *Primates*, 40(2): 383-396.
- Ricklan, D.E. 1987. Functional anatomy of the hand of *Australopithecus africanus*. *Journal of Human Evolution*, 16: 643–664.
- Roberts, N. The Holocene—an environmental history. Oxford: Basil Blackwell Inc.; 1989. pp. 121.
- Roberts ,D. and Berger, L.R. 1997. Last Interlacial (c. 117 kyr) human footprints from South Africa. *South African Journal of Science*, 93:349–50.
- Rose, M.D. 1991. The process of bipedalization in hominids. In: Origine(s) de la bipédie chez les Hominides. (eds Senut B, Coppens Y), pp. 37–48. Paris: CNRS.
- Rose, M.D. 1977. Positional behaviour of olive baboons (*Papio Anubis*) and its relationship to maintenance and social activities. *Primates*, 18:59-116.
- Roux, W. 1881. Der zu“chtende Kampf der Teile, oder die ‘Teilauslee’ im Organismus (Theorie der ‘funktionellen Anpassung’). Leipzig: Wilhelm Engelmann.

- Rubin, C.T. and Lanyon, L.E. 1985. Regulation of bone mass by mechanical strain magnitude. *Calcified Tissue International*, 37: 411–417.
- Ruff, C. 1988. Hindlimb articular surface allometry in Hominoidea and Macaca, with comparisons to diaphyseal scaling. *Journal of Human Evolution*, 17: 687–714.
- Ruff, C. and Runestad, J.A. 1992. Primate limb bone structure adaptations. *Annual Review of Anthropology*, 21: 407–433.
- Ruff, C., Walker, A. and Trinkaus, E. 1994. Postcranial robusticity in *Homo*. III: Ontogeny. *American Journal of Physical Anthropology*, 65: 191–197.
- Ruff, C., Holt, B. and Trinkaus E. 2006. Who’s afraid of the big bad Wolff?: ‘Wolff’s law’ and bone functional adaptation. *American Journal of Physical Anthropology*, 129: 484–498.
- Ryan, T.M. and Ketcham, R.A. 2002a. The three-dimensional structure of trabecular bone in the femoral head of strepsirrhine primates. *Journal of Human Evolution*, 43: 1–26.
- Ryan, T.M. and Ketcham, R.A. 2002b. Femoral head trabecular bone structure in two omomyid primates. *Journal of Human Evolution*, 43: 241–263.
- Ryan, T.M. and Ketcham, R.A. 2005. The angular orientation of trabecular bone in the femoral head and its relationship to hip joint loads in leaping primates. *Journal of Morphology*, 265: 249–263.
- Ryan, T.M. and Krovitz, G.E. 2006. Trabecular bone ontogeny in the human proximal femur. *Journal of Human Evolution*, 51: 591–602.
- Ryan, T.M. and Shaw, C.N. 2012. Unique suites of trabecular bone features characterize locomotor behaviour in human and nonhuman anthropoid primates. *PLoS ONE* 7, e41037.
- Ryan, T.M. and Shaw, C.N. 2013. Trabecular bone microstructure scales allometrically in the primate humerus and femur. *Proceedings of the Royal Society B* 280, 20130172.
- Ryan, T.M. and Shaw, C.N. 2015. Gracility of the modern *Homo sapiens* skeleton is the result of decreased biomechanical loading. *Proceedings of the National Academy of Science USA* 112, 372–377.
- Ryan, T.M. and van Rietbergen, B. 2005. Mechanical significance of femoral head trabecular bone structure in *Loris* and *Galago* evaluated using micromechanical finite element models. *American Journal of Physical Anthropology*, 126: 82–96.
- Ryan, T.M. and Walker, A. 2010. Trabecular bone structure in the humeral and femoral heads of anthropoid primates. *The Anatomical Record*, 293: 719–729.
- Ryan, T.M., Colbert, M., Ketcham, R.A., *et al.* 2010. Trabecular bone structure in the mandibular condyles of gouging and non-gouging platyrrhine primates. *American Journal of Physical Anthropology*, 141: 583–593.
- Saers, J.P., Cazorla-Bak, Y., Shawm C.N., Stock, R.T. and Ryan, T.M. 2016. Trabecular bone structural variation throughout the human lower limb. *Journal of Human Evolution*, 97:97-108 doi: 10.1016/j.jhevol.2016.05.01

- Salmon, P.L., Ohlsson, C., Shefelbine, S.J. and Doube, M. 2015. Structure Model Index does not measure rods and plates in trabecular bone. *Frontiers in Endocrinology*, 6:181-191 doi: 10.3389/fendo.2015.00162
- Sarrafian SK. 1993. Biomechanics of the subtalar joint complex. *Clin Orthop Relat Res*, 290: 17e26.
- Saparin, P., Scherf, H., Hublin, J.J., *et al.* 2011. Structural adaptation of trabecular bone revealed by position resolved analysis of proximal femoral of different primates. *The Anatomical Record*, 294: 55–67.
- Schaller, G. E. 1963. The mountain gorilla: Ecology and behavior. Oxford, England: Univer., Chicago Press.
- Scherf, H. 2007. Locomotion-related femoral trabecular architectures in primates. Ph.D. Dissertation, Darmstadt University of Technology, Darmstadt, Germany.
- Scherf, H. 2008. Locomotion-related femoral trabecular architectures in primate: high-resolution computed tomographies and their implications for estimates of locomotor preferences of fossil primates. In: *Imaging Anatomical*. (eds Endo, Frey RH, FreyR), pp. 39–59. Japan: Springer.
- Scherf, H., Harvati, K. and Hublin, J.J. 2013. A comparison of proximal humeral cancellous bone of great apes and humans. *Journal of Human Evolution*, 65: 29–38.
- Sealy, J. 2006. Diet, mobility and settlement pattern among Holocene hunter-gatherers in southernmost Africa. *Current Anthropology*, 47: 569–595.
- Sealy, J. and Pfeiffer, S. 2000. Diet, body size and landscape use among Holocene people in the Southern Cape, South Africa. *Current Anthropology*, 41(4): 642–655
- Senut, B. and Tardieu, C. 1985. Functional aspects of Plio-Pleistocene hominid limb bones: implications for taxonomy and phylogeny. In (E. Delson, Ed.) *Ancestors: the Hard Evidence*, pp. 193–201. New York: A. R. Liss.
- Schilling, A.M., Tofanelli, S., Hublin, J.J., *et al.* 2014. Trabecular bone structure in the primate wrist. *Journal of Morphology*, 275: 572–585.
- Schmitt, D. and Hanna, J. 2004. Substrate alters forelimb to hindlimb peak force ratios in primates. *Journal of Human Evolution*, 46: 149–159.
- Shaw, C.N. and Ryan, T.M. 2012. Does skeletal anatomy reflect adaptation to locomotor patterns? Cortical and trabecular architecture in humans and nonhuman anthropoids. *American Journal of Physical Anthropology*, 147: 187–200.
- Simkin, A., Ayalon, J. and Leichter, I. 1987. Increased trabecular bone density due to bone-loading exercises in postmenopausal osteoporotic women. *Calcified Tissue International*, 40: 59–63.
- Simkin, A., Leichter, I., Swissa, A., *et al.* 1989. The effect of swimming activity on bone architecture in growing rats. *Journal of Biomechanics*, 22: 845–851.

- Sinclair, K.D., Farnsworth, R.W., Pham, T.X., *et al.* 2013. The artiodactyl calcaneus as a potential ‘control bone’ cautions against simple interpretations of trabecular bone adaptation in the anthropoid femoral neck. *Journal of Human Evolution*, 64: 366–379.
- Skedros, J.G., Hunt, K.J., Bloebaum, R.D. 2004. Relationships of loading history and structural and material characteristics of bone: development of the mule deer calcaneus. *Journal of Morphology*, 259: 281–307.
- Skedros, J.G., Knight, A.N., Farnsworth, R.W., *et al.* 2012. Do regional modifications in tissue mineral content and microscopic mineralization heterogeneity adapt trabecular bone tracts for habitual bending? Analysis in the context of trabecular architecture of deer calcanei. *Journal of Anatomy*, 220: 242–255.
- Skerry, T.M., Lanyon, L.E. 1995. Interruption of disuse by short duration walking exercise does not prevent bone loss in the sheep calcaneus. *Bone*, 16: 269–274.
- Smith, E.L., Gilligan, C., McAdam, M., *et al.* 1989. Detering bone loss by exercise intervention in premenopausal and postmenopausal women. *Calcified Tissue International*, 44: 312–321.
- Snyders, R.C. 1952. Quadrupedal and bipedal locomotion of lizards. *Copeia*, 2:64-70.
- Snyders, R.C. 1962. Adaptations for bipedal locomotion of lizards. *American Zoologist*, 2: 191-203.
- Sockol, M.D., Raichlen, D.A. and Pontzer, H., 2007. Chimpanzee locomotor energetics and the origin of human bipedalism. . *Proceedings of the National Academy of Science USA* 104, 12265e12269.
- Stern, J.T. Jr. 1975. Before bipedality. *Yearbook of Physical Anthropology* 19, 59–68.
- Stern, J.T. Jr and Susman, R.L. 1991. ‘Total morphological pattern’ versus the ‘magic trait:’ conflicting approaches to the study of early hominid bipedalism. In: *Origine(s) de la bipédie chez les Hominides.* (eds Senut B, Coppens Y), pp. 99–112. Paris: CNRS.
- Stock J, Pfeiffer S. 2001. Linking structural variability in long bone diaphyses to habitual behaviors: foragers from the Southern African Later Stone Age and the Andaman Islands. *American Journal of Physical Anthropology*, 115:337–48.
- Stratford, D.J., Bruxelles, L., Clarke, R.J., Kuman, K., 2012. New stratigraphic interpretations of the fossil and artefact-bearing deposits of the Name Chamber, Sterkfontein. *South African Archaeology Bulletin*. 67, 159e167.
- Stratford, D.J., 2013. Biofabric analysis of palaeocave deposits. *Journal of Taphonomy*, 11: 21e40.
- Su, A., 2011. The functional morphology of subchondral and trabecular bone in the hominoid tibiotalar joint. Ph.D. Dissertation, Stony Brook University.
- Su, A., Wallace, I.J. and Nakatsukasa, M. 2013. Trabecular bone anisotropy and orientation in an Early Pleistocene hominin talus from East Turkana, Kenya. *Journal of Human Evolution*, 64: 667–677.

- Su, A. and Carlson, K.J. 2017. Comparative analysis of trabecular bone structure and orientation in South African hominin tali. *Journal of Human Evolution*, 106: 1-18
- Sugardjito, J. and van Hooff, J. 1986. Age-sex class differences in the positional behavior of the Sumatran orangutan (*Pongo pygmaeus abelii*) in the Gunung Leuser National Park, Indonesia. *Folia Primatologica (Basel)*, 47:14–25.
- Sugiyama, T., Price, J.S., Lanyon, L.E. 2010. Functional adaptation to mechanical loading in both cortical and cancellous bone is controlled locally and is confined to the loaded bones. *Bone*, 46: 314-321
- Susman, R.L. 2004. *Oreopithecus bambolii*: an unlikely case of hominidlike grip capability in a Miocene ape. *Journal of Human Evolution*, 46:103–115.
- Swartz, S.M., Parker, A. and Hou, C. 1998. Theoretical and empirical scaling patterns and topological homology in bone trabeculae. *Journal of Experimental Biology*, 201: 573–590.
- Tardieu, C. 1983. L'articulation du Genou. Analyse, morphofonctionnelle chez les Primates et Hominides fossils. Cah. Paleoanthropologie. C.N.R.S. Ed., p 108
- Thompson, S., MacMillen, E., Richard, M., 1980. The energetic cost of bipedal hopping in small mammals. *Nature*. 287. 223-4. 10.1038/287223a0.
- Thorpe, S.K.S. and Crompton, R.H. 2006. Orangutan positional behaviour and the nature of arboreal locomotion in hominoidea. *American Journal of Physical Anthropology*, 131: 384–401.
- Thulborn, R.A. 1984. Preferred gaits of bipedal dinosaurs. *Alcheringa*, 8: 243-252.
- Thulborn, R.A. 1989. The Gaits of dinosaurs. In *Dinosaur Tracks and Traces* (eds. D.D.Gillette, M.G.Lockley), pp.39-50. Cambridge University Press, Cambridge
- Townsley, W. 1948. The influence of mechanical factors on the development and structure of bone. *American Journal of Physical Anthropology*, 6: 25–45.
- Trinkaus E. 2005. Anatomical evidence for the antiquity of human footwear use. *Journal of Archaeological Science*, 32: 1515-1526.
- Tsegai, Z.J., Kivell, T.L., Gross, T., *et al.* 2013. Trabecular bone structure correlates with hand posture and use in hominoids. *PLoS ONE* 8, e78781.
- Tuttle, R.H. and Cortwright, D. 1988. Positional behavior, adaptive complexes, and evolution. In: Schwartz J, editor. *Orang-utan biology*. New York: Oxford University Press. p 311–330.
- Ulrich, D., van Reitbergen, B., Laib, A., *et al.* 1999. The ability of three-dimensional structural indices to reflect material aspects of trabecular bone. *Bone*, 25: 55–60.
- Vereecke, E.E., D'Août, K., De Clercq, D., Van Elsacker, L., Aerts, P. 2003. Dynamic plantar pressure distribution during terrestrial locomotion of bonobos (*Pan paniscus*). *American Journal of Physical Anthropology*, 120, 373e383.
- Viola, T.B. 2002. Locomotion dependent variation in the proximal femoral trabecular pattern in primates. MSc Thesis, University of Vienna, Vienna, Austria.

von Meyer, G.H. 1867. Die architektur der spongiosa. *Archiv für Anatomie, Physiologie und Wissenschaftliche Medicin*, 34: 615–628.

Wainwright, P.C., Mehta, R.S. and Higham, T.E. 2008. Stereotypy, flexibility and coordination: key concepts in behavioral functional morphology. *Journal of Experimental Biology*, 211: 3523–3528.

Wallace, I.J., Demes, B., Mongle, C., et al. 2014. Exercise-induced bone formation is poorly linked to local strain magnitude in the sheep tibia. *PLoS ONE* 9, 99108.

Ward, F.O. 1838. *Outlines of Human Osteology*. London: Henry Renshaw.

Ward, S.C. and Susman, R.W. 1979. Correlates between locomotor anatomy and behavior in two sympatric species of Lemur. *American Journal of Physical Anthropology*, 50: 575–590.

White, T. D., Asfaw, B., Beyene, Y., Haile-Selassie, Y., Lovejoy, O. C., Suwa, G. & WoldeGabriel, G. 2009 *Ardipithecus ramidus* and the paleobiology of early hominids. *Science*, 326:75–86. (doi:10.1126/science.1175802)

Willems, C., Stassijns, G., Cornelis, W and D’Août. 2016. Biomechanical implications of walking with indigenous footwear. *American Journal of Physical Anthropology*, 162:782-793 doi: 10.1002/ajpa.23169.

Wolff ,J. 1986. *The law of bone remodelling*. Berlin: Springer.

Wunderlich, R. 1999. Pedal form and plantar pressure distribution in anthropoid primates. Ph.D. Dissertation, Stony Brook University.

Yamaguchi, S., Sasho, T., Kato, H., Kuroyanagi, Y. and Banks, S.A. 2009. Ankle and subtalar kinematics during dorsiflexion-plantarflexion activities. *Foot and Ankle International*, 30 (4): 361-6. doi: 10.3113/FAI.2009.0361.

Zeininger, A., Patel, B.A., Zipfel, B., Carlson, K.J., 2016. Trabecular architecture in the StW 352 fossil hominin calcaneus. *Journal of Human Evolution*, 97: 145-158.

Zipfel, B. and Berger, L.R. 2007. Shod versus unshod: The emergence of forefoot pathology in modern humans? *The Foot*, 17: 205-213.

Zipfel, B and Berger, L.R. 2009. Partial hominin tibia (StW 396) from Sterkfontein, South Africa. *Palaeontological Society Southern Africa*, 44: 71-75

Zipfel, B., Kidd, R.S., Clarke, R.J., 2010. The ‘second australopithecine species hypothesis’ in Sterkfontein Member 4: the post-cranial evidence. In: Proceedings of the 16th Conference of the Palaeontological Society of Southern Africa (Howick, 5-8 August, 2010). Interpak Books, Pietermaritzburg, pp. 124e125.

CHAPTER 7: APPENDICES

Table A1: Tukey-HSD for interspecific pairwise comparisons in distal tibia of extant primates (p=0.05)

Parameter	VOI	Significant pairwise	p	
BV/TV	3	<i>Papio>Homo</i>	0,0205	
		<i>Pongo>Homo</i>	0,0267	
		<i>Papio>Pan</i>	0,0463	
	6	<i>Homo>Papio</i>	0,0041	
	Tb.Th	1	<i>Pongo>Pan</i>	0,0163
		<i>Pongo>Homo</i>	0,0382	
3		<i>Pongo>Papio</i>	0,0015	
		<i>Pongo>Homo</i>	0,0274	
		<i>Pongo>Pan</i>	0,0241	
		<i>Gorilla>Papio</i>	0,0334	
7		<i>Pongo>Homo</i>	0,0017	
		<i>Pongo>Pan</i>	0,0133	
Tb.Sp		1	<i>Homo>Papio</i>	<0,0001
			<i>Homo>Pongo</i>	<0,0001
	<i>Gorilla>Papio</i>		0,0015	
	<i>Pan>Papio</i>		0,0039	
	<i>Homo>Pan</i>		0,0183	
	<i>Homo>Gorilla</i>		0,0264	
	2		<i>Homo>Papio</i>	<0,0001
			<i>Homo>Pongo</i>	<0,0001
			<i>Gorilla>Papio</i>	<0,0001
			<i>Pan>Papio</i>	<0,0001
		<i>Gorilla>Pongo</i>	<0,0001	
		<i>Homo>Pan</i>	<0,0001	
		<i>Pan>Pongo</i>	<0,0001	
		<i>Homo>Gorilla</i>	0,0002	
	3	<i>Homo>Papio</i>	<0,0001	
		<i>Homo>Pongo</i>	<0,0001	
		<i>Pan>Papio</i>	<0,0001	
		<i>Gorilla>Papio</i>	<0,0001	
		<i>Pan>Pongo</i>	<0,0001	
		<i>Gorilla>Pongo</i>	<0,0001	
		<i>Homo>Gorilla</i>	0,0003	
		<i>Homo>Pan</i>	0,0005	
		4	<i>Gorilla>Papio</i>	<0,0001
			<i>Homo>Papio</i>	<0,0001
	<i>Gorilla>Pongo</i>		<0,0001	
	<i>Gorilla>Pan</i>		<0,0001	
	<i>Pan>Papio</i>		0,0011	
	<i>Pongo>Papio</i>		0,0026	
	5		<i>Gorilla>Papio</i>	<0,0001
			<i>Homo>Papio</i>	0,0001
<i>Gorilla>Pongo</i>		0,0018		
<i>Gorilla>Pan</i>		0,0025		
		<i>Pan>Papio</i>	0,0176	

		<i>Pongo>Papio</i>	0,0229
	6	<i>Homo>Papio</i>	<0,0001
		<i>Homo>Pan</i>	0,0002
		<i>Homo>Pongo</i>	0,0002
		<i>Gorilla>Papio</i>	0,001
	7	<i>Gorilla>Pan</i>	<0,0001
		<i>Gorilla>Pongo</i>	<0,0001
		<i>Homo>Pan</i>	0,0025
		<i>Homo>Pongo</i>	0,0042
		<i>Gorilla>Papio</i>	0,0041
	8	<i>Homo>Papio</i>	<0,0001
		<i>Homo>Pan</i>	<0,0001
		<i>Homo>Pongo</i>	0,0003
		<i>Homo>Gorilla</i>	0,0402
		<i>Gorilla>Papio</i>	0,0457
	9	<i>Homo>Pongo</i>	<0,0001
		<i>Homo>Papio</i>	<0,0001
		<i>Homo>Pan</i>	<0,0001
		<i>Homo>Gorilla</i>	0,0006
Conn.D	1	<i>Pan>Gorilla</i>	0,0005
		<i>Pan>Pongo</i>	0,0009
		<i>Papio>Gorilla</i>	0,0083
		<i>Pan>Homo</i>	0,0259
		<i>Papio>Pongo</i>	0,0140
	2	<i>Papio>Gorilla</i>	0,0014
		<i>Papio>Pongo</i>	0,0023
		<i>Homo>Gorilla</i>	0,0391
	3	<i>Papio>Gorilla</i>	<0,0001
		<i>Pan>Gorilla</i>	0,0123
		<i>Homo>Gorilla</i>	0,0313
		<i>Papio>Pongo</i>	0,0170
	7	<i>Pan>Pongo</i>	0,0074
		<i>Homo>Pongo</i>	0,0481
DA	1	<i>Papio>Homo</i>	<0,0001
		<i>Pan>Homo</i>	<0,0001
		<i>Gorilla>Homo</i>	0,0001
		<i>Pongo>Homo</i>	0,0012
	2	<i>Gorilla>Homo</i>	0,0043
		<i>Pongo>Homo</i>	0,0061
	3	<i>Papio>Homo</i>	0,0025
		<i>Papio>Pan</i>	0,0184
	4	<i>Papio>Gorilla</i>	<0,0001
		<i>Papio>Pongo</i>	0,0003
		<i>Papio>Pan</i>	0,0016
		<i>Papio>Homo</i>	0,0142
	5	<i>Papio>Pongo</i>	0,0147
	6	<i>Papio>Homo</i>	0,0211
		<i>Papio>Gorilla</i>	0,0128
	7	<i>Papio>Homo</i>	0,0166
	8	<i>Papio>Homo</i>	<0,0001
		<i>Pongo>Homo</i>	0,0015
		<i>Papio>Gorilla</i>	0,0036

		<i>Pan>Homo</i>	0,0183
		<i>Papio>Pan</i>	0,0493
	9	<i>Papio>Homo</i>	0,0035
		<i>Papio>Pongo</i>	0,0027
		<i>Papio>Gorilla</i>	0,0331
SMI	2	<i>Pan>Homo</i>	0,0079
		<i>Pan>Pongo</i>	0,0095
		<i>Pan>Gorilla</i>	0,0146
		<i>Pan>Papio</i>	0,0213
	3	<i>Papio>Homo</i>	0,0142
		<i>Pongo>Homo</i>	0,0155
		<i>Pan>Homo</i>	0,0243
	4	<i>Pongo>Homo</i>	0,0012
		<i>Pan>Homo</i>	0,0158
	5	<i>Pongo>Homo</i>	<0,0001
		<i>Pan>Homo</i>	0,0005
		<i>Gorilla>Homo</i>	0,0026
		<i>Papio>Homo</i>	0,0076
	6	<i>Papio>Homo</i>	<0,0001
		<i>Pan>Homo</i>	<0,0001
		<i>Pongo>Homo</i>	0,0001
		<i>Gorilla>Homo</i>	0,0018
BS/BV	1	<i>Papio>Gorilla</i>	<0,0001
		<i>Pan>Gorilla</i>	0,0003
		<i>Pongo>Gorilla</i>	0,0039
		<i>Papio>Homo</i>	0,0324
	2	<i>Papio>Gorilla</i>	<0,0001
		<i>Homo>Gorilla</i>	0,0459
		<i>Papio>Pan</i>	0,0265
		<i>Papio>Pongo</i>	0,0344
	3	<i>Papio>Gorilla</i>	<0,0001
		<i>Papio>Homo</i>	<0,0001
		<i>Pan>Gorilla</i>	<0,0001
		<i>Papio>Pongo</i>	<0,0001
		<i>Pongo>Gorilla</i>	<0,0001
		<i>Papio>Pan</i>	<0,0001
		<i>Homo>Gorilla</i>	0,0021
	4	<i>Papio>Gorilla</i>	<0,0001
		<i>Pan>Gorilla</i>	0,0002
		<i>Homo>Gorilla</i>	0,0027
		<i>Papio>Pongo</i>	0,0053
	5	<i>Papio>Gorilla</i>	<0,0001
		<i>Homo>Gorilla</i>	0,0011
		<i>Pan>Gorilla</i>	0,0005
	6	<i>Homo>Gorilla</i>	<0,0001
		<i>Papio>Gorilla</i>	0,0003
		<i>Pan>Gorilla</i>	0,0007
		<i>Pongo>Gorilla</i>	0,0075
	7	<i>Pan>Gorilla</i>	<0,0001
		<i>Papio>Gorilla</i>	<0,0001
		<i>Homo>Gorilla</i>	0,0013
		<i>Pongo>Gorilla</i>	0,0122

	8	<i>Pan</i> > <i>Gorilla</i>	<0,0001
		<i>Papio</i> > <i>Gorilla</i>	<0,0001
		<i>Homo</i> > <i>Gorilla</i>	0,0049
		<i>Pongo</i> > <i>Gorilla</i>	0,005
	9	<i>Papio</i> > <i>Gorilla</i>	<0,0001
		<i>Pan</i> > <i>Gorilla</i>	<0,0001
		<i>Homo</i> > <i>Gorilla</i>	0,0015
		<i>Pongo</i> > <i>Gorilla</i>	0,0005

Table A2: Tukey-HSD for intraspecific pairwise comparisons in distal tibia of extant primates (p=0.05)

Species	Parameter	Significant pairwise	p
<i>Homo</i>	Tb.Sp	VOI2>VOI7	0,0124
		VOI8>VOI9	0,0431
	DA	VOI9>VOI1	0,0324
		VOI6>VOI1	0,0454
<i>Pan</i>	BV/TV	VOI8>VOI5	0,0007
		VOI8>VOI4	0,0057
		VOI9>VOI5	0,0099
		VOI8>VOI2	0,0236
		VOI3>VOI5	0,0458
	Tb.Sp	VOI5>VOI9	<0,0001
		VOI4>VOI9	<0,0001
		VOI2>VOI9	<0,0001
		VOI1>VOI9	<0,0001
		VOI5>VOI7	<0,0001
		VOI4>VOI7	<0,0001
		VOI2>VOI7	<0,0001
		VOI5>VOI6	<0,0001
		VOI4>VOI6	<0,0001
		VOI1>VOI7	<0,0001
		VOI8>VOI9	<0,0001
		VOI3>VOI9	<0,0001
		VOI2>VOI6	<0,0001
		VOI5>VOI3	<0,0001
		VOI4>VOI3	<0,0001
		VOI5>VOI8	<0,0001
		VOI1>VOI6	0,0132
		VOI4>VOI8	0,0179
		VOI6>VOI9	0,022
	VOI2>VOI3	0,0327	
	BS/BV	VOI7>VOI5	0,004
		VOI7>VOI2	0,0104
VOI7>VOI6		0,0276	
VOI7>VOI4		0,0346	
VOI8>VOI5		0,0377	
<i>Gorilla</i>	BV/TV	VOI3>VOI5	0,006
		VOI3>VOI4	0,0114
	Tb.Th	VOI3>VOI4	0,0004

		VOI3>VOI5	0,0009
		VOI9>VOI4	0,0041
		VOI9>VOI5	0,0076
		VOI2>VOI4	0,0399
	Tb.Sp	VOI4>VOI9	<0,0001
		VOI5>VOI9	<0,0001
		VOI4>VOI3	<0,0001
		VOI5>VOI3	<0,0001
		VOI7>VOI9	0,0001
		VOI2>VOI9	0,0008
		VOI4>VOI6	0,0011
		VOI5>VOI6	0,0033
		VOI8>VOI9	0,004
		VOI4>VOI1	0,0063
		VOI1>VOI9	0,0099
		VOI4>VOI8	0,0152
		VOI5>VOI1	0,0173
		VOI7>VOI3	0,0186
		VOI5>VOI8	0,0388
		VOI6>VOI9	0,0452
	DA	VOI9>VOI4	0,0003
		VOI2>VOI4	0,0015
		VOI1>VOI4	0,0026
		VOI6>VOI4	0,0331
		VOI8>VOI4	0,0482
	BS/BV	VOI3>VOI5	0,0096
		VOI3>VOI4	0,0176
		VOI2>VOI5	0,0455
Pongo	BV/TV	VOI3>VOI5	<0,0001
		VOI3>VOI4	<0,0001
		VOI3>VOI6	0,0003
		VOI2>VOI5	0,0038
		VOI1>VOI5	0,0130
		VOI2>VOI4	0,0166
		VOI9>VOI5	0,0166
		VOI3>VOI7	0,0352
		VOI1>VOI4	0,0491
	Tb.Th	VOI3>VOI4	0,0016
		VOI2>VOI4	0,0046
		VOI3>VOI5	0,0456
	Tb.Sp	VOI5>VOI9	<0,0001
		VOI5>VOI3	<0,0001
		VOI4>VOI9	<0,0001
		VOI4>VOI3	<0,0001
		VOI5>VOI7	<0,0001
		VOI8>VOI9	<0,0001
		VOI4>VOI7	<0,0001
		VOI8>VOI3	<0,0001
		VOI5>VOI2	<0,0001
		VOI5>VOI6	<0,0001
		VOI4>VOI2	0,0001

		VOI5>VOI1	0,0004
		VOI4>VOI6	0,0005
		VOI1>VOI9	0,0011
		VOI1>VOI3	0,0011
		VOI4>VOI1	0,0021
		VOI6>VOI9	0,0042
		VOI6>VOI3	0,0043
		VOI2>VOI9	0,0142
		VOI2>VOI3	0,0147
		VOI5>VOI8	0,0436
	SMI	VOI4>VOI2	0,0005
		VOI4>VOI8	0,0012
		VOI5>VOI2	0,0014
		VOI5>VOI8	0,0031
		VOI4>VOI3	0,0129
		VOI5>VOI3	0,0296
		VOI4>VOI7	0,0338
	BS/BV	VOI3>VOI5	<0,0001
		VOI3>VOI4	0,0002
		VOI9>VOI5	0,0025
		VOI1>VOI5	0,0031
		VOI8>VOI5	0,0074
		VOI9>VOI4	0,0126
		VOI1>VOI4	0,0152
		VOI8>VOI4	0,0332
		VOI2>VOI5	0,0335
		VOI7>VOI5	0,037
<i>Papio</i>	BV/TV	VOI3>VOI6	0,0007
		VOI2>VOI6	0,0152
		VOI3>VOI5	0,0155
		VOI7>VOI6	0,0261
		VOI3>VOI4	0,0407
	Tb.Sp	VOI5>VOI3	<0,0001
		VOI4>VOI3	<0,0001
		VOI8>VOI3	<0,0001
		VOI5>VOI9	<0,0001
		VOI7>VOI3	<0,0001
		VOI4>VOI9	<0,0001
		VOI8>VOI9	<0,0001
		VOI7>VOI9	<0,0001
		VOI5>VOI6	<0,0001
		VOI5>VOI1	<0,0001
		VOI2>VOI3	0,0002
		VOI5>VOI2	0,0003
		VOI1>VOI3	0,0007
		VOI6>VOI3	0,0007
		VOI4>VOI6	0,012
		VOI4>VOI1	0,0129
		VOI8>VOI6	0,0154
		VOI8>VOI1	0,0165
		VOI4>VOI2	0,0305

		VOI8>VOI2	0,0384
	Conn.D	VOI3>VOI6	0,0005
		VOI1>VOI6	0,0012
		VOI2>VOI6	0,0045
		VOI3>VOI9	0,0053
		VOI3>VOI8	0,0074
		VOI1>VOI9	0,0108
		VOI1>VOI8	0,0149
		VOI3>VOI5	0,0184
		VOI2>VOI9	0,0340
		VOI1>VOI5	0,0351
		VOI2>VOI8	0,0454
	DA	VOI9>VOI2	<0,0001
		VOI6>VOI2	<0,0001
		VOI8>VOI2	<0,0001
		VOI9>VOI5	0,0001
		VOI9>VOI1	0,0001
		VOI4>VOI2	0,0020
		VOI3>VOI2	0,0038
		VOI9>VOI7	0,0043
		VOI7>VOI2	0,0109
		VOI9>VOI3	0,0121
		VOI9>VOI4	0,0218
	BS/BV	VOI3>VOI6	<0,0001
		VOI3>VOI5	<0,0001
		VOI3>VOI8	0,0066
		VOI1>VOI6	0,0133
		VOI3>VOI4	0,0155
		VOI1>VOI5	0,0250
		VOI3>VOI7	0,0331
		VOI3>VOI9	0,0349
		VOI2>VOI6	0,0420

Table A3: Pearson's Correlation by VOI for trabecular parameters examined in distal tibia.

VOI1							
	BV/TV	SMI	Tb.Th	Tb.Sp	Conn.D	DA	BS/BV
BV/TV	1	-0,3955	0,3397	-0,0832	0,0467	0,2753	0,5949
SMI	-0,3955	1	-0,6921	0,0225	-0,0161	-0,112	0,0331
Tb.Th	0,3397	-0,6921	1	-0,1014	-0,2518	0,0808	-0,2112
Tb.Sp	-0,0832	0,0225	-0,1014	1	-0,3756	-0,2889	-0,2168
Conn.D	0,0467	-0,0161	-0,2518	-0,3756	1	0,1409	0,4551
DA	0,2753	-0,112	0,0808	-0,2889	0,1409	1	0,1793
BS/BV	0,5949	0,0331	-0,2112	-0,2168	0,4551	0,1793	1
VOI2							
	BV/TV	SMI	Tb.Th	Tb.Sp	Conn.D	DA	BS/BV
BV/TV	1	-0,5433	0,5526	-0,1959	-0,0223	0,1928	0,5085
SMI	-0,5433	1	-0,6827	-0,0717	0,1019	-0,0441	-0,1794
Tb.Th	0,5526	-0,6827	1	-0,1543	-0,4083	0,2225	0,0049
Tb.Sp	-0,1959	-0,0717	-0,1543	1	-0,1162	-0,3844	-0,2469
Conn.D	-0,0223	0,1019	-0,4083	-0,1162	1	-0,2308	0,497
DA	0,1928	-0,0441	0,2225	-0,3844	-0,2308	1	-0,0614
BS/BV	0,5085	-0,1794	0,0049	-0,2469	0,497	-0,0614	1
VOI3							
	BV/TV	SMI	Tb.Th	Tb.Sp	Conn.D	DA	BS/BV
BV/TV	1	-0,3467	0,658	-0,4506	-0,0548	-0,038	0,3528
SMI	-0,3467	1	-0,4275	-0,4373	0,1929	0,4028	0,0885
Tb.Th	0,658	-0,4275	1	-0,0833	-0,5147	-0,2666	-0,2732
Tb.Sp	-0,4506	-0,4373	-0,0833	1	-0,2329	-0,4097	-0,4835
Conn.D	-0,0548	0,1929	-0,5147	-0,2329	1	0,1133	0,6629
DA	-0,038	0,4028	-0,2666	-0,4097	0,1133	1	0,3238
BS/BV	0,3528	0,0885	-0,2732	-0,4835	0,6629	0,3238	1
VOI4							
	BV/TV	SMI	Tb.Th	Tb.Sp	Conn.D	DA	BS/BV
BV/TV	1	-0,6167	0,5146	0,115	0,2643	-0,0526	0,5559
SMI	-0,6167	1	-0,6533	-0,2084	-0,0662	-0,0207	-0,3007
Tb.Th	0,5146	-0,6533	1	0,3144	-0,2739	-0,15	0,0025
Tb.Sp	0,115	-0,2084	0,3144	1	-0,2272	-0,5516	-0,52
Conn.D	0,2643	-0,0662	-0,2739	-0,2272	1	-0,0556	0,3858
DA	-0,0526	-0,0207	-0,15	-0,5516	-0,0556	1	0,3525
BS/BV	0,5559	-0,3007	0,0025	-0,52	0,3858	0,3525	1
VOI5							
	BV/TV	SMI	Tb.Th	Tb.Sp	Conn.D	DA	BS/BV
BV/TV	1	-0,6952	0,3691	0,122	0,3942	-0,052	0,6413
SMI	-0,6952	1	-0,5318	-0,2372	-0,2594	0,0807	-0,4106
Tb.Th	0,3691	-0,5318	1	0,2405	-0,2334	-0,3072	0,0961
Tb.Sp	0,122	-0,2372	0,2405	1	-0,2566	-0,2836	-0,4266
Conn.D	0,3942	-0,2594	-0,2334	-0,2566	1	-0,0027	0,47
DA	-0,052	0,0807	-0,3072	-0,2836	-0,0027	1	0,1236
BS/BV	0,6413	-0,4106	0,0961	-0,4266	0,47	0,1236	1
VOI6							
	BV/TV	SMI	Tb.Th	Tb.Sp	Conn.D	DA	BS/BV
BV/TV	1	-0,5376	0,3668	0,3812	0,1124	-0,1774	0,4593
SMI	-0,5376	1	-0,4999	-0,5312	-0,1343	0,3138	-0,134
Tb.Th	0,3668	-0,4999	1	0,0737	-0,3296	-0,2858	-0,0391

Tb.Sp	0,3812	-0,5312	0,0737	1	0,163	-0,3251	-0,0021
Conn.D	0,1124	-0,1343	-0,3296	0,163	1	0,0556	0,328
DA	-0,1774	0,3138	-0,2858	-0,3251	0,0556	1	0,1045
BS/BV	0,4593	-0,134	-0,0391	-0,0021	0,328	0,1045	1
VOI7							
	BV/TV	SMI	Tb.Th	Tb.Sp	Conn.D	DA	BS/BV
BV/TV	1	-0,5813	0,1834	0,0407	0,1962	0,0918	0,5925
SMI	-0,5813	1	-0,542	-0,1078	0,0362	0,1729	-0,3817
Tb.Th	0,1834	-0,542	1	-0,1204	-0,5083	0,1678	-0,006
Tb.Sp	0,0407	-0,1078	-0,1204	1	-0,1353	-0,3315	-0,4031
Conn.D	0,1962	0,0362	-0,5083	-0,1353	1	-0,1225	0,3839
DA	0,0918	0,1729	0,1678	-0,3315	-0,1225	1	0,0855
BS/BV	0,5925	-0,3817	-0,006	-0,4031	0,3839	0,0855	1
VOI8							
	BV/TV	SMI	Tb.Th	Tb.Sp	Conn.D	DA	BS/BV
BV/TV	1	-0,4661	0,3644	-0,2029	0,2123	0,0032	0,5026
SMI	-0,4661	1	-0,4819	-0,0971	-0,1565	0,0698	-0,214
Tb.Th	0,3644	-0,4819	1	-0,2007	-0,3554	0,1519	-0,1785
Tb.Sp	-0,2029	-0,0971	-0,2007	1	0,0694	-0,4189	-0,3147
Conn.D	0,2123	-0,1565	-0,3554	0,0694	1	-0,2595	0,4753
DA	0,0032	0,0698	0,1519	-0,4189	-0,2595	1	0,1219
BS/BV	0,5026	-0,214	-0,1785	-0,3147	0,4753	0,1219	1
VOI9							
	BV/TV	SMI	Tb.Th	Tb.Sp	Conn.D	DA	BS/BV
BV/TV	1	-0,3612	0,4954	-0,2346	-0,0576	-0,2273	0,3975
SMI	-0,3612	1	-0,3795	-0,3284	0,0488	0,2484	-0,0157
Tb.Th	0,4954	-0,3795	1	-0,1309	-0,5541	-0,0909	-0,3528
Tb.Sp	-0,2346	-0,3284	-0,1309	1	-0,0245	-0,0697	-0,2108
Conn.D	-0,0576	0,0488	-0,5541	-0,0245	1	-0,1922	0,3323
DA	-0,2273	0,2484	-0,0909	-0,0697	-0,1922	1	-0,0274
BS/BV	0,3975	-0,0157	-0,3528	-0,2108	0,3323	-0,0274	1

Table A4: Trabecular properties of fossil hominins from Sterkfontein Member 4 in relation to comparative extant species. NH= Non-human like, H= human-like, B= Both, U= Unique

Specimen	Trabecular parameter							
	VOI Number	BV/TV	Tb.Th	Tb.Sp	Conn.D	DA	SMI	BS/BV
StW 358	1	NH	B	NH	NH	H	U	B
	2	B	B	NH	NH	H	U	B
	3	U	H	NH	NH	B	U	B
	4	B	H	NH	B	B	U	B
	5	H	U	NH	NH	B	U	H
	6	U	U	NH	NH	B	U	H
	7	H	U	NH	B	B	U	B
	8	U	B	NH	NH	B	U	NH
	9	U	U	U	NH	B	B	U
StW 389	1	B	H	NH	NH	B	B	B
	2	B	H	NH	U	H	B	B
	3	B	H	NH	U	B	B	NH
	4	B	B	NH	NH	NH	H	B
	5	B	B	B	U	B	H	H
	6	B	B	B	U	B	H	H
	7	B	B	NH	U	B	B	B
	8	B	H	NH	U	B	B	NH
	9	U	H	NH	U	U	B	U
StW 515	1	H	U	NH	U	H	H	B
	2	B	U	NH	U	B	B	B
	3	B	U	NH	U	U	B	U
	4	B	U	NH	U	B	B	B
StW 567	1	B	B	U	NH	U	H	B
	2	H	B	U	U	U	U	U
	3	B	B	NH	U	U	H	NH
	4	B	B	NH	NH	NH	U	B
	5	H	B	U	NH	B	U	H
	6	H	B	NH	NH	B	H	H
	7	H	B	NH	NH	B	H	B
	8	B	B	U	NH	B	H	NH